Master's thesis

NTNU
Norwegian University of Science and Technology
Faculty of Engineering
Department of Energy and Process Engineering

Erlend Nytrø Balstad

# Evaluation of possible heat pump configurations for waste heat recovery at +CityXChange Sluppen

Master's thesis in Energy and Environmental Engineering
Supervisor: Armin Hafner
June 2020

NTNU
Norwegian University of
Science and Technology

Erlend Nytrø Balstad

# Evaluation of possible heat pump configurations for waste heat recovery at +CityXChange Sluppen

Master's thesis in Energy and Environmental Engineering
Supervisor: Armin Hafner
June 2020

Norwegian University of Science and Technology
Faculty of Engineering
Department of Energy and Process Engineering

NTNU
Norwegian University of
Science and Technology

# Preface

This paper is the Master Thesis of Erlend Nytrø Balstad, a continuation of the work Project work done during the fall of 2019 and the work done during an summer internship for Statkraft Varme AS. I would like to thank Professor Armin Hafner (NTNU) for valuable guidance and adiveses, helping me realize this thesis. Also a special thanks should be granted to Morten Einar Fossum and Åmund Utne (Statkraft Varme AS), who as advisors during the summer internship provided me with valuable experiences and insights into Statkraft Varme and the +CityxChange project. I would also like to thank Bjørn Ove Berthelsen, Trondheim Kommune and the other +CityxChange partners for allowing students to participate in the project.

Further thanks to; Ignat Tolstorebrov for providing the EES software, Marcel Ahrens for advice and insight into the Dymola/Modelica software. Vegard Klungtveit (ABK-Qviller) providing practical advises and technical knowledge about HTHPs. Sondre Leonhardsen (Kjeldsberg Eiendomsforvaltning) for providing access to the electricity measurements at Sluppenveien 10. Mauro Dallai (Mario Dorin S.p.a) for advice on high temperature compressors and the technical specifications of the chosen compressor models, And Torgeir Viking Skiple (Statkraft Varme AS) for for providing temperature measurements of the district heating grid. I would also like to thank my fellow students for a good social and study environment.

Trondheim, June 2020

Erlend Nytrø Balstad

# Abstract

Facing climate change there is a need for new technologies and better utilization of available resources. The goal of +CityxChange, a part of Horizon 2020, is to promote new and innovative energy solutions. The objective of this thesis is to evaluate possible heat recovery heat pump configurations for waste heat recovery at Sluppenveien 10, a part of developing PEB at Sluppen-Tempe in Trondheim. Both heat recovery to the district heating grid and for hot water production are considered.

High temperature heat pumps (HTHPs) capable of heat sink temperatures $>100°C$ exist, few are commercially available and even fewer capable of waste heat recovery $< 30°C$. The main obstacles to development in HTHP technology are limitations in compressor suction and discharge temperatures, high initial costs and few installations tested in real life conditions. It is therefore a need for large scale pilot installations documenting the profitability and reliability under real life conditions.

Different methods of heat recovery have been investigated through the development five dynamic simulation models of potential heat recovery heat pump configurations in Dymola [1]. The simulation models have been tested under realistic operating conditions, both the steady state at design point and dynamic performance at part load conditions have been studied. The models were set to have an evaporator capacity of 60 kW and suitable compressors were selected from compressor manufacturers.

For heat recovery to the district heating grid two R290/R600 cascade heat pumps have been investigated, Model A1 and A2. The results show that the models achieved a steady state heating/combined COP of 1.71/2.53 and 1.78/2.68 of the A1 and A2 configuration respectively. The Model A2 configuration achieved 11.3 K lower Propane compressor discharge gas temperature than the A1 configuration, and a higher COP as a result of increased specific cooling capacity. Both models were tested for realistic weekly cooling load curve estimated from electricity measurements take by the building owner. The models were able to follow a average weekly cooling load curve of the cold store from 62.5 kW down to 45 kW. For cooling demands over 62.5 kW additional cooling has to be delivered by the existing chillers. The part load simulations did not achieve a lower COP compared to the design point simulations, caused by variable compressor efficiencies not being implemented in the models, a limitation of the models.

The three hot water producing heat pump models; B1, B2 and C1 have been developed. Where the B1 and B2 models are R290/R600 cascade heat pumps similar to A1 and A2, and the C1 configuration is a more conventional $CO_2$ heat pump. The model B1, B2 and C1 configurations achieved a heating/cooling COP of; 2.38/3.88, 3.06/5.23 and 3.28/5.66 respectively. Showing that the COP of the R290/R600 cascade heat pump can be significantly improved by adding a water pre-heater/propane sub-cooler, but inferior to the COP of the $CO_2$ heat pump. The cascade solution is also concluded to be overly complicated for hot water production because the same heat sink temperature can be achieved with a less advanced heat pump. The $CO_2$ heat pump is however more susceptible to increased heat sink inlet temperatures, which limits its possible area of application.

The annual hot water demand of Austmann and 3T is not known, but estimated to be very small compared to the possible hot water production by the heat recovery heat pumps. If heat should be recovered by means of hot water production large amounts of water has to be exported out of the area with M-TES. Due to the uncertainty in cooling demand of the cold storage facility an energy- and economic analysis have been performed with the amount of full load hours (FLH) of the heat recovery heat pumps as an independent variable. The results show that at an assumed 8500 FLH 513.1 MWh of heat can be recovered and 705.0-1060.4 MWh of heat can be delivered depending on method of heat recovery and heat pump configuration. The hot water producing heat pumps achieved the highest COP and thus the best alternative from an energy point of view.

The economical analysis show that the Model A1 and A2 heat pump configurations recovering heat to the district heating grid, have the highest investment costs estimated to 1 650 000 NOK. Similar for the hot water producing heat pumps B1, B2 and C1 the investment cost is estimated to be; 1 500 000, 1 230 000 and 1 205 000 NOK. At very low FLH the hot water producing heat pumps achieve the lowest annual costs, however at $>$1000 FLH the annual costs of heat recovery by hot water increases significantly due to high cost of M-TES. The calculated LCOG of heat recovery to district heating and hot water production is approximately 0.31 NOK/kWh and 0.81-0.73 NOK/kWh respectively. Heat recovery by hot water production is not profitable compared to district heating due to higher LCOG than the average district heating price. For FLH over 3600 hours heat recovery to the district heating grid achieves a LCOG lower than the average district heating price and thus the best economical alternative. However the most amount of heat is likely to be recovered in the summer, the value of the recovered heat is therefore low from the district heating company's point of view. Assuming the heat is sold for half the district heating price, the maximum investment cost of the Model A2 configuration is estimated to be 468 000/482 000. Substantial investment support from +CityXChange is therefore needed.

# Sammendrag

Klimautfordringene har skapt et behov for økt ressursutnyttelse og innovative løsninger. Formålet med +CityxChange, en del av Horizon 2020, er å etablere pilotprosjekter med innovative energiløsninger. Formålet med denne masteroppgaven er å evaluere høytemperatur varmepumpe (HTVP) konfigurasjoner for gjenvinning av lavtemperatur spillvarme fra Sluppenveien 10, en del av etableringen av PEB på Sluppen-Tempe i Trondheim. Både gjenvinning av varme til fjernvarme og for tappevannsproduksjon har blitt evaluert.

HTVPer i stand til varmeavgivelse $>$100°C eksisterer, men få er kommersielt tilgjengelige og enda færre kan gjenvinne lavtemperatur spillvarme under $<$30°C. HTVPer i stand til å gjenvinne lavtemperatur spillvarme finnes, men begrenset til småskala lab-installasjoner. De største utfordringene til utvikling av HTVP-teknologi er; begrensninger i kompressor sugegass- og trykkgasstemperatur, høye investeringskostnader og få eksisterende storskala anlegg. For å gjøre teknologien mer kommersiell er det behov for flere storskala testanlegg for å dokumentere lønnsomhet og pålitelighet under reelle forhold.

Forskjellige metoder for gjenvinning av overskuddsvarme har blitt vurdert ved å utvikle fem dynamiske simuleringsmodeller av potensielle varmepumpe konfigurasjoner i Dymola [1]. Simuleringsmodellene har blitt testet under realistiske driftsforhold både stabilt ved design punkt og dynamisk ytelse ved del-last forhold har blitt studert. Modellene ble satt til å ha en fordamperytelse på 60 kW og passende kompressor modeller har blitt valgt fra produsentene Dorin og Bitzer.

For varmegjenvinning til fjernvarme har det blitt utviklet to R290/R600 kaskadevarmepumper, Model A1 og A2. Resultatene viser at modellene oppnådde en stabil tilstand varme/kombinert COP av 1.71/2.53 og 1.78/2.68 for hhv. Model A1 og A2 konfigurasjonen. Model A2 konfigurasjonen oppnådde en 11.3 K lavere Propan kompressor trykkgass temperatur, og høyere COP som følge av økt spesifikk kjølekapasitet. Begge modellene har blitt testet under en realistisk ukentlig kjøle-lastkurve estimert fra elektrisitetsmålinger foretatt av byggeier. Modellene var i stand til å følge kjølebehovet fra 62.5 kW ned til 45 kW. For høyere kjøle behov må de eksisterende kjølemaskinene være i drift. Del-last simuleringene oppnådde ikke en lavere COP sammenliknet med driftspunkt simuleringene, dette skyldes at reduserte kompressorvirkningsgrader ved del-last ikke er inkludert i og en begrensning av simuleringsmodellene,

Tre tappevanns produserende varmepumpe modeller; B1, B2 og C1 har blitt utviklet. Hvor B1 og B2 er R290/R600 kaskade varmepumper slik som A1 og A2, og C1 konfigurasjonen er en mer konvensjonell $CO_2$ varmepumpe. Model B1, B2 og C1 konfigurasjonene oppnådde en varme/kombinert COP av hhv; 2.38/3.88, 3.06/5.23 og 3.28/5.66. Noe som viser at COP'en av R290/R600 varmepumpen kan bli økt signifikant ved å implementere en vann forvarmer/ propan underkjøler, men fortsatt underlegen COP'en til $CO_2$ varmepumpen. Kaskadeløsningen er også vurdert til å være overkomplisert for tappevannsproduksjon da samme varmeavgivelses temperatur kan oppnås med en mindre avansert varmepumpe. $CO_2$ varmepumpen er forøvrig mer følsom for økt inngående varmesluk temperatur, noe som begrenser dens mulige bruksområder.

Det årlige tappevannsforbruket til Austmann og 3T er ukjent, men estimert til å være lite sammenliknet med den mulige årlige produksjonen av tappevanns varmepumpene. Hvis varme skal gjenvinnes ved tappevannsproduksjon må store mengder tappevann eksporteres ut av området med M-TES.

På grunn av usikkerheten knyttet til kjølebehovet til kjølelageret, har energi- og kostnadsanalysen blitt foretatt med mengden full last timer (FLT) som en uavhengig variabel. Resultatene viser at ved en antatt 8500 FLT, 513.1 MWh varme kan gjenvinnes og 1060.4-705.0 MWh varme leveres avhengig av valgt metode og varmepumpe konfigurasjon. Tappevannsvarmepumpene oppnådde høyest COP og er derfor det beste alternativet fra et energi-standpunkt.

kostnads og lønnsomhetsanalysen viste at varmepumpe konfigurasjonene Model A1 og A2 hadde høyest investeringskostnader estimert til å være 1 650 000 NOK. Tilsvarende for tappevannsvarmepumpene B1, B2 og C1, har investeringskostnadene blitt estimert til å være; 1 500 000, 1 230 000 og 1 205 000 NOK. Ved veldig lave FLT oppnådde tappevannsvarmepumpene lavest årlige kostnader, men ved $>$1000 FLT øker de årlige kostnadene raskt på grunn av de høye kostnadene knyttet til M-TES. Den beregnede LCOG for gjenvunnet varme til fjernvarme og tappevannsproduksjon er hhv omtrent 0.31 NOK/kWh og 0.81-0.73 NOK/kWh. varmegjenvinning ved tappevannsproduksjon er ikke lønnsomt sammenliknet med fjernvarme på grunn av en høyere LCOG enn den gjennomsnittlige fjernvarmeprisen. For FLT over 3600 oppnådde gjenvinnings-varmepumpene til fjernvarme en lavere LCOG enn den gjennomsnittlige fjernvarmeprisen og derfor det beste alternativet fra en økonomisk standpunkt. Likevel vil antageligvis mest varme gjenvinnes om sommeren, verdien av den gjenvunnede varmen vil derfor være lav sett fra fjernvarme selskapets perspektiv. Ved å anta at varmen selges for halvparten av fjernvarmeprisen har den maksimale investeringskostnaden blitt estimert til å være 468 000/482 000. Det vil derfor være behov for betydelig investeringsstøtte fra +CityXChange.

# Table of Contents

# List of Tables

# List of Figures

# Nomenaclature

## Abbreviations

| | | |
|---|---|---|
| AC | = | Annual costs |
| CDT | = | Compressor discharge temperature |
| CF | = | Counter flow |
| CFCs | = | Clorofluorocarbons |
| +CityxChange | = | Positive city exchange |
| COP | = | Coefficient of performance |
| CST | = | Compressor suction temperature |
| CVCC | = | Closed vapour compression cycle |
| DA | = | Demonstration area |
| DC | = | Data center |
| DH | = | District heating |
| DHW | = | Domestic hot water |
| EES | = | Engineering equations solver |
| EU | = | European union |
| FLH | = | Full load hours |
| GWP | = | Global warming potential |
| HC | = | Hydrocarbon |
| HCFCs | = | Hydroclorofluorocarbons |
| HFCs | = | Hydrofluorocarbons |
| HFOs | = | Hydrofluoroolefins |
| HP | = | Heat pump |
| HSiIT | = | Heat sink inlet temperature |
| HSiOT | = | Heat sink outlet temperature |
| HSoIT | = | Heat source inlet temperature |
| HSoOT | = | Heat source outlet temperature |
| HTC | = | High temperature cycle |
| HTHP | = | High temperature heat pump |
| IHX | = | Internal heat exchanger |
| LCOG | = | Levelized cost of generation |
| LMTD | = | Logarithmic mean temperature difference |
| LTC | = | Low temperature cycle |
| LTDH | = | Low temperature district heating |
| MTC | = | Medium temperature cycle |
| M-TES | = | Mobile thermal energy storage |
| NTNU | = | Norwegian university of science and technology |
| ODP | = | Ozone depletion potential |
| O&M | = | Operation and maintenance cost |
| PEB | = | Positive energy block |
| PED | = | Positive energy district |
| PF | = | Parallel flow |
| SCOP | = | Seasonal coefficient of performance |
| SLV10 | = | Sluppenvegen 10 |
| SLV17A | = | Sluppenvegen 17A |
| SP | = | State point |
| TFA | = | Trifluoroacetic acid |
| UN | = | United nations |
| VHC | = | Volumetric heating capacity |
| VCHP | = | Vapor compression heat pump |
| ZEA | = | Zero emission area |
| ZEN | = | Zero emission neighborhood |

t

## Symbols

| | | | |
|---|---|---|---|
| a | = | annuity factor | |
| $A$ | = | Area | $[m^2]$ |
| B | = | Annual net benefit | [NOK] |
| $C_P$ | = | Heat capacity | $[kJ/kgK]$ |
| $e$ | = | Electricity cost | [NOK/kWh] |
| $h$ | = | enthalpy | $[kJ/kgK]$ |
| $I_0$ | = | Investment costs | [NOK] |
| $k$ | = | Isentropic coefficient | $[-]$ |
| $L$ | = | Length | $[m]$ |
| $\dot{m}_R$ | = | Refrigerant mass-flow | $[kg/s]$ |
| $n$ | = | Polytropic coefficient | $[-]$ |
| $n$ | = | Compressor speed | $[rpm]$ |
| $n$ | = | Economic lifetime | [year] |
| $p_C$ | = | Condensation pressure | $[bar]$ |
| $p_E$ | = | Evaporation pressure | $[bar]$ |
| $p_{im}$ | = | Intermediate pressure | $[bar]$ |
| $T_E$ | = | Evaporation Temperature | $[°C]$ |
| $T_C$ | = | Condensation Temperature | $[°C]$ |
| $\Delta T$ | = | Temperature difference | $[K]$ |
| $\dot{Q}_E$ | = | Evaporator heat capacity | $[kW]$ |
| $\dot{Q}_C$ | = | Condenser heat capacity | $[kW]$ |
| $r$ | = | interest rate | [-] |
| $U$ | = | Overall heat transfer coefficient | $[W/m^2K]$ |
| $v_0$ | = | Cylinder clearance volume | $[m^3]$ |
| $\dot{V}$ | = | Volume-flow | $[m^3/h]$ |
| $V_{Nom}$ | = | Nominal displacement | $[m^3/h]$ |
| $\dot{W}_C$ | = | Mechanical compressor work-input | $[kW]$ |
| $\approx$ | = | Approximately | |
| $\pi$ | = | Pressure ratio | [-] |
| $\phi_0$ | = | Cylinder charge ratio | $[-]$ |
| $\rho$ | = | Mass density | $[kg/m^3]$ |
| $\lambda$ | = | Volumetric Compressor Efficiency | $[-]$ |
| $\eta_{Is}$ | = | Isentropic Compressor Efficiency | $[-]$ |
| $\eta_{Eff.Is}$ | = | Effective Isentropic Compressor Efficiency | $[-]$ |
| $\eta_v$ | = | Expansion Related Volumetric Losses | $[-]$ |
| $\eta_v$ | = | Non-Expansion Related Volumetric Losses | $[-]$ |

Chapter 1

# Introduction

## 1.1 About the Master Thesis

The main goal of this Masters Thesis is to develop and evaluate thermal energy solutions for waste heat recovery at Sluppen-Tempe, a part of the +CityxChange project in Trondheim. This work is a continuation of an summer internship for Statkraft Varme AS and the Project work performed in the fall semester of 2019. The summer internship and project work mainly focused on Sluppenveien 17A, the focus of this masters thesis is therefore waste heat recovery at Sluppenveien 10.

### 1.1.1 Motivation

Climate change is a growing threat to our common future, the sea level is rising and weather patterns are changing. At the same time the worlds demand for energy is increasing, and is expected to grow by 20-30% within 2040 [2], mainly driven by economic growth in the developing world. Facing climate change while maintaining economic growth is a tremendous challenge in need of new solutions. To face these challenges the United Nations (UN) have created 17 goals for sustainable development [3]. They include: *7: Affordable and clean energy*, *11: Sustainable cities and communities* and *13: Climate action*. Coherent with the sustainable development goals the European Union (EU) has decided to reduce $CO_2$ emissions compared to 1990 levels and increase energy efficiency, both by 20% [4]. The development of new technologies to increase utilization of available resources is important to achieve reduced $CO_2$ emissions, meanwhile maintaining economic growth.

For instance $\approx 36\%$ of the total energy consumption in Norway is related to building use and operation [5]. At the same time a study from 2007 by Norsk Energi in collaboration with Enova [6] found that Norway has $19.2\,TWh$ of available waste heat from industry. Thereof $3.3\,TWh$ is in the low temperature range $25$ to $40°C$. Developing new methods to utilize this excess heat is therefore vital to reducing the energy consumption and $CO_2$ emissions in Norway. This can be achieved through use of state of the art heat pump technology.

### 1.1.2 Task Description

Task description The goal of +CityXChange Sluppen is to achieve a plus energy district (PED). To reach the goal heat must be recovered from the energy system of Sluppenvegen 10 and 17A by means of heat pumps. Sluppenvegen 17A has available waste heat from process cooling, i.e. mainly data center cooling. Sluppenvegen 10 has available waste heat from a cold store refrigeration system. Up to now, there are four independent refrigeration units providing a few 100 kW of cooling. The exact required cooling demand is uncertain since there are no measurement devices. Most of the building is cooled by a unit with a maximum capacity of 346 kW. An evaluation of possible high temperature heat pump configurations for waste heat recovery at Sluppenvegen 17A was performed in the Project work. The aim of the Master thesis is therefore to analyze the energy flows and develop system architectures for waste heat utilization at Sluppenvegen 10. The Sluppen already have an existing district heating grid. High temperature heat recovery to the existing district heating grid and local low temperature heat recovery to buildings not connected to the district heating grid should both be considered. The developed energy system architectures should be compared and evaluated in terms of; System performance, energy efficiency, economy and long-term commercial applicability for future installations. Tasks to be considered:

- Review relevant literature eg. HVAC, Industrial refrigeration and thermal energy systems.
- Evaluate possible energy systems for waste heat recovery by means of heat pumps, suitable for the +CityxChange project.
- Evaluate different heat pump configurations and thermal energy systems in terms of: System performance, energy efficiency, costs and profitability.
- Develop dynamic simulation model(s) of possible energy systems for +CityxChange
- Draft version of possible scientific paper
- Proposals for further work

### 1.1.3 Overview

As previously stated this Masters Thesis is a continuation of an summer internship for Statkraft Varme AS and the Project Work performed during the fall of 2019, both of which a part of the +CityxChange project. This section is therefore intended as an overview of which tasks have been performed during which period.

#### Summer Internship

The main task of the summer internship for Statkraft Varme AS, a partner in the +CityxChange project, was to perform a feasibility study of how waste heat can be recovered from the Sluppen Area. The work was especially related to the Sluppenveien 17A installation, due to the buildings connection to Statkrafts district heating grid in Trondheim. A large part of the work consisted of gathering information about the +CityxChange buildings and the two existing technical installations at Sluppenveien 10 and Sluppenveien 17A, analysing energy measurements and proposing possible heat pump configurations for waste heat utilization.

#### Project Thesis

Based on the proposed heat pump configurations, it was decided to move on with a 2-step cascade heat pump utilizing propane and butane as working fluids. This was done in collaboration with the +CityxChange partners. The main focus of the project work performed during the fall of 2019 was therefore to develop dynamic simulation model(s) of the proposed heat pump configurations for SLV17A in Dymola/Modelica using the TIL media and component libraries. In the start of 2020 the planning of the heat pump configuration at SLV17A is close to completion and possible suppliers and manufactures are currently being involved. It was therefore decided to focus on focusing developing a similar method of waste heat utilization for SLV10 in this masters thesis.

#### Continuation of the Project Thesis

As previously stated this Master thesis is a continuation of the project work, both with a focus on heat recovery heat pumps at Sluppen. A lot of the literature studies and theory of the project thesis is therefore still relevant for the Master thesis. In agreement with my supervisor Armin Hafner it was decided to reuse part of the project thesis relevant to the master thesis. In stead of spending time re-writing usable sections it was considered more productive to use the most amount of time trying to solve the challenges of +CityXChange. The following sections are therefore taken either in its entirety or partly from the project thesis. Section; 2.1, 2.2, 2.3, 2.4, 2.6, 4.4.1, First paragraph of the ”Conclusion”, First two paragraphs of the ”Abstract” and ”Sammendrag”.

### 1.1.4 Goal and Structure

The goal of this thesis is to evaluate different methods of heat recovery at Sluppenveien 10, and constitute an assessment basis for the +CityxChange project. This is done by developing dynamic HTHP simulation models and performing an energy and economical analysis. The eight parts of this thesis are:

**+CityxChange**
Presenting the +CityxChange project in general and the different demonstration areas in Trondheim. This section also explains the role of this thesis within +CityxChange. And gives a brief introduction into the +CityXChange and other comparable projects.

**Theory and Literature review**
Containing relevant theory and literature regarding HTHPs for waste heat recovery. Including but not limited to; Basic heat pump principles, heat pump components, industrial heat pump configurations, working fluids, state of the art HTHP technology, Thermal energy storage and economic parameters.

**System Description and Preliminary Work**
This chapter describes the solution for Sluppenveien 17A worked on during the Project Work. It also is devoted to describing the existing technical installations at Sluppenveien 10 as well as the existing electricity measurements taken at Sluppenveien 10.

**Method**
Explaining the methodology used developing the heat recovery heat pumps models. The process of developing initial steady state models is first presented, the general approach of developing dynamic models. Lastly the method of performing the energy and economical analysis is presented.

**Results and Discussion**
This chapter presents and discusses detailed results of the developed models under relevant operating conditions. It has been chosen to focus on presenting detailed results of the Model A1 heat pump configuration, followed by the most important results of the remaining models. Lastly the developed heat recovery heat pump configurations are compared in terms of; performance, technical feasibility, costs and profitability.

**Conclusion**
Containing the most important findings of this thesis, from both literature review and simulation models. Predicted system performance in terms of COP as well as practical findings regarding reliability and costs.

**Further Work**
Some of the tasks given in the tasks description should be further investigated. This chapter therefore gives a series of proposals for futher work to be performed during research following this thesis.

**Appendices**
Containing other relevant information. Including EES-scripts, data from the compressor manufacturer, detailed Dymola model input parameters and additional results of the simulation models.

## 1.2 +CityxChange and the Sluppen-Tempe Area

+CityxChange is a smart city project funded by the European Union [7]. The project is a part of the European Unions research and innovation program *Horizon 2020* , under the scope *Smart cities and communities* [8]. The goal of the project is to develop sustainable cities for the future. The two *Light house cities* Trondheim and Limerick are to develop sustainable and climate-friendly demo projects in urban environments. Positive Energy Blocks (PEB) are to be created through innovative solutions in energy markets, implementing new technology and business models. The demo projects will be replicated in the five *Follower Cities*; Alba Iulia, Pisek, Võru, Smolyan and Sestao [9]. And eventually scaled up creating Positive Energy Districts and cities. +CityxChange is lead by the Norwegian University of Science and Technology (NTNU) in collaboration with the two light house cities, represented by Trondheim Municipality and Limerick City and County Council.

+CityxChange in Trondheim consists of three demonetisation areas (Figure 1.1): DA1 Sluppen-Tempe, DA2 Brattøra and DA3 Campus Gløshaugen. All in proximity to the city centre. This thesis will focus on thermal energy solutions of DA1 Sluppen-Tempe.

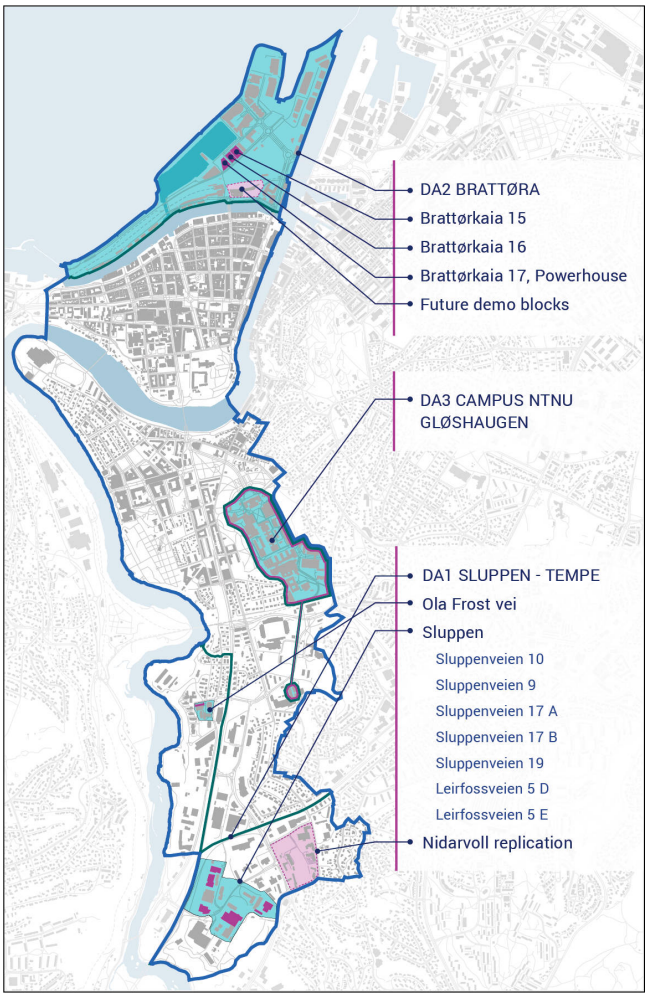


**Figure 1.1:** +CityxChange Demo Areas in Trondheim [10]

### 1.2.1 The Sluppen-Tempe Area

Sluppen-Tempe is an area with several office and light-industry buildings. Where the majority of the properties on the 180 000 $m^2$ area are owned by Kjeldsberg Eiendomsforvaltning AS. Sluppen Positive Energy Block Sluppen-Tempe consist of in total eight buildings. The location of all +CityxChange buildings at Sluppen-Tempe except Ola Frost vei is shown in Figure 1.2 on the following page. Figure 1.2 also shows a simplified overview of the road and district heating infrastructure in the area. This is of importance when considering how the excess thermal energy in the area can be utilized.

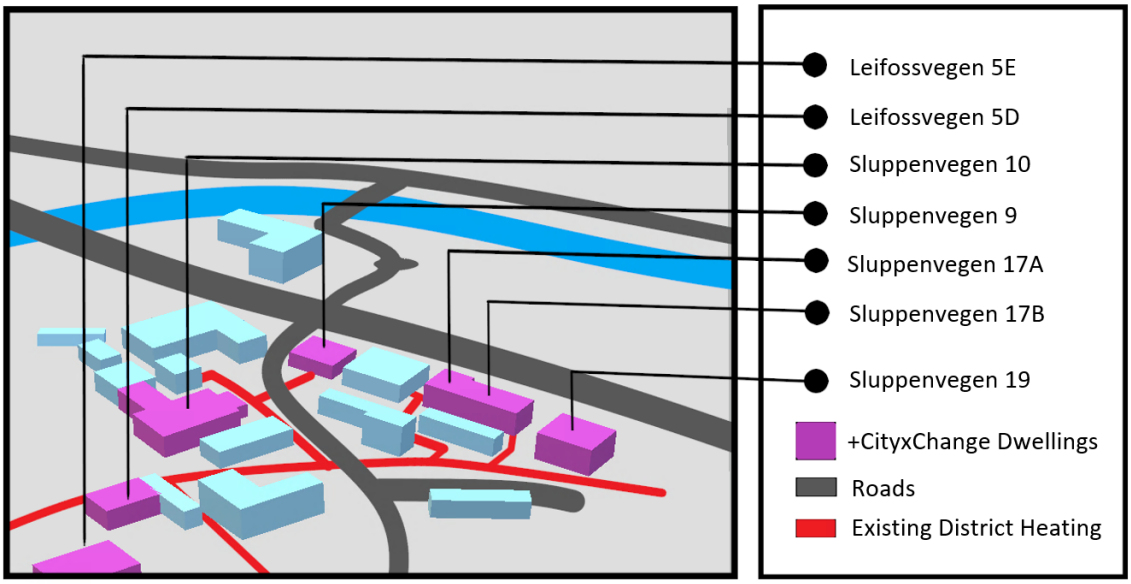


**Figure 1.2:** Simplified 3D overview of the +CityxChange buildings at Sluppen-Tempe. Ola Frost vei is not included due to its distance from the other +CityxChange buildings.

Figure 1.3 below shows which of the buildings in the area are currently connected to the district heating grid as well as sources of, and recipients of waste heat in the area. Two of the buildings Sluppenveien 10 and Sluppenveien 17A have excess waste heat which can be utilized. The heat sources in the two buildings are cold storage and cooling of a computer centre for Sluppenveien 10 and Sluppenveien 17A respectively. In Sluppenveien 10 the current system has no form of excess heat utilization, in the case of Sluppenveien 17A some excess heat is utilized within the building. The technical installations of both systems is described in Section 3.1. Waste heat utilization at Sluppenveien 17A was evaluated during the project thesis, this masters thesis is therefore to focus on waste heat utilization at Sluppenveien 10.

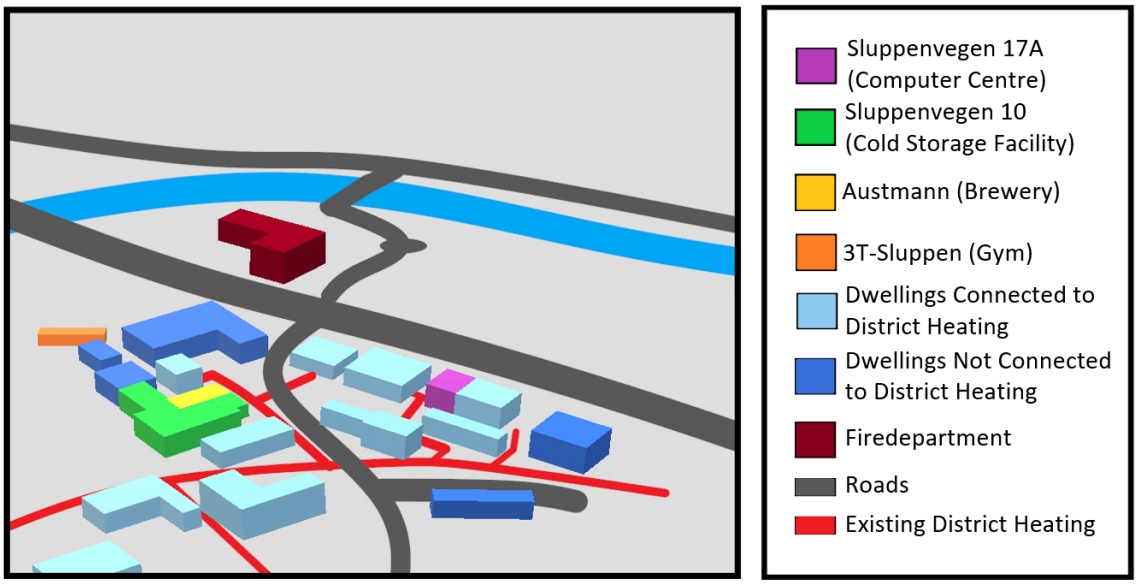


**Figure 1.3:** Simplified 3D overview of the Sluppen-Tempe Area.

Unlike Sluppenveien 17A is Sluppenveien 10 not connected to the existing district heating infrastructure in the area. The building is a cold storage facility owned by Kjeldsberg Eiendom, but occupied by BaRe through NHP Eiendom. Being a cold storage facility it is likely to have excess heat available from the existing chillers, especially during the summer period. The lack of district heating connection, period of waste heat availability as well as ownership structure of the building is of importance when considering potential methods of waste heat recovery from Sluppenveien 10. Some of the most promising possible recipients of the excess waste heat are; Austmann a local brewery located in the same building as BaRe, 3T Sluppen a fitness center as well as connecting the building to the existing district heating grid, all of which is shown in Figure 1.3. It was therefore in this thesis decided to focus on waste heat recovery to the district heating grid and hot water production by means of heat pumps.

## 1.3 Other Comparable PED and ZEA Projects

The +CityxChange project and the concept of positive energy districts (PED) is very innovative and new. Therefore few developed comparable projects exists. Due to the lack of comparable projects both existing PED and zero emission areas (ZEA) have been included in the literature review.

#### Ectogrid — Medicon Village, Sweden

Medicon Village is a center for research and innovation in life sciences located close to Lund University in Sweden. Medicon Valley is the result of an large biopharmaceutical company moving its business from Lund, creating 80 000 $m^2$ of available technologically advanced real estate. Over 50% of the floor space is high technology labs and is currently inhabited by over 120 companies and over 1600 employees [11]. Medicon Village is currently expanding and the worlds first Ectogrid is to be built by E.ON [12].

Ectogrid is a new an innovative thermal energy system able to deliver both heating and cooling on both a community and city level. The Ectogrid is able to adapt its low temperature level to the surroundings in order to minimize losses. The Ectogrid is both a thermal energy distribution system and a thermal energy battery adding flexibility to the energy system allowing for more intermittent renewable energy and reuse of excess waste heat [13]. When completed the ectogrid at Medicon Valley is going to connect 15 residential and commercial buildings, delivering 10 GWh of heating and 4 GWh of cooling, with only 3 GWh of supplied energy to the system. This is to be achieved through reuse of available thermal energy sources and the 11 GWh of heat balancing capacity of the system [12]. The intended Ectogrid at Medicon Valley is illustrated in Figure 1.4.

**Figure 1.4:** Ectogrid - Medicon Village, Sweden [14].

### Zero-Zero — Suurstoffi, Switzerland

Zero-Zero is new zero emission district currently being developed by Zug Estates AG in Rotkreuz, outside Luzern in Switzerland. The approximately 165000 $m^2$ large area will consist of a combination of offices, supermarkets, residential buildings and other commercial buildings, including the new campus of Luzern University of applied sciences [15]. When completed in 2020 the area is going to be self sufficient of primary energy, which is going to be achieved through electricity production from PV-panels and utilization of excess waste heat from the buildings. Heating and cooling of the area is to be delivered by a low temperature district heating and cooling network and decentralized heat pumps. The LTDH network has been in operation since 2012 and is connected to 215, 150 meter deep ground borehole heat exchangers [16]. When completed the ground borehole system is going to consist of additional 840, 280 meter deep bore holes [17]. The area was built in 3 construction periods; 2010-2012, 2012-2014 and 2013-2018. Allowing measurements from the first periods to be used for improved planning of the later construction periods.

Measurements showed that the actual electricity demand of the LTDH network and heat pumps was 800 MWh/a, significantly higher than the expected 360 MWh/a [16]. Simulations in IDA-ICE showed that the increased heating demand was caused by higher indoor air temperatures and higher ventilation heat losses than initially predicted. A wood pellet oven was therefore installed to supply extra heat to the LTDH network in order to avoid a decrease in ground storage temperature [16]. Despite the installation of the pellet oven, the temperature of the geothermal storage decreased by about 0.6 K [16]. Proving the importance of accurately estimating the total heating demand in advance. An illustration of the Suurstoffi Zero-Zero area with bore holes can be seen in Figure 1.5 below.

**Figure 1.5:** Zero-Zero Concept Suurstoffi Switzerland [18].

Chapter 2

# Theory and Literature review

This chapter will present an overview of relevant literature and present the most important theory for the topics covered in this thesis. Including but not limited to: basic heat pump principles, heat pump components, and working fluids. The chapter includes a literature review of existing high temperature heat pump technologies and systems for waste heat recovery.

## 2.1 Heat Pump principles

The term heat pump can be defined as a machine that transfers heat from a low temperature source to a high temperature source, by means of mechanical work input. Several different heat pump principles exist, most of which have in common that they exploit the latent energy difference of evaporation and condensation. This thesis will focus on the closed vapor compression cycle CVCC. The cycle uses a circulating working fluid and controls the evaporation and condensation temperature of the fluid by regulating the pressure. The evaporator extracts heat from a low temperature heat source $\dot{Q_E}$ and transfers it to the working fluid at low evaporation pressure and temperature. The working fluid is then compressed to a high pressure, increasing the temperature. Heat $\dot{Q_C}$ from the working fluid at high pressure is then transferred to the high temperature heat sink through the condenser. Next the pressure of the working fluid is lowered by the expansion valve. The cycle then continues as long as the compressor receives a power input $\dot{W}$.

In order to comprehend the heat pump process the CVCC is often drawn into the Ts or pH (Temperature-entropy or pressure-enthalpy) diagram. Each working fluid has its own set of unique pH- and Ts- diagram. The CVCC as described in Figure 2.1 is drawn into the diagrams can be seen in Figure 2.2.

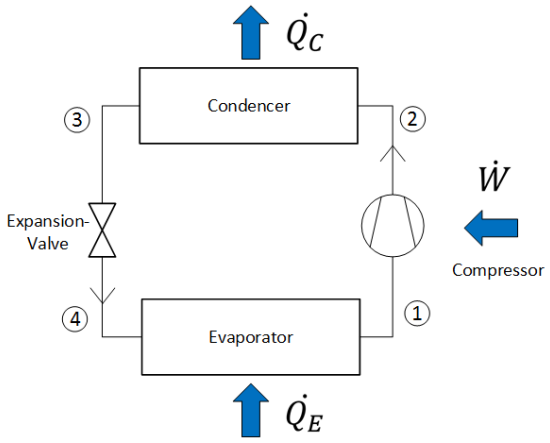


**Figure 2.1:** Simple Closed vapor compression cycle.

**The 4 stages of the CVCC**

- **1-2 Compression:** The working fluid is compressed in the compressor, increasing the pressure. The isentropic compression work is calculated with the following formula: $\dot{W}_{is} = \dot{m}_R \cdot (h_2 - h_1)$. The actual compression work is calculated using the isentropic efficiency $\eta_{is}$ and Formula 2.1.

$$\dot{W}_{Comp} = \frac{\dot{W}_{is}}{\eta_{is}} = \frac{\dot{m}_R \cdot (h_2 - h_1)}{\eta_{is}} \tag{2.1}$$

- **2-3 Isobaric heat rejection in condenser:** The working fluid condenses and heat is rejected to the heat sink. If heat losses to the surroundings is neglected, then the amount of heat rejected in the condenser is equal to the sum of heat absorbed in the evaporator and the compressor work. Or the mass flow rate times the change in enthalpy over the condenser.

$$\dot{Q}_C = \dot{Q}_E + \dot{W}_{Comp} = \dot{m}_R \cdot (h_3 - h_2) \tag{2.2}$$

- **3-4 Isenthalpic Expansion:** The expansion valve reduces the pressure by expanding the working fluid. This happens under constant enthalpy.

$$h_4 = h_3 \tag{2.3}$$

- **4-1 Isobaric heat extraction:** Due to the low pressure and low temperature of the working fluid, heat is absorbed by evaporation. The amount of absorbed heat can be calculated by product of mass flow rate times enthalpy difference across the evaporator. Or the product of U-value $[W/m^2k]$, surface area and the logarithmic mean temperature difference of the evaporator. The logarithmic mean temperature difference is defined as in Equation 2.7, and the temperature differences are defined as in Equation 2.8a and 2.8b, for a counter-flow (CF) and parallel-flow (PF) heat exchanger respectively.

$$\dot{Q_E} = \dot{m_R} \cdot h_1 - h_4 = U \cdot A \cdot LMTD|_{Heat-exchanger} = \dot{V} \cdot \rho \cdot C_p \cdot \Delta T|_{Heat-source} \quad (2.4)$$

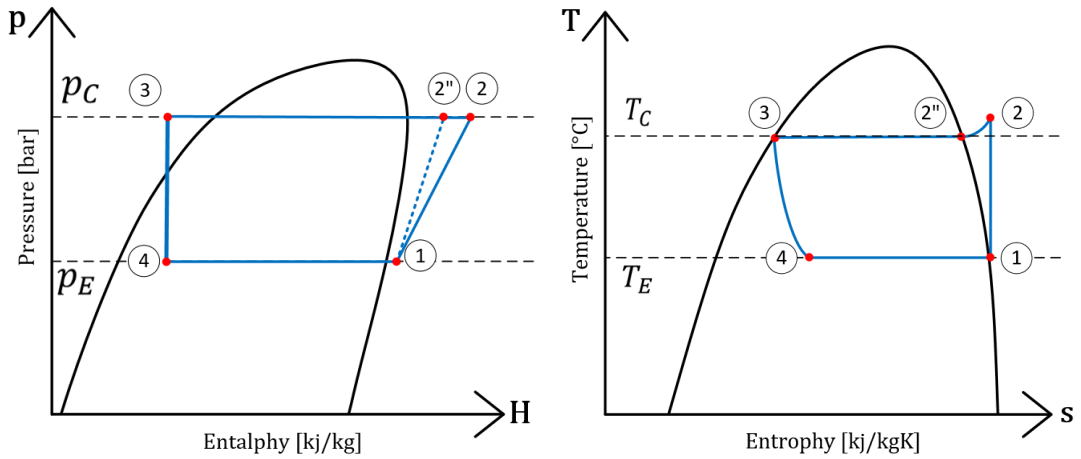


**Figure 2.2:** (a) Left: pH-Chart Example (b) Right: Ts-Chart Example

To describe the performance of the system it is usual to calculate the coefficient of performance (COP). The COP is the ratio of thermal energy delivered from system versus work input. Depending on if the system is a heat pump or a refrigeration system the goal is to deliver or remove heat. The COP of the system is therefore defined in different ways depending on the function of the system. $COP_{HP}$ for heat pumps, $COP_{Ref}$ for refrigeration systems and $COP_{Comb}$ for combined refrigeration and heating systems. See Equation: 2.5a, 2.5b and 2.5c.

$$COP_{HP} = \frac{\dot{Q}_c}{\dot{W}}[-] \quad (2.5a) \qquad COP_{Ref} = \frac{\dot{Q}_e}{\dot{W}}[-] \quad (2.5b) \qquad COP_{Comb} = \frac{\dot{Q}_c + \dot{Q}_e}{\dot{W}}[-] \quad (2.5c)$$

$$COP_{Carnot} = \frac{T_{HSiOT}}{T_{HSiOT} - T_{HSoIT}} \quad (2.6)$$

## 2.2 Heat Pump Components

### 2.2.1 Heat exchangers

The second law of thermodynamics determines that heat will always flow in the direction of high to low temperature, when a temperature difference exists. To reverse the direction of heat transfer mechanical work has to be done. In a heat pump the most important heat transfer happens in the evaporator and the condenser. Pipes and other components also experience heat loss to the surroundings, but this is often neglected.

The heat transfer in a heat exchanger is often assumed to be proportional to the mean temperature difference over the heat exchanger. But due to the non-linear behaviour of heat transfer, the *Logarithmic mean temperature difference* (LMTD) has to be used instead of the arithmetic mean temperature difference. The definition of LMTD vary with flow direction in the heat exchanger. For counter-flow heat exchangers Equation 2.7 and 2.8a has to be used, for parallel-flow heat exchangers Equation 2.7 and 2.8b is correct. Figure 2.3 show a general fluid temperature distribution of the two mentioned types of heat exchangers. The heat transfer properties vary with, fluid-type, fluid-velocity, fluid-state and many other factors it is therefore difficult to determine exactly. In general heat transfer coefficients for gases are in the range 50-100 $W/m^2K$. Whereas liquid heat transfer coefficients are usually significantly higher, in the range of 2000-5000 $W/m^2K$ [19].

$$LMTD = \frac{\Delta T_1 - \Delta T_2}{ln(\frac{\Delta T_1}{\Delta T_2})} \tag{2.7}$$

$$\Delta T_{1,CF} = T_{h,i} - T_{c,o}$$
$$\Delta T_{2,CF} = T_{h,o} - T_{c,i} \tag{2.8a}$$

$$\Delta T_{1,PF} = T_{h,i} - T_{c,i}$$
$$\Delta T_{2,PF} = T_{h,o} - T_{c,o} \tag{2.8b}$$

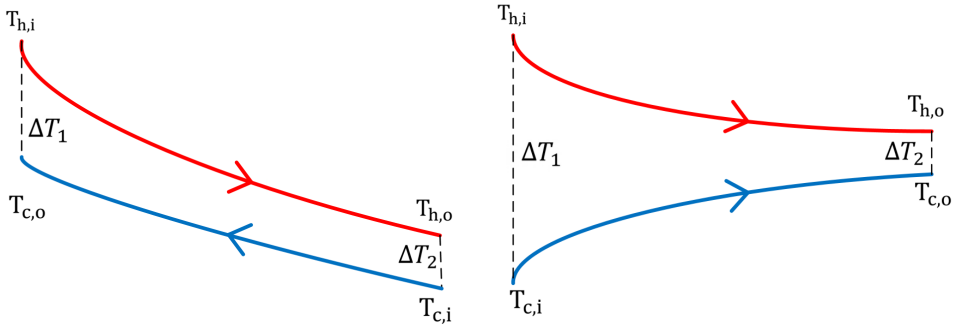


**Figure 2.3:** (a) Left: LMTD Counter-flow (b) Right: LMTD Parallel-flow

Several types of heat exchangers exist; shell-and-tube, tube-in-tube and various types of plate heat exchangers are some of the most commonly used types.

### Shell-and-tube heat exchanger

Shell-and-tube heat exchangers are very commonly used in older heat pump installations. Especially for large indirect heating and refrigeration installations with a secondary circuit. Two types of shell-and-tube heat exchangers exist, filled and dry type [20]. The filled type where the working fluid flows outside of the pipes is illustrated in Figure 2.4. Due to the design the shell-and-tube heat exchanger requires a large space and filling ratios, but relatively good heat transfer properties [20]. The heat transfer properties of the shell-and-tube heat exchanger are usually in the range 500-900$W/m^2K$ for evaporators and 600-1100 $W/m^2K$ for condensers [20].

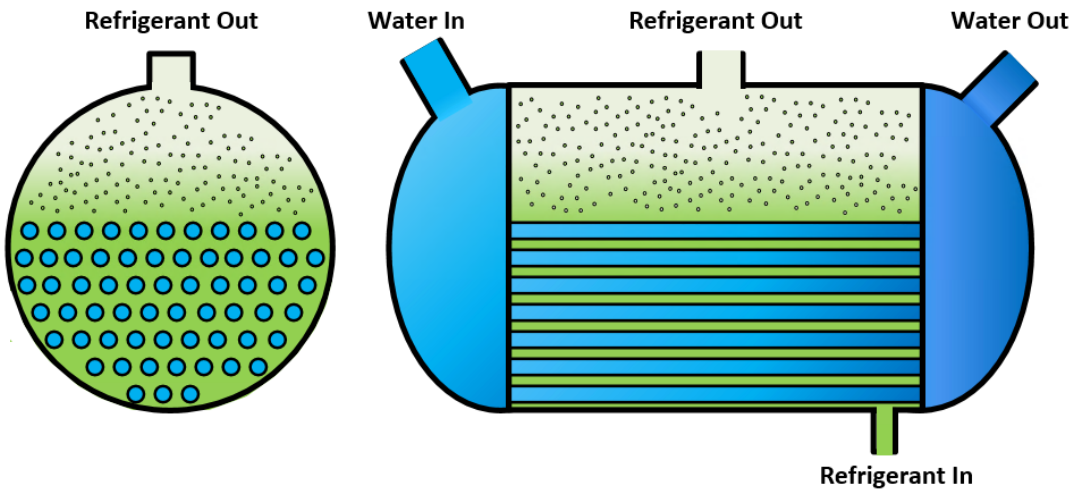


**Figure 2.4:** Sketch Shell-and-tube Heat Exchanger. Drawn with inspiration from [20].

### Plate heat exchanger

In modern installations, the plate heat exchanger is often the preferred solution. It consists of several parallel plates. The hot and cold fluid circulates in every other canal between the plates, usually in counter flow direction. The capacity of the heat exchanger is determined by the number of plates, plate size, temperature difference, choice of plate material and working fluid used. The capacity varies from a few $kW$ to several $MW$ [20]. Plate heat exchangers are compact and have very good heat transfer properties. The compactness reduces working fluid filling ratio, which is advantageous for flammable or expensive working fluids [20]. The design and flow pattern of a counter flow plate heat exchanger is illustrated in Figure 2.5.

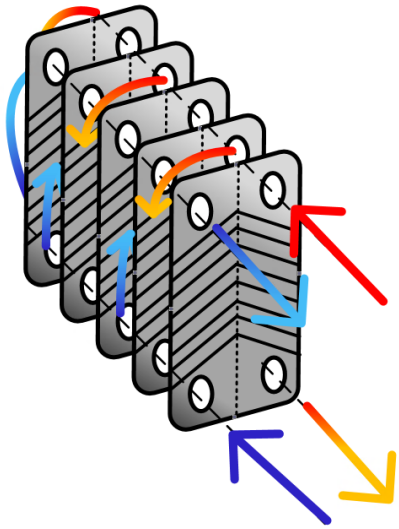

**Figure 2.5:** Sketch Plate Heat Exchanger. Drawn with inspiration from [20].

**Table 2.1:** Common heat transfer rates for different types of heat exchangers. The values are based on R-22/HFK working fluids [20].

| Common heat exchanger heat transfer rates | | | |
|---|---|---|---|
| Heat exchanger type | Evaporator | Condenser | |
| Shell-and-tube | 500-900 | 600-1100 | $[W/m^2K]$ |
| Tube-and-tube | – | 500-800 | $[W/m^2K]$ |
| Plate | 1200-1500 | $\approx 1500$ | $[W/m^2K]$ |

### 2.2.2 Compressor

The compressor is one of the key components in the CVCC heat pump, increasing the pressure from the evaporation pressure $p_E$ to the condensation pressure $p_C$. Many different types of compressors exists. Scroll-,Screw-, Turbo- and Piston-compressors are some of the most common types. It is decided that the heat pump installations at Sluppen-Tempe are going to use semi-hermetic piston compressors. The other types of compressors are therefore not further elaborated in this thesis. The basic construction of a piston compressor with its corresponding Pv-chart for an isentropic compression process can be seen in Figure 2.6.

The compression process is a non-reversible process, due to among other; heat, friction, leakage, re-expansion and valve losses. In heat pump calculations the process if often treated as isentropic, the different kinds of losses are taken into account using the isentropic- and volumetric efficiencies, $\eta_{is}$ and $\lambda$. The piston compressor has a deadspace $v_0$ over the piston at max stroke, this is to avoid the piston hitting the cylinder top and enable safe opening and closing of the suction and discharge valves. $v_0$ is often given as the charge ratio $\phi_0 = (v_0/v_{swept})$. The value of $\phi_0$ varies from 3% to 8% for medium to large compressors, and for small compressors $\phi_0$ varies from 5% to 15% [21].

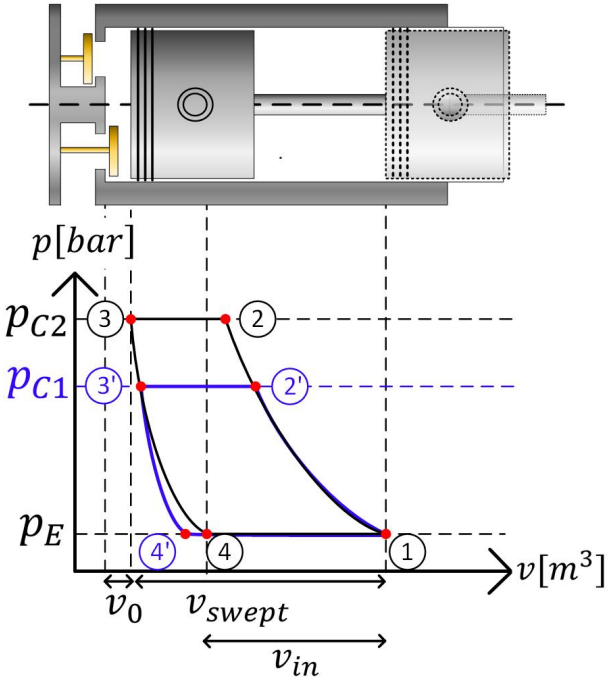


**Figure 2.6:** Pv-chart for an arbitrary piston compressor, for two different pressure ratios; $p_{C1} < p_{C2}$ Drawn with inspiration from [21].

For a piston compressor $\lambda = \eta_v \cdot \eta_d$. Where $\eta_v$ represents volumetric losses due to re-expansion of working fluid in the clearance volume. And $\eta_d$ represents other volumetric losses as; valve resistance, leakage and heat losses. The volumetric losses due to re-expansion of gasses in the clearance volume for an insentropic compression process can be calculated using Equation 2.9, where $k = C_p/C_v$ of the working fluid. In general the volumetric- and isentropic efficiencies decrease with increased pressure ratio. This is illustrated in Figure 2.6, and can be estimated with Equation 2.9-2.11, assuming constant isentropic coefficient $k$.

$$\eta_v = 1 - \phi_0[(\frac{p_C}{p_E})^{\frac{1}{k}} - 1] \tag{2.9}$$

$$\lambda_{Vol} = \frac{V_{Suction}}{V_{Svept}} = \frac{\dot{m}}{\rho_{Suction} * n * V_{Displacement}} \tag{2.10}$$

$$\eta_{is} = \frac{W_{is}}{V_{W_{Compressor}}} = \frac{\dot{m}(h_{isDischarge} - h_{suction})}{W_Compressor} \tag{2.11}$$

## 2.3 Working Fluids

### 2.3.1 Choice of Working Fluid

There are several factors impacting the choice of working fluid, some are related to the cycle itself, other pure practical. Some of these factors are the thermo-physical properties of the working fluid, price and availability. In the early stages of heat pump development these were the most important factors to consider. The working fluids commonly used during the early stages of heat pumps were flammable. As a result of the desire to develop safe non-flammable working fluids, chlorofluorocarbons (CFCs) and eventually hydrochlorofluorocarbons (HCFCs) were developed. Due to their superior thermo-physical properties combined with low price and good availability the CFCs and HCFCs often were the preferred choice of working fluid. Initially they were thought to do no harm to the environment, unfortunately this turned out to be wrong. In fact the CFCs and HCFCs are harmful to the ozone layer. The chemicals harmfulness to the ozone layer is measured by the ozone depletion potential (ODP). The production and use of chemicals harmful to the ozone layer is regulated by the Montreal Protocol of 1987 [22]. Which aimed to phase out CFCs by 1996 and HCFCs by 2030. Hydrofluorocarbons (HFCs) were introduced to replace the high ODP CFCs and HCFCs because of their harmfulness to the ozone layer.

As a replacement to the high ODP CFCs and HCFCs, HFCs were developed. The HFCs do not degrade the ozone layer, but are still harmful to the environment, due to their contribution to global warming. The working fluids impact on global warming is measured by the global warming potential (GWP) of the substance. The Kyoto Protocol of 1997, the F-gas directive of 2006 and the Kigali amendment to the Montreal Protocol of 2016 regulates the use of working fluids with high GWP [23],[24], [22].

Hydrofluoroolefins (HFOs) are the latest addition to synthetic working fluids. The HFOs are unsaturated molecules of hydrogen, fluorine and carbon and show promising potential with zero ODP and very low GWP. HFOs have a lower GWP compared to HFCs due to a short atmospheric life time [25]. There are however concerns related to the decomposion of HFOs in the atmosphere. One of the most frequently used HFOs, R1234yf decomposes in the atmosphere forming trifluoroacetic acid (TFA) and hydrogen fluoride (HF) [25],[26]. To evaluate the potential long term health- or environmental impact of TFA and HF further studies should be performed.

#### R134a

One commonly used refrigerant in existing heat pump and refrigeration systems today are R134a, this is also one of the refrigerants used in the existing chillers at SLV10. The refrigerant was initially developed as a replacement for R12 a CFC [20]. R134a was believed to be a good replacement due to the zero ODP. According to NS-EN 378 Part 1 [27] the refrigerant is classified under the A1 safety classification, thus non-flammable and non-poisonous. One of the main disadvantages of R134a is the high GWP value of 1430 [27] ,it is therefore restricted by the F-gas regulation and leakage preventing measures are important.

#### R410A

R410A is a zeotrop 50%/50% blend of the HFCs R125 and R32 [20]. As R134a is has the safety classification A1, and thus have similar non-flammable and non-poisonous properties. It also have 0 ODP and 2088 GWP [27]. It is a common refrigerant in existing chiller installations and is used in 3 out of the 4 existing chiller installations at SLV10. R410A is a undesirable choice of refrigerant in new installations due to the high GWP.

### 2.3.2 Natural Working fluids

Natural working fluids, are as the name indicates, a class of working fluids naturally occurring in nature. Among these are: Water (R718), Ammonia (R717), $CO_2$ (R744) and the hydrocarbons (HC). The thermal properties and impact on health and environment of this class of working fluids have been thoroughly investigated and studied. They have zero ODP and low GWP compared to the HFCs. Ammonia is highly toxic and the HCs are highly flammable, impacting the safety and operation. Key parameters of some natural refrigerants are shown in Table 2.2.

**Table 2.2:** Key properties of working fluids commonly used in heat pumps. [28].

| ASHRAE number | IUPAC name | ODP | GWP | Molarmass (g mol$^{-1}$) | Normal boiling point (°C) | Critical Temperature (°C) | Critical Pressure (bar) |
|---|---|---|---|---|---|---|---|
| R290 | Propane | 0 | 3.3 | 44.1 | -42.1 | 96.7 | 42.48 |
| R600 | Butane | 0 | 4.0 | 58.1 | 0.0 | 152.0 | 37.96 |
| R600a | IsoButane | 0 | 3.0 | 58.1 | -11.7 | 134.7 | 36.40 |
| R601 | Pentane | 0 | 4.0 | 72.1 | 36.1 | 196.6 | 33.58 |
| R601a | Isopentane | 0 | 4.0 | 72.1 | 27.7 | 187.8 | 33.78 |
| R717 | Ammonia | 0 | 0.0 | 17.0 | -33.3 | 132.4 | 112.80 |
| R718 | Water | 0 | 0.2 | 18.0 | 100.0 | 373.9 | 220.60 |
| R744 | $CO_2$ | 0 | 1.0 | 44.0 | -78.0 | 31.0 | 73.80 |

### Water $H_2O$

Water has several advantageous properties which makes it a suitable choice of working fluid for some heat pump applications. It has a high enthalpy of evaporation, good heat transfer properties, such as a high isobaric specific heat capacity ($C_P$) of ($\approx 4.2[kJ/kgK]$)[29]. Water is also cheap, easily available and environmentally friendly with zero ODP and low GWP. Water is less suitable for low temperature levels due to a high specific volume and low pressure evaporation under atmospheric pressure, which limits its use in vapor compression heat pumps (VCHP)[29]. Water/Steam has the potential of especially high temperature heat delivery levels up to 200 $°C$, through a mechanical vapor recompression process [30]. This is possible by utilization of oil-free steam compressors, removing the lubrication problems of classic high temperature compressors.

### Carbon dioxide $CO_2$

$CO_2$ is a well suited working fluid for many heat pump and refrigeration applications due to the good thermophysical properties, low GWP (GWP=1) and zero ODP. $CO_2$ heat pumps have low pressure ratios $\pi$ increasing compressor efficiencies and good heat transfer properties. $CO_2$ has a low critical temperature and high critical pressure of 31.1 $°C$ and 73.8 $bar$ [20]. Heat pump installations using $CO_2$ as a working fluid therefore often operate in a trans-critical process at high pressures. In a trans-critical process the condenser is replaced with a gas-cooler. The high pressure level has both advantages and disadvantages. Among the advantages are: high energy density and volumetric heating capacity (VHC) resulting in small component sizes. The VHC of $CO_2$ increases with increased sub-cooling, system performance of $CO_2$ heat pumps are therefore low for high heat sink inlet temperatures (HSiIT). $CO_2$ is especially suitable as a working fluid for heat pumps with a stable heat source temperature and large temperature glide at the heat sink, like for instance domestic hot water heat pumps [20].

### Hydrocarbons $C_nH_m$

Hydrocarbons have been used as working fluids in heat pump and refrigeration cycles since the early developments in heat pump technology due to their good thermophysical properties. Hydrocarbons have favorable heat transfer properties resulting in efficient heat exchange [30]. They are however highly flammable, thus in the A3 safety rating classification. For many years hydrocarbons were not considered suitable working fluids due to the problems with flammability. In the recent years hydrocarbons are once again considered a good choice of working fluid due to their good environmental properties, with zero ODP and low GWP. To cope with the flammability issue safety routines and measures are needed. Due to the problems with flammability, hydrocarbons are mostly used in small installations with limited working fluid charge. If existing standards and regulations are followed the working fluid charge can be increased to achieve desired capacities [25].

#### Propane R290

Propane (R290, $C_3H_8$) is a common hydrocarbon used as working fluid in heat pumps and refrigeration units today. It has a low GWP of 3 and good thermal properties[27]. It is highly flammable with a lower flammability level (LFL) of 2.1 $vol\%$ [31] and is classified as A3 safety rating according to the european standard NS-EN 378 [27],[32],[33],[34]. Compared to R134a Propane has almost double the heat of evaporation [35] resulting in lower working fluid charges. Unlike ammonia Propane has no limitations regarding choice of component materials and is comparable to R22/R505 [31]. This makes Propane a good choice as a replacement working fluids for existing HFK installations. At low oil temperatures and high suction gas temperatures problems with the solubility of Propane in oil can occur. This can cause problems with lubrication and compressor malfunction. It is therefore for high evaporation temperatures important to choose an oil with high viscosity index [31]. When using Propane as a working fluid the gas might condense in the compressor, to avoid this it is important to have sufficient $\Delta T_{Superheat}$, use an oil heater and place the compressor in a heated room [31].

#### Butane R600

Butane (R600, $C_4H_10$) has similar characteristics as Propane, both advantages and disadvantages. It has the same safety classification A3 according to NS-EN 378 [27],[32],[33], [34]. It is non toxic and with a GWP of 4 and zero ODP, thus health-vise and environmentally friendly[27]. In high temperature applications Butane can be used instead of Propane due to the higher critical temperature 152$°C$ compared to 96.7$°C$. R600 has a high VHC compared to for instance R601 [36]. It is also thermodynamically closer to R290, existing R290 compressors can therefore be used for R600 with minor modifications [36]. Prototype heat pumps with R600 as a working fluid, capable of HSiOT above 100$°C$ exist [37].

## 2.4 Industrial Heat Pump Configurations

This section describes industrial modifications and improvements to the simple CVCC, with a main focus on high temperature applications.

### 2.4.1 Internal Heat Exchanger (IHX)

The internal heat exchanger (IHX) transfers heat from the working fluid leaving the condenser to the working fluid leaving the evaporator. This sub-cooles the condensed fluid and super-heats the evaporated fluid. Increased sub-cooling increases volumetric heating capacity (VHC), resulting in reduced working fluid mass flow $\dot{m}_R$ and thus reduced compression work. The IHX also assures sufficient superheat of the suction gas, avoiding problems with compression of liquid working fluid in the compressor. The IHX thus increases system performance and COP [31]. The IHX also increases the discharge gas temperature.

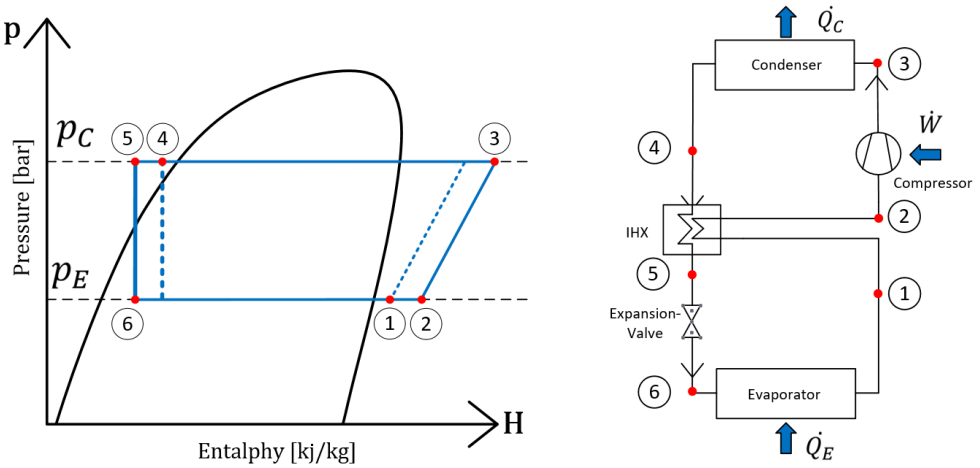


**Figure 2.7:** (a) Left: pH-Chart IHX Example (b) Right: Example IHX System sketch

### 2.4.2 Multi stage heat pumps

For high temperature lifts and correspondingly high pressure ratios $\pi$ result in increased compression work and high discharge temperatures on the high pressure side of the compressor. High discharge temperatures can lead to the dissolution of oil/working fluid and lubrication problems [20]. This increases mechanical wear and tear especially in the compressor, lowering the lifetime of the system and might result in break down. Isentropic efficiency and system performance also decreases with increasing pressure ratio $\pi$ due to increased compressor and expansion losses [20]. This can be improved by dividing the process into separate steps, the most usual methods of improving the system performance are: Inter-cooling, economizer, cascade heat pump, subcooling and internal heat exchanger. These advanced configurations increase system performance, but also investment costs. For heat pump cycles with two stage compression and expansion the intermediate pressure is often defined by Equation 2.12, this method of determining the intermediate pressure also reduces the discharge temperature of the high pressure compressor [38].

$$p_m = \sqrt{p_E \cdot p_C}[38] \tag{2.12}$$

#### Inter-cooling

Inter-cooling is a method of improving system performance by using a two-step compression and expansion. The system consists of a intermediate pressure vessel where the discharge gas of the low-pressure compressor is fully or partially cooled down by the expanded working fluid form the condenser. The working fluid is then expanded again from the intermediate pressure to evaporation pressure. This has several advantages: Decreasing compression losses due to a smaller compression ratio for the compressors, lower expansion losses due to two expansion steps and lower discharge temperature of the working fluid [20]. There exists two types of inter-cooling, full and partial, depending on if the discharge gas from the first compressor stage is cooled fully or partially to saturation. The system sketch and pH-diagram of a fully inter-cooled heat pump can be seen in Figure 2.8.

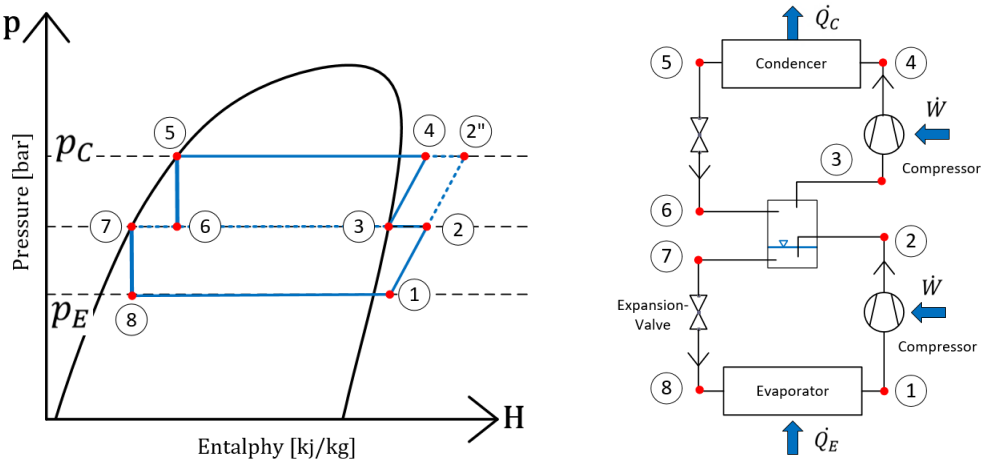


**Figure 2.8:** (a) Left: pH-Chart Inter-cooling Example (b) Right: Example Inter-cooling System sketch

### Economizer

The economizer solution is a two step expansion and one step compression cycle. A portion of the working fluid, after the high pressure expansion-valve is re-compressed from an intermediate pressure, the remaining working fluid is further expanded in the low pressure expansion-valve to the evaporation pressure. This reduces expansion losses, the discharge temperature from the compressor and the compressor work decreases as well. For screw compressors this is often the preferred solution [20]. System sketch and a pH-chart for an arbitrary economizer solution is shown in Figure 2.9.

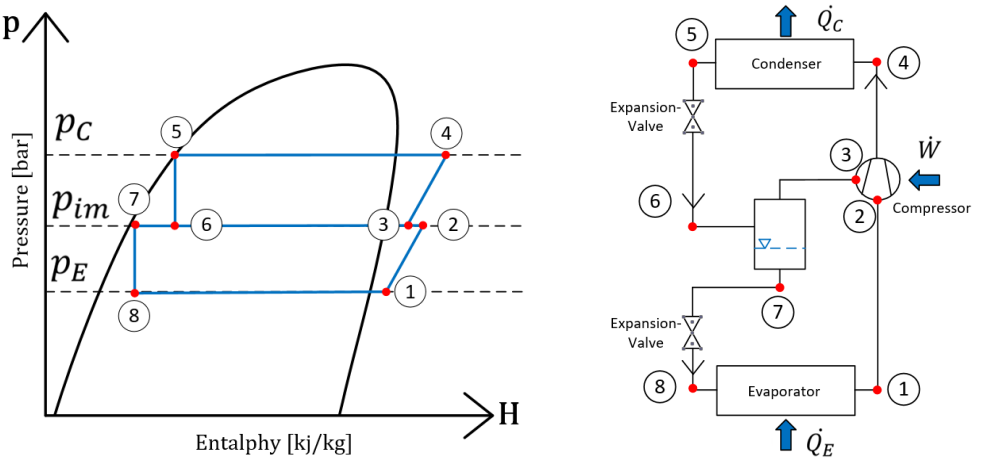


**Figure 2.9:** (a) Left: pH-Chart Economizer Example (b) Right: Example Economizer System sketch

### Cascade Heat Pump

Cascade heat pumps consist of two or more separate working fluid cycles, Figure 2.10 show an arbitrary cascade heat pump with two cycles. The two cycles are here after mentioned as: the low temperature cycle (LTC) and high temperature cycle (HTC), based on their respective evaporation and condensation temperatures. The two cycles are connected through an cascade heat exchanger which acts as the condenser of the LTC and the evaporator of the HTC. The cascade system has the same advantages due to multiple stages of compression and expansion as mention in for inter-cooling and the economizer. The physical separation into two cycles makes it possible to use two different working fluids thus optimizing the thermophysical performance of the working fluid for the intended temperature range. In order to transfer heat in the cascade heat exchanger the condensation temperature of the LTC has to be 2-3 K higher than the evaporation temperature of the HTC [39], increasing temperature lift and compression work which is detrimental to system performance. The advantage of a more suitable working fluid therefore has to be evaluated against the disadvantages of losses in the cascade heat exchanger.

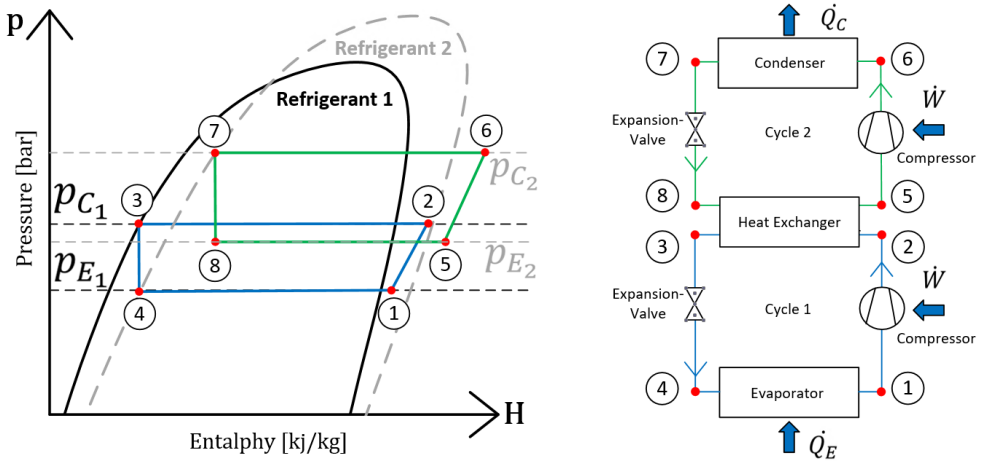


**Figure 2.10:** (a) Left: pH-Chart Cascade Example (b) Right: Example Cascade System sketch

### 2.4.3 Trans-critical CVCC

The low critical point of working fluids like $CO_2$, results in a trans-critical CVCC for heat pump applications. The process is characterised by evaporation at constant temperature below critical point,like ordinary CVCC. Heat delivery however happens above critical point at a gliding temperature range. The gas does therefore not condensate and the condenser has to be replaced with a gas-cooler. The low critical temperature of $Co_2$ result in a lower theoretical COP than traditional CVCC, but practical advantages as high compressor efficiency, low pressure losses and good heat transfer properties makes trans-critical $CO_2$ Heat pumps perform at least as good as traditional CVCC [20]. Trans-critical $CO_2$ heat pumps are well suited with stable temperature heat sources and large temperature glide on the heat sink, like for instance DHW production [20]. An example of a trans-critical CVCC drawn into the pH- and Ts-diagrams is illustrated in Figure 2.11 below.

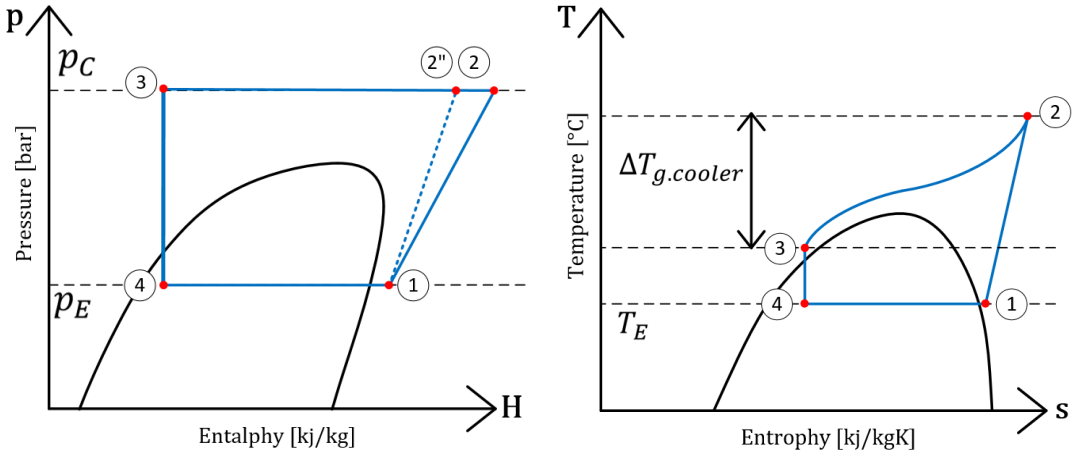


**Figure 2.11:** (a) Left: Trans-critical pH-Chart Example (b) Right: Trans-critical Ts-Chart Example

### Optimal Gas Cooler Pressure

As previously mentioned trans-critical heat pumps does not have a constant condensation temperature, but the gas gradually densifes over a temperature range in the gas cooler. Like conventional CVCC heat pumps heat rejection occurs at a constant pressure. Figure 2.12 shows the pH-diagram of an trans critical $CO_2$ Heat pump with variable gas cooler pressure from 80 to 110 bar. The diagram was made using the program engineering equations solver (EES), by assuming a -10°C evaporation temperature, 0.7 isentropic and volumetric compressor efficiency and 45 °C $CO_2$ leaving the gas cooler. As seen from the figure, the flat shape of the isobars of $CO_2$ close to the critical point lead to a large difference in gas cooler leaving $CO_2$ enthalpy for relatively small changes of gas cooler pressure. This increases both volumetric cooing and heating capacity, resulting in a reduced mass flow through the compressor and thus reduced compression work. As the gas cooler pressure increase the state point of $CO_2$ leaving the gas cooler moves to the left of the critical point, where $dh/dp$ is smaller resulting in a smaller impact of increased pressure on the leaving gas cooler enthalpy. An increased gas cooler pressure also increases the LMTD of the gas cooler, moving the pinch point towards the low temperature side of the gas cooler.

Increased gas cooler pressure leads to an increase in discharge gas enthalpy and temperature, resulting in an increased compression work( Equation 2.1 ). Also as previously mentioned, increased compression ratio in general reduces both volumetric and isentropic efficiency of compressors, resulting in additional increase of compression work. Due to this there exists an optimal gas cooler pressure for all trans-critical heat pump cycles, where effect of increased volumetric heating and cooling capacities are counteracted by increased compression work.

Chen [40] have done an investigation of optimum gas cooler pressure of a trans-critical heat pump cycle through a pinch point analysis. As a result Chen [40] derived a equation estimating the optimum gas cooler pressure given by the; inlet and outlet heat sink water temperature, evaporation temperature and minimum temperature difference in the heat exchanger. According to Chen [40], the optimum gas cooler pressure can be estimated using Equation 2.13

$$P_{Opt} = 1.7691 + 8.146 \cdot 10^{-2} \cdot T_{W.In} - 3.713 \cdot 10^{-3} \cdot T_{W.In}^2 + 7.039 \cdot 10^{-5} \cdot T_{W.In}^3 + 0.1915 \cdot T_{W.Out} \\ -2.110 \cdot 10^{-3} \cdot T_{W.Out}^2 + 1.134 \cdot 10^{-5} \cdot T_{W.Out}^3 + 0.631 \Delta T_{min} - 0.153 \Delta T_{min}^2 + 1.013 \cdot 10^{-2} \cdot \Delta T_{min}^3 \\ +3.419 \cdot 10^{-2} \cdot T_E - 1,876 \cdot 10^{-4} * T_E^2 + 1.440 \cdot 10^{-5} \cdot T_E^3 \quad [40] \tag{2.13}$$

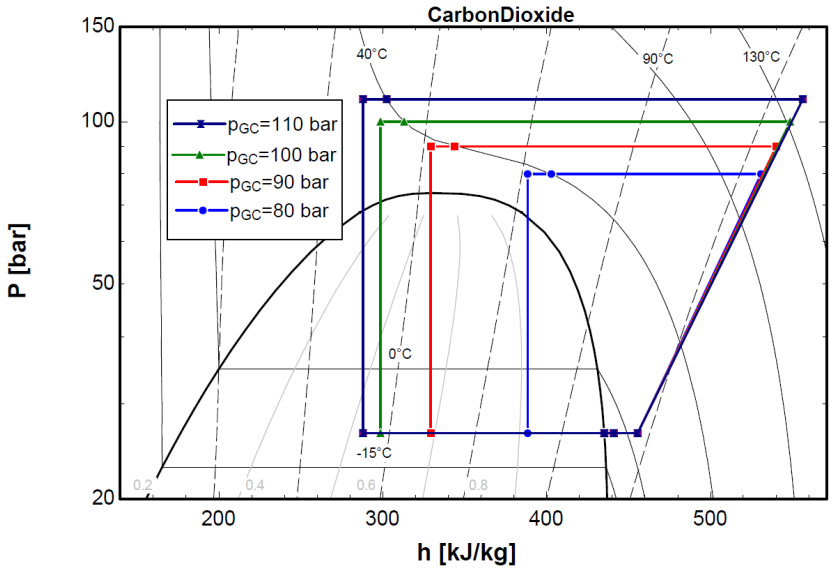


**Figure 2.12**

## 2.5 Hot Water Production

### 2.5.1 General

Production of domestic hot water is in Norway traditionally done with electricity and pre-heated thermally stratified hot water tanks [41]. The hot water tanks are usually made out of stainless steel and made to withstand high pressures caused by expansion of water at increasing temperatures. For large buildings several hot water tanks are usually connected together either in series or parallel. The main focus of this thesis is waste heat recovery, the detailed description of the domestic hot water system within the buildings is therefore not further described.

One important topic to consider when producing tap water is sufficient water temperature to avoid growth of legionella. Legionella pneumophila is a bacteria naturally occurring in water, when growth to high concentrations the bacteria is harmful to human health, causing legionaries decease. The bacteria thrives in the biofilm of bacteria, algae and other microorganisms usually forming in water. Legionella growth occurs in water temperatures between 20-50 °C, but the optimum growth temperature is 35-37 °C [41]. The bacteria starts to inactivate and die at water temperatures above 55 °C and can only live for short periods at temperatures above 70 °C [41]. It is therefore important that the water temperature in domestic hot water systems is sufficiently high to avoid growth of legionella. According to the Norwegian building code TEK17 circulating hot water should keep a minimum of 65 °C to avoid growth of legionella [42].

### 2.5.2 Breweries

The brewery process and beer production in particular is very intensive in both energy and water consumption [43]. Thermal energy and water among other used for; the brewing process itself, pasteurization of finished product, sanitation water and cleaning water.

**Energy Usage in Breweries**

A literature study have been performed in order to investigate the energy consumption of the brewery process. Kubule, Zogla, Ikaunieks and Rosa [44] investigated the possible energy efficiency improvements in the brewing industry by analyzing a small brewery in Latvia. The brewery had an annual production of 15 000 - 17 000 hl of beer and the study found a annual specific thermal energy consumption of 219.2 to 231.3 MJ/hl in the period of 2011 to 2013. This is however inclusive thermal energy consumption for space heating.

Muster-Slawitsch, Weiss, Schnitzer and Brunner [45] investigated the potential for reducing thermal energy consumption in breweries by investigating small and medium sized Austrian breweries. They found a specific thermal energy demand of 43.6 and 104,5 MJ/hl for the small and medium sized brewery, excluding energy consumption for space heating. Of this was around 26-54 MJ/hl used for wort boiling. The studied breweries had an annual production of 20 000-50 000 and 800 000 hl/year [45].

Table 2.3 below shows an overview of several studies investigating the energy consumption of breweries, including the two studies described above. The specific thermal energy consumption found in the varies significantly from 43.6 MJ/hl to 231.3 MJ/hl. Where in general smaller breweries have a larger specific energy consumption than larger breweries. Some of the studies also have included space heating demand others not.

**Table 2.3:** Literature overview: Energy consumption of beer production.

| Source | Brewery Size | Production | Thermal Energy Consumption | Electricity Consumption |
|---|---|---|---|---|
| Kubule 2016 [44] | Small Size | 15 000 - 17000 hl/y | 219.2-231.3 [a] MJ/hl | 81-92 MJ/hl |
| Muster-Slawitsch 2011 [45] | Small Size | 20 000 - 50 000 hl/y | 104.5 [b] MJ/hl | - |
| Muster-Slawitsch 2011 [45] | Medium Size | 800 000 hl/y | 43.6 [b] MJ/hl | - |
| EU Commission 2019 [46] | All Sizes | 20 000 -500 000 hl/y | 87-121 [c] MJ/hl | - |
| Sturm 2013 [47] | Medium Size | 250 000 hl/y | 160-180 [a] MJ/hl | 45-60 |
| Brewing Association [48] | - | - | 70 % of total [a] | - |
| Canadian Brewing Industry [43] | All Sizes | <100 000 to >500 000 | 150 [c] MJ/hl | 8-12 kWh/hl |
| Campden BRI [49] | Large breweries | > 500000 hl/y | 141-207 [d] MJ/hl | |

[a] Inclusive space heating, [b] Exclusive space heating, [c] Not specified, [d] Total energy consumption.

### Water Consumption in Breweries

As previously mentioned the brewery of beer has a high water consumption, both in the process itself as well as; cleaning of products, used equipment, pasteurization and cooling water [46]. According to "Best Available Techniques (BAT) Reference Document for the Food, Drink and Milk Industries. Industrial Emissions Directive 2010/75/EU (Integrated Pollution Prevention and Control)" [46] is the reported specific water consumption of several EU breweries often below 0.6 $m^3/hl$ of beer. Campden BRI a part of Bristol University in the UK [49], have in collaboration with the brewing industry performed a global study of energy and water consumption in 225 breweries world wide [50]. The study concluded that the average water consumption had dropped by 17% from 5.2 hl/hl in 2008 to 4.3 hl/hl in 2012.

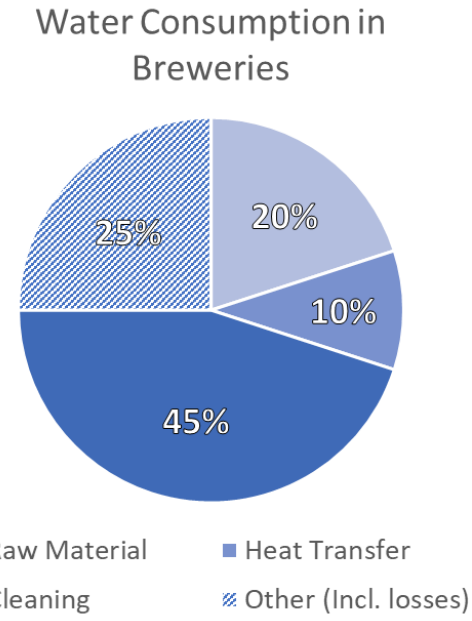


**Figure 2.13:** Distribution of water consumption i breweries [43].

Few studies have investigated the distribution of water within the brewery, but according to the Canadian Industry Program for Energy Conservation report "Guide to energy efficiency opportunities in the Canadian brewing industry" [43] is; 20% of water used as raw material in product, 10% For heat transfer, 45% fro cleaning and 25% Other applications including losses. This is illustrated in Figure 2.13.

## 2.6 High Temperature Heat Pumps Literature review

### 2.6.1 Status and overview of technologies

The temperature level of high temperature heat pumps (HTHP) is not consistently defined in literature. In this paper it is therefore decided to use Arpagaus' definition of HTHP, which is heat pumps capable of heat sink outlet temperatures (HSiOT) above 100°$C$ [51]. Arpagaus performed a thorough market overview, reviewing current research and technology status of HTHPs capable of HSiOT of 90-160°$C$. Among the most important findings of the study are; There is a large potential for waste heat recovery from industry in Europe. Over 20 HTHPs from 13 manufacturers are capable of HSiOT above 90°$C$, but few are able to deliver HSiOTs over 120 °$C$. Arpagaus also concludes that some important barriers to development in HTHP technology are; Long pay back periods, usually above 3 years. Limited availability of low GWP working fluids and few pilot and demonstration heat pumps. HTHPs exist in a wide area of installed capacity, ranging from a few $kW$ to several $MW$ [51]. Different HTHP technologies exist, for instance Jensen [52] studied the development of ammonia-water hybrid absorption-compression heat pump and Bamigbetan [53] has developed a prototype vapor-compression HTHP using a two-cascade system with Propane (R290) and Butane (R600) as working fluids. Consistent with the goals of +CityXChange and to aid further developments in HTHPs with natural working fluids, this study will focus on high temperature vapor-compression heat pumps with natural working fluids.

### 2.6.2 Working fluids for high temperature heat pumps

Several studies have evaluated the thermo-physical properties and suitability of different working fluids for high temperature heat pumps. Frate, Ferrari and Desideri analysed the suitability of high temperature heat pump working fluids [54]. For HTHP applications the critical temperature has to be sufficiently higher than the heat sink temperature, this limits the number of suitable working fluids.

Frate, Ferrari & Desideri analyzed suitable working fluids with a critical temperature $T_{Crit}$ above 125°$C$ and saturation pressure above 0.05 bar at 40°$C$ [54]. The working fluids were tested for different operating ranges from 50°$C$ HSoIT and up to 150°$C$ HSiOT, concluding that some hydrocarbons especially cyclo-pentane and iso-pentane are suitable for high temperature heat pumps achieving a high COP [54]. The study concludes that there are challenges related to the high flammability of hydrocarbons and proposes R1336mzz(Z) and R1234ze(Z) as viable alternatives. Frate, Ferrari & Desideri importantly concludes that working fluids with moderately reduced COP can be the preferred choice due to the advantages high volumetric heating capacity (VHC). High VHC reduces compressor size and costs. R1233zd(E) is proposed as a good compromise between high VHC and COP at HSiOT above 140°$C$ [54]. In their study Frate, Ferrari & Desideri didn't consider the potential health and environmental consequences of atmospheric decomposition of HFOs pointed out by Hafner [25].

The researchers at SINTEF Energy Research and NTNU have focused on improving energy efficiency through high temperature heat pumps utilizing natural working fluids. Nekså, Bantle, Schlemminger and Bamigbetan [30] describes the research and technology development in HTHPs utilizing ammonia, water and hydrocarbons as working fluid. Nekså, Bantle, Schlemminger and Bamigbetan also mentions ammonia-water mixture as a viable HTHP option, in a Osenbrück cycle. This has the advantage of achieving high temperatures with much lower operating pressures compared to using pure ammonia in a VCHP [30].

Of the low GWP hydrocarbons, Butane, Pentane and their respective isomers is well suited for high temperature delivery due to their high critical temperature. Bamigbetan, Eikevik, Nekså, Bantle and Schlemminger performed a theoretical analysis of suitable working fluids for high temperature heat delivery [36]. They found that R601 and R601a is capable of delivering a maximum heat sink outlet temperature (HSiOT) of 134 °C and for R600 and R600a the maximum HSiOT was 128 °C. According to Bamigbetan, Eikevik, Nekså, Bantle and Schlemminger R601 achieved the highest simulated COP, however the suction temperature is more restricted for R601 and R601a compared to R600 and R600a. The low volumetric heating capacity of R601 results in a 2-3 times larger compressor size compared to R600. This is likely to increase investment costs. R600 also has the advantage of a broader operating range and is thermodynamically closer to R290 [36]. There exists commercially available compressor technology for R290 which can be used with R600 with small modifications. The optimum working fluid is therefore dependent on the intended project and if maximum COP, cost or operating range is the main decision criteria.

### 2.6.3 High temperature heat pumps with natural working fluids

Verdink, Rieberer and Mosi have developed a theoretical model of a trans-critical single cycle R600 heat pump using Modelica and the TIL thermal component library [55]. At 80/75$°C$ HSoIT/HSoOT and 100/170 HSiIT/HSiOT a COP of 2.64 was achieved [55]. Using a IHX and 20 K superheat the COP increased to 2.77 [55]. Another advantage of the IHX was decreased high side pressure, from 47 to 43 bar [55]. The model was validated against a test rig developed by Mosi. The test rig has a condensation capacity of 45 $kW$ at a HSoIT/HSoOT of 70/65$°C$ and a HSiIT/HSiOT of 80/110$°C$ [55]. The developed theoretical model predicted CDTs of 5-10 K higher than HSiOT [55].

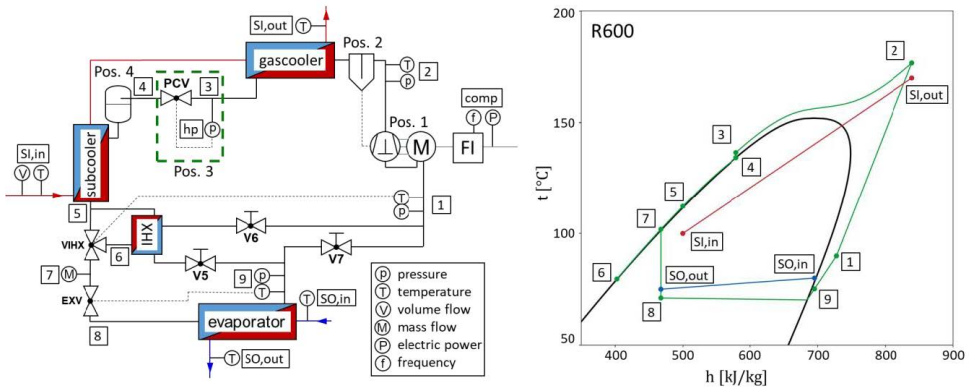


**Figure 2.14:** Schematic and Th-chart of model developed by Verdink, Rieberer and Mosi [55].

Wemmers, van Haasteren, Kremers and van der Kamp developed a 160 $kW$ R600 pilot heat pump capable of producing hot process water and steam at 0.5-2.4 $bar$ [56]. The heat pump is a single cycle R600 heat pump utilizing waste heat in moist air from paper production at a temperature of 60°$C$. A $COP_{steam}$ in the range of 3.7-2.0 was achieved with steam pressures of 0.5-2.4 $bar$ respectively. The combined $COP_{steam+hotwater}$ achieved was 5.1-4.4 under the same steam pressures [56]. The temperature difference over the heat exchangers was lower than the 5$K$ assumed, similar for the isentropic efficiency of the R600 compressor was 0.8 instead of the assumption of 0.85 [56].

As previously mentioned, Bamigbetan has in collaboration with SINTEF Energy Research, developed a 20 kW prototype cascade heat pump using Propane (R290) and Butane (R600) as working fluids [53]. The heat pump is capable of waste heat recovery at 30°$C$ and HSiOT of 115°$C$. For temperature lifts of 58-72 and 98-101 $K$ the average heating COPs was found to be 3.1 and 2.1 respectively [53]. The heat pump is also tested with a evaporation temperature of -1°$C$ to +1°$C$ and 113°$C$ to 118°$C$ condensation temperature, delivering chilled ice-water at 4°$C$ and hot water at 85°$C$ to 116°$C$ [37]. The combined heating and cooling COP achieved was 2.6-2.8 [37].

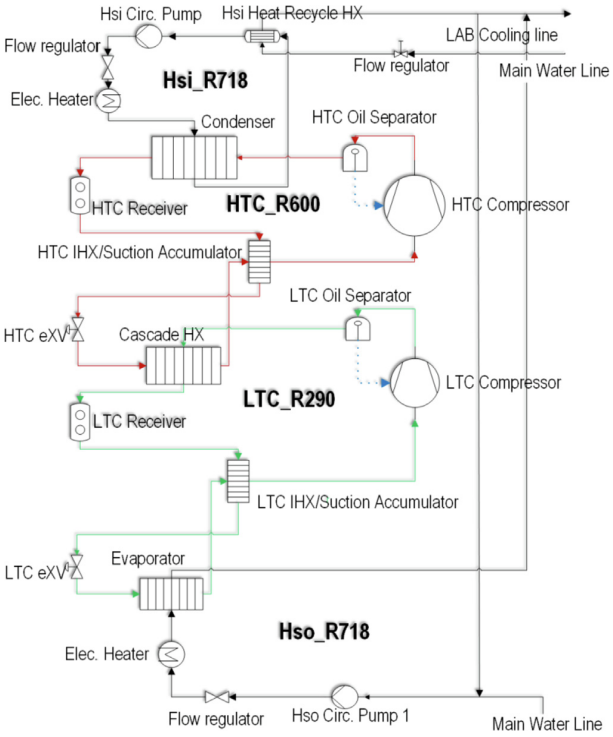


**Figure 2.15:** Schematics of cascade heat pump developed by Bamigbetan [53].

Often the maximum HSiOT is not restricted by $T_{Crit}$, but by the maximum compressor discharge temperature (CDT) or maximum compressor suction temperature (CST), given by the available compressor technology. For hydrocarbons the maximum CDT is 140°$C$ and the highest CST is 80°$C$ [36]. No commercially available hydrocarbon compressors are able to handle these temperature conditions, Bamigbetan therefore developed a prototype R600 semi-hermetic piston compressor [57]. The compressor is a modified R290 compressor with 4 cylinders manufactured by Mario Dorin S.p.A., with a displacement of 48.82 $m^3/h$ and a rated maximum operating pressure of 31 $bar$ [53], [57]. The maximum operating pressure was under 22 bar significantly lower than the maximum rated pressure [53]. The HTC prototype R600 compressor achieved an average isentropic efficiency of 84%, average total compressor efficiency of 74% and an average volumetric efficiency of 82% [53]. The average isentropic, total and volumetric efficiency of the LTC was 65%, 60% and 74% [53].

### 2.6.4 Heat pumps for waste heat recovery

Energy demanding industries such as: food, chemical and paper industries require heat up to 150°$C$ for drying, evaporating and distilling processes [58]. Kosmadakis analyzed the potential for waste heat recovery using high-temperature heat pumps in EU-industries [58]. Concluding that high-temperature industrial heat pumps have the potential of 28.37 $TWh/year$ heat recovery, equivalent to $\approx 15\%$ of the total heat consumption in the range 100-200°$C$ of EU-industries [58].

#### Heat recovery from data centers (DC)

The IT-companies and especially data centers (DC) are very energy demanding and it has been estimated that DCs accounted for 1.1-1.5% of the worlds electricity use in 2010 [59]. The electricity consumption of DCs mostly converts to heat, studies have shown that 97% of the electricity consumption can be captured as waste heat [60]. The waste heat is rarely utilized even though several technical solutions exist [61]. One of the possible solutions for utilizing waste heat from DCs is with HTHPs. In his Master's thesis Stenberg simulated DC waste heat recovery by means of HP delivering 75°$C$ water to the DH grid in Helsinki, Finland [62]. Concluding that waste heat recovery by HP to the DH grid is profitable in this case was profitable compared to free cooling and the estimated pay back time heat recovery/cooling equipment was less than 2 years. The profitability of waste heat recovery systems depend of the selling price to the DH company. From the DH company's point of view this has to be less than marginal production cost of the conventional heat production. The value of the recovered heat is also dependent of the quality of the heat. Heat recovered to the supply side of DH network is of more value than heat recovered to the return side because no improvement of heat quality is needed by the DH company.

## 2.7 Heating and cooling loads

Heating and cooling loads of buildings are dependent on the buildings; physical construction, use and purpose as well as the surrounding environment. This thesis focuses on waste heat recovery from a cold storage facility, this section will therefore mostly cover cooling load calculations.

For an enclosed space, an increase in thermal energy will result in an increase in sensible temperature when no phase change occurs. For a cold storage facility this means that all thermal energy added has to be removed by the refrigeration system, in order to maintain a constant air temperature. Some common sources of heat gain to a cold storage facility are; Transmission loads, Infiltration loads, Internal Loads, Product loads and refrigeration equipment related loads.

### Transmission loads

Transmission loads are heat transmission through walls, floors, ceilings and other building parts due to the temperature difference between storage room and ambient. Transmission loads can be calculated using Equation 2.14, where U is the heat transfer coefficient $[W/m^2K]$, A is the surface area and $\Delta T$ is the temperature difference between the storage and surroundings. Calculated as a sum of all building parts individually. Proper calculation of transmission loads rely on the U-value, which is dependent on building construction and insulation thickness in particular. For building parts exposed to solar radiation the solar heat gain should be included by adjusting the temperature difference.

$$\dot{Q}_t = \sum_i UA\Delta T|_i \tag{2.14}$$

### Infiltration loads

Cold storage facilities as other buildings, face heat losses through air exchanges with the ambient. Both through infiltration and ventilation. For cold storage's this is both a sensible heat gain due to the sensible temperature difference between the storage room air and ambient temperature, but also a latent heat gain caused by moist outdoor air is mixed with the dry chilled storage room air. For cold storage facilities below freezing temperature this moisture causes ice-formation on floors, walls and refrigeration evaporators, a health and safety risk for the workers and increasing energy consumption fro de-frosting of evaporators.

### Internal loads

All electrical equipment like; fans, pumps, computers, forklifts, lights ect. emit heat when used. For cold storage facilities this leads to an increased refrigeration load. An other source of heat gain are product processing, like glue melting or shrink wrapping [63] and heat gain from persons. Person related heat gain depend on; temperature levels, activity level and number of persons present.

### Product loads

The main refrigeration load contributions of products stored in refrigeration facilities are lowering the product temperature to the storage air temperature and heat generated by live products [63]. According to the ASHRAE Handbook for Refrigeration [63], heat required to lover the temperature of products can be described by Equation 2.15. Where $m$, $Cp$ and $\Delta T$ are the mass, heat capacity and temperature difference between initial product temperature and storage temperature respectively.

For freezer refrigeration facilities the latent heat of freezing also needs to be calculated. It is however important to consider that the thermophysical properties of food are complex and depend on product chemical composition and temperature, especially during phase change [63].

$$\dot{Q}_{prod} = m \cdot C_p \cdot \Delta T \tag{2.15}$$

## 2.8 Thermal energy systems

### 2.8.1 District Heating

A common thermal energy system is district heating. District heating is a network of connected pipes between buildings of a neighborhood, district or entire towns. This enables the buildings to be supplied with thermal energy from either a centralised waste incineration plant or a series of decentralized heat producing units. The development of district heating is commonly divided in 4 generations, from high temperature steam systems to low temperature water, close to ambient temperature.

The first generation district heating (1GDH), initially introduced in the US in the 1880s, used pressurized steam as a heat carrier. This technology was used in most district heating systems both in USA and Europe until the 1930s [64]. The system consists of pressurized steam pipes in concrete ducts.Today this technology is considered outdated due to the high temperature levels resulting in large heat losses and risk of steam explosions causing a safety risk.

The second generation district heating (2GDH) is some times referred to as Soviet district heating systems because it was commonly used in the former Soviet Union and USSR. The systems uses pressurized hot water as a heat carrier, often with supply temperatures $100°C$. This technology succeeded the 1GDH and was commonly used until the 1970s [64]. 2GDH typically consist of water pipes in concrete ducts and large material intensive components [64]. This technology is often used in combination with combined heat and power plants (CHP). As 1GDH, 2GDH has substantial losses and bad energy efficiency due to the high temperature levels.

The third generation district heating (3GDH) is an improved version of 2GDH with reduced water temperatures, often below $100°C$. This system was introduced in the 1970s and often known as the ”Scandinavian district heating system” [64]. This is because the system is commonly used in Scandinavian countries. 3GDH typically has prefabricated parts, buried insulated pipes and compact plate heat exchangers [64]. This is the most common DH system today and used as a replacement of 1GDH and 2GDH.

#### Low-Temperature District heating

The typical trend in district heating technology development is reduced supply temperatures and increased energy efficiency. State of the art 3GDH has a supply/return temperature of 80/40 $°C$. Future developments in district heating technology is referred to as 4GDH, a low temperature district heating system (LTDH) with supply and return temperature of 55/25 $°C$ [65]. Lower temperature levels are advantageous due to reduced heat losses and the possibility to apply flexible, less cost extensive pipe materials [64]. LTDH enables efficient implementation of heat pumps and utilization of available renewable and waste heat resources. LTDH can meet the space heating demand for both new and existing buildings with floor heating, but is not able to deliver sufficient temperature levels for domestic hot water (DHW). This is due to the increased legionella risk at water temperatures below 50 $°C$, one of the main disadvantages of LTDH [66].

However this problem can be solved with; Thermal, chemical or physical treatments. Thermal treatment involves heating the water to over 70 $°C$ for 30 minutes, which is recommended by the WHO. Chemical treatment involves adding an chemical substance killing the legionella bacteria. The most common chemical treatment is chlorine and hydrogen peroxide, but ionization with copper/silver ions is also possible [66]. As an alternative to thermal or chemical treatment, physical treatments like membrane filtration and UV-sterilization exist [66].

### 2.8.2 Thermal energy storage, TES

Thermal energy storage (TES) is the method of storing thermal energy in order to balance the time-mismatch of supply and demand or heating and cooling. In heating and ventilation of buildings and commercial refrigeration TES has several benefits as; increased energy efficiency, reduced peak loads and load shifting from high energy cost periods to low cost periods. Typically TES is divided into categories dependent on how the thermal energy is stored and for how long. Thermal energy can be stored as sensible or latent heat, utilizing the thermal energy of temperature change and latent heat of phase change. The size and capacity of the TES is dependent on operation strategy and for how long periods of time the energy is to be stored. Both sensible and latent TES can be stored for either long or short periods of time. Short term TES is TES for periods of hours to several days, while for long term TES the energy can be stored in periods of up to several months.

#### Sensible Heat TES

Sensible heat storage is achieved by charging or discharging the thermal energy of a liquid or a solid through changing the substances temperature. The most typical form of sensible heat storage is water as in domestic hot water tanks and concrete for thermal energy storage in building constructions. A mediums thermal storage abilities is dependent on the; mass of medium, heat capacity and temperature shift of the medium. The sensible heat storage capacity of a medium can be expressed by the following equation:

$$Q_{Stored-Sensible} = \frac{m \cdot c_p \cdot \Delta T}{3600s} = \frac{V \cdot \rho \cdot c_p \cdot \Delta T}{3600s}[kWh] \tag{2.16}$$

From Equation 2.16 it is evident that high density and heat capacity is advantageous for sensible heat storage. Increasing storage capacity without needing to increase stored medium volume or temperature level. Reduced stored volume reduces the physical size of the TES system and reduced temperature reduces the need for thermal insulation from the surroundings, both of which is advantageous in terms of reduced installation costs. This is also explains why concrete and water is often used for sensible TES, water has a high specific heat capacity of 4,2 $[kJ/kgK]$ and relatively high density of $\approx 1000[kg/m^3]$. Likewise concrete has a specific heat capacity $C_p$ of $\approx 0.88[kJ/kgK]$ [67] and density $\rho$ of $2200 - 2300[kg/m^3]$ [68]. The mentioned materials are also cheap and widely available. Water can also be utilized in cold TES, but the risk of freezing limits the range of possible temperature levels.

#### Latent Heat TES

Latent heat storage utilized the latent heat change of a phase changing material (PCM), usually between liquid/solid phase for charging and discharging thermal energy. Phase change happens at constant temperature and by using materials with high latent heat of phase change large thermal storage capacities can be achieved. The heat storage capacity of latent TES is described by the following equation:

$$Q_{Stored-Latent} = \frac{m \cdot \Delta h_{pc}}{3600s} = \frac{V \cdot \rho \cdot \Delta h_{pc}}{3600s}[kWh] \tag{2.17}$$

Where $\Delta h_{pc}$ in Equation 2.17 is the enthalpy difference of phase change of the storage medium. The traditional and most commonly know PCM used for cold TES is ice. Ice melts at $0°C$ and has a phase change enthalpy of 334 $kJ/kg$ [69].The amount of energy required for melting 1 $m^3$ of ice is 85.4 kWh, equivalent to a temperature increase of the same amount of liquid water by approximately 70 K. Such high temperature changes of sensible heat storage is not practical, storing the same amount of energy in sensible heat storage would therefore require around four times the stored volume compared to latent heat storage of ice.

Many different TES technologies exist with different advantages and disadvantages. The optimal choice of TES technology has to be evaluated for each specific project. Some important system performance indicators to consider is; Storage Capacity, Energy and power density, Response time, energy efficiency, self-discharge rate, Life expectancy and economics of operation [70].

#### Short term TES (Diurnal)

Short term of diurnal TES is used for matching the demand and supply offset in short periods of time, usually between low and high load periods of a day. The most common type of diurnal TES system is

the thermally stratified hot water storage tank for domestic hot water. Thermally stratified means that the tank has a vertical temperature gradient where the hottest water gathers at the top and the temperature gradually decreases closer to the bottom of the tank, this effect is caused by the difference in density of hot and cold water. Diurnal TES can be used for load shifting and peak shaving. Load shifting means offsetting a high load period to a more suitable period of the day, for example from a high energy cost period to a low energy cost period. Peak shaving is distributing the high load period over a longer period of time thus reducing the maximum load. Reduced maximum load means smaller installed cooling or heating capacities, reducing investment cost of equipment and peak load of the local energy system. Figure 2.16 below shows an example of diurnal TES used for an cold storage facility on a warm summer day. By charging the TES system during the night and discharging during high cooling load conditions at mid-day, energy cost savings is likely to be achieved and needed installed capacity of the cooling machines is reduced from over 500 kW to around 300 kW. This is however just an example, actual peak load reduction and cost savings vary from case to case, dependent on; cooling demand and size and type of TES system.

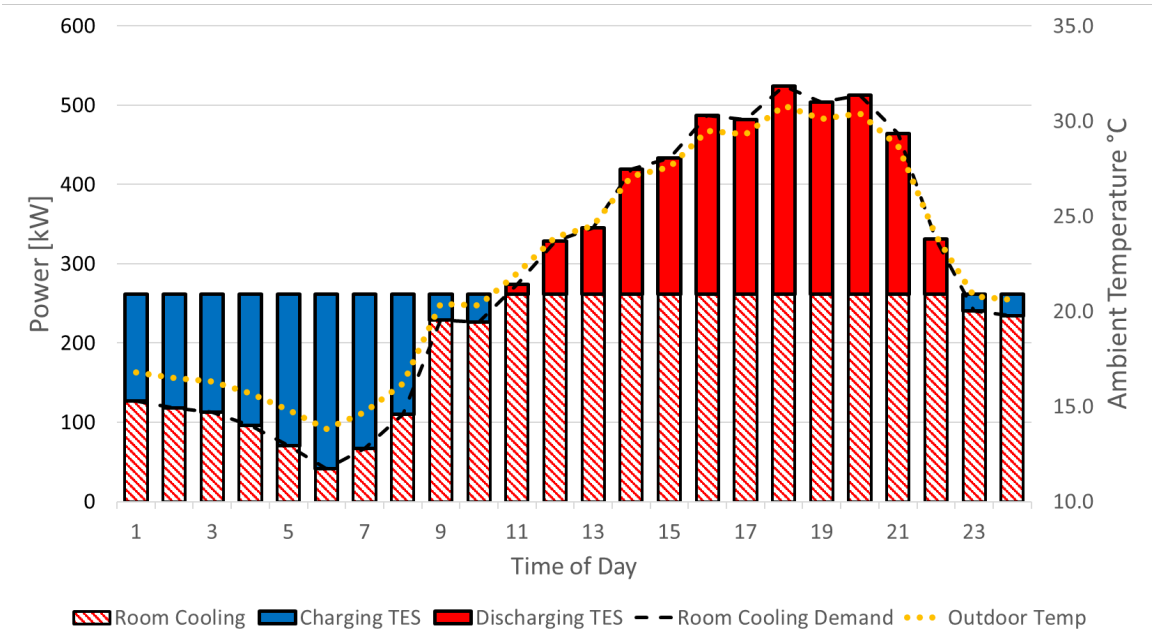


**Figure 2.16:** Short term TES — Example cold store

### Long term TES (Seasonal)

Long therm or seasonal thermal storage is a promising technology for reducing both heating and cooling demand of dwellings. Most long term TES (LT-TES) are sensible TES systems utilizing available, renewable thermal energy like geothermal energy [70]. In summer cooling demand can be reduced by utilizing free cooling with low temperature water. The resulting increase in water temperature then assures energy efficient and good operating conditions for example a geothermal heat pump. reducing

both installed heating and cooling capacity, energy usage and thus both installation heat pump installation and energy cost. However this has to be evaluated against the increased investment cost by the TES system. Figure 2.17 below illustrates the principle of LT-TES for an medium size office building. Some of the most common sensible LT-TES technologies are the; Aquifer thermal storage, borehole thermal storage and cavern thermal storage [70]. LT-TES utilizing both sensible and latent cold energy storage in PCM or storing snow from the winter also exists. An example of the later is used at Gardermoen Airport [71].

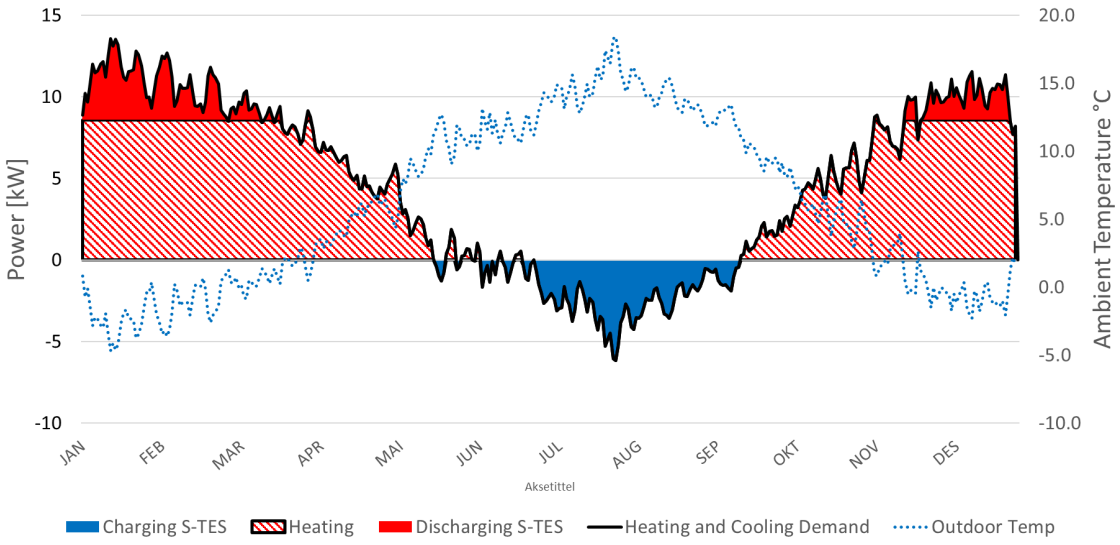


**Figure 2.17:** Long term TES — Example non-residential building.

### 2.8.3 Mobile Thermal Energy Storage (M-TES)

When the heat source and heat customer are not located in near proximity to each other mobile thermal energy storage (M-TES) can be viable option for transporting thermal energy. The concept of M-TES involves charging a thermal battery at the heat source and then transporting the M-TES either by truck, rail or other way of transportation to the customer, where the heat is discharged. Figure 2.18 below, illustrates the concept of M-TES.

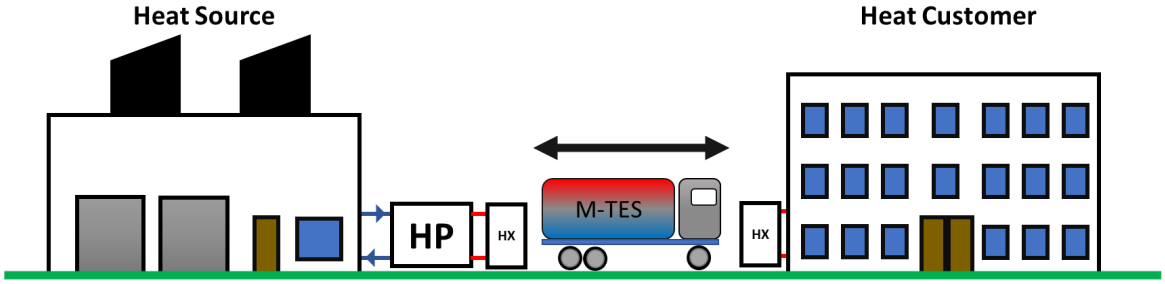


**Figure 2.18:** The concept of M-TES

Some studies suggest Latent M-TES using Erythritol as phase change material (PCM) is a good option for waste heat recovery from the industry [72]. In Västerås Sweden, a pilot project investigated using M-TES with Erythritol as PCM for waste heat recovery from the industry [72], [73], [74], [75]. The heat customer of the project is low temperature district heating grid. Erythritol was chosen due to its high energy density (330 kJ/kg), environmentally friendliness and suitable temperature rang for the project [75]. Erythritol is sugar and alcohol, with a melting point of 118 °C[75]. It is therefore suitable for high temperature waste heat sources. The M-TES system was for a transportation distance of 30 km more attractive than an oil boiler , and the cost estimated to be in the range of 0.03-0.06 USD/kWh. The price of PCM had the most impact on cost of heat transportation [73]. They also evaluated using sensible M-TES with water, concluding that Water M-TES is competitive to Erythritol M-TES, especially for small transportation distances and small building areas [73].

According to Guo, Li, Zhao, Li and Yan [75] the charging time of the system was more than four times the discharge time, short charging times increased the amount of heat supplied and thus the profitability. In most application transportation by truck is most practical, but an economical assessment of M-TES by Chiu, Castro Flores, Martin and Lacarriere [72] transportation by both rail and maritime was more economical. They found a levelized cost of thermal energy of; 49, 62 and 86 Eur/MWh for maritime, rail and road transportation. Their conclusion was based on a economic pay back time of 12 years and 4% interest rate [72].

Deckert, Scholz, Binder and Hornung [76] investigated the economical efficiency of Latent M-TES using Sodium Acetate Hydrate. Using 20 ft containers with 1.3 MWh of latent heat storage and a total storage capacity of 2 MWh including sensible heat. The container was charged at a temperature of 85 °C, with an average charging power of 120 kW. The PCM has a melting point of 58 °C and latent heat exchange occurred in the range of 50-60 °C. They concluded that the system achieved an energy efficiency of over 90% and the storage capacity was increased with decreased heat sink temperature. The economic assessment was based on 200 cycles per year of 1500 kWh, transported 5.6 km. Which resulted in costs of 5 ct/kWh. Table 2.4 below summarises the found costs of M-TES in literature.

**Table 2.4:** Literature overview: Specific costs of mobile thermal storage (M-TES)

| Source | Technology | Specific energy storage cost | Storage cost in NOK/MWh |
|---|---|---|---|
| Li 2013 | PCM Erythritol | 0.03-0.06 USD/kWh | 300-600* NOK/MWh |
| Deckert 2014 | PCM Sodium Acetate Hydrate | 5 ct/kWh | 550* NOK/MWh |
| Chiu 2016 | PCM Erythritol | $49^{(a)}$, $62^{(b)}$, $86^{(c)}$ EUR/MWh | 539-946* NOK/MWh |

Transportation method:$^{(a)}$ Maritime, $^{(b)}$ Rail, $^{(c)}$ Road.

*Assuming an exchange rate of EUR/NOK of 11. and USD/NOK of 10.

## 2.9 Principles of Cost & Investment analysis

This section is devoted to describing basic cost and investment principles in general and heat pump projects in particular. Including a description of typical costs and income of heat pump installations as well as a short introduction of common economic therms.

### 2.9.1 Costs and Income of heat pumps

Heat pumps are complex technical installations and typically large capital investments. The capital investment cost vary for different heat pump installations and is dependent on, but not limited to; Type of heat pump, Size of installation, refrigerant used, complexity of installation, manufacturer prices ect. In general the capital investment cost of heat pumps is given as a ratio between total investment costs [NOK] and installed capacity [kW]. Figure 2.19 show the specific investment cost [NOK/kW] plotted against installed capacity [kW] for several heat pump installations. The data is however from the year 2000 and might be outdated, but it illustrates that specific investment cost varies from installation to installation, especially for small capacities. In the contrary heat pumps are energy efficient and thus have low operational costs compared to other heating and cooling systems, like for instance electricity.

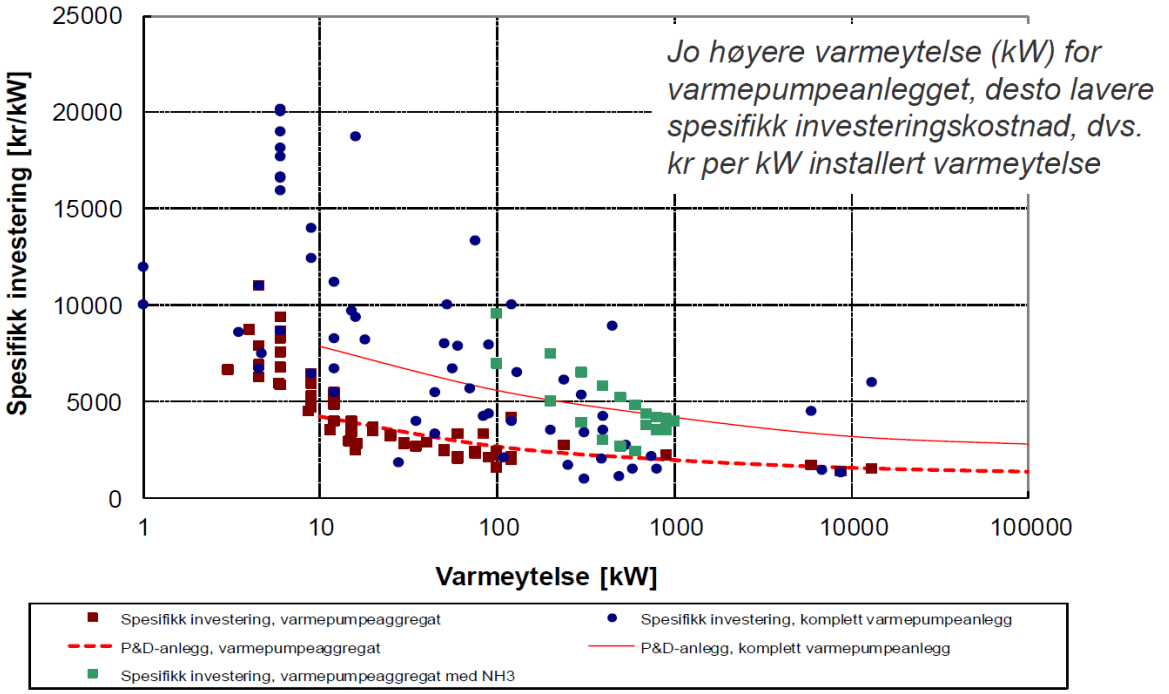


**Figure 2.19:** Spesific investment cost of heat pump installations in 2000 [77].

Despite the actual investment cost of a heat pump varies from installtation to installation have Norges Vassdrags- og Energidirektorat (NVE) developed an Excel-sheet of standard values for documentation of costs in the Norwegian energy sector [78]. Heat pump costs according to NVE [78] for geothermal heat pumps with capacities from 35 to 150 kW delivering hot water at 55 °C and 70 °C respectively, excluding energy wells and heat extraction system is shown in Table 2.5 and 2.6 below. Geothermal heat pumps was chosen because they were considered to be most comparable to the intended SLV10 heat pump installation, both in capacity and uses brine/water as heat source/sink at the evaporator/condenser.

**Table 2.5:** Heat Pump Costs According to NVE: Heat Pump Brine to Water 55 °C [78].

| | | | | |
|---|---|---|---|---|
| Capacity | 35 | 75 | 150 | kW |
| Heat Pump Unit | 100 000 | 170 000 | 300 000 | NOK/Unit |
| Installation Cost | 115 500 | 247 500 | 495 000 | NOK/Installation |
| Specific Unit Cost | 2 875 | 2 267 | 2 000 | NOK/kW |
| Spcsific Installation Cost | 3 300 | 3 300 | 3 300 | NOK/kW |
| Specific Construction Interests | 274 | 248 | 236 | NOK/kW |
| Sum Specific Investment Costs | 6449 | 5815 | 5536 | NOK/kW |
| Fixed Operational Costs | 40 | 40 | 40 | NOK/kW/year |
| Total Specific Costs | 6489 | 5855 | 5576 | NOK/kW |

**Table 2.6:** Heat Pump Costs According to NVE: Heat Pump Brine to Water 70 °C [78].

| | | | |
|---|---|---|---|
| Capacity | 35 | 150 | kW |
| Heat Pump Unit | 315 000 | 500 000 | kr/Unit |
| Installation Cost | 115 500 | 495 000 | kr/Installation |
| Specific Unit Cost | 9 000 | 3 333 | kr/kW |
| Specific Installation Cost | 3 300 | 3 300 | kr/kW |
| Specific Construction Intrests | 548 | 296 | kr/kW |
| Sum Specific Investment Costs | 12848 | 6929 | kr/kW |
| Fixed Operational Costs | 70 | 70 | kr/kW/year |
| Total Specific Costs | 12918 | 6999 | kr/kW |

The variable operational costs are dependent on; energy efficiency , operation method, full load hours and electricity prices. And thus varies significantly from installation to installation. It has therefore been decided not to use the variable from NVE [78], but calculate the variable operational costs for the +CityxChange installations based on dynamic heat pump simulation models described in 4.4.

### 2.9.2 Discounting and time-value of money

The values of money is time dependent, having money today is worth more than expecting money in the future. Due to this effect it is in all profitability and cost analyses necessary to discount the different cash flows in the project for the time they occur. The time-value of money is dependent on the real interest rate which is given by the nominal interest from the bank corrected for inflation. The formula for calculating the real interest rate can be seen in Equation 2.18 below.

$$real\ interest\ rate = \frac{n_r - b}{1 + b} \quad [20] \tag{2.18}$$

Where $n_r$ and $b$ are the nominal interest rate and annual inflation rate.

#### Cost analysis

A cost analysis is as the name implies an analysis of the costs related to the project or possible investment evaluated. Some common cost analysis results of a cost analysis are annual costs (AC) and levelized cost of energy (LCOE). The annual costs of an heat pump system is the sum of all annual; investments costs, energy costs and operational and maintenance costs, levelized for the economic lifetime of the installation. The annual cost is described by Equation 2.20, where; $I_0$ is the investment cost, $a$ is the annuity factor, $W_E$ is the annual energy consumption, $e$ is the energy price, $O\&M$ are annual operation and maintenance costs and $n$ is the economic lifetime of the project.

$$a = \frac{r}{1 - (1 + r)^{-n}} \quad [77] \tag{2.19}$$

$$AC = \sum I_0 * a + \sum W_E * e + \sum O\&M \quad [77] \tag{2.20}$$

The LCOE is descirbed by Equation and is defined as annual costs of the system divided by the annual amount of energy produced. See Equation 2.21. For a heat pump installation $Q_{Produced}$ can be heating, cooling or the sum of delivered heating and cooling. Both AC and LCOE can be used to compare different methods of energy production.

$$LCOE = \frac{AC}{\sum Q_{Produced}} \quad [77] \tag{2.21}$$

### Profitability analysis

Profitability analysis is comparable to cost analysis, but instead of the actual costs, the profitability of a project is evaluated for a pre-determined rate of return. The rate of return should be larger than the real interest rate to account for; risk, tied capital and desired profit margin. Several measurements of profitability exists including; net present value (NPV) and pay off time. The formulas for NPV and pay off times can be seen in Equation 2.22 and 2.23, where $B$ is the net annual income or saving compared to other alternative systems considered.

$$NPV = \sum_{i}^{n}(\frac{B_i}{(1+r)^i}) - I_0 \approx B \cdot \frac{1-(1+r)^{-n}}{r} - I_0 \quad [20] \tag{2.22}$$

$$Pay\ off\ time = \frac{\ln(1-(I_0/B)*r)^{-1}}{\ln(1+r)} \quad [20] \tag{2.23}$$

### Sensibility analysis

Often in reality the exact investment costs can be difficult to pre-determine. It might then be interesting how sensible the profitability of the project is to changes in either investment costs or annual net income. Some measures of this are maximum investment and minimum annual income, defined as the maximum investment and minimum annual income required to make the NPV of an investment 0.

$$Maximum\ investment\ cost = \sum_{i}^{n}(\frac{B_i}{(1+r)^i}) \approx B \cdot \frac{1-(1+r)^{-n}}{r} \quad [20] \tag{2.24}$$

Chapter 3

# Preliminary Work and System Descriptions

## 3.1 Existing Technical Installations

This chapter contains a detailed system description of the existing technical installations at Sluppenveien 17A and 10. As well as measurements and proposed solutions on how HTHPs for waste heat recovery can be implemented with the existing technical installations.

### 3.1.1 Sluppenveien 17A

Sluppenveien 17A has available excess thermal energy from the cooling system of a computer server. The system consists of two alternating chillers with 264 kW of cooling capacity each. The chillers use R407C as working fluid and has a total charge rate of 28 kg. The high GWP of R407C results in a potential environmental risk equivalent to over 30 tonnes of $CO_2$ emissions if a refrigerant leakage should occur. Some of the condenser heat is recovered to the buildings hydronic heating system, but the majority of the excess heat is emitted to the surroundings through room mounted gas coolers. Measurements performed during the spring of 2019 show that the chillers operate on only part load. On average was the condenser heat measured to approximately $90kW$, where $\approx 9$ kW is recovered internally in the building and $\approx 81$ kW is emitted to the surroundings.

The main purpose of the technical installation is to provide safe and reliable cooling of the computer servers. It is therefore important that measures for improving energy efficiency and waste heat recovery does not impact the reliable delivery of cooling to the computer servers. It is therefore decided to implement the intended waste heat recovery heat pump before the existing chillers in the computer server cooling cycle return pipe. Figure 3.1 below show the existing technical chiller installation and intended implementation of the heat recovery heat pump. Based on the mentioned measurements it is estimated that an heat recovery heat pump with 60 kW of evaporator capacity would have good and stable operating conditions.

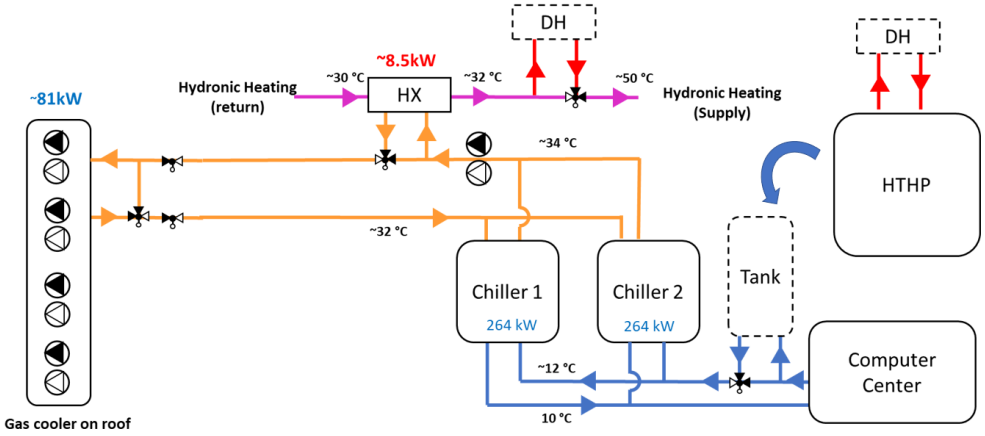


**Figure 3.1:** System sketch of the existing installation Sluppenveien 17A and intended implementation of HTHP for waste heat recovery.

### SLV17A — High temperature heat pump

For Sluppenveien 17A waste heat is to be recovered from the computer server cooling system to the district heating supply line using a 2-step R290/R600 cascade high temperature heat pump. This heat pump was the main focus during the project thesis performed during the fall of 2019. Figure 3.2 below show the developed dynamic simulation model in *Dymola 2020*, based on the *TIL Media* and *TIL Component* libraries. The SLV17A 2-step cascade model was set to have a evaporation/condensation temperature of $7°C/103°C$, and assumed $3K$ temperature difference in the cascade heat exchanger. With a heat sink and heat source inlet/outlet temperature of $75/100°C$ and $12/10°C$ the model achieved a combined heating and cooling COP of 3.59 and heating COP of 2.29.

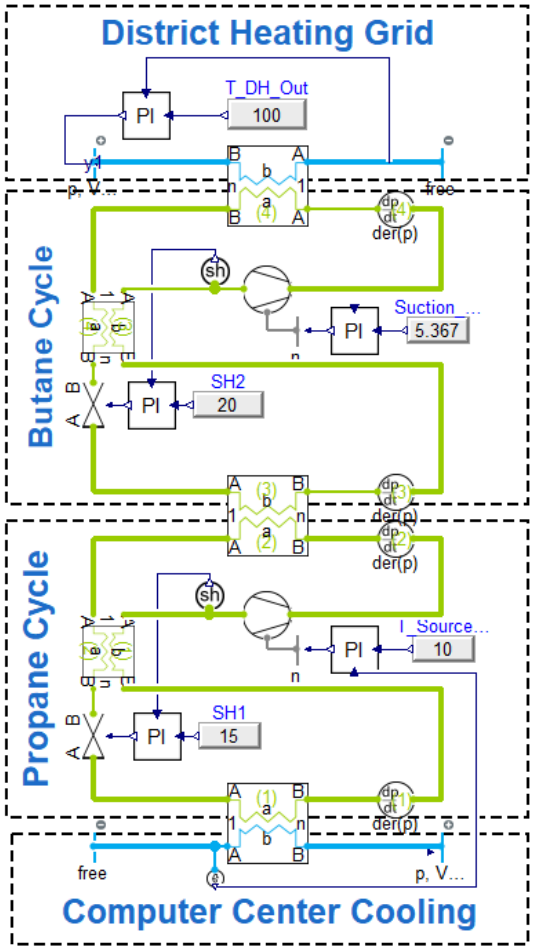


**Figure 3.2:** SLV17A — Developed Dymola model of high temperature R290/R600 cascade heat recovery heat pump.

The model has a design evaporator capacity of 60 kW, but absolute maximum evaporator capacity was set to 68 kW, according to the compressor manufacturer. The model was tested with variable cooling loads from 30-120 $kW$. The model was able to maintain the $10°C$ and $100°C$ set-points of the evaporator and condenser outlet water temperature at cooling loads $< 68kW$ as per design. The $100°C$ set point of the condenser outlet water temperature was maintained at cooling loads under 60 kW due to a variable heat sink water volume flow.

A series of assumptions and simplifications was made developing the simulation model. The model does for instance not include heat losses to the ambient or pressure drop through components. But it is believed to give an realistic indication of the performance of the actual heat pump installation.

### 3.1.2 Sluppenveien 10 — Existing Installations

Sluppenveien 10 is an old light-industry building constructed in the 1970s. Today the building is mainly a cold storage facility operated by BaRe and Norfresh. The building has over 6600 $m^2$ of cold storage areas, mainly used for storing pre-refrigerated fruit and vegetables until redistribution to local supermarkets. Besides from being a cold storage facility the building also have office areas and a local brewery, Austmann. The building has available waste heat from the existing chillers of the cold storage facilities, the exact amount is however unknown due to a lack of measurements.

Due to the age of the building and the technical installations it has been a challenging and time consuming task to gather information and technical specifications of the building and refrigeration system. The existing refrigeration system consists of in total 4 cooling machines. Each cooling machine has an air cooled condenser placed on the outside of the building, which means that the extracted heat is emitted to the surroundings. The temperature of the storage rooms wary depending on the type of products stored in the room. For instance fruit and flowers. The temperature in the storage rooms is: 2-4°C, 10-12°C, 8-12°C, 16°C and 10-20°C, see Figure 3.3. Three of the cooling machines belongs to BaRe and the $4^{th}$ belongs to Norfresh. The room partitioning of the chillers as well as cold storage room air temperature set points can be seen in Figure 3.3 and 3.4 below.

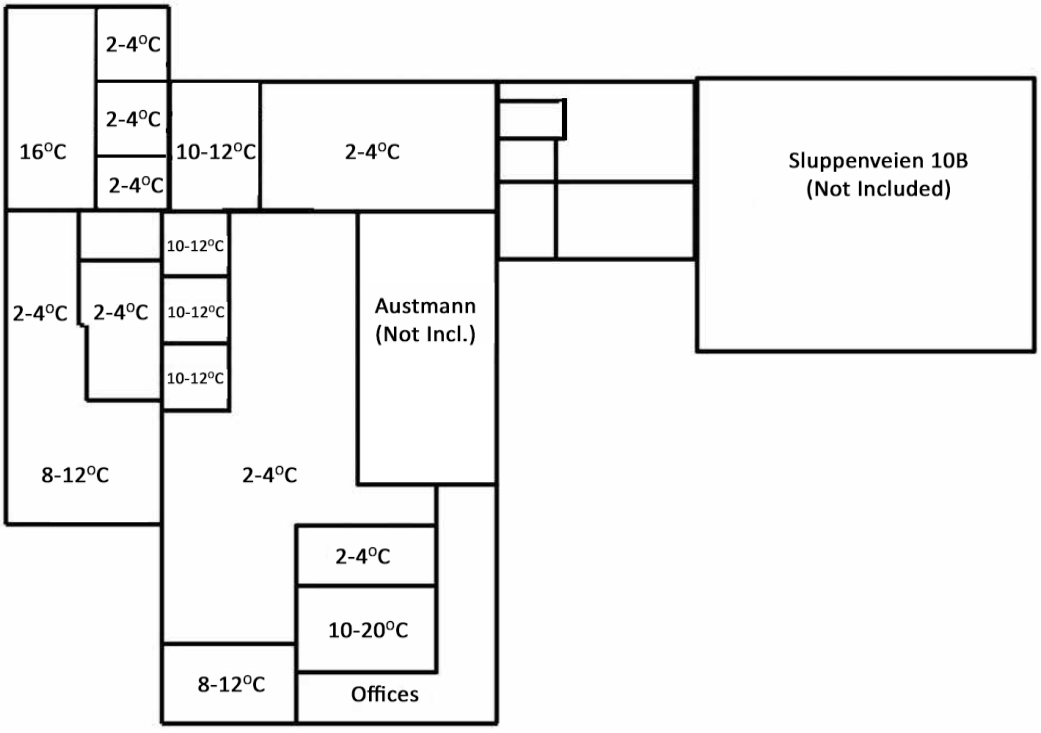


**Figure 3.3:** SLV10: Floor plan with storage room set-point air temperatures.

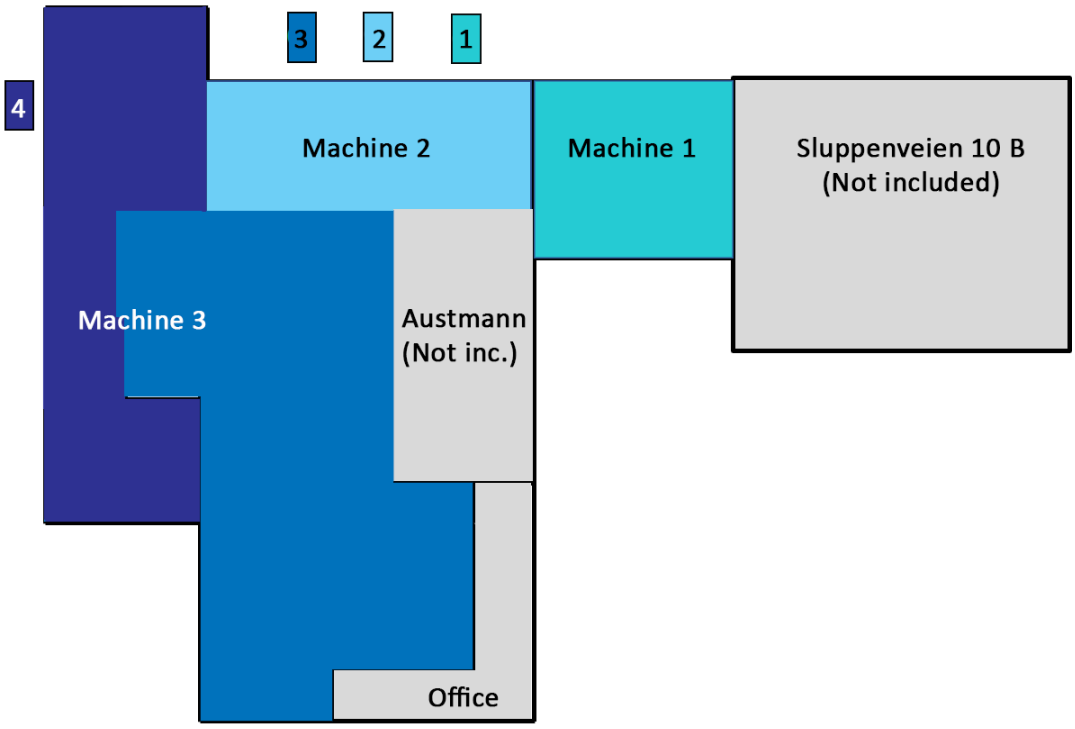


**Figure 3.4:** SLV10: Cooling machine zone overview

The existing chillers will hereby be referred to as; chiller 1,2,3 and 4, as indicated in Figure 3.4. Chiller 1,2 and 3, have an installed cooling capacity of 117, 121 and 338 kW respectively. Chiller 3 is however newer and likely to have better energy efficiency. From a system performance point of view it is therefore desirable to operate chiller 3 as much as possible. Little is known about chiller 4. An overview of the existing chiller information can be seen in Table 3.1 below. Most information is know about the newest and largest unit, chiller 3. It was installed in 2013 and is a DAIKIN EWAD-480D-SL air cooled chiller. Detailed information about chiller 3 can be seen in Table B.4 on the following page.

**Table 3.1:** SLV10 — Existing Chiller Information. Numbers according to Figure 3.4.

| Chiller | $\dot{Q}_{Evap}$ | Refrigerant | Ref. Charge | Installation date | Model |
|---|---|---|---|---|---|
| 1 | 121 kW | R410a | 20 kg | Unknown | ACM SCAEYJ-F 151 PAC1 |
| 2 | 117 kW | R410A | 23.7 kg | Unknown | BlueBox ZETA ECHOS/ST 12.2 |
| 3 | 338 kW | R134a | 68 kg | 08.2014 | DAIKIN EWAD 480D-SL |
| 4 | 145 kW | R410A | 2x26 kg | 11.2010 | DAIKIN EWYQ 150 DAYNB-Q |

**Table 3.2:** SLV10 Chiller 3 Information

| Machine 3 — Information | | |
|---|---|---|
| Model | DAIKIN EWAD-480D-SL | |
| Cooling Capacity | 338 | kW |
| Unit Power input | 136 | kW |
| Fluid | Ethylene Glycol 40% | |
| Water temp. (In/Out) | -2.0 / -6.0 | $°C$ |
| Nominal Water flow | 21.5 | l/s |
| Refrigerant | R134a | |
| Refrigerant Charge | 68 | kg |
| Compressor | 2xSymetric Single Screw | |
| Part-Load Operation | Stepless 100-25% | |


**Figure 3.5:** DAIKIN EWAD 480D-SL Chiller

Table 3.3 below shows the energy performance of the Daikin EWAD 480D-SL under variable part load operation, calculated according to the standard EN14511. The efficiencies are calculated for an ambient air temperature of 28 $°C$. Higher than the yearly average air temperature in Trondheim, which is 4.7 $°C$ [79].

**Table 3.3:** DAIKIN EWAD-480D-SL Energy performance according to the user manual [80]

| Part Load [%] | $T_E$ In [$°C$] | $T_E$ Out [$°C$] | T Ambient [$°C$] | $\dot{Q}_{Evap}$ [kW] | $\dot{W}_{Comp+Pump}$ [kW] | $\dot{W}_{Fan}$ [kW] | COP [-] |
|---|---|---|---|---|---|---|---|
| 100 | -2.0 | -6.0 | 28.0 | 338 | 129 | 6.27 | 2.49 |
| 75 | -3.0 | -6.0 | 28.0 | 253 | 100 | 6.27 | 2.37 |
| 50 | -4.0 | -6.0 | 28.0 | 168 | 68.9 | 3.14 | 2.33 |
| 25 | -5.0 | -6.0 | 28.0 | 107 | 44.2 | 3.14 | 2.27 |

## 3.2 Sluppenveien 10 — Electricity Measurements

This section is dedicated to presenting and discussing the electricity measurements taken by the building owner Kjeldsberg Eiendomsforvaltning [81]. It has been decided to present these results in the Existing Technical Installation chapter because it is not the results this master thesis, the results are solely presented and illustrated. The measurements are presented in this chapter because as the existing technical installations the electricity measurements form a basis for the chosen methods of waste heat recovery.

No measurements of available thermal energy for waste heat recovery have been performed at Sluppenveien 10, the exact potential for waste heat recovery is therefore uncertain. However the electric energy consumption of the Daikin chiller have been measured daily since the beginning of 2015 by the building owner, Kjeldsberg Eiendomsforvaltning AS. New regulations on electricity measurements was introduced in Norway in 2019, making it mandatory to installed an advanced electricity measuring device (AMS). Detailed measurements of the electricity consumption of chiller 3 therefore exists in hourly increments since 08.02.2019. The electricity measurements have therefore been used a basis for estimating the cooling demand and potential for waste heat recovery of Sluppenveien 10.

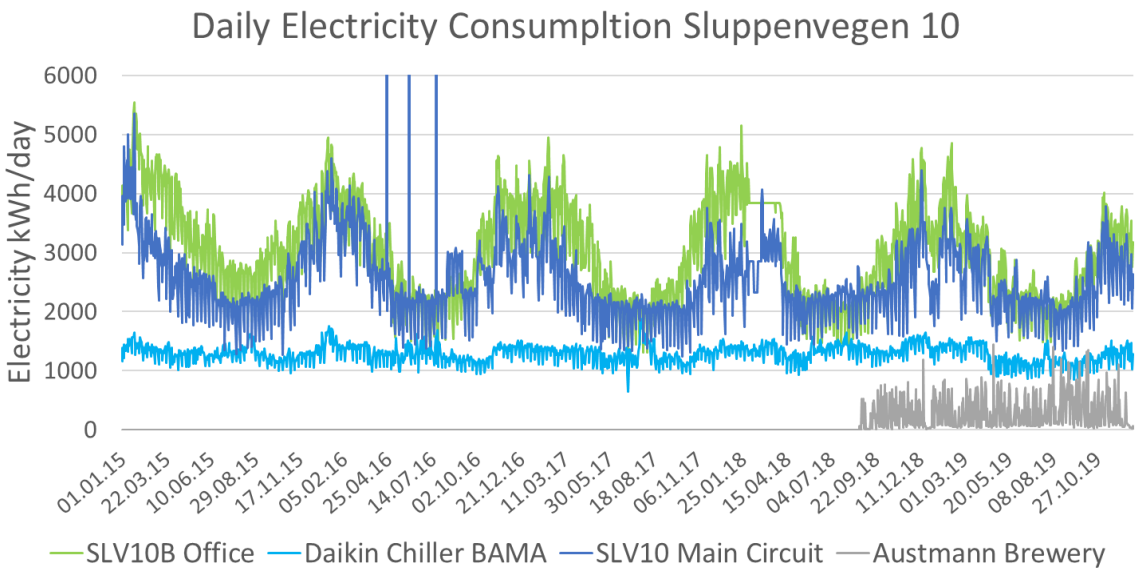


**Figure 3.6:** Sluppenveien 10 daily electricity consumption, measured from 2015 to 2019 [81].

Figure 3.6 above show the daily measured electricity consumption of the 4 measuring devices installed at Sluppenveien 10 by Kjeldsberg; SLV10B, Chiller 3 BAMA, SLV10 Main Circuit and Austmann Brewery. The measurement devices measure electricity consumption of the main electrical circuits of the building. The SLV10B unit measures the total electricity consumption of Sluppenveien 10B, Chiller 3 BAMA measures the electricity consumption the refrigeration system. It is believed that Chiller 3 BAMA only includes the Daikin EWAD 480D Chiller, but the building owner was not certain, it was therefore assumed that the measurements from Chiller 3 BAMA includes all chillers in order to not over estimate the available waste heat. In order to maintain the loading docks frost-free during winter, electric heaters are installed. It is however unknown whether the heaters are installed on the circuit for the refrigeration system or SLV10 Main Circuit. The Austmann device measures electricity consumption mainly to production units in the brewery. Lastly the SLV10 Main circuit measures the total electricity consumption of Sluppenveien 10, excluded the chiller and Austmann consumption. The same measurements only for 2019 is shown in Figure 3.7 below. The hourly measurements from 08.02.2019-07.02.2020 show an annual electricity consumption of chiller 3 of 446 436 kWh/a.

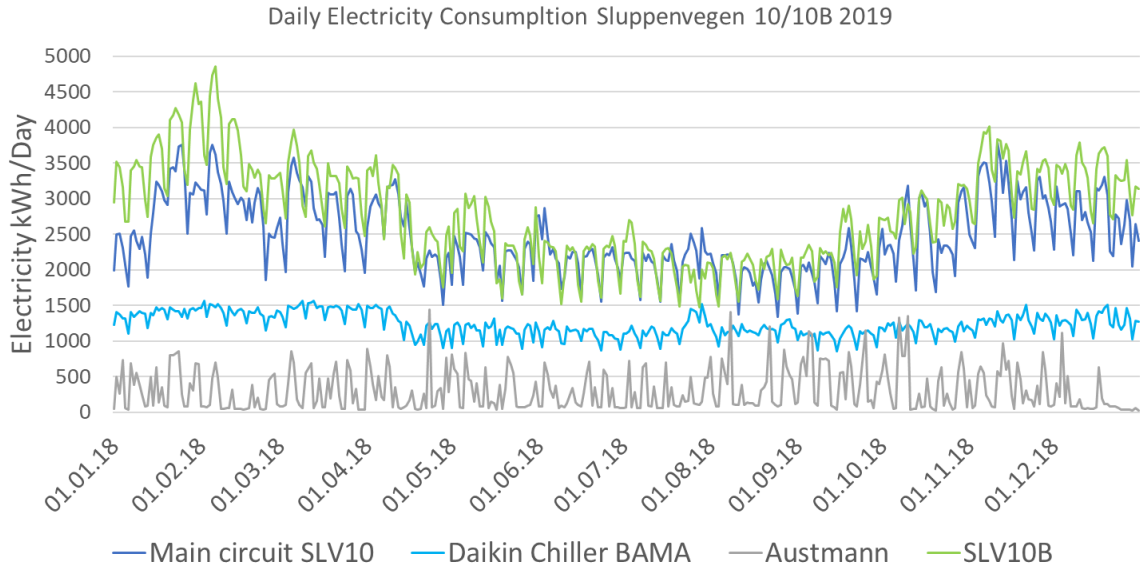


**Figure 3.7:** Sluppenveien 10, daily electricity consumption for 2019 [81].

Being mainly office spaces the Sluppenveien 10B and Sluppenveien 10 main circuit shows and increased electricity consumption in winter, as would be expected of old office buildings. The electricity consumption of Austmann is characterized by very variable electricity consumption, likely coinciding with use of power demanding production units.

The electricity consumption of the chiller unit is stable around 1200 kWh/day throughout the year. Not as would be expected of a cold storage facility, which is an increase in cooling demand during summer due to increased infiltration and transmission losses. Figure 3.8 below show the measured hourly chiller 3 electricity load for 2019 plotted against ambient air temperatures from Meterologisk Institutt [82]. The figure seems to indicate that the degree of correlation between the actual chiller electricity consumption and the ambient air temperature is either very small or that there is no correlation at all. A small tendency towards increased chiller electricity can be seen for especially high and low ambient temperatures, but due to few measuring points no clear conclusion can be made. The seemingly lack of correspondence between cooling demand and outdoor temperature might be caused by low chiller efficiencies at part load resulting in high electricity consumption also in low cooling load conditions. An other possible explanation for the increased electricity consumption at low ambient temperatures might be that the Chiller 3 Bama measurement device includes the consumption of the electric heaters.

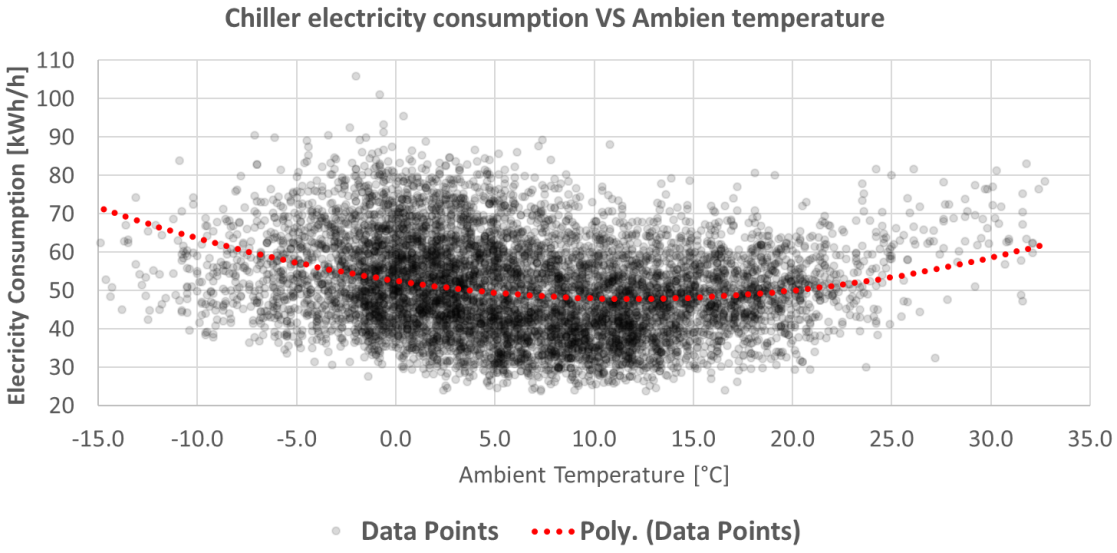


**Figure 3.8:** Temperature dependency of chiller electricity consumption [81].

Figure 3.9 show the hourly measured electricity consumption of chiller 3 for most of 2019. In the figure the data is illustrated as a scatter-plot with the measured time of week as X-axis. The average electricity consumption for all measured weeks is indicated in red. The data show a visible peak in electricity consumption around; 05:00, 12:00 and 17:00 on weekdays, correlating to when the storage facility receives trucks with new products. According to the cold store manager Cato Mosling Vonstad most of the rooms have installed electrical heating leading which also have high electricity consumption in the previously mentioned time periods during the winter period [83]. It is however unclear if these heaters are included in the electricity measurements. The increase in electricity consumption at low ambient temperatures shown in Figure 3.8 might indicate that they are. This is one possible explanation for the usage dependency, but lack of seasonal variation of measured chiller electricity demand.

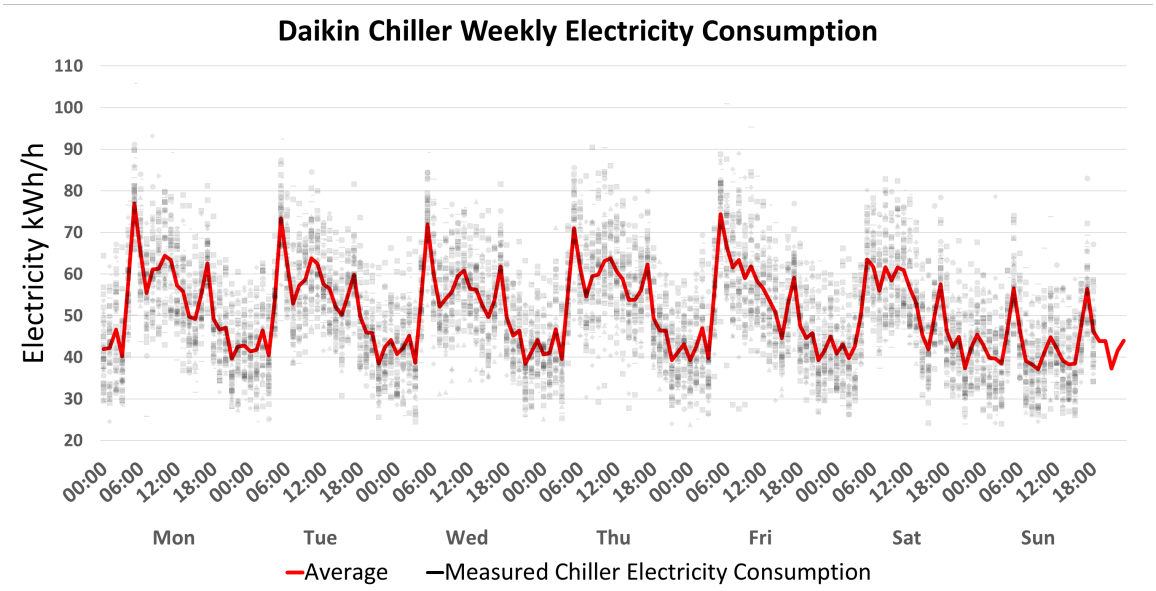


**Figure 3.9:** Daikin Chiller, weekly electricity consumption for 2019, measured in hourly increments [81].

### Integration of Heat recovery HTHP

As for Sluppenveien 17A reliable delivery of cooling is of most importance, it is therefore decided that the high temperature heat pump is to be installed "in front of" the chillers. This means installing 3 heat exchangers to extract heat from the brine before it enters the chiller. The heat is transferred from the heat exchangers to the heat pump evaporator through a secondary circuit. To fulfill the funding requirements from the EU, an innovative solution with $CO_2$ as brine in the secondary circuit was chosen. The system overview can be seen in Figure 3.10. This solution would allow the existing chillers to be able to operate even if the heat recovery heat pump is not. When the HTHP is in operation the existing chillers covers the remaining cooling demand. This solution makes it possible to dimension the heat recovery heat pump evaporator capacity lower than the maximum cooling demand of the cold storage facility, increasing full load operational hours, assuring reliable and good operation conditions for the HTHP. This also maximizes recovered heat while holding the capital investment costs of the HTHP low. The solution is illustrated in Figure 3.10.

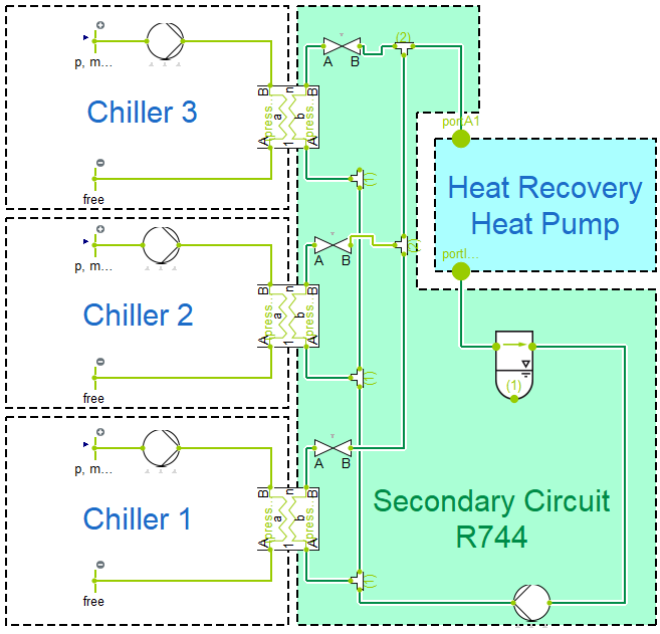


**Figure 3.10:** High temperature heat pump solution with $CO_2$ secondary circuit.

Chapter 4

# Methodology

This chapter describes the procedure and methodology used when developing the steady state and dynamic heat recovery heat pump simulation models. The first section describes the method of estimating the cooling demand of the cold store, followed by the development of the steady state heat pump models in Engineering Equations Solver (EES). Subsequently the general modeling approach in Dymola is described, with examples from the developed heat pump models, and how the models have been tested and validated.

## 4.1 Estimation of Cooling Demand from electricity measurements

The measured electricity consumption of the existing chillers presented in Section 3.2 combined with the energy efficiency given by the chiller data-sheets was used to estimate the cooling demand and available waste heat at Sluppenveien 10. The part-load percentage of the chiller was estimated using Table 3.3 and hourly electricity measurements from 08.02.2019-07.02.2020, the COP was the calculated by interpolation from Table 3.3. Lastly the cooling demand was calculated using Equation 2.5b. The COP of chiller 3 at different part loads can be seen in Figure 4.1. For the measured period no load over 81% of installed cooling capacity was measured and for part-loads under 25% the COP was assumed to be as for 25% Part load.

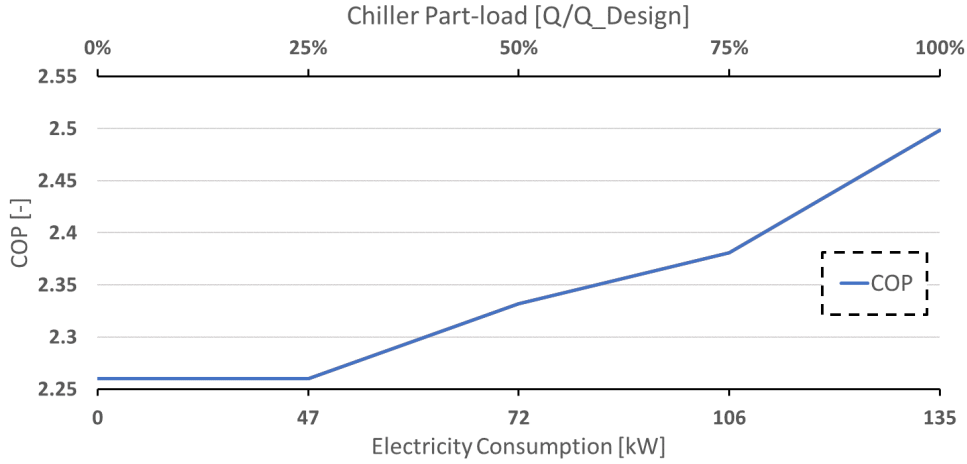


**Figure 4.1:** Estimated Chiller COP at part load based on Table 3.3.

Figure 4.2 below shows the estimated cooling demand for an average week based on the method described above and average measured hourly electricity consumption from Figure 3.9. This weekly load profile was used for testing av validating the dynamic simulation models described later on. For yearly energy simulations an similar load curve based on the actual hourly measured electricity consumption was used. It was decided to visualize the load curve with a average week in stead of the entire year because the yearly load curve showed little seasonal variation and a weekly load curve being more visible.

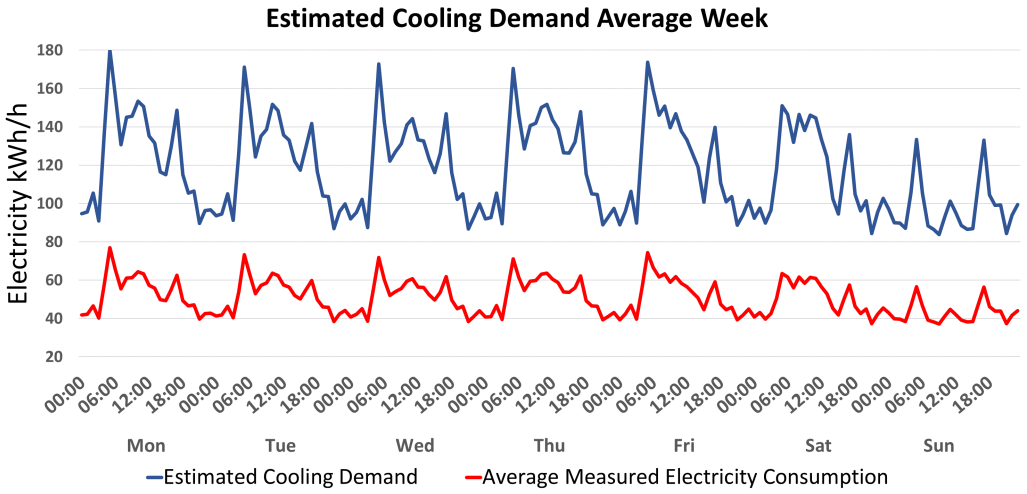


**Figure 4.2:** Estimated cooling load average week.

The load-duration diagram for the estimated cooling demand of the cold storage facility is illustrated in Figure 4.3 below. Estimated cooling demand has a maximum of 274 kW, average of 116 kW and minimum of 54 kW. The maximum occurring 03.02.2020 at 5 am and the minimum 30.06.2019 at 9 pm. 87.7% of the measurement period the estimated cooling demand is between 80 and 180 kW, corroborating that the weekly average cooling demand in Figure 4.2 is presentable for the entire year.

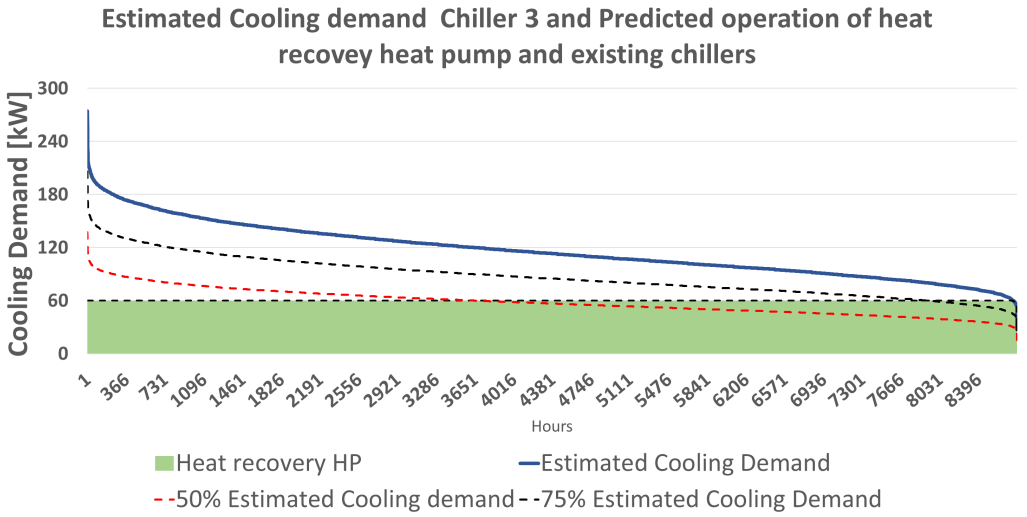


**Figure 4.3:** Sorted estimated cooling demand and waste heat recovery heat pump with 60 kW evaporator capacity.

In order to investigate the consequence of the uncertainty of the estimated cooling demand the duration load-curve and full load hours have been calculated for 50% and 75% of the estimated cooling demand as well.

Despite that the estimated cooling demand rarely is less than 80 kW it was in collaboration with the +CityxChange partners to limit the evaporator capacity of the intended waste heat recovery heat pumps to 60 kW. This was done to assure stable operating conditions and avoid part load operation due to the uncertainty of the actual cooling demand of the cold store. An additional advantage is that the intended installation for Sluppenveien 17A, which is more developed also has 60 kW evaporator capacity. This opens the possibility for using a similar system as developed for Sluppenveien 17A, possibly saving both workload, time and costs for +CityxChange.

## 4.2 Chosen methods of waste heat recovery

As previously mentioned in Section 1.2, is Sluppenveien 10 not connected to the district heating grid at Sluppen. This makes the choice of waste heat recovery method at Sluppenveien 10 more challenging compared to Sluppenveien 17A, but it also opens the possibility for new and innovative solutions. The two most promising methods of waste heat recovery are considered to be:

- Recover heat delivered to the district heating supply line, below supply line temperature.
- Production of how water to neighbouring dwellings, for instance 3T or Austmann.

#### Waste heat recovery to District heating grid

For the first method, waste heat recovery to the district heating grid, a secondary circuit would have to be made from the cold store existing chillers to the closest access point of the district heating grid. Then a similar heat pump as developed for Sluppenveien 17A might be used to recover heat to the district heating supply line. Delivering heat at the district heating gird supply line temperature might be infeasible due to the high temperature lift (over 110 K), as a plan B it has therefore been considered to deliver heat at a as high as possible temperature to the district heating supply line. However this is undesirable from the district heating grid operator point of view and should therefor be avoided if possible.

Figure 4.4 on the consecutive page show the two models chosen to evaluate waste heat recovery to the district heating grid. The models are based on the solution developed for SLV17A (See section 3.1.1). Due to the high temperature lift by the low temperature R290 cycle and thus risk of low compressor efficiencies and high discharge temperatures, it has been decided to evaluate the effect of 2-step compression and expansion in the LTC. Both models have a evaporation and condensation

temperature of -15 and 56°C for the R290 LTC and 53 and 103 °C for the R600 HTC. The evaporation temperature of the R600 HTC is limited to a maximum of 53 °C due risk of compressor lubrication problems at higher temperatures due to reduced viscosity of the lubrication oil.

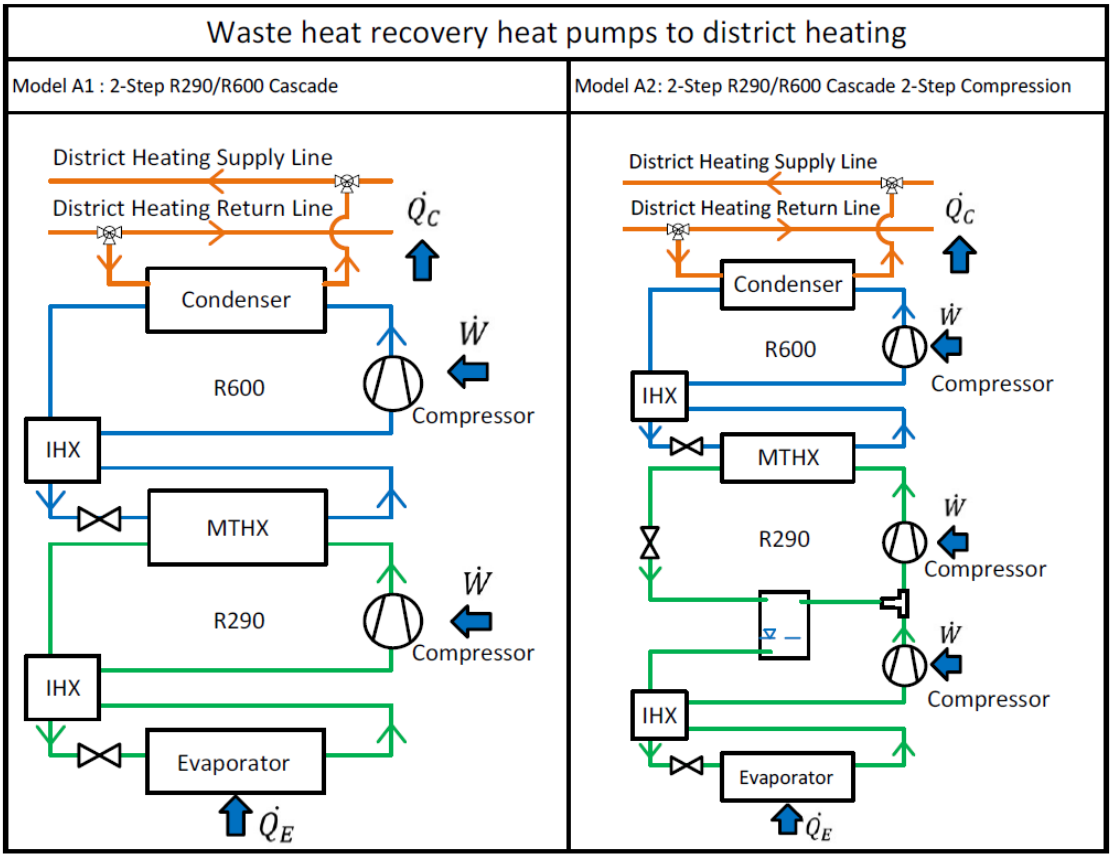


**Figure 4.4:** Overview of chosen models for waste heat recovery to district heating.

### Waste heat recovery by hot water production

The second option is production of hot water to neighbouring buildings, where the most promising recipients of hot water are; the fitness center 3T Sluppen and the brewery Austmann. Due to the COVID-19 virus crisis limiting the progress of the +CityxChange project 3T and Austmann have not yet become official partners of the +CityxChange project. The solutions presented in this thesis are therefore pure hypothetical with the intention of identifying possible waste heat recovery solutions for +CityxChange. Of the same reason it has not been possible to perform measurements or determine the hot water demand of 3T and Austmann in particular. The hot water demands have therefore been assumed based on general values in the presented theory.

For production of hot water the heat sink inlet water temperature is significantly lower compared to re-heating of district heating return line water to the supply line. This opens up the possibility to use $CO_2$ heat pumps which are inefficient for high heat sink inlet temperatures due to high vapour content of the evaporator inlet. It has therefore been decided to compare the performance of a 2-step R290/R600 cascade similar to Sluppenveien 17A, with a more conventional $CO_2$ heat pump solution for production

of hot water. Figure 4.5 and 4.6 on the next page show the 3 chosen models for hot water production. 2 using a hydrocarbon R290/R600 cascade solution (Model B1 and B2) and one using $CO_2$ as refrigerant, Model C1. All of which producing hot water at 70 °C.

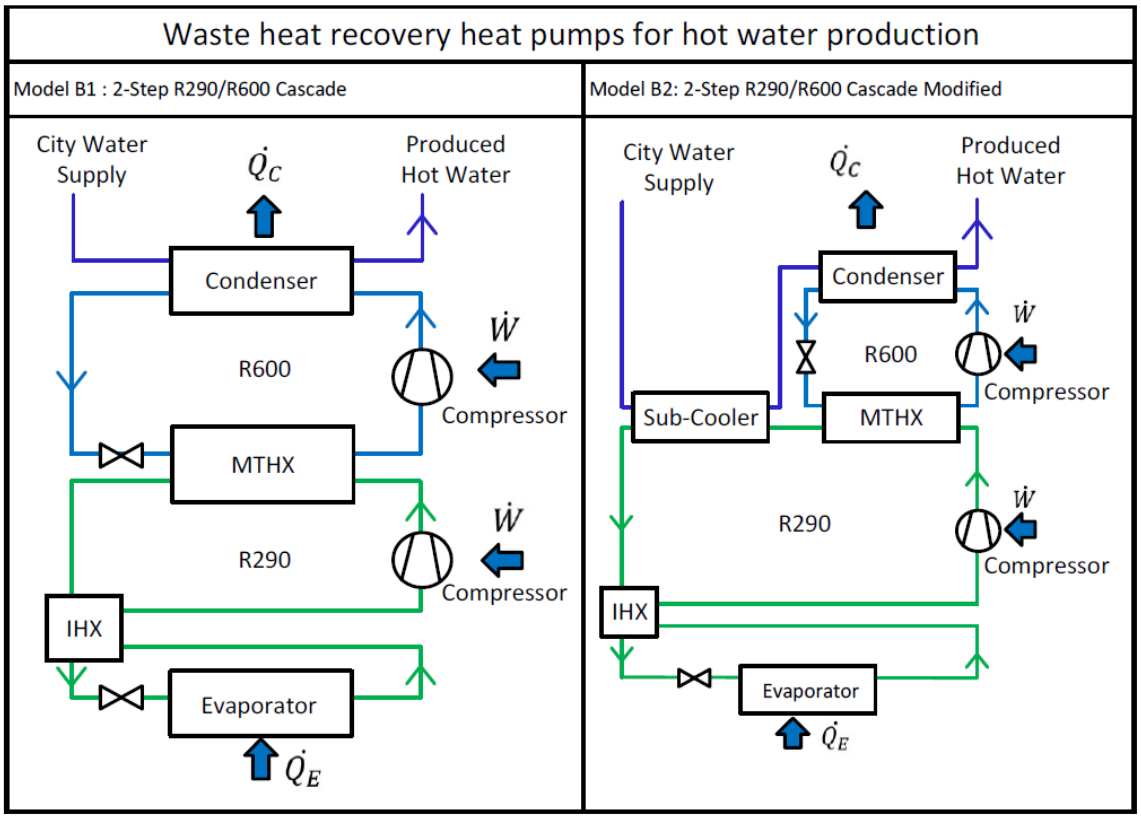


**Figure 4.5:** Overview of chosen models for hot water production with 2-Step R290/R600 Cascade Heat Pump as SLV17A solution.

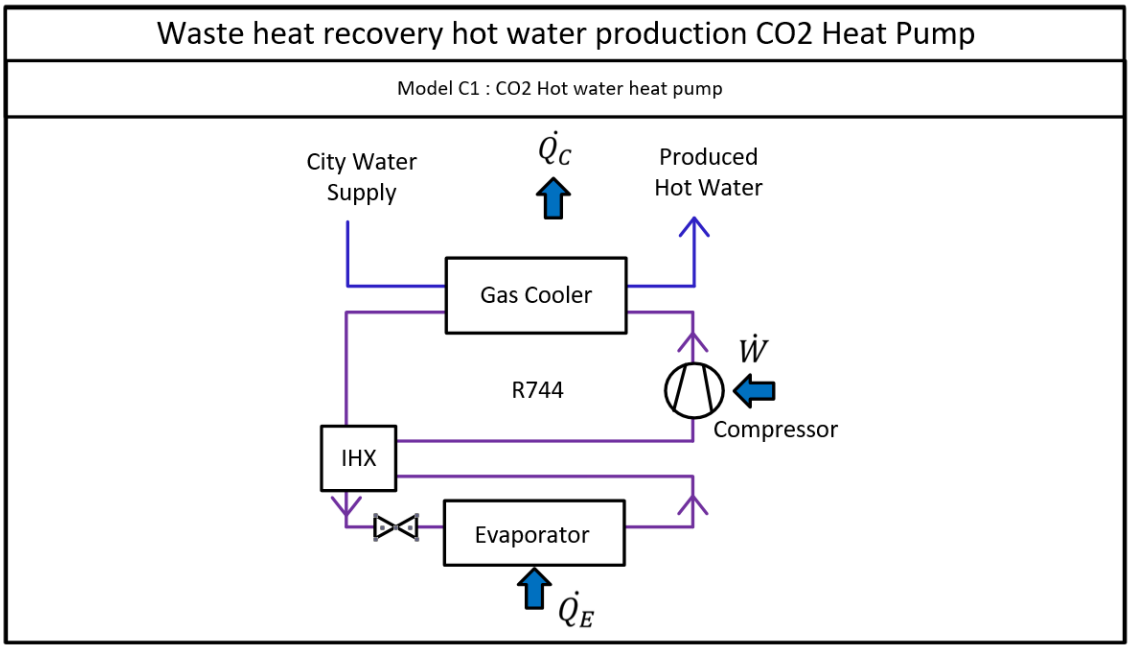


**Figure 4.6:** Overview of chosen models for hot water production with $CO_2$ heat pumps.

### 4.2.1 Recipients of Hot Water

The hot water demand of a building is difficult to determine precisely because it is greatly dependent of user behavior. In the case of +CityxChange Austmann and 3T, a local brewery and fitness center is believed to have large hot water demands. Their actual power demand for hot water production varies with usage, for instance when Austmann cleans their brewing equipment or 3T has a lot of customers showering at the same time. This user behaviour of the two possible recipients is not known, because the attempts on contacting the respective companies have been unsuccessful. In this thesis the hot water demand is therefore investigated in an energy point of view through estimating the average annual power demand for hot water. It is therefore assumed that the two recipients have large accumulation tanks to account for hourly or daily variations in hot water demand.

#### 3T/Austmann

For the case of Austmann the hot water demand is estimated based on the presented theory in Section 2.5.2. The found literature is inconclusive, the thermal energy demand found is varying from case to case and depends on the size of brewery. In order to estimate the hot water demand of Austmann is has therefore been assumed that the brewery has a water consumption of 4.3 hl/hl the average brewery water consumption in 2012 according to Campden BRI [50]. 45% of the water consumption is then assumed to be hot water demand. This has been assumed because according to the Canadian Industry Program for Energy Conservation report [43] 45% of the water consumption of breweries are used for cleaning applications. The total production capacity of Austmann is also uncertain, no reliable source of the breweries annual production have been found and the attempts on contacting Austmann have not been successful. But according to the Wikipedia page for Austmann the production in 2015 was 250 000 liters [84]. This is not a reliable source and the production is likely to have changed since 2015, but the annual production of 250 000 liters is assumed to be true due to a lack of more reliable information. This results in an annual hot water demand of approximately 483750 liters.

$$V_{Hot-Water} = 4.3 * Production * 0.45 \tag{4.1}$$

For the fitness center 3T, the hot water demand have been calculated using standard values from SN/TS 3031:2016 "Energy performance of buildings, Calculation of energy needs and energy supply" [85]. The standard gives general values for energy demand for hot water based on building category. The most suitable building category for 3T Sluppen is "Idrettsbygg". According to SN/TS 3031:2016 this building category has an energy demand for hot water of 22.73 $Wh/m^2$ from 07:00 to 18:00 and 0 $Wh/m^2$ the remaining hours of the day. Yet in the updated version of the standard, SN-NSPEK 3031:2020 [86] the energy demand for hot water of this building category is changed to 4.5 $Wh/m^2$ during the same operating hours. This focus of this thesis is not to discuss the reason for this change of standardized hot water demand from SN/TS 3031:2016 to SN-NSPEK 3031:2020, but it illustrates that energy demand for hot water is difficult to determine precisely and varies substantially for different buildings and user patterns.

The Standards SN/TS 3031:2016 and SN-NSPEK 3031:2020 also has standardized values for annual operating days. SN/TS 3031:2016 recommends five days a week and 44 weeks of operation annually. The same number of operating days as for school buildings, which are closed during summer and in school holidays. This is not the case for 3T Sluppen which are open all days of the week the entire year. In this thesis it has therefore been decided to use the daily energy demand for hot water from SN/TS 3031:2016 and SN-NSPEK 3031:2020, but changing the amount of operating days to 7/52 days/weeks because it is assumed to be more suitable for 3T Sluppen.

3T Sluppen is estimated to have a length and width of 80x25 meters resulting in a total area of approximately 2000 $m^2$. The hot water demand of 3T Sluppen were then calculated using Equation 4.2 and 4.3 below, where P is the average hourly power demand for hot water according to the mentioned standards and $h_d$ is the amount of hours with hot water demand per day.

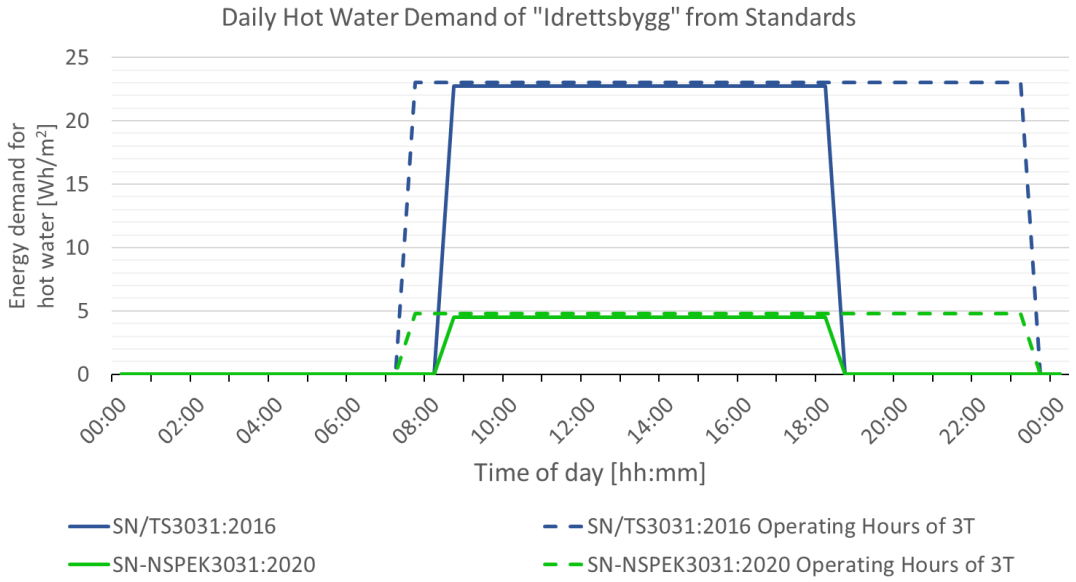


**Figure 4.7:** Daily hot water demand curve for building category "Idrettsbygg" from Standards SN/TS 3031:2016 and SN-NSPEK3031:2020 Table A.2. [85], [86]

$$E_{HotWater} = \frac{P \cdot \dot{h_d} \cdot days \cdot Area}{10^3}[kWh] \tag{4.2}$$

$$V_{Hot_Water} = \frac{E_{HotWater}}{3600 \cdot C_p \cdot \Delta T_{Water} \cdot \rho} \cdot 1000[liter] \tag{4.3}$$

### Export of Hot water by M-TES

In this thesis the main focus is heat pump configurations for waste heat recovery, it is therefore assumed that excess hot water production over the demands of Austmann and 3T Sluppen is exported out of the area by for instance mobile thermal energy storage (M-TES). The solution of M-TES is not investigated in detail besides how the chosen method of M-TES impacts the choice of heat recovery heat pump configuration.

## 4.3 Initial Calculations in EES

In order to get an impression of suitable advanced high temperature heat pump configurations for the intended heat pump installations initial simplified calculations were performed using the refrigerant calculator in Engineering Equations Solver EES, which uses thermal properties from the Refprop refrigerant library. The results of the initial calculations are presented in Section 5.1.1, 5.1.2, 5.1.3 and 5.1.4. All developed models utilizes the same heat source and $CO_2$ secondary circuit and thus are set to have the same evaporation temperature of the LTC. The developed EES scripts are attached in Appendix E

### 4.3.1 EES — Model A1

A similar 2-step cascade heat pump as for SLV17A is also a possible solution for SLV10. The schematics of the solution can be seen in Figure 4.8. The developed model of the 2-step R290/R600 cascade heat pump developed in EES was as for SLV17A used to calculate the initial starting parameters for the dynamic simulation model in Dymola. The two compressors are set to have a suction gas superheat of 15K and 20K for the Propane and Butane compressor respectively.

The most important difference for the 2-step cascade heat pump for SLV10 compared to the intended heat pump at SLV17A, is the lower heat source temperature. Thus a lower evaporation temperature of -15$°C$. Input parameters for, and results of the A1 EES-model can be seen in Table 4.1,5.1 and 5.2. The volumetric and isentropic compressor efficiencies was assumed to be 0.6 and 0.7 for the LTC R290 compressor. Likewise for the R600 Compressor the compressor efficiencies were assumed to be identical to the efficiencies of the R600 compressor intended for Sluppenveien 17A. This was assumed due to the identical evaporation and condensation temperature of the R600 cycles in the respective heat pump models.

**Table 4.1:** Model A1 — Input parameters EES-model

| | LTC | HTC | Unit |
|---|---|---|---|
| Working Fluid | R290 | R600 | — |
| $T_E$ | -15 | 53 | $°C$ |
| $T_C$ | 56 | 103 | $°C$ |
| $T_{Sh_{Evap}}$ | 4 | 9 | K |
| $T_{Sh_IHX}$ | 11 | 11 | K |
| $T_{SubCooling}$ | 5.8 | 7.3 | K |
| Isentropic Efficiency $\eta$ | $\approx 0.6$ | 0.66 | — |
| Volumetric Efficiency $\lambda$ | $\approx 0.7$ | 0.84 | — |

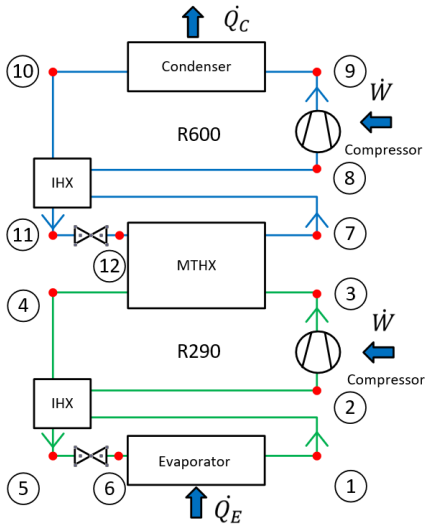


**Figure 4.8:** Schematics of Model A1

### 4.3.2 EES — Model B1

The B1 model is in many aspects similar to the A1 model, but slightly modified for hot water production. The evaporation and condensation temperatures were set to -15/33 °C and 30/73 °C for the Propane and Butane cycle respectively. The condensation temperature of 73 °C was chosen in order to produce 70 °C hot water, assuming 3 K temperature difference in the heat exchanger. The temperature levels in the cascade heat exchangers were set to 33/30 °C in order to have similar temperature lifts of the two cascade cycles, a slightly lower temperature lift of the HTC was chosen to avoid problems with high compressor discharge temperatures and following operation and maintenance problems. The compressor efficiencies of both compressors were in the initial EES modeling assumed to be 0.7 and 0.8 for the volumetric and isentropic efficiency respectively. The heat sink inlet and outlet temperature of the hot water produced was set to 4 °C and 70 °C. Due to the low heat sink inlet temperature the internal heat exchanger of the R600 cycle has been removed in order to allow more sub-cooling of the condenser.

**Table 4.2:** Model B1 — Input parameters EES-model

| | LTC | HTC | Unit |
|---|---|---|---|
| Working Fluid | R290 | R600 | — |
| $T_E$ | -15 | 30 | $°C$ |
| $T_C$ | 33 | 73 | $°C$ |
| $T_{Sh_{Evap}}$ | 4 | 9 | K |
| $T_{Sh_IHX}$ | 11 | 11 | K |
| $T_{SubCooling}$ | 6.5 | 39 | K |
| Isentropic Efficiency $\eta$ | 0.7 | 0.7 | — |
| Volumetric Efficiency $\lambda$ | 0.8 | 0.8 | — |

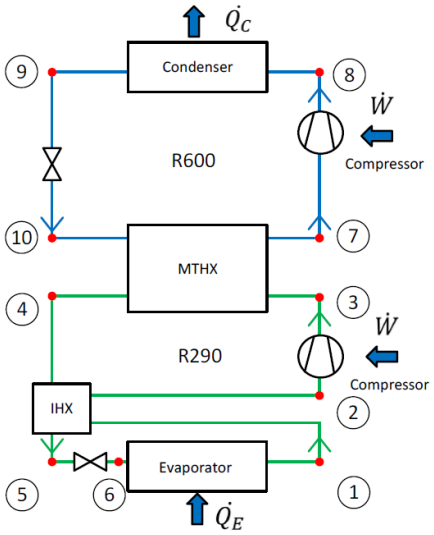


**Figure 4.9:** Schematics of Model B1

### 4.3.3 EES — Model B2

The B2 model is a similar R290/R600 cascade heat pump as B1 intended for hot water production. With the same assumed inlet and outlet water temperatures of the heat sink. The main difference between the two models is an extra heat exchanger added to the R290 LTC, the heat exchanger pre-heats the hot water going in to the R600 condenser, thus reducing the amount of heat going through the Butane cycle. This should in theory reduce the mass flow of the Butane cycle and compression work, thus increasing COP. This solution also increases the amount of subcooling of the Propane cycle, an additional benefit of this solution. The original idea was to pre-heat the water to a temperature around 50 °C, then using the butane cycle just to heat the water the additional 20 decrees. However this resulted in a compression ratio of the Butane cycle falling below 2, this idea was therefore disregarded due to the low compression ratio and fear of low Butane compressor isentropic efficiency. The evaporation and condensation temperatures of the two cycles were therefore set equal the the temperatures of the B1 model.

**Table 4.3:** Model B2 — Input parameters EES-model

| | LTC | HTC | Unit |
|---|---|---|---|
| Working Fluid | R290 | R600 | — |
| $T_E$ | -15 | 30 | $°C$ |
| $T_C$ | 33 | 73 | $°C$ |
| $T_{Sh_{Evap}}$ | 4 | 9 | K |
| $T_{Sh_IHX}$ | 11 | 11 | K |
| $T_{SubCooling}$ | 33.2 | 39 | K |
| Isentropic Efficiency $\eta$ | 0.7 | 0.7 | — |
| Volumetric Efficiency $\lambda$ | 0.8 | 0.8 | — |

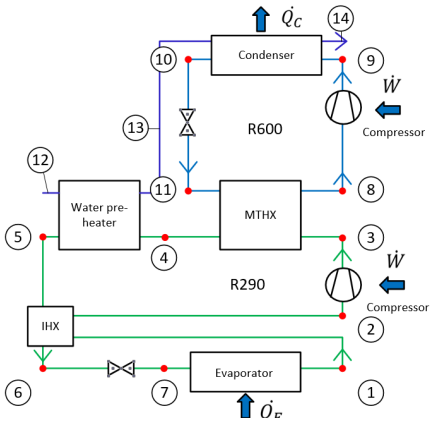


**Figure 4.10:** Schematics of Model B2

### 4.3.4 EES — Model C1

A more traditional method of hot water production is using a trans-critical $CO_2$ heat pump. It was therefore also developed a $CO_2$ heat pump model in order to compare the performance of the R290/R600 cascade heat pumps against a more traditional hot water producing heat pump. The $CO_2$ heat pump was set to have the same evaporation temperature as the previously described models. Being a trans-critical heat pump, the model does not have a constant condensation temperature, but a constant gas cooler pressure. The gas cooler pressure was initially set to 95 bar, calculated from Equation 2.13 in the presented theory. But later reduced to 90 bar in order to reduce discharge gas temperature. The volumetric and isentropic efficiency of the compressor was assumed to be 0.8 and 0.7 as the previous models.

**Table 4.4:** Model C1 — Input parameters EES-model

| | LTC | Unit |
|---|---|---|
| Working Fluid | R744 | — |
| $T_E$ | -15 | $°C$ |
| $P_C$ | 90 | $bar$ |
| $T_{Sh_{Evap}}$ | 0 | K |
| $T_{Sh_IHX}$ | 10 | K |
| $T_{Out-Gas}$ | 7 | K |
| Isentropic Efficiency $\eta$ | $\approx 0.7$ | — |
| Volumetric Efficiency $\lambda$ | $\approx 0.8$ | — |

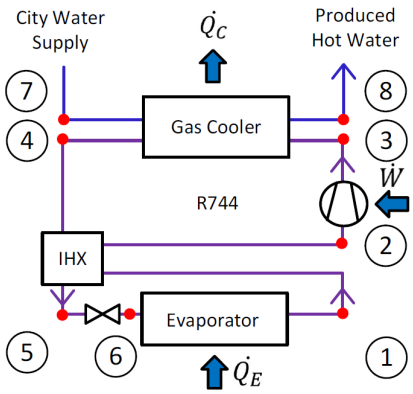


**Figure 4.11:** Schematics of proposed 2-step cascade HTHP SLV10

### 4.3.5 Calculation of compressor efficiencies

For all models a suitable compressor was chosen using software available from the compressor manufacturers Mario Dorin Spa. [87] and Bitzer [88]. The volumetric and isentropic compressor efficiencies were for each operating point and compressor calculated using compressor polynomials and coefficients attached in Appendix C.6, Table C.33 in combination with Equation 2.10 and 2.11. The polynomials calculate shaft power of the compressors and refrigerant mass flow at various evaporation/condensation temperatures. The isentropic efficiency calculated is thus the Effective isentropic efficiency including heat losses to the ambient and other losses. Heat losses to the ambient is in this thesis assumed to be 10% of the compressor shaft power. By doing so, the isentropic efficiency excluding heat losses which is needed as an input in Dymola can be estimated using Equation 2.11 by subtracting 10% from the compressor shaft power. The difference between the isentropic and effective isentropic efficiency is further described in Subsection 4.4.1.

Using the method described above for a fixed evaporation temperature of and variable condensation temperature in EES [89] the compressor efficiencies was plotted for variable pressure ratios. Figure 4.12 below show the calculated Volumetric, Isentropic and Effective isentropic efficiency for the Dorin Propane compressor "HEX4500CS" for -15 °C evaporation temperature and a condensation temperature ranging from 0 to 90 °C. For this compressor at this evaporation temperature the minimum and maximum condensation temperature is 20 °C and 65°C respectively given by the Dorin Software [87]. This is illustrated in the figure with the dotted lines showing the minimum and maximum pressure ratio.

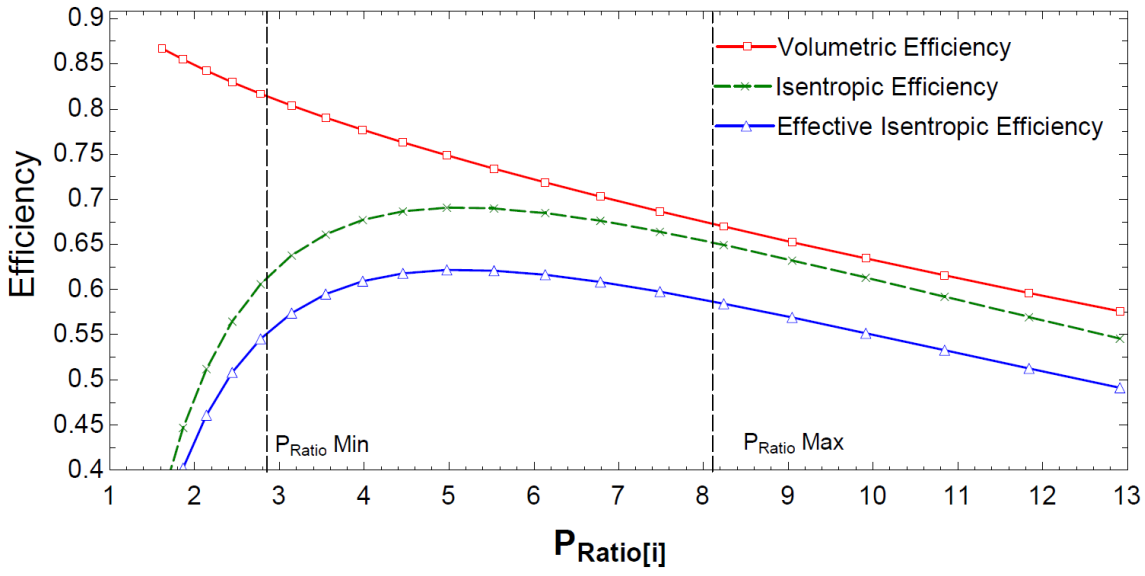


**Figure 4.12:** Volumetric and isentropic compressor efficiency for Dorin HEX4500CS R290 Compressor for variable pressure ratios.

## 4.4 Dynamic Modeling in Dymola

5 Dynamic simulation models of possible HTHP configurations have been developed using the program Dymola 2020 [1], and the TLK-Thermo GmbH refrigerant and component libraries [90]. Based on the object oriented programming language Modelica, Dymola and the TLK-Thermo GmbH libraries provide tools to model advanced thermal systems and run transient simulations of complex heat pump configurations. The TIL 3.5.0 component library contains several pre-modeled components such as; heat exchangers, valves, pumps and compressors. The refrigerant library TIL-Media contains a variety of commonly used refrigerants and secondary fluids.

Several assumptions and simplifications have been made to create the models, they are therefore a simplified representation of reality. The validity of the models therefore rely on the assumptions made. All models simulated for a time period of 3600 seconds or more, with one time interval per second. It was assumed that any errors due to incorrect initialization values would have stabilized after one hour of simulation.

### 4.4.1 General Modeling Approach

#### General System Model

A total of 5 simulation models have been developed in Dymola using parameters described in Section 4.3.1-4.3.4. This subsection describes the general method of developing all Dymola models, with examples from the 2-Step Cascade R290/R600 Model. Figure 4.13 shows the complete Dymola model of the developed 2-Step Cascade Solution similar to SLV17A, the model is however simplified for illustrative purposes. The model consists out of two closed vapour compression cycles (CVCC), a LTC R290 cycle and a HTC R600 cycle, connected through a cascade heat exchanger.

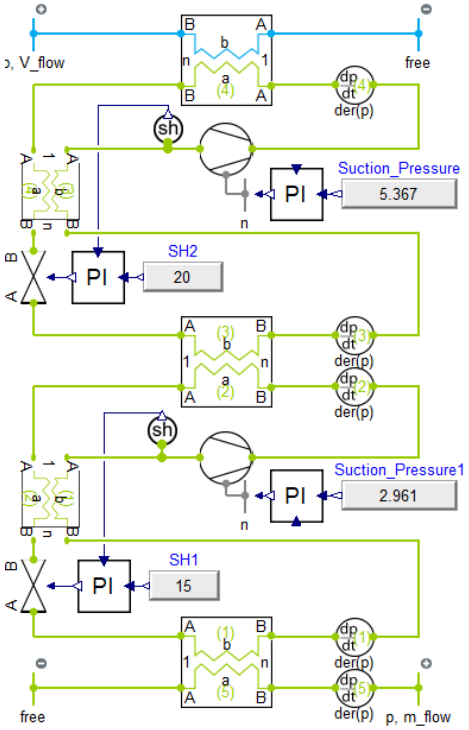


**Figure 4.13:** Simplified Cascade HTHP model snipped from Dymola.

Each CVCC is modeled with a evaporator, compressor, condenser, internal heat exchanger and expansion valve. All evaporators, condensers and internal heat exchangers are modeled as counter flow plate heat exchangers. The compressors was initially modeled with constant isentropic and volumetric efficiency. For each CVCC the amount of superheat is regulated by the expansion valve through a PI-controller. The Compressor speed is regulated by PI-controllers as well to maintain a set evaporation pressure.

Detailed input parameters for all major components of the developed models can be seen in Appendix C.1-C.30. The detailed modeling of the different component will first be presented, then the method of combining the separate components into a complete system as seen in Figure 4.13.

### Heat Exchangers

As previously mentioned, the evaporator, condenser, cascade heat exchanger and IHXs was modeled in Dymola using the pre-modeled heat exchanger "ParallelFlowHX" in the TIL Component library. The entire heat pump installation was dimensioned to have an design evaporator capacity of 60 $kW$, partly due to the uncertainties in cold store cooling demand and this value correlating to the capacity of the more developed SLV17A cascade. The needed surface area of each heat exchanger was initially calculated using Equation 4.4. The evaporator, cascade heat exchanger and condenser was assumed to have a width and length of 0.3 m and 0.6 m. Likewise for the IHXs the measurements of 0.3m x 0.1m was assumed.

$$\dot{Q} = \dot{V} \cdot \rho \cdot C_P \cdot \Delta T = U \cdot A \cdot LMTD_{HX} = \dot{m}_R \cdot \Delta h \tag{4.4}$$

Equation 4.4 assumes a constant heat transfer coefficient $U[W/m^2K]$ for the entire heat exchanger surface. It is known from theory that the heat transfer properties of a liquid is superior to the heat transfer properties of the corresponding gas under similar conditions. For the evaporator, cascade heat exchanger and the condenser the rate of heat transfer is not constant, because phase change occurs. Equation 4.4 was therefore modified by assuming that subcooling and superheat happens on a fixed fraction of the total heat exchanger length. The fraction of heat exchanger length on which superheat of the refrigerant occurs ($\frac{L_{Sh}}{L_{total}}$) was assumed to be 0.2.

$$\dot{Q} = U_{no-sh} \cdot (1 - \frac{L_{Sh}}{L_{total}}) \cdot A_{total} \cdot LMTD_{no-sh} + U_{gas} \cdot \frac{L_{Sh}}{L_{total}} A_{total} \cdot LMTD_{sh} \tag{4.5}$$

**Table 4.5:** U-values of Propane and Butane used in determining the needed heat exchanger area.

| U-value | | | | | |
|---|---|---|---|---|---|
| | R290 | R600 | R744 | Water | |
| Condensing vapour-liquid mixture | 800 | 800 | 800 | 1500 | $[W/m^2K]$ |
| Evaporating vapour-liquid mixture | 600 | 600 | 600 | 1500 | $[W/m^2K]$ |
| Gas | 100 | 100 | 100 | | $[W/m^2K]$ |

The heat transfer properties of the heat exchangers turned out to be difficult to determine precisely. The heat transfer properties vary with; temperature range, fluid type, fluid-phase, fluid velocity and many other parameters. It was therefore decided to simplify the problem by assuming constant heat transfer coefficients based on the presented theory in Table 2.1. The presented theory gives a combined heat transfer coefficient for both water and working fluid, but the Dymola model requires individual heat transfer coefficients for each fluid. It was chosen to use the heat transfer coefficients presented in Table 4.5, where the heat transfer coefficient is decreasing in size for liquids, condensing fluid, evaporating fluid and gases. Based on the parameters given in Table 5.2 and U-values in Table 4.5 the heat transfer area and thus number of plates in the; evaporator, cascade heat exchanger, condenser and IHXs were determined using Equation 4.5 and 4.4 respectively.

### Compressors

The compressors was modeled using the ”EffCompressor” component in the TIL 3.5.0 component library. The input parameters of this component are: rotational speed (Hz), displacement ($m^3$) as well as fixed volumetric and isentropic compressor efficiencies. The compressor efficiencies of a given compressor can be calculated using Equation 2.10 and 2.11 in combination $W_C$ and $\dot{m}$ estimated from compressor polynomials given by the manufacturer.

Several attempts of implementing variable compressor efficiencies using compressor polynomials and ”statePoints” was made in Dymola, with little success. Both modifying the EffCompressor-model and creating a new custom compressor model was unsuccessful. It is believed that the problems occurred due to limitations in the TIL-Component library not allowing for input of compressor efficiencies from components in the Dymola-model which are not included in the TIL Component library.

Based on the estimated cooling demand in Figure 4.3 it is believed that a heat recovery heat pump with 60 kW evaporator capacity would have very stable operating conditions and over full-load hours over 8000, per year. Thus little variation in pressure ratio and compressor efficiencies. It was therefore decided to use constant volumetric and isentropic efficiency, calculated in EES at the respective compressors operation point and type of compressor chosen from manufacturer.

For all compressors a compressor model was chosen based on the desired evaporation, suction and condensation temperature and desired refrigerant volume flow calculated in EES. The displacement in Dymola was then calculated with Equation 4.6, where $V_{Nom}$ is the nominal displacement of the compressor at 50 Hz. The Eff Compressor model in the TIL Component library has three inputs for compressor efficiencies; Volumetric-, Isentropic- and Effective Isentropic efficiency. Volumetric efficiency is used for calculation of refrigerant mass flow, while the isotropic and effective isentropic efficiencies are used for calculation of compressor outlet state point and shaft power respectively. Due to friction losses and heat losses to the ambient the effective isentropic efficiency is lower than the isentropic efficiency. The TIL Component library definition of volumetric, isentropic and effective isentropic efficiency can be seen in Figure 4.14 below.

$$V_{Disp} = \frac{V_{Nom}}{3600 \cdot 50} \tag{4.6}$$

| value | equation | type of losses |
|---|---|---|
| volEff | $\lambda_{eff} = \frac{m_{dot}}{V_{displacement} \cdot n \cdot \rho_{Suction}}$ | Ratio of the actual mass flow rate and the theoretically possible mass flow rate. |
| isEff | $\eta_{isen} = \frac{h\_isentropic_{Discharge} - h_{Suction}}{h_{Discharge} - h_{Suction}}$ | Ratio of the enthalpy increase during an isentropic compression and the actual enthalpy increase during the compression. |
| effIsEff | $\eta_{effIsen} = \frac{m\_flow\left(h\_isentropic_{Discharge} - h_{Suction}\right)}{P_{shaft}}$ | Ratio of the isentropic enthalpy transported to the VLEFluid and the supplied mechanical power. |

**Figure 4.14:** Definition of Volumetric, Isentropic and Effective Isentropic efficiency used in the TIL Component "EffCompressor" snipped from the TIL Component library information document [90].

In order to make the models more dynamic and able to handle different operating conditions a variable compressor speed was implemented. This was done in Dymola using an "Mechanical Rotatory Boundary" and a PI-controller. For the LTC R290 cycle the compressor PI-Controller was set to have a fixed evaporator pressure of 2.916$bar$, correlating to an evaporation temperature of -15$°C$. The HTC R600 compressor PI-Controller was set to maintain a constant evaporation temperature of 53$°C$ when set to deliver heat to the district heating. This was achieved by regulating the evaporation pressure.

$$P_{Shaft} = Given\ by\ compressor\ polynomial \quad p = f(T_E, T_C) \tag{4.7}$$

$$\dot{m}_{Actual} = Given\ by\ compressor\ polynomial \quad m = f(T_E, T_C) \tag{4.8}$$

### Expansion Valves

In both CVCC the refrigerant mass-flow $\dot{m}_R$ and the amount of suction gas superheat is regulated by the expansion valves using a PI-Controller. For the R290 and R600 cycle the desired suction gas superheat was set to 15K and 20K respectively. Both expansion valves were modeled using the "Orifice Valve" a part of the "VLE Fluid Components" group in the TIL 3.5.0 Component library. The PI-controller adjusts $\dot{m}_R$ and superheat by changing the effective flow area of the orifice valves. The LTC and HTC expansion valve PI-controller were set to maintain a superheat of 15 K and 20 K respectively at the compressor inlet. For the developed $CO_2$ hot water heat pump models the valve was set to maintain a fixed gas cooler pressure. The effective valve flow area at design conditions was calculated in EES using Equation 4.9 below.

$$A_{Valve} = \frac{\dot{m}_{Ref}}{\sqrt{(P_C - P_E) \cdot 2\rho_{inlet}}} \tag{4.9}$$

### Combining the components

The process of combining the different components into a complete system, was simplified by initially modeling the R290 LTC and the R600 HTC as to separate cycles, with fixed heat source and heat sink conditions. The heat sink and heat source conditions were fixed to the values achieved in the initial calculations in EES (See Tables 5.1, 5.3, 5.5 and 5.7 ), using ”over-determined” and ”under-determined” boundaries in the TIL Component library.

For both cycles the process of combining the components was done by combining the evaporator and expansion valve of the respective cycle. With fixed heat source conditions, a PI-controller was introduced to regulate the superheat out of the evaporator. The condenser and compressor were then also implemented creating a complete CVCC. Lastly the IHX was implemented and sized to achieve the desired superheat at the compressor suction side. ”StatePoints”, pressure and temperature sensors were put before and after each component to get a better overview of the cycle. Figure 4.15 and 4.16 show the complete Propane and Butane cycles used when combining the different components, the figure does not include the ”statePoints” and sensors. Custom ”display-boxes” was also created, displaying COP, Compressor-displacement as well as evaporator- and condenser power.

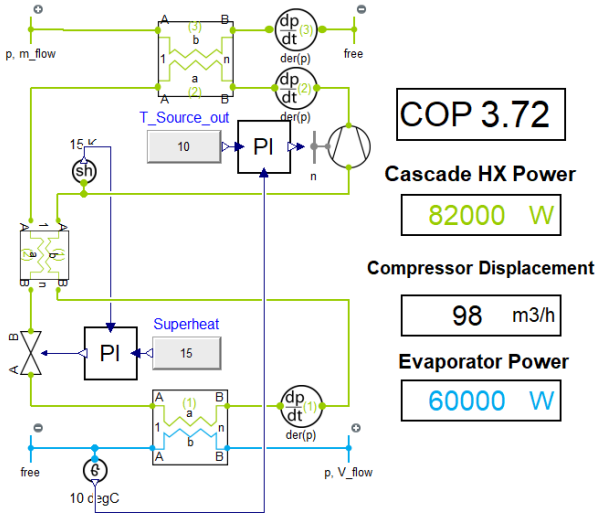


**Figure 4.15:** LTC Propane CVCC Heat pump developed in Dymola.

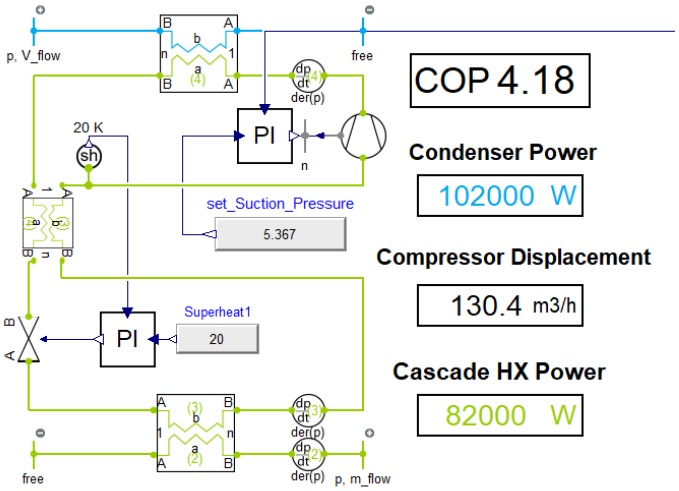


**Figure 4.16:** HTC Butane CVCC Heat pump developed in Dymola.

The number of plates in each heat exchanger was manually changed from the initial calculated area from Equation 4.5, while keeping a constant volume/ mass-flow through the compressor. Too low/high Evaporation pressure was solved by increasing/decreasing the heat exchanger surface area. Likewise for the condenser to high/low condensation pressure was solved by increasing/decreasing the condenser surface area. This was done in small increments of 5-10 plates until similar results as in the EES-model was achieved. Lastly the two cycles were combined into one cascade heat pump system, as seen in Figure 4.13.

### 4.4.2 CO2-Secondary circuit

All developed dynamic heat pump simulation models in Dymola uses the same $CO_2$ Circuit intended to transport the waste heat from the heat source to where the heat pump model is placed. The placement of the heat recovery heat pump could vary based on if the waste heat is delivered to the district heating grid or to hot water production. The focus of this thesis is therefore only to describe the basic principle of the $CO_2$ circuit. The $CO_2$ circuit model mainly consist of two heat exchangers and a circulation pump. Heat is extracted from the existing chiller ethyleneglycol-circuit by evaporation of $CO_2$ at 26.6 bar. The $CO_2$ then is transported in an insulated pipe to the evaporator, where the $CO_2$ is condensed back to liquid phase. The circulation pump is controlled using a PI-regulator regulating the mass-flow of $CO_2$ in order to maintain the -6°C supply temperature set point of ethyleneglycol to the cold store. The maximum mass flow of the circulation pump is limited so the set point temperature is only achieved if the cooling demand of the cold store is less than the evaporation capacity of the heat recovery heat pump. Additional cooling demand is therefore covered by the existing chillers. The ethyleneglycol inlet temperature is calculated using Table 3.3 and the estimated cooling demand shown in Figure 4.2. Due to limitations in choice of brine in the TIL Media library, 40% Mass-fraction propyleneglycol/water mixture was set in the simulation models in stead of ethyleneglycol. It is assumed that propyleneglycol has thermo-physical properties comparable to ethyleneglycol.

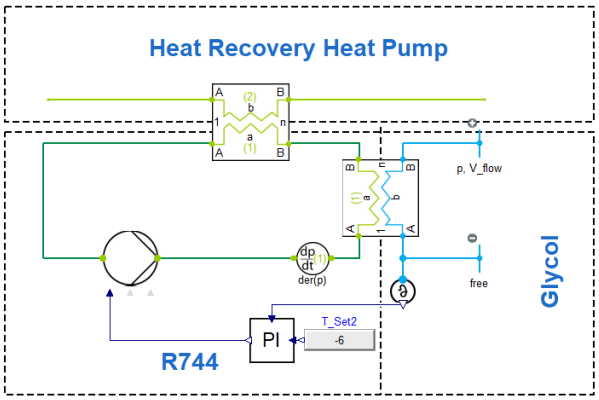


**Figure 4.17:** $CO_2$-Circuit — Simplified Cascade HTHP model snipped from Dymola.

### 4.4.3 Dymola — Model A1

A dynamic simulation model of the ”Model A1” heat pump configuration have been developed in Dymola using the general method described in Section 4.4.1 and the results of the initial calculation in EES (Section 5.1.1 ). The LTC and HTC is set to have a constant evaporation temperature of -15 °C and 53 °C respectively and a temperature lift of 71 and 50 K, for the LTC and the HTC. According to the initial steady state calculation of this heat pump configuration should the LTC and HTC compressor have a nominal refrigerant volumetric flow rate of about 225 and 149 $m^3/h$. From using the Dorin Compressor selection software [87] at these conditions the two compressors ”HEX7500CC” and ”HEX7501CS” was found to be most suitable for the Propane Cycle. According to the Dorin Software they have a volumetric flow rate of 199.86 and 221.75 $m^3/h$ and evaporator capacity of 59.5 and 65.5 kW at the conditions described in Table 4.1.The largest compressor ”HEX7501CS” because it was the most suitable compressor with for an evaporator capacity above 60 kW.

For the Butane Cycle the choice of compressor was not so simple using the Dorin Software because Butane is not a viable choice of refrigerant in the software. It was therefore assumed that the Propane compressors in the software would be able to use Butane as refrigerant as well, this was done based on the presented refrigerant theory and the fact that Dorin was able to convert a Propane Compressor to Butane for the Sluppenveien 17A heat pump configuration. An other limitation in the Dorin Software was the maximum evaporation temperature of 0 °C and 10 °C for Propane ”CS” and ”CC” models. The choice of Butane compressor was therefore done in the software by selecting R290 as refrigerant and adjusting the desired evaporator capacity until a compressor with suitable volumetric flow was recommended by the software. The compressor HEX5000CC and HEX4500CS were the closest match to the volumetric flow rate of 149 $m^3/h$ from EES. The ”CC” model was selected due to the 10 °C higher maximum suction temperate than the ”CS” model.

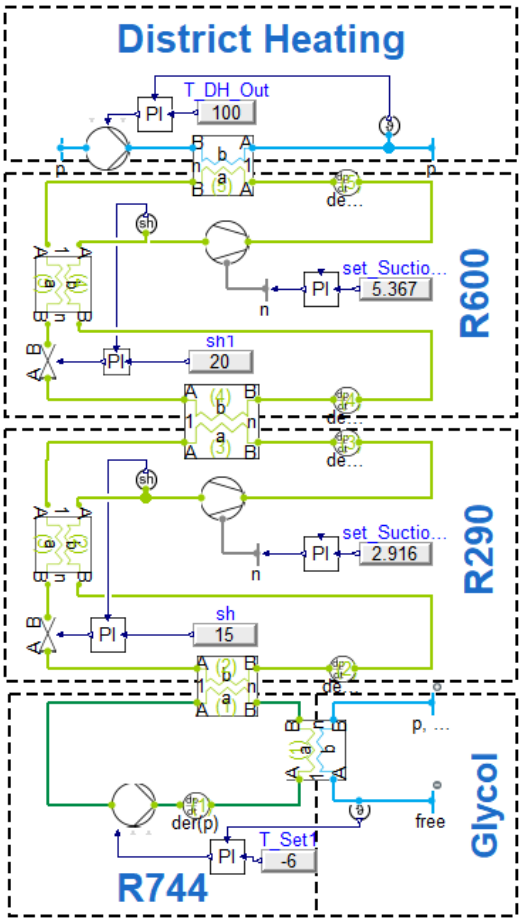


**Figure 4.18:** Model A1 — Simplified Cascade HTHP model snipped from Dymola.

It was assumed that this compressor is able to handle the 73 °C suction temperature of the Butane cycle by choosing a more advanced lubrication oil with a higher viscosity index. Using Equation 4.6 the Displacement of the LTC and HTC compressors was set to $1.2319 \cdot 10^{-}3$ and $8.5288 \cdot 10^{-}4\ m^3$ in the Dymola Model.

The volumetric and isentropic efficiencies of the two compressors was calculated using the method described in Section 4.3.5. For the Propane compressor the evaporation and condensation temperature was used directly into the EES calculation of the compressor efficiencies. The polynomials are only applicable for Propane as refrigerant and therefore not suitable for calculation of Butane compressor efficiencies. The original idea was to plot the efficiency curves of each compressor model for a range of pressure ratios and assuming that the Butane compressor efficiencies were similar as a Propane compressor operating under the same pressure ratio. However the compressor inlet density and isentropic compression work is different for Butane and Propane which have an impact on the calculated efficiencies. Due to the uncertainty of estimating the Butane compressor efficiencies using the polynomials it was assumed that this would result in no improved accuracy than assuming constant efficiencies from theory. The Volumetric-, Isentropic- and Effective Isentropic efficiencies of the Butane compressor was therefor assumed to be 0.8, 0.7 and 0.6 respectively. Figure 4.19 below show that the HEX7501CS compressor is operating within the operational area approved by the manufacturer.

**Table 4.6:** Model A1 — Compressor input parameters in Dymola Model

| | LTC (R290) | HTC (R600) | Unit |
|---|---|---|---|
| Chosen Compressor | HEX7501CS | HEX5000CC | $[kg/s]$ |
| Nominal Displacement (50 Hz) | 221.75 | 153.52 | $[m^3/h]$ |
| Displacement in Dymola | $1.2319 \cdot 10^{-}3$ | $8.5288 \cdot 10^{-}4$ | $[m^3]$ |
| Pressure ratio $\pi$ | 6.68 | 3.01 | $[--]$ |
| Volumetric Efficiency | 0.70 | $\approx 0.8$ | $[--]$ |
| Isentropic Efficiency | 0.69 | $\approx 0.7$ | $[--]$ |
| Eff. Isentropic Efficiency | 0.62 | $\approx 0.6$ | $[--]$ |

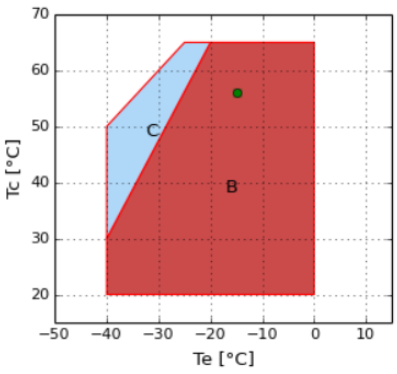


**Figure 4.19:** Model A1 — Operation point of HEX7501CS Compressor, Snipped from Dorin Software [87]

### 4.4.4 Dymola — Model A2

No initial calculations calculations was performed on the Dymola Model A2 this is because this model was created by modifying the Dymola Model A1 to have two stage compression and expansion in the Propane Cycle. The intermediate pressure of the Propane cycle was set to 7.54 bar according to Equation 2.12. The model was simulated with a cooling load of 60 kW and with PI-controllers at each compressor maintaining the set suction pressure of the respective compressor. The initial simulation resulted in a volumetric refrigerant flow rate of; 131.6, 79.2 and 157.3 $m^3/h$ for the LTC, MTC and HTC compressor respectively at set suction pressures of; 2.916, 7.54 and 5.367 bar. The choice of compressor models were then done using the Dorin Software [87] and selecting compressors with nominal displacement at 50 Hz close to the volumetric refrigerant flow rate achieved in the initial simulation. The chosen compressor models and their respective displacement and efficiencies in Dymola is shown in Table 4.7 below.

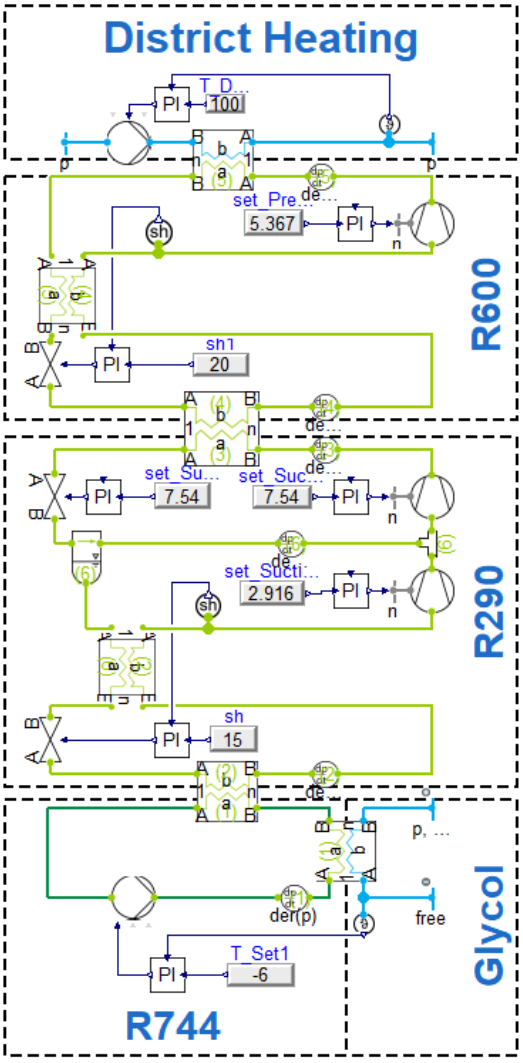


**Figure 4.20:** Model A2 — Simplified Cascade HTHP model snipped from Dymola.

**Table 4.7:** Model A2 — Compressor input parameters in Dymola Model

| | LTC (R290) | MTC (R290) | HTC (R600) | Unit |
|---|---|---|---|---|
| Chosen Compressor | HEX4000CC | HEX2500CC | HEX5000CC | $[kg/s]$ |
| Nominal Displacement (50 Hz) | 127.5 | 75.83 | 153.52 | $[m^3/h]$ |
| Displacement in Dymola | $7.0833 \cdot 10^-4$ | $4.2127 \cdot 10^-4$ | $8.5288 \cdot 10^-4$ | $[m^3]$ |
| Pressure ratio $\pi$ | 2.59 | 2.58 | 3.01 | $[--]$ |
| Volumetric Efficiency | 0.82 | 0.92* | $\approx 0.8$ | $[--]$ |
| Isentropic Efficiency | 0.59 | 0.81* | $\approx 0.7$ | $[--]$ |
| Eff. Isentropic Efficiency | 0.53 | 0.73* | $\approx 0.6$ | $[--]$ |

*Calculated with an evaporation temperature of 17°C, which is higher than the maximum evaporation temperature of 10°C set the compressor manufacturer.

### 4.4.5 Dymola — Model B1

Since the development of the heat recovery heat pump installation for Sluppenveien 17A is more progressed, it is interesting to investigate if this heat pump configuration is applicable for hot water production at Sluppenveien 10. The results of the initial calculations resulted in a pressure ratio of 3.98 and 3.06, and refrigerant flow rate of 151.2 and 143.4 $m^3/h$, for the Propane and Butane cycle respectively. The selection of compressors and calculation of compressor efficiencies was done using the same method as described in Section 4.4.3 and the selected compressors as well as compressor input parameters in the Dymola model is shown in Table 4.8. As for the previous models, the Volumetric-, Isentropic- and Effective Isentropic efficiencies of the Butane compressor was therefor assumed to be 0.8, 0.7 and 0.6 respectively. From Figure 4.22 it can be seen that the propane compressor operates within its valid operational area. The compressor diagram for the butane compressor is not included due to the Dorin Software not supporting Butane as a refrigerant.

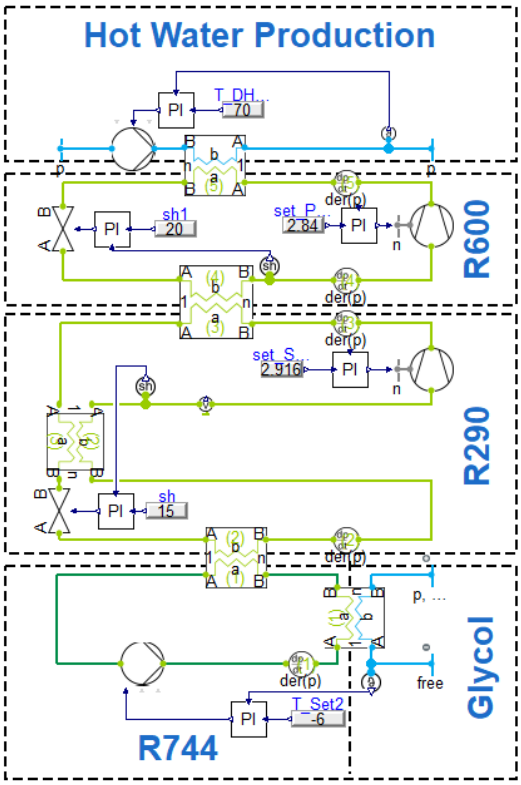


**Figure 4.21:** Model B1 — Simplified Cascade HTHP model snipped from Dymola.

**Table 4.8:** Model B1 — Compressor input parameters in Dymola Model

| | LTC (R290) | HTC (R600) | Unit |
|---|---|---|---|
| Chosen Compressor | HEX4500CS | HEX5000CC | $[kg/s]$ |
| Nominal Displacement (50 Hz) | 153.52 | 153.52 | $[m^3/h]$ |
| Displacement in Dymola | $8.529 \cdot 10^{-4}$ | $8.529 \cdot 10^{-}4$ | $[m^3]$ |
| Pressure ratio $\pi$ | 3.98 | 3.06 | $[--]$ |
| Volumetric Efficiency | 0.78 | $\approx 0.8$ | $[--]$ |
| Isentropic Efficiency | 0.68 | $\approx 0.7$ | $[--]$ |
| Eff. Isentropic Efficiency | 0.61 | $\approx 0.6$ | $[--]$ |

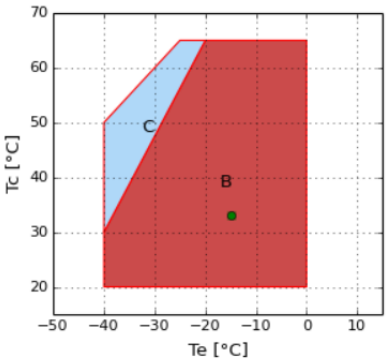


**Figure 4.22:** Model B1 — Operation point of HEX4500CS Compressor, Snipped from Dorin Software [87]

### 4.4.6 Dymola — Model B2

In order to further improve the performance of the R290/R600 cascade heat pump for hot water production the B1 model was modified as described in Section 4.3.3. The model is identical to the B1 model except the water pre-heating heat exchanger and the number of plates in the Propane IHX, Cascade HX and Butane Condenser was adjusted in order to compensate for the changed heat transfer rates and LMTD. The selection of compressors and calculation of compressor efficiencies have been done with the same method as described in previous subsections. The compressor input values in Dymola and the operational point of the Propane compressor can be seen in Table 4.9 and Figure 4.24 below. As for the previous models, the Volumetric-, Isentropic- and Effective Isentropic efficiencies of the Butane compressor was therefor assumed to be 0.8, 0.7 and 0.6 respectively.

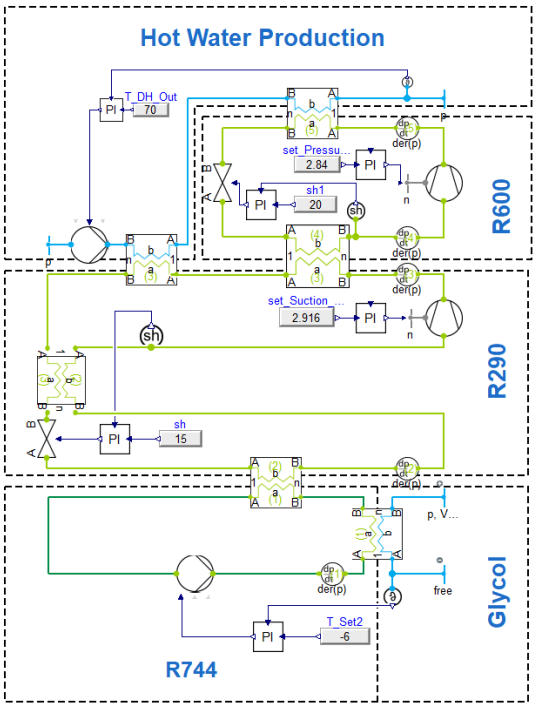


**Figure 4.23:** Model B2 — Simplified Cascade HTHP model snipped from Dymola.

**Table 4.9:** Model B2 — Compressor input parameters in Dymola Model

| | LTC (R290) | HTC (R600) | Unit |
|---|---|---|---|
| Chosen Compressor | HEX3500CS | HEX2500CC | $[kg/s]$ |
| Nominal Displacement (50 Hz) | 127.52 | 75.83 | $[m^3/h]$ |
| Displacement in Dymola | $7.084 \cdot 10^{-}4$ | $4.2127 \cdot 10^{-}4$ | $[m^3]$ |
| Pressure ratio $\pi$ | 3.98 | 3.06 | $[--]$ |
| Volumetric Efficiency | 0.78 | $\approx 0.8$ | $[--]$ |
| Isentropic Efficiency | 0.68 | $\approx 0.7$ | $[--]$ |
| Eff. Isentropic Efficiency | 0.62 | $\approx 0.6$ | $[--]$ |

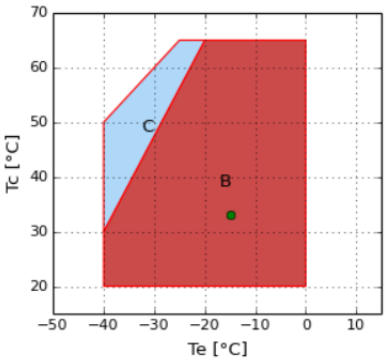


**Figure 4.24:** Model B2 — Operation point of HEX3500CS Compressor, Snipped from Dorin Software [87]

### 4.4.7 Dymola — Model C1

The $CO_2$ hot water heat pump model is different from the previously described models, especially in the way the gas cooler pressure and compressor inlet superheat is maintained. The gas cooler pressure is controlled by regulating the expansion valve effective flow area. The compressor inlet superheat is assured by the internal heat exchanger and a separator tank placed at the evaporator outlet. The separator tank assures at least 0 °superheat in to the IHX and thus no liquid droplets at the compressor inlet. The $CO_2$ compressor efficiencies were calculated using the same method as described for the previous models, but a compressor from the manufacturer Bitzer was also considered. The Bitzer compressor 4DTE-25K was chosen because it was recommended by the Bitzer compressor selection software [88] . Table 4.10 below show the input parameters in Dymola for the two chosen compressors from Dorin and Bitzer. The acceptable operation area of the two compressors are quite similar, it was therefore decided to only include the compressor diagram of the Dorin compressor shown in Figure 4.26. A comparison of the compressor efficiencies of the two compressors have been done in Section 5.1.4.

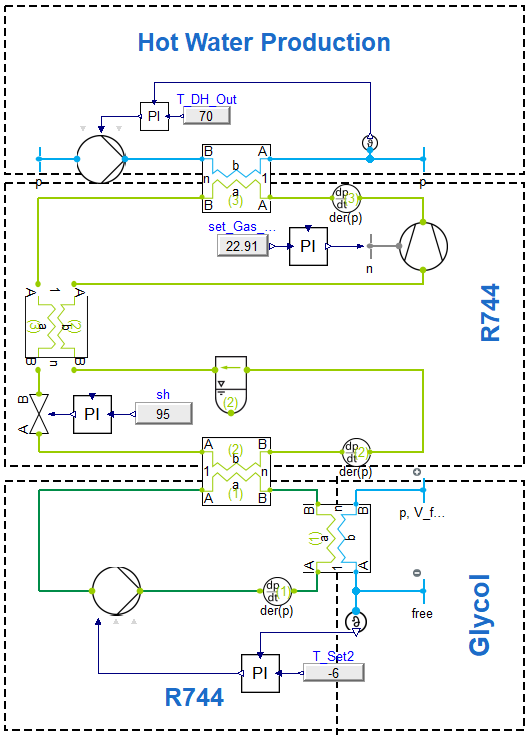


**Figure 4.25:** Model C1 — Simplified Cascade HTHP model snipped from Dymola.

**Table 4.10:** Model C1 — Compressor input parameters in Dymola Model. For set gas cooler pressure 90 bar.

| | R744 | R744 | Unit |
|---|---|---|---|
| Chosen Compressor | CD3501H | 4DTE-25K | $[kg/s]$ |
| Nominal Displacement (50 Hz) | 23.30 | 22.0 | $[m^3/h]$ |
| Displacement in Dymola | $1.294 \cdot 10^{-}4$ | $1.222 \cdot 10^{-}4$ | $[m^3]$ |
| Pressure ratio $\pi$ | 3.93 | 3.93 | $[--]$ |
| Volumetric Efficiency | 0.72 | 0.76 | $[--]$ |
| Isentropic Efficiency | 0.70 | 0.74 | $[--]$ |
| Eff. Isentropic Efficiency | 0.63 | 0.66 | $[--]$ |

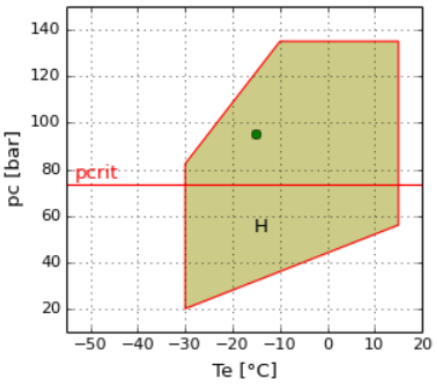


**Figure 4.26:** Model C1 — Operation point of CD3501H Compressor, Snipped from Dorin Software [87]

## 4.5 Simulations and Validation

### 4.5.1 Generating a input signal in Dymola

The estimated cooling demand is converted into a heat source inlet temperature of the heat pump by using 4.10 below, assuming a constant $C_p$ and volume flow from the technical drawing of the system. The set point temperature of the heat sink outlet is set to -6 °C according to the technical specifications of the chiller user manual [80]. A custom converter block was created in Dymola calculating the heat sink inlet temperature of the heat pump given a set point temperature and cooling demand as inputs. The $C_P$ and Volume flow of the brine is assumed constant during the simulations. The simulation models were then tested for 100%, 75% and 50% of the estimated cooling demand assuming that the weekly distribution shown in Figure 4.28 is the same in all three conditions and is representable for the entire year.

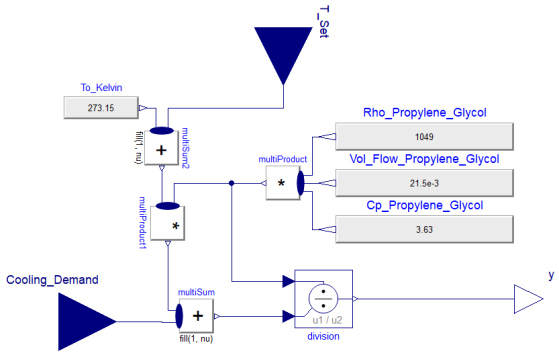


**Figure 4.27:** Custom converter block created in Dymola, converting cooling demand to heat sink inlet temperature.

$$Q = \dot{m}_{Glycol} \cdot C_P \cdot (T_{inlet} - T_{Setpoint}) \tag{4.10}$$

### 4.5.2 Weekly Simulations

All of the previously described models were designed for an nominal evaporation capacity of 60 kW, while the $CO_2$-secondary circuit mass flow and heat exchanger were sized up in order to handle cooling demands up to approximately 68kW. This was done in order to test the performance of the performance of the heat pump configuration at cooling demands slightly above design condition. It also opens the option to set a maximum evaporation capacity between 60 and 68 kW by limiting the maximum speed of the compressors. The minimum evaporator capacity was set to 36 kW, 60% of design condition.

In order to test how the developed simulation models handled different cooling demands the developed models were tested under realistic weekly cooling loads. Figure 4.28 below show the testing pulse used for weekly simulations in Dymola. The signal was made from the estimated cooling demand from weekly average electricity measurements in Figure 4.2 by dividing the estimated cooling demand by the maximum estimated cooling demand of an average week. The cooling demand input in Dymola is then generated by multiplying the signal pulse by the maximum weekly cooling demand. This method

of generating a weekly cooling demand signal in Dymola was chosen because it enables the cooling demand to be easily changed in Dymola by changing the maximum cooling demand constant the signal pulse is multiplied with. The simulation models in Dymola was simulated for 100%, 75% and 50% of the estimated cooling demand in Figure 4.2 in order to investigate the possible consequences of the uncertain cooling demand. From the estimated cooling demand it is assumed that the cooling demand during the summer period with high ambient temperatures is higher than 60 kW at all times of the week. Due to long simulation times and size of result-files from Dymola it has been decided not to simulate the 100% and 75% of the estimated cooling demand because the results would be identical to the steady state simulation.

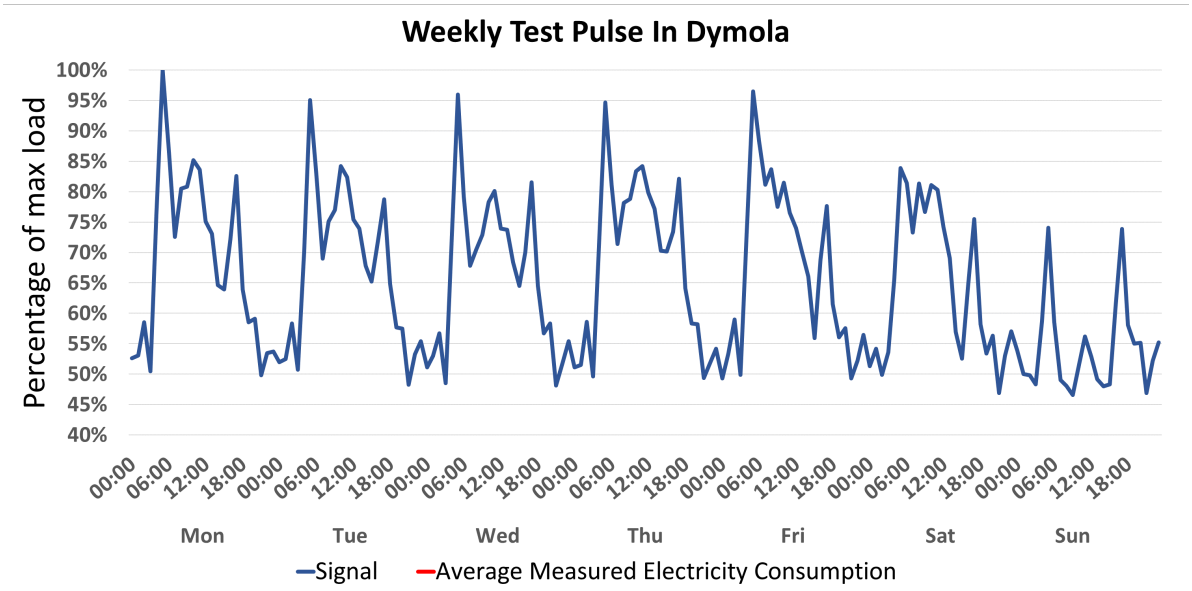


**Figure 4.28:** Weekly Testing pulse used for estimation of SCOP at various max cooling demands in Dymola.

In spring and autumn it is likely that the cooling demand if the cold store is significantly lower than during the summer period. This is not shown in the electricity measurements because it is believed electric heaters are installed on the same electricity circuit as the chillers. In order to investigate the heat recovery heat pump performance in a likely spring/autumn operation the simulation models are simulated for 50% of the peak estimated cooling demand load curve seen in Figure 4.2 assuming the same daily and weekly variation load curve seen in Figure 4.28 above. For this operation scenario the cooling demand during low load periods is less than 60 kW. Due to this the results of the weekly simulation can not be simplified by using the steady state simulation and the full weekly simulation have to be performed in Dymola. In the weekly simulation the Propane compressor speed is limited to a maximum of 50 Hz to avoid the heat recovery heat pumps exceeding their maximum evaporator capacity. Similar for the Butane compressor the maximum compressor speed was limited to 55 Hz. The maximum Butane compressor speed was set higher than the maximum Propane compressor speed in order to secure that the Butane compressors were at all operating conditions able to maintain a Butane evaporation temperature lower than the condensation temperature of Propane in the cascade heat exchanger. This eliminated heat flow in the wrong direction in the cascade heat exchanger as a possible source of problems.

It was initially intended to simulate the Dymola models for an entire year and thus calculate the annual energy flows and SCOP of the heat recovery heat pump configurations. Due to long simulation times of several hours of the weekly simulations the plan to do annual simulations was disregarded as infeasible.

## 4.6 Economy and energy planning- method

### 4.6.1 Energy Analysis

Due to the uncertainty in cooling demand of the cold store it has been a challenging task to perform an energy analysis of the developed heat recovery heat pump configurations. The load duration curve of the estimated cooling demand shown in Figure 4.3 indicates that the full load hours of an heat recovery heat pump with 60 kW evaporator capacity operates at full load for 8722 hours annually. However in this thesis the maximum full load hours of the system is limited to 8500 assumed to account for maintenance. The impact of the uncertainty in cooling demand is considered by also performing an energy analysis with 6375 and 4250 annual full load hours correlating to 75% and 50% of the maximum full load hours. This method is severely simplified and and does not result in real life energy flows of the actual heat pump installations, but due to the large amount of uncertainty in both cooling demand of the cold store, existing chiller COP and hot water demand of 3T and Austmann, it is assumed that a more advanced energy flow analysis would not result in significant increased accuracy.

Equation 4.11-4.13 below were used to calculate the annual; delivered cooling, delivered heating and compressor electric shaft power of the heat recovery heat pumps. Equation 4.14 is used to calculated the reduced electricity consumption of the existing chillers, this is calculated in order to create a basis for evaluating the value of delivered cooling by the heat recovery heat pump.

$$Delivered\ \ Cooling\ \ Q_C = \dot{Q}_{Evap} \cdot FLH \tag{4.11}$$

$$Delivered\ \ Heating\ \ Q_H = \sum \dot{Q}_{Cond} \cdot FLH \tag{4.12}$$

$$Electricity\ \ Consumption\ \ EL_{Cons.} = \sum W_{Compressor} \cdot FLH \tag{4.13}$$

$$Reduced\ \ Electricity\ \ Consumption\ \ Chillers\ \ EL_{Reduced} = \frac{Q_C}{COP_{Chiller}} \tag{4.14}$$

### 4.6.2 Economical Analysis

#### Investment Costs & Maintenance

The investment costs of the heat recovery heat pumps have been difficult to determine precisely, the investment costs have therefore been calculated based on general cost of heat pumps from NVE seen in Table 2.5 and 2.6. The investment costs of the developed heat recovery heat pump installations were calculated by assuming the unit costs and installation costs in Table 2.5 and 2.6 varies linearly between the heat pump sizes in the table. For the Propane/Butane cascade heat pump the total unit cost have been estimated as if the two cascade cycles were two separate heat pumps. The unit cost of the propane unit are calculated from Table 2.5 and the Butane unit from Table 2.6. For the case of the Butane Cycle 25% is added to the unit cost in Table 2.6 in order to account for additional costs due to Butane not being a common choice of refrigerant. For the installation cost the Propane/Butane cascade heat pump is calculates as one unit assuming the same installation cost as in Table 2.5 and 2.6.

#### Cost of Electricity

The cost of electricity in Norway usually consists of a cost of electric power [NOK/kWh] plus the grid tariff. In this thesis only the cost of electric power is considered not the gird tariff, this is because the building owner already has to pay the grid tariff for the existing chillers at Sluppenveien 10 the grid tariff would therefore not impact the profitability of the heat recovery heat pumps. The focus of this thesis is to calculate the additional annual cost of installing a heat recovery heat pump at Sluppenveien 10.

The market cost of electric power varies with supply and demand, for Norway the electricity price in general is higher in the winter period with low precipitation and high electricity consumption. The actual market cost of electric power during one specific hour of operation in the future is therefore hard to predict. The cost of electricity is therefore in this thesis calculated as the average electricity price from 2012 to the first quarter of 2019 from ”Statistisk Sentralbyrå, SSB” [91]. It was decided to use an average historical cost of electricity over a long period from SSB in stead of the actual cost of electricity in for instance 2019 because it was believed that the average historical cost of electricity would be a better representation of the cost of electric power consumption over the entire life time of the heat pumps. Using the historical cost of electricity from SSB the average cost of electricity was calculated to be 0.288 NOK/kWh exclusive the electricity tax and VAT. The general electricity tax in Norway is 15.83 øre/kWh. Electricity consumption directly connected to either electricity production, district heating production or computer centers with over 0.5 MW of electric power consumption is however entitled to a reduced electricity tax of 0.5 øre/kWh according to ”Skattedirektoratet” [92]. In this thesis it is assumed that the heat recovery heat pumps are entitled to a reduced electricity tax, at least for the case of Model A1 and A2 producing hot water to the district heating gird this seems reasonable. With 0.5 øre/kWh of electricity tax and 25% VAT the average historical cost of electricity is estimated to be 0.36 NOK/kWh.

### Value of delivered Cooling

The price of the delivered cooling to the cold storage facility from the heat recovery heat pumps is not known exactly. In this thesis it has therefore been assumed that the value of the delivered cooling is set to the reduced cost of electricity of the existing chillers caused by the additional cooling delivered from the heat recovery heat pump. The reduced electricity consumption of the existing chillers is estimated by assuming a constant cooling COP of 2.49 for the existing chillers and Equation 2.5b. The COP of 2.49, correlates to the full load COP of Daikin EWAD -480D-SL Chiller. The highest COP from the Daikin Chiller User manual in Table 3.3 was chosen in order to not over estimate the value of delivered cooling. Choosing a lower COP would result in a larger reduction of existing chiller electricity consumption per kW of cooling delivered from the heat recovery heat pump.

The developed heat recovery heat pumps are then compared in terms of annual costs and levelized cost of heat generation (LCOG) for different full load hours, interest rates and economical life times of the heat pump. Since the cooling demand and full load hours (FLH) of operation of the heat pumps is uncertain it has been attempted to as much as possible calculate the annual costs and LCOG as a function of the FLH. The annual costs and LCOG have been calculated for all models with the interest rates of; 6%, 12% and 18%. The interest rate of 6% was chosen because it is the official discounting interest used for documentation of costs in the energy sector in Norway used by NVE [78]. the remaining two rates of interest were chosen to represent a low and common demand for profitability respectively. For the cost analysis the lifetimes of 10, 15 and 20 years have used.

In the calculation of profitability and maximum investment costs it has in this thesis been assumed an profitability demand of 20% and the maximum investment cost is calculated for a pay back time of 5 and 10 years. It is also assumed that the hot water is sold for 0.6 NOK/kWh the same as the average district heating price in Norway [93] and the heat recovered to the district heating gird is sold for the half of that, 0.3 NOK/kWh.

Chapter 5

# Results & Discussion

This chapter contains the most important results and discussion of the developed heat recovery heat pump models. Both initialization values for the EES-models and more detailed results of different operation scenarios from the dynamic Dymola models will be presented. Since the 5 developed models of the different heat recovery heat pump configurations have been developed using a similar method and assumptions, it has been decided to focus on validating and presenting detailed results of the Model A1 model. Then the most important results of the remaining 4 models are presented followed by a comparison. Additional results of the other developed Models not prioritized in this chapter are attached in Appendix D.

Due to the large amount of models and results, it has been chosen to structure the results in the following way; First the results of the initial calculations is presented for all models, then the Dymola simulation results of the heat recovery models to district heating, Model A1 and A2 is presented and discussed, followed by the hot water producing heat pump models B1,B2 and C1. Subsequently a the developed heat recovery heat pump configurations are compared from both a technical, energy and economical point of view.

## 5.1 All Models — Initial Calculation in EES

### 5.1.1 Model A1 — Initial Calculations in EES

**Table 5.1:** Model A1 — Initial values from EES to be used in further calculations

| | LTC (R290) | | | | | HTC (R600) | | | |
|---|---|---|---|---|---|---|---|---|---|
| Point Nr | T | P | h | s | Point Nr | T | P | h | s |
| Unit | [$°C$] | [bar] | [kJ/kg] | [kJ/kgK] | | [$°C$] | [bar] | [kJ/kg] | [kJ/kgK] |
| 1 | -11 | 2.916 | 564.3 | 2.416 | 7 | 62.0 | 5.367 | 678.0 | 2.498 |
| 2 | 0 | 2.916 | 582.6 | 2.485 | 8 | 73.0 | 5.367 | 700.5 | 2.564 |
| 3 | 95.2 | 19.48 | 720.6 | 2.600 | 9 | 121.9 | 16.17 | 773.1 | 2.627 |
| 4 | 56 | 19.48 | 356.2 | 1.508 | 10 | 103.0 | 16.17 | 471.7 | 1.829 |
| 5 | 50.2 | 19.48 | 338.0 | 1.452 | 11 | 95.7 | 16.17 | 449.2 | 1.797 |
| 6 | -15 | 2.916 | 338.0 | 1.540 | 12 | 53.0 | 5.367 | 449.2 | 1.797 |

Table 5.1 the previous page show the initial thermodynamic values from the initial calculation in EES of the Model A1 heat pump configuration. These values formed the basis of creating a dynamic heat pump model in Dymola by using these cycle points as initial values of dynamic simulation model. This was done in order to make the dynamic simulation model converge faster reducing simulation time.

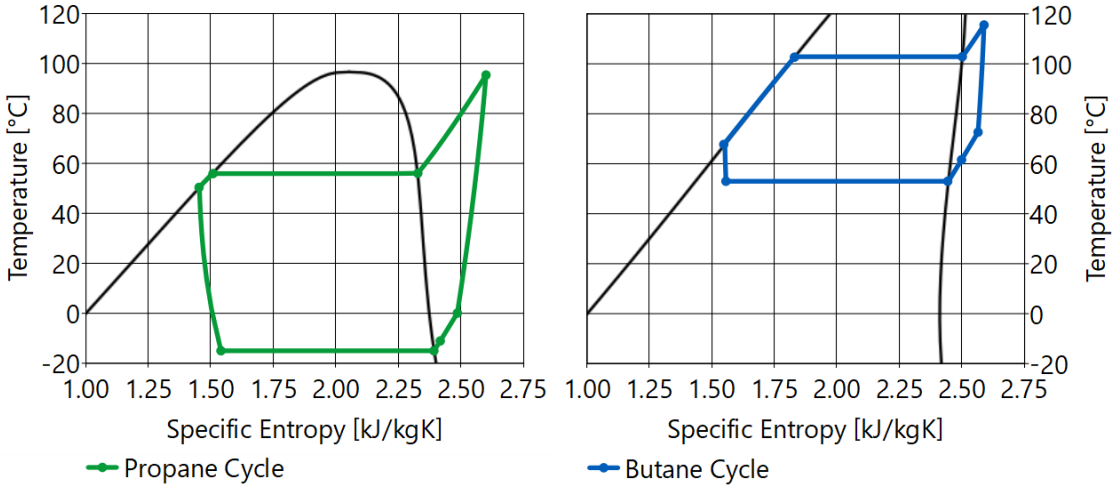


**Figure 5.1:** Model A1 — Ts-Chart inital values from EES-model.

Figure 5.1 above and Figure 5.2 below show the initial cycle points from Table 5.1 drawn into the Ts- and pH-chart of Propane and Butane respectively. From the pH-chart it is evident that the Propane cycle has a higher compression ratio than Butane due to the higher temperature lift of the cycle. The high compression ratio and temperature lift results in a high compression work, discharge enthalpy and thus temperature. This could be reduced by decreasing the evaporation temperature of the Butane cycle, but would result in an increased Butane cycle discharge temperature. Which should be avoided. The evaporation temperature of Butane is limited by the compressor manufacturer to a maximum 53 °C. This configuration is therefore chosen in order to minimize Butane compressor discharge temperature.

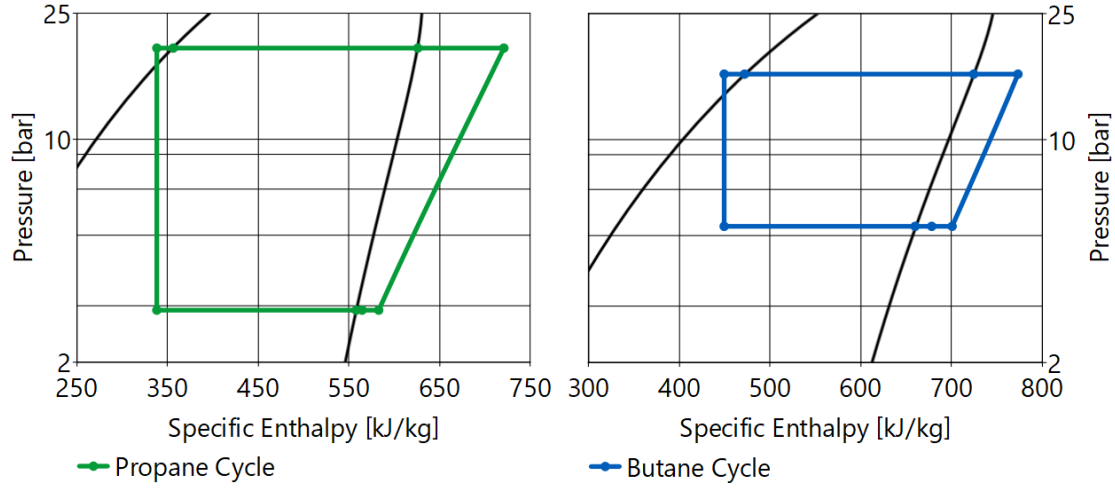


**Figure 5.2:** Model A1 — pH-Chart initial values from EES-model.

Table 5.2 below show the most important calculated values for the Model A1 2-step cascade heat pump configuration from EES. This was used as an initial indication of the performance of the system as well as formed the basis of compressor selection and estimation of compressor efficiencies. This is further described in section 4.3.5.

**Table 5.2:** Model A1 — Results from Initial Calculations in EES using Equation 2.1-2.11

| | LTC (R290) | HTC (R600) | Unit |
|---|---|---|---|
| $\dot{m}_R$ | 0.2651 | 0.3138 | $[kg/s]$ |
| $\dot{Q}_E$ | 60.0 | 96.58 | $[kW]$ |
| $\dot{W}_C$ | 36.58 | 22.78 | $[kW]$ |
| $\dot{Q}_C$ | 96.58 | 119.4 | $[kW]$ |
| $\dot{V}_S$ | 225.2 | 149.6 | $[m^3/h]$ |
| $pressure\ ratio\ \pi$ | 6.68 | 3.01 | $[--]$ |
| Cycle COP | 2.64 | 5.24 | $[--]$ |
| Total COP | 2.01 | | $[--]$ |

### 5.1.2 Model B1 — Initial Calculations in EES

Table 5.3 below show the initial thermodynamic values from the initial calculation in EES of the Model B1 heat pump configuration. These values formed the basis of creating a dynamic heat pump model in Dymola by using these cycle points as initial values of dynamic simulation model. From the calculated condensation pressures of the two cycles it is evident that this configuration as a reduced pressure ratio compared to the two previously described Model A1.

**Table 5.3:** Model B1 — Initial values from EES to be used in further calculations

| LTC (R290) | | | | | HTC (R600) | | | | |
|---|---|---|---|---|---|---|---|---|---|
| Point Nr | T | P | h | s | Point Nr | T | P | h | s |
| Unit | $[°C]$ | [bar] | [kJ/kg] | [kJ/kgK] | | $[°C]$ | [bar] | [kJ/kg] | [kJ/kgK] |
| 1 | -11 | 2.916 | 564.3 | 2.416 | 7 | 50 | 2.839 | 664.7 | 2.54 |
| 2 | 0 | 2.916 | 582.6 | 2.485 | 8 | 94.2 | 8.675 | 734.0 | 2.597 |
| 3 | 68.17 | 11.61 | 682.3 | 2.574 | 9 | 34 | 8.675 | 281.7 | 1.277 |
| 4 | 33 | 11.61 | 287.8 | 1.298 | 10 | 30 | 2.839 | 281.7 | 1.281 |
| 5 | 26.5 | 11.61 | 269.5 | 1.238 | | | | | |
| 6 | -15 | 2.916 | 269.5 | 1.275 | | | | | |

Figure 5.3 and Figure 5.4 below show the initial cycle points from Table 5.3 drawn into the Ts- and pH-chart of Propane and Butane respectively. At first sight they are similar to the Cycle Charts of model A1 in Figure 5.1 and 5.1, but the discharge temperatures of the cycles are significantly lower due to reduced condensation temperatures. The subcooling of the butane cycle is also increased due to the low temperature of the heat sink inlet.

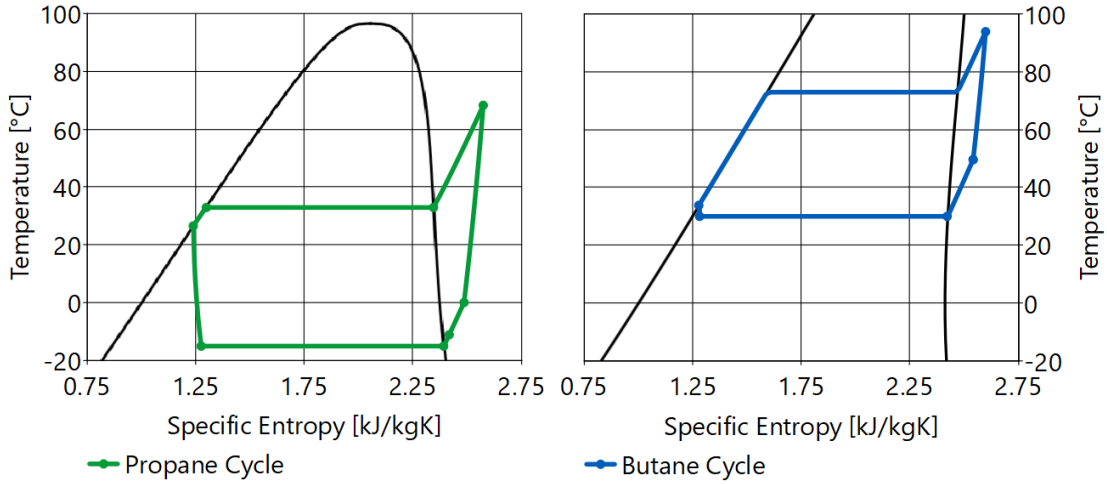


**Figure 5.3:** Model B1 — Ts-Chart initial values from EES-model.

From the pH-Chart in Figure 5.4 it can be seen that the compression ratios of the two cycles are much more similar compared to the Model A1 configuration where the Propane cycle has a significantly higher pressure ratio than the Butane cycle. The volumetric cooling capacity of the Butane cycle is also increased due to the increased subcooling. Which reduces refrigerant mass flow, compression work and thus increases COP.

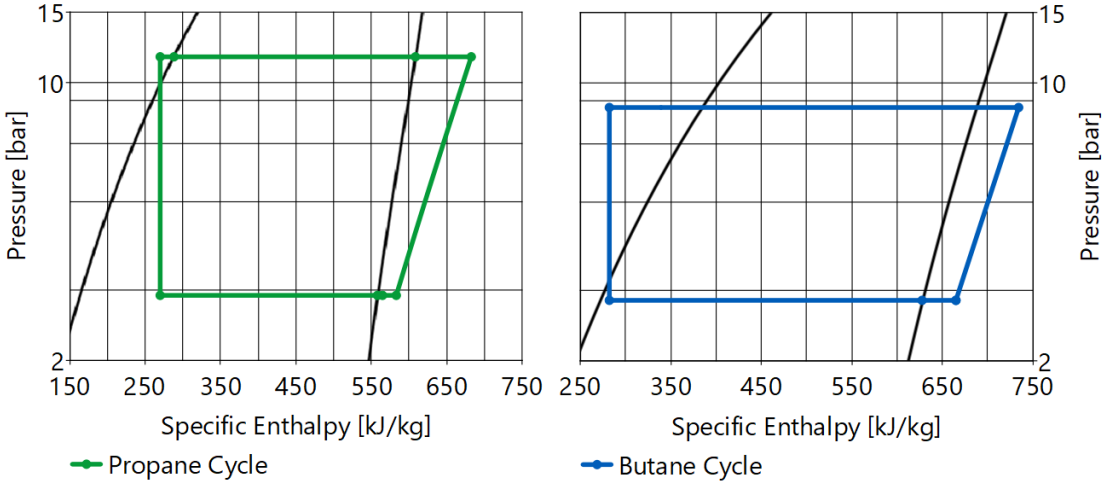


**Figure 5.4:** Model B1 — pH-Chart initial values from EES-model.

Table 5.4 below show the most important values of the Model B1 heat pump configuration calculated in EES. Compared to the values of The A1 model in Table 5.2 both refrigerant mass flow and compressor work is reduced, as an effect of the reduced temperature lifts, compression ratio and increased volumetric heating capacities. This results in a significant increase of COP from 1.89 to 2.72.

**Table 5.4:** Model B1 — Results from Initial Calculations in EES using Equation 2.1-2.11.

| | LTC (R290) | HTC (R600) | Unit |
|---|---|---|---|
| $\dot{m}_R$ | 0.2065 | 0.2097 | $[kg/s]$ |
| $\dot{Q}_E$ | 60.0 | 80.29 | $[kW]$ |
| $\dot{W}_C$ | 20.29 | 14.54 | $[kW]$ |
| $\dot{Q}_C$ | 80.29 | 94.83 | $[kW]$ |
| $\dot{V}_S$ | 151.3 | 143.4 | $[m^3/h]$ |
| $pressure\ ratio\ \pi$ | 3.981 | 3.055 | $[--]$ |
| Cycle COP | 3.957 | 6.522 | $[--]$ |
| Total COP | 2.723 | | $[--]$ |

### 5.1.3 Model B2 — Initial Calculations in EES

Table 5.5 below show the initial thermodynamic values from the initial calculation in EES of the Model B1 heat pump configuration. These values formed the basis of creating a dynamic heat pump model in Dymola by using these cycle points as initial values of dynamic simulation model. From the table it can be seen that the subcooling of the Propane cycles in the Model B2 is higher than the B1 configuration. Increasing the specific cooling capacity of the Propane cycle with approximately 70 kJ/KgK.

**Table 5.5:** Model B2 — Initial values from EES to be used in further calculations

| LTC (R290) | | | | | HTC (R600) | | | | |
|---|---|---|---|---|---|---|---|---|---|
| Point Nr | T | P | h | s | Point Nr | T | P | h | s |
| Unit | $[°C]$ | [bar] | [kJ/kg] | [kJ/kgK] | | $[°C]$ | [bar] | [kJ/kg] | [kJ/kgK] |
| 1 | -11 | 2.916 | 564.3 | 2.416 | 8 | 50 | 2.839 | 664.7 | 2.560 |
| 2 | 0 | 2.916 | 582.6 | 2.485 | 9 | 94.19 | 8.675 | 734 | 2.597 |
| 3 | 68.17 | 11.61 | 682.3 | 2.574 | 10 | 34 | 8.675 | 281.7 | 1.277 |
| 4 | 33 | 11.61 | 419.2 | 1.728 | 11 | 30 | 2.839 | 281.7 | 1.281 |
| 5 | 7 | 11.61 | 218.0 | 1.061 | | | | | |
| 6 | -0.2 | 11.61 | 199.8 | 0.9945 | | | | | |
| 7 | -15 | 2.916 | 199.8 | 1.005 | | | | | |

Figure 5.5 and Figure 5.6 below show the initial cycle points from Table 5.1 drawn into the Ts- and pH-chart of Propane and Butane respectively. The pressure ratios and the Butane cycle is the same as for the Model B1 configuration in Section 5.1.2. While the Propane cycle has an increased liquid subcooling as previously discussed.

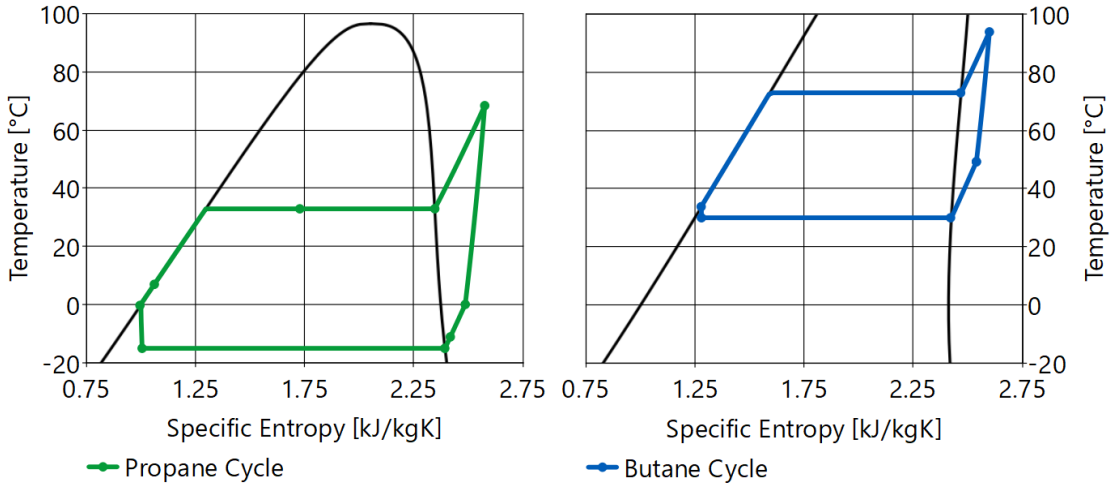


**Figure 5.5:** Model B2 — Ts-Chart initial values from EES-model.

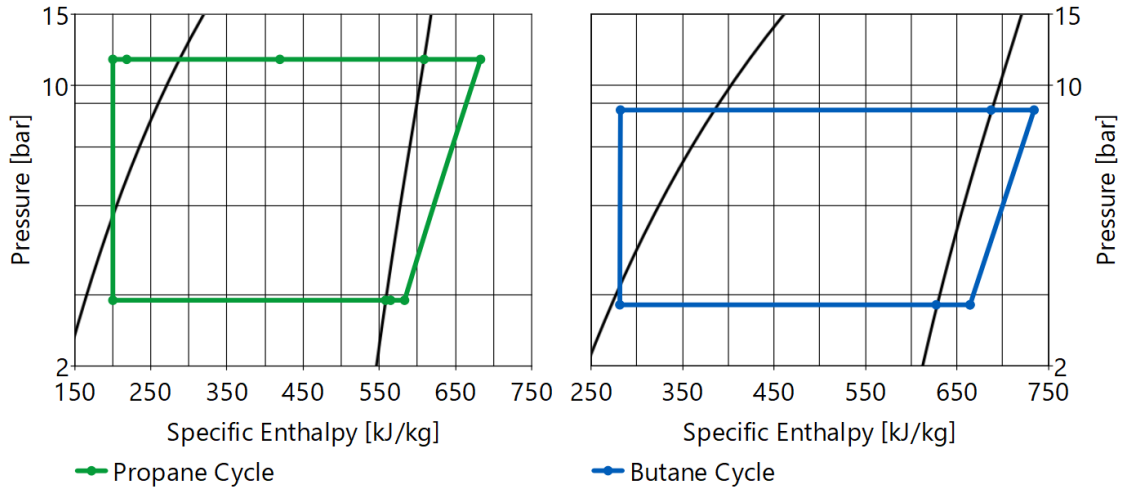


**Figure 5.6:** Model B2 — pH-Chart initial values from EES-model.

Table 5.6 below show the most important values of the Model B2 heat pump configuration calculated in EES. Compared to the values of The B1 model in Table 5.4 both refrigerant mass flow and compressor work of the Propane cycle. Despite the initial EES calculation Ts- and pH-charts of the Model B1 and B2 configuration Butane Cycles being identical the Model B2 has a much lower Butane mass flow and Butane compressor work compared to the B1 model. One of the possible explanations for this is the reduced heat transfer through the cascade heat exchanger of the B2 configuration. The impact of the modification is noticeable in the increase of COP from 2.72 to 3.47 from the B1 to B2 model configuration.

**Table 5.6:** Model B2 — Results from Initial Calculations in EES using Equation 2.1-2.11.

| | LTC (R290) | HTC (R600) | Unit |
|---|---|---|---|
| $\dot{m}_R$ | 0.1646 | 0.1131 | $[kg/s]$ |
| $\dot{Q}_E$ | 60.0 | 43.3 | $[kW]$ |
| $\dot{Q}_{W.Pre-Heater}$ | 33.11 | - | $[kW]$ |
| $\dot{W}_C$ | 16.41 | 7.84 | $[kW]$ |
| $\dot{Q}_C$ | 76.41 | 51.14 | $[kW]$ |
| $\dot{V}_S$ | 122.4 | 77.3 | $[m^3/h]$ |
| $pressure\ ratio\ \pi$ | 3.981 | 3.055 | $[--]$ |
| Cycle COP | 4.66 | 6.52 | $[--]$ |
| Total COP | 3.47 | | $[--]$ |

### 5.1.4 Model C1 — Initial Calculations in EES

Table 5.7 show the initial calculated values in EES for the Model C1 configuration. As the previously described models this formed the basis of crating a dynamic simulation model in Dymola. Due to the high temperature lift and concern for high discharge gas temperatures the gas cooler pressure was decreased to 90 bar, despite Equation 2.13 indicates the 95 bar is optimal from an energy performance point of view. It is assumed that 90 bar gas cooler pressure is sufficient for hot water production at 70 °C. Due to the high pressures of the $CO_2$ cycle the Model C1 configuration is likely to need more advanced heat exchangers compared to the previously described models, especially on the heat sink side. However, in this thesis it is assumed that the same heat exchangers can be used for all the developed heat recovery heat pump configurations.

**Table 5.7:** Model C1 — Initial values from EES to be used in further calculations

| Trans-Citical R744 Cycle | | | | |
|---|---|---|---|---|
| Point Nr | T | P | h | s |
| Unit | $[°C]$ | [bar] | [kJ/kg] | [kJ/kgK] |
| 1 | -15 | 22.91 | 436.4 | 1.924 |
| 2 | -5 | 22.91 | 449.4 | 1.974 |
| 3 | 119 | 90 | 538 | 2.034 |
| 4 | 7 | 90 | 211.9 | 1.004 |
| 5 | 1.3 | 90 | 198.9 | 0.9745 |
| 6 | -15 | 22.91 | 198.9 | 1.004 |

Figure 5.7 on the following page show the pH- and Ts-chart of the trans critical $CO_2$ cycle from EES. The pH-chart is similar to the previous pH-charts despite the heat sink pressure being trans critical. The Ts-chart on the other hand is distinct from the previous Ts-charts due to the large temperature variation in the gas cooler.

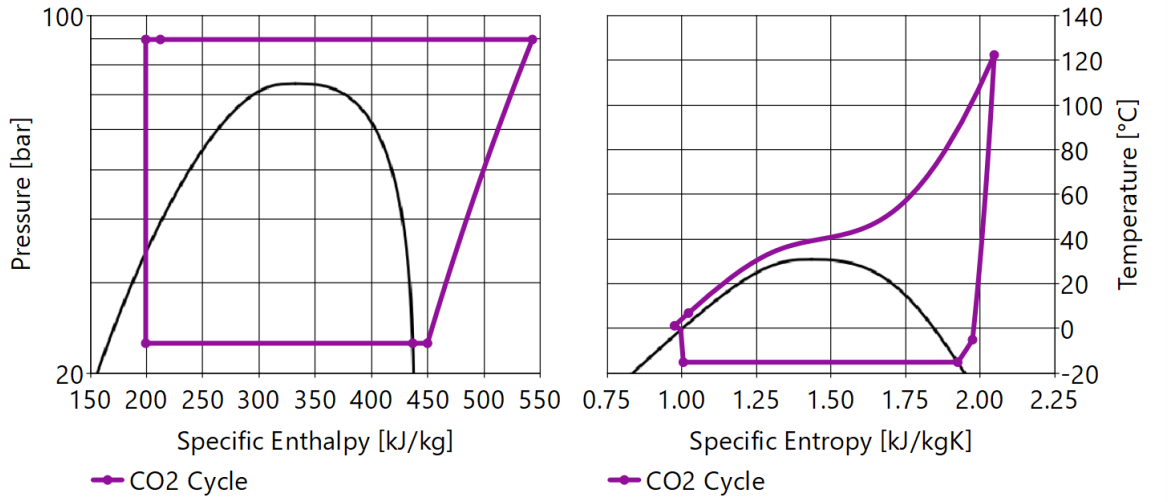


**Figure 5.7:** Model C1 — Ts-Chart and pH-Chart inital values from EES-model.

Table 5.8 show the most important results of the initial EES calculations for the Model C1 configuration. The refrigerant mass flow is comparable to the Model A1 configuration, but larger than the other previously described models. Yet the heating COP of 3.68 is higher than all the other heat recovery heat pump configurations in this thesis. The higher COP of the $CO_2$ heat pump configuration is as expected because it is a heat pump configuration well suited for hot water production and known for its high COP. More precisely the Model C1 configuration has only one refrigeration cycle reducing both total temperature lift and pressure ratio. The $CO_2$ heat pump also have higher compressor efficiencies compared to the other models, but this is not included in the EES calculations. This is because the compressor efficiencies were set equal for all models in EES in order to compare only the heat pump configurations not the advancement of compressor technology. This is however included in the Dymola simulation models.

**Table 5.8:** Model C1 — Results from Initial Calculations in EES using Equation 2.1-2.11.

| | Trans-Crit. R744 Cycle | Unit |
|---|---|---|
| $\dot{m}_R$ | 0.2526 | $[kg/s]$ |
| $\dot{Q}_E$ | 60.0 | $[kW]$ |
| $\dot{W}_C$ | 22.4 | $[kW]$ |
| $\dot{Q}_C$ | 82.4 | $[kW]$ |
| $\dot{V}_S$ | 21.3 | $[m^3/h]$ |
| $pressure\ ratio\ \pi$ | 3.93 | $[--]$ |
| Cycle COP | 3.68 | $[--]$ |

**Choice of Compressor**

As previously mentioned in Section 4.4.7 two compressors were considered for the Model C1 configuration. One from each of the two compressor manufacturers Bitzer and Dorin. Figure 5.8 below show the estimated compressor efficiencies for the two compressors Dorin CD3501H and Bitzer 4DTE-25K using the method described in Section 4.3.5. In the Figure the design operation point of the Model C1 configuration is illustrated in red at a pressure ratio 3.9. Which is well within the operational range of the two compressors illustrated by the minimum and maximum pressure ratio. From the figure it can be seen that the Bitzer compressor efficiencies were estimated to be higher than the Dorin compressor for the intended design point of the Model C1 heat recovery heat pump configuration. Due to this the Bitzer compressor was chosen for the Dynamic Dymola simulation model. If this is the case in real life conditions is not known, the efficiencies are estimated from polynomials given by the compressor manufacturers which sell a product and thus want to show the best possible performance of their product. The isentropic efficiencies were also estimated by assuming a 10% of compressor shaft power being heat losses. Whether this is the fact is not known and it is not constant for all operational points and likely not to be the same for different compressor models. The results shown in Figure 5.8 below therefore rely on the assumptions made when estimating the efficiencies.

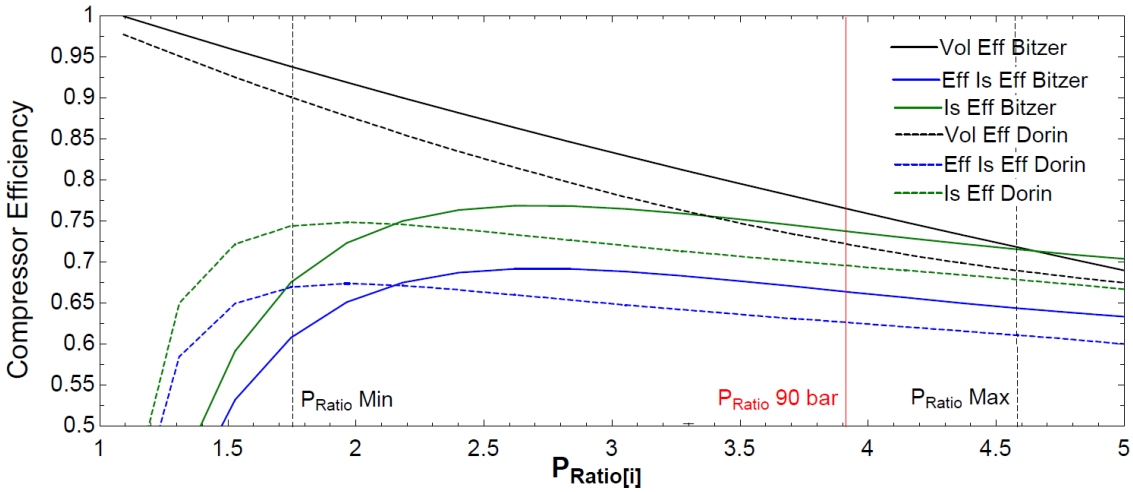


**Figure 5.8:** Estimated Volumetric and isentropic compressor efficiency for Dorin CD3501H and Bitzer 4DTE-25K $CO_2$ Compressors.

## 5.2 Heat recovery to District heating — Model A1 & A2

This section is dedicated to presenting and discussing the results of the heat recovery heat pump configurations Model A1 and A2 delivering heat to the district heating grid. First the steady state performance of the models at the design point with design cooling demand and 50 Hz speed of compressors, followed by the testing pulse simulations testing the performance of the model under variable cooling demand input. Lastly the results of the weekly simulations are presented.

### 5.2.1 Model A1 and A2 — Steady state simulations

Figure 5.9-5.11 on the following pages show the results of the steady state simulation with 60 kW of cooling demand for the two models A1 and A2. The graphs show the; COP Heating, COP Combined, Compressor Shaft Power, Refrigerant mass flow, Compressor discharge temperature, Compressor suction superheat and compressor speed of the two developed models. The results show that all the measured values stabilize before one hour of simulation and the respective values at the end of the simulation is presented in Table 5.9.

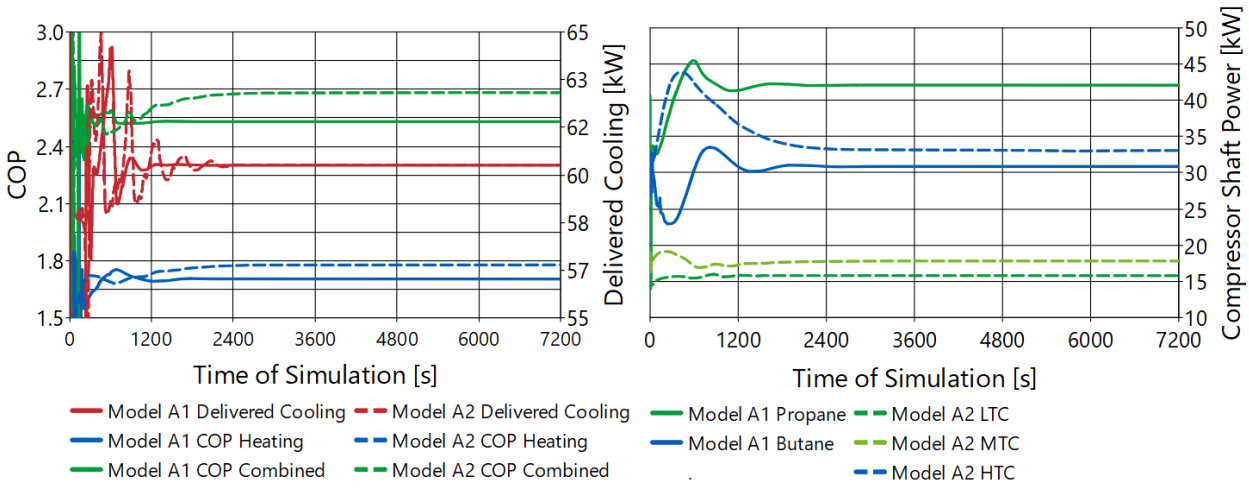


**Figure 5.9:** Model A1 and A2 — COP Heating & Combined and Compressor Shaft Power.

The results of the steady state simulation show that both simulation models behave as intended from the initial calculation in EES. All of the chosen compressor models operate close to or at 50 Hz frequency at design cooling demand of 60 kW, and the 15 and 20 K set superheat of the LTC and HTC is achieved. The model A2 configuration achieves a higher COP and lower propane compressor discharge temperatures compared to the A1 configuration. Caused by increased subcooling of the propane cycle and dividing the low temperature cycle in two compression and expansion steps.

The reduction of compressor discharge temperature can be seen in Figure 5.10, where the highest propane compressor discharge temperature is reduced from 98.8 to 87.5 °C by dividing the propane cycle in two compression and expansion steps. This reduces the wear and tear of the compressors increasing compressor life time and reducing the risk of compressor failure. However the improvements of reduced compressor discharge temperature might be cancelled out be the detrimental effect of the high suction gas superheat of 25 K for the MTC. It is therefore uncertain whether the A1 or A2 configuration achieve the best compressor performance and lifetime.

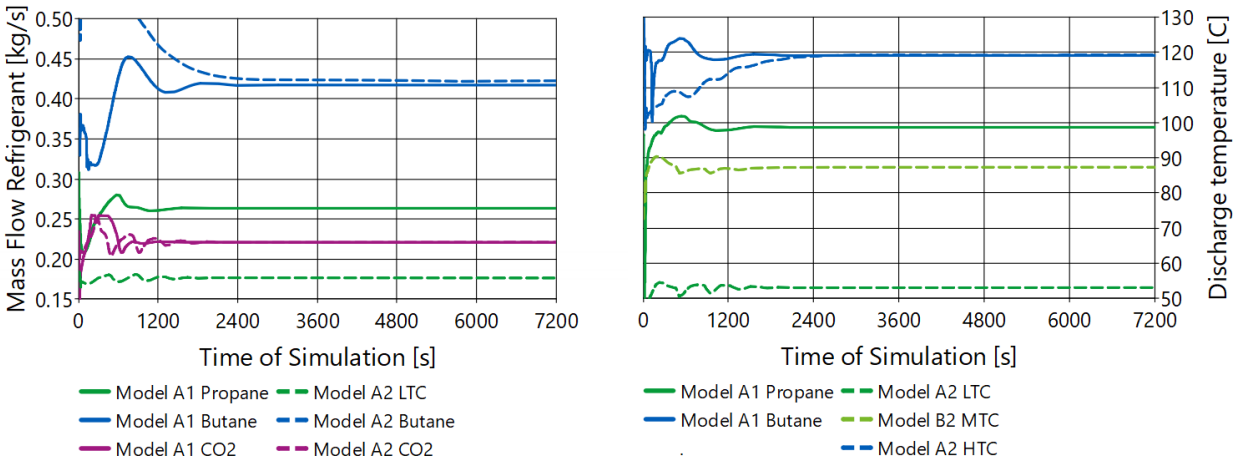


**Figure 5.10:** Model A1 and A2 — Refrigerant mass flow and compressor discharge temperature.

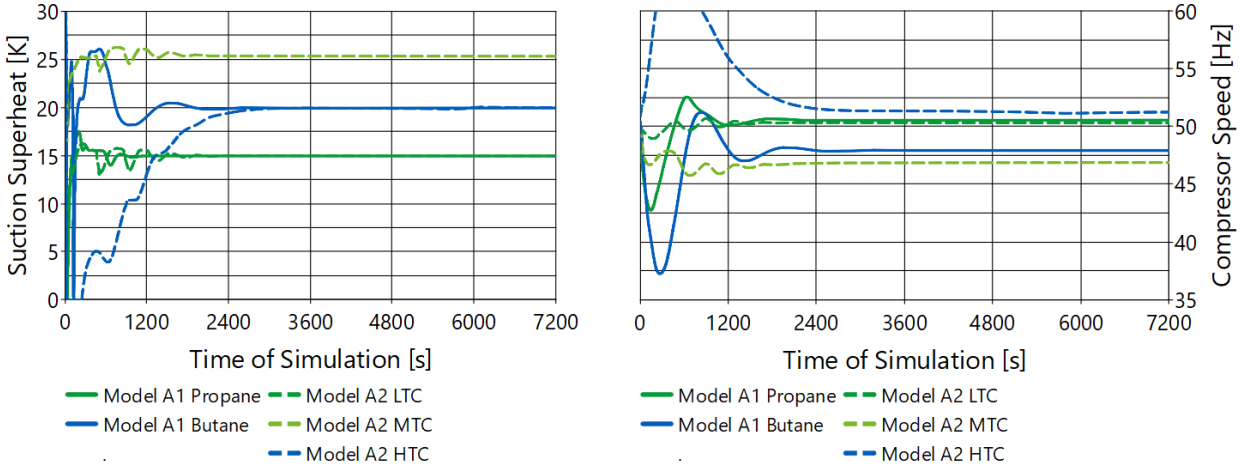


**Figure 5.11:** Model A1 and A2 — Compressor suction superheat and Compressor speed.

Figure 5.12 and 5.13 on the consecutive page show the steady state pH- and Ts-Charts of the Propane and Butane cycle of the Model A1 and Model A2 Dymola simulation models. The charts are snipped from the simulation time of 7150 seconds where the model results have stabilized as seen in Figure 5.9-5.11 above. The initial state points of the Model A1 from EES is also illustrated by the shaded area within the pH- and Ts-Charts. This has not been done for the Model A2 configuration because it was derived from the model A1 Dymola model, thus no initial EES calculations of the Model A2 configuration have been performed. As seen from the figures the results of the steady state simulation in Dymola and initial EES calculated values are close to identical for the Model A1 configuration, affirming that the steady state performance of the Dymola model is as intended. For the Butane cycle no visible difference of the steady state Dymola results of the Model A1 and A2 can be seen, as per design. For the Propane cycle state charts of the Model A2 configuration it is evident that the implementation of two step compression, expansion and intermediate pressure separator successfully reduces the Propane compressor discharge temperature and increased the specific cooling capacity of the evaporator.

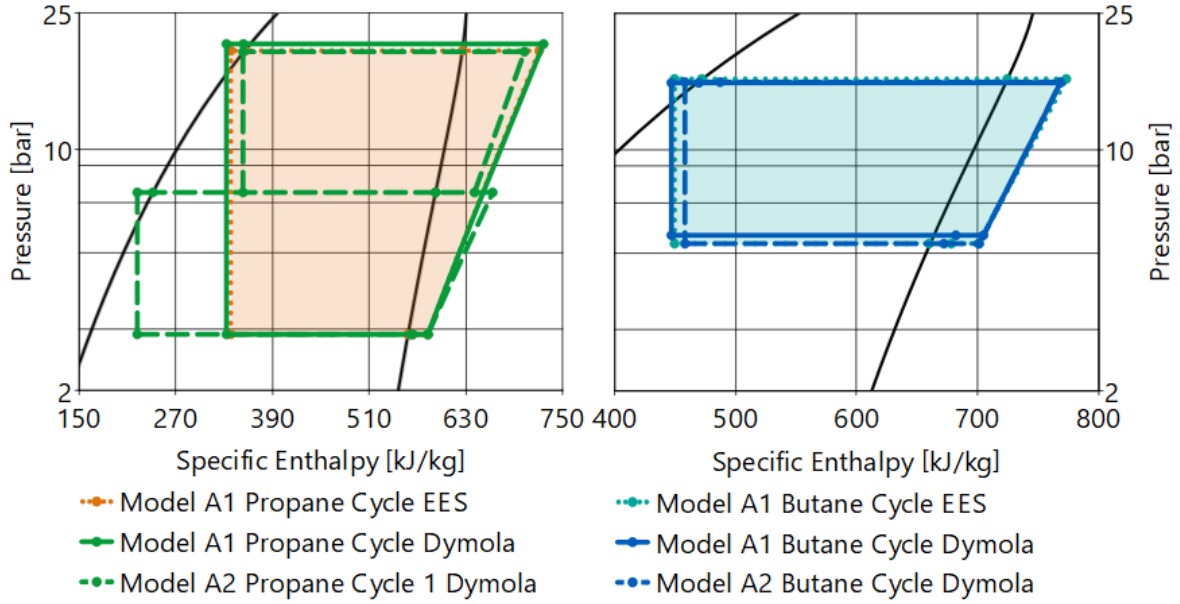


**Figure 5.12:** Model A1 and A2 — Steady state pH-Chart From Dymola.

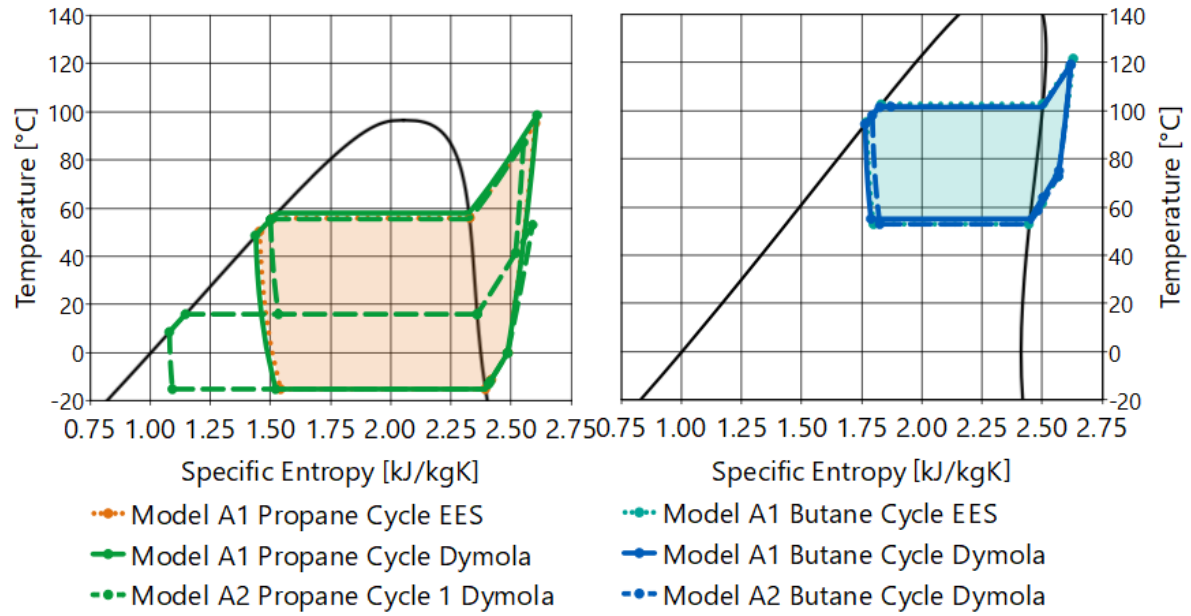


**Figure 5.13:** Model A1 and A2 — Steady state Ts-Chart From Dymola.

Table 5.9 below show the steady state results of the Model A1 and A2 Dymola simulation models after 7150 seconds of simulations when the results have stabilized as seen from Figure 5.9-5.11. In order to present the comparable values of the two Dymola models in the table the compressor superheat, discharge temperature and shaft power is presented for the low temperature cycle (LTC), intermediate temperature cycle (MTC) and high temperature cycle (HTC).

**Table 5.9:** Model A1 and A2 — Results of steady state simulation

| Parameter | Model A1 | Model A2 | Unit |
|---|---|---|---|
| COP Heating | 1.71 | 1.78 | [-] |
| COP Combined | 2.53 | 2.68 | [-] |
| LTC Compressor Speed | 50.58 | 50.34 | [Hz] |
| MTC Compressor Speed | - | 46.91 | [Hz] |
| HTC Compressor Speed | 47.95 | 51.27 | [Hz] |
| LTC mass flow | 0.2640 | 0.1770 | [kg/s] |
| Butane mass flow | 0.4176 | 0.4231 | [kg/s] |
| CO2 mass flow | 0.2215 | 0.2216 | [kg/s] |
| LTC Compressor Superheat | 15.0 | 15.0 | [K] |
| MTC Compressor Superheat | - | 25.4 | [K] |
| HTC Compressor Superheat | 19.9 | 20.0 | [K] |
| LTC Compressor Discharge Temp. | 98.8 | 53.2 | [°C] |
| MTC Compressor Discharge Temp. | - | 87.5 | [°C] |
| HTC Compressor Discharge Temp. | 119.2 | 119.4 | [°C] |
| LTC Compressor Shaft Power | 42.16 | 15.85 | [kW] |
| MTC Compressor Shaft Power | - | 17.88 | [kW] |
| HTC Compressor Shaft Power | 30.94 | 33.14 | [kW] |
| Delivered Cooling | 60.36 | 60.36 | [kW] |
| Delivered Heat | 124.75 | 119.12 | [kW] |
| Heat Sink Water Volume flow | 0.8651 | 0.8261 | [l/s] |

### 5.2.2 Model A1 and A2 — Weekly Simulations

As explained in Section 4.5.2 the developed Dynamic simulation models in Dymola have all been simulated for an average week of operation with 50% of the estimated peak cooling demand. For 100% and 75% of peak cooling demand the cooling demand in low load periods of the day is over 60 kW, the heat recovery heat pumps would then operate steadily at maximum cooling demand the entire week. The entire weekly simulations have therefore only been done for 50% of estimated cooling demand. The results of the weekly simulations of Model A1 and A2 is shown in Figure 5.14-5.20 on the following pages.

Figure 5.14 below show the delivered cooling of the heat recovery heat pump configurations A1 and A2 for 50% of the estimated weekly load curve. From Figure 5.14 below it can be seen that both simulation models are able to follow the input cooling demand signal for the low load periods of the week. However during mid-day on weekdays the cooling demand of the cold storage facility exceeds the maximum evaporator capacity of the heat recovery heat pump models. The heat recovery heat pumps therefore operate at maximum capacity from approximately 05:00 to 18:00 on week days. On weekends it is less activity in the cold storage facility, with less workers and less products going in and out of the storage. As a results of this the cooling demand is smaller compared to weekdays and the heat recovery heat pumps operate mostly at part load. This can also be seen in the Heat source outlet glycol temperature in Figure 5.15 below, where the outlet glycol temperature exceeds the -6 °C set point during mid-dag, indicating that the existing chillers also need to be in operation. The 100 °C heat sink water temperature set point are maintained at all times during the weekly simulation due to the variable water volume flow rate.

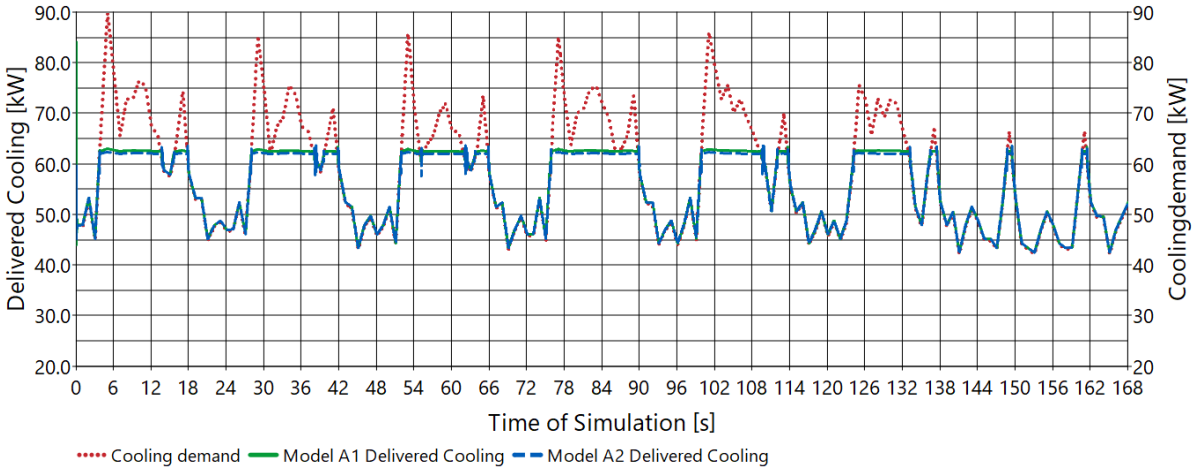


**Figure 5.14:** Model A1 and A2 — Weekly Simulation, delivered cooling. Input 50% of estimated cooling demand.

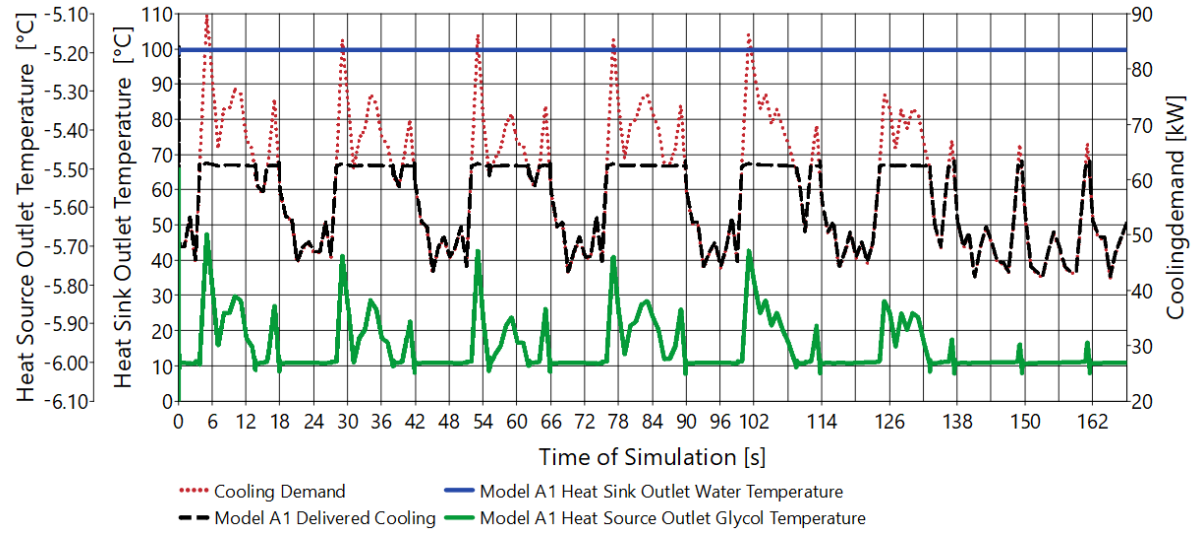


**Figure 5.15:** Model A1 and A2 — Weekly Simulation, Heat sink outlet water temperature and heat source outlet glycol temperature at 50% of estimated cooling demand.

Figure 5.16 below show the Propane- and Butane cycle pressure ratio of the Model A1 and A2 heat recovery heat pump configuration. As for the steady state simulations the Propane cycle pressure ratio of the Model A1 configuration is significantly higher than the pressure ratio of the Butane cycle, and the Model A2 configuration. During the weekly simulation the pressure ratios show little deviation from the steady state pressure ratios. This is as should be expected when the models have a fixed evaporation pressure of both Propane and Butane cycles and fixed temperature at the heat sink outlet. At part load the simulation models at part load should therefore operate at state points close to the steady state state point seen in Figure 5.12 and 5.13.

The small variation in pressure ratio seen in Figure 5.16 below is believed to be caused by a reduction in heat exchanger LMTD at part load caused by the constant heat transfer rate U and area A and reduced heat transfer Q. The reduction in LMTD could then be calculated using the heat exchanger energy balance in Equation 4.4. The reduced LMTD combined with the fixed evaporation pressure of both cycles and fixed heat sink temperatures this caused a reduced condensation pressure of both cycles. For the Butane cycles this effect can be seen in Figure 5.16 below causing reduced pressure ratio in low load conditions. However for the Model A1 Propane cycle the opposite effect is found with increased pressure ratio at part load. The variation in pressure ratio is however very small a might be caused by inaccuracy or small numerical errors in the simulation model.

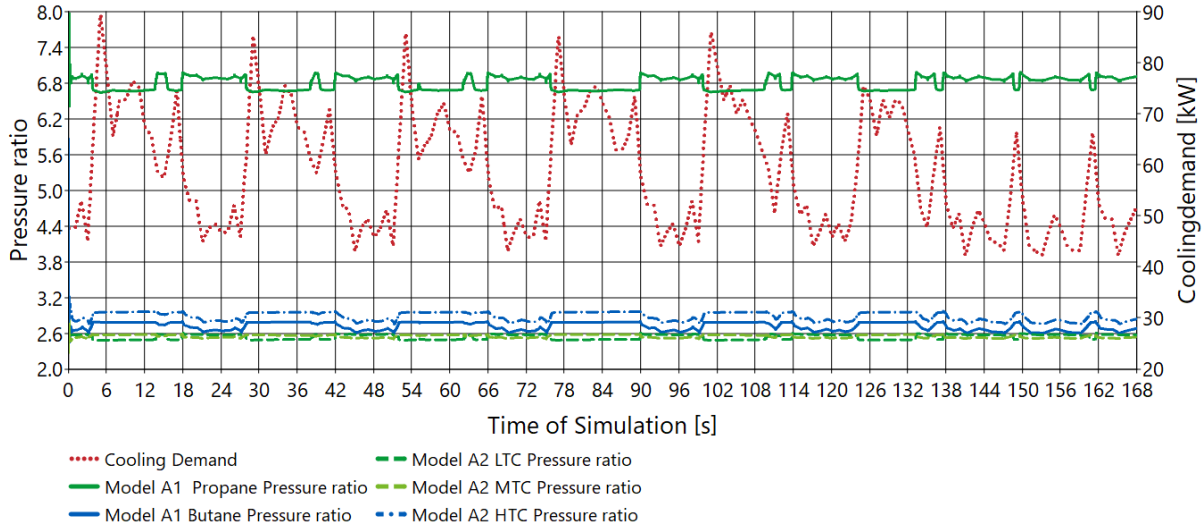


**Figure 5.16:** Model A1 and A2 — Weekly Simulation, Cycle pressure ratio. Input 50% of estimated cooling demand

Figure 5.17 below show the evaporation and condensation pressure of the Model A1 Propane Cycle. The figure show a very small variation in both evaporation and condensation pressure. The evaporation pressure is in the range of 2.9 to 3.0 bar and condensation pressure in the range of 20.1 to 20.4 bar, where the highest pressures are achieved at high load conditions. The variation of both evaporation and condensation pressure is however so small that no clear conclusion can be made because the uncertainty of the simulation models is believed to be larger than the variation of evaporation and condensation pressure. At low load condition is can also be seen that the condensation pressure is more unstable than

at high load conditions. This might cause inaccuracies in calculation of pressure ratio and one possible explanation for the increase in Model A1 Propane Cycle pressure ratio at part load seen in Figure 5.16 above.

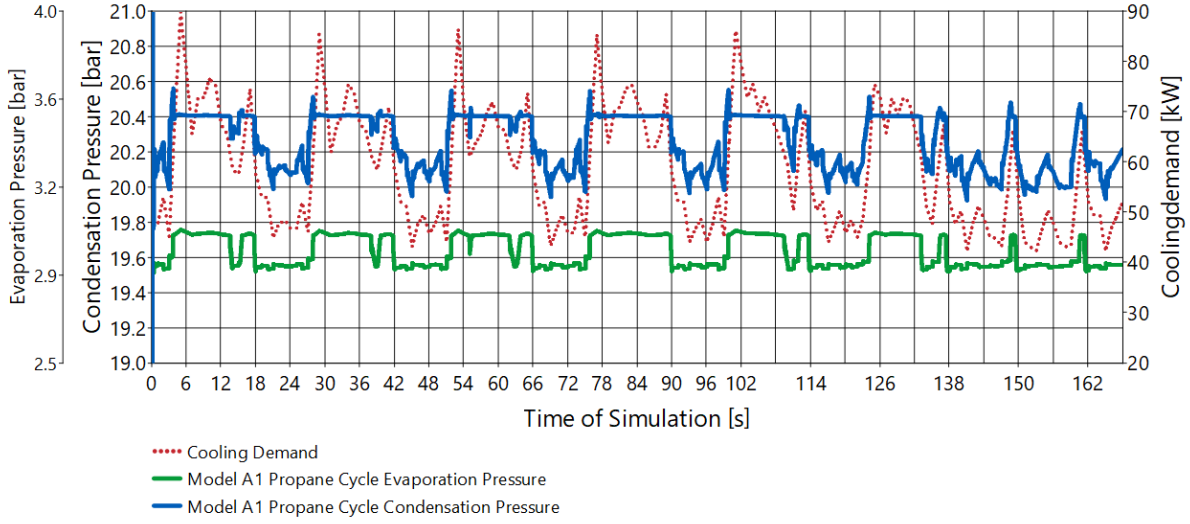


**Figure 5.17:** Model A1 — Weekly Simulation, Propane Cycle evaporation and condensation pressure. Input 50% of estimated cooling demand

Figure 5.18 below show the heating and combined heating and cooling COP of the Model A1 and A2 heat recovery heat pump configuration for an average week of operation simulated with 50% of the estimated peak cooling demand. The results of the weekly simulation show in general a higher heating COP and combined COP for the Model A2 configuration, same as the steady state results. The results also show small variation in COP at different cooling demand. This is believed to be caused by inaccuracies in measured evaporation and condensation pressure resulting in inaccurate pressure ratio, compressor shaft power and thus leading to variations in COP. The variation in COP at different cooling loads is further discussed in Section 5.5.

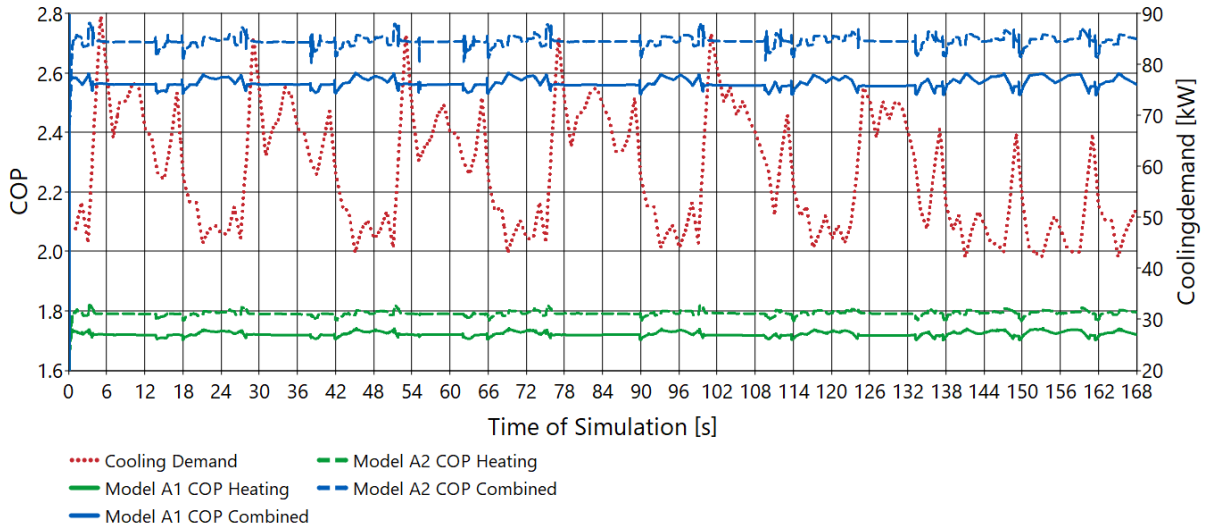


**Figure 5.18:** Model A1 and A2 — Weekly Simulation, COP Heating and Combined COP Heating & Cooling.

Figure 5.19 below show the compressor speed in hertz for the Propane and Butane Cycle of the Model A1 heat recovery heat pump configuration. It was chosen to only include the speed of the Model A1 compressors in the diagram because the LTC, MTC and HTC compressors of the Model A2 configuration showed the same behavior as the A1 compressors. The diagram and behaviour of the compressors would therefore be easier to see by reducing the number of graphs in the diagram. From the figure it can be seen that the compressor operate at design condition of 50 Hz during mid-day and at part load during night and weekends. During low load periods the minimum compressor speed does not fall far below 35 Hz, 70% of design speed. Which is assumed to be within the operational range of the compressors.

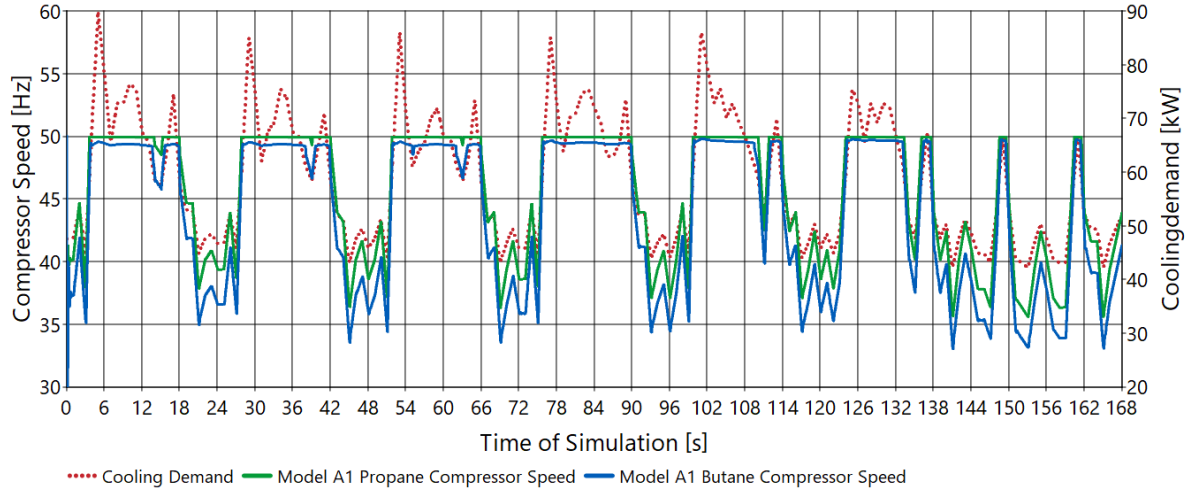


**Figure 5.19:** Model A1 and A2 — Weekly Simulation, Compressor speed at 50% of estimated cooling demand.

Figure 5.20 show the suction gas superheat of the Model A1 and A2 heat pump configuration compressors. The results show little variation from the steady state results in Figure 5.11 implying that the simulation models are able to maintain the set compressor suction heat for all conditions during the weekly simulation.

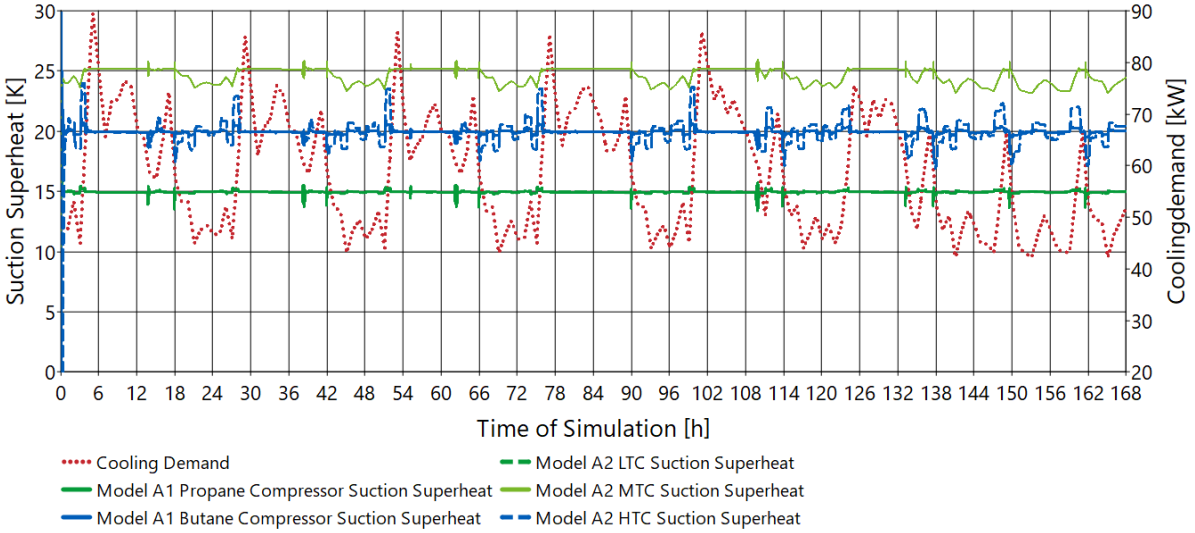


**Figure 5.20:** Model A1 and A2 — Weekly Simulation, Compressor suction superheat. Input 50% of estimated cooling demand.

## 5.3 Heat recovery by hot water production — Model B1 and B2

### 5.3.1 Model B1 and B2 — Steady state simulations

Figure 5.21 and 5.22 below show the steady state pH- and Ts-Charts of the hot water producing heat recovery heat pump configurations Model B1 and B2. The steady state charts from Dymola of both models are near identical to the initial calculated values from EES, implying that the models operate as intended. The pH- and Ts-charts of the initial EES calculation is presented and discussed in Section 5.1.2 and 5.1.3. Since the state charts from Dymola and EES are so similar the results are not further discussed in this section.

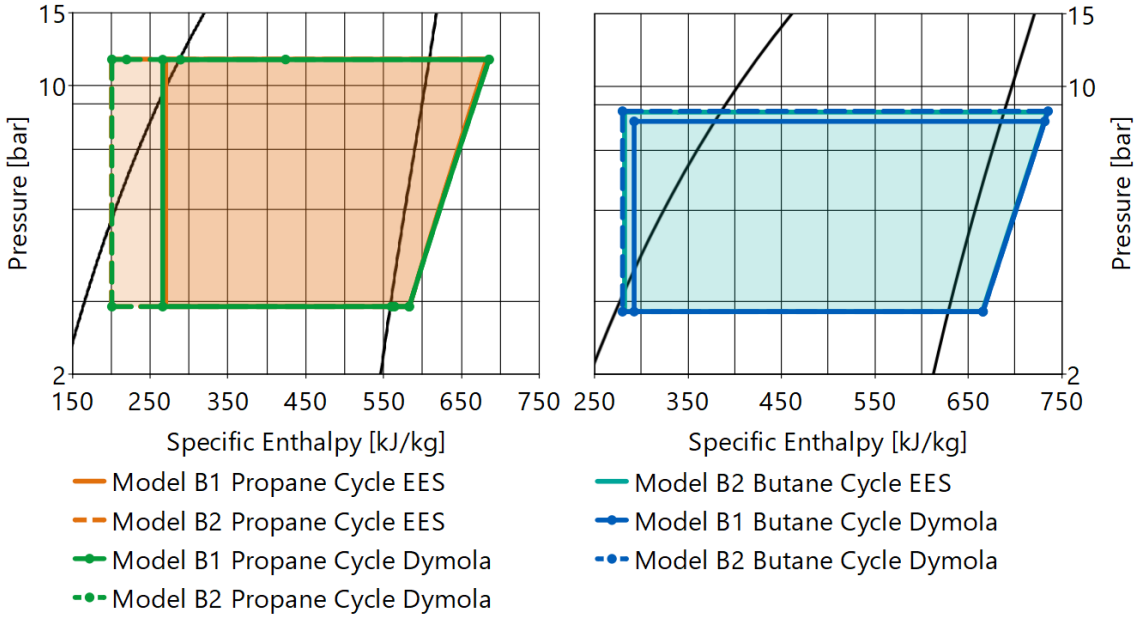


**Figure 5.21:** Model B1 and B2 — Steady state pH-Chart From Dymola.

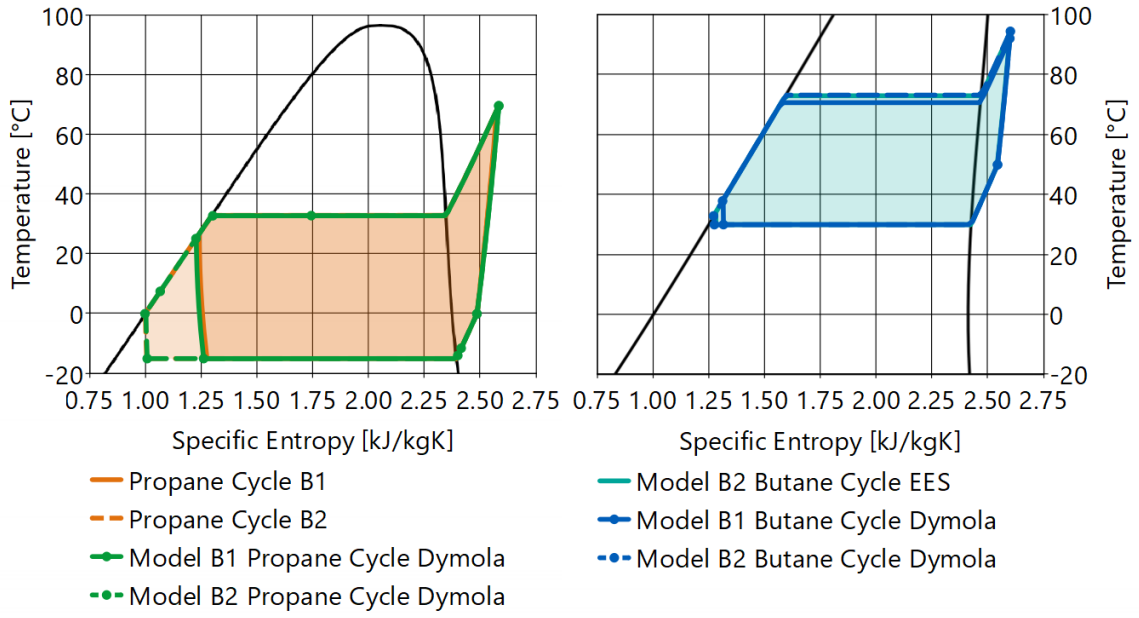


**Figure 5.22:** Model B1 and B2 — Steady state Ts-Chart From Dymola.

Table 5.10 below show the final results of the steady state simulation of the Model B1 and B2 heat recovery heat pump configuration. The results of the steady state simulation was performed at design condition with 60 kW of cooling demand and 4°C/70 °C heat sink inlet/outlet temperature. The results stabilized towards the results shown in Table 5.10 in a similar amount of time as the Model A1 and A2 steady state results shown in Figure 5.9-5.11. The results of the Model B1 and B2 configuration are therefore only presented in a tabularized form.

**Table 5.10:** Model B1 and B2 — Results of steady state simulation

| Parameter | Model B1 | Model B2 | Unit |
|---|---|---|---|
| COP Heating | 2.38 | 3.06 | [-] |
| COP Combined | 3.88 | 5.23 | [-] |
| Propane Compressor Speed | 51.01 | 49.71 | [Hz] |
| Butane Compressor Speed | 48.54 | 50.78 | [Hz] |
| Propane mass flow | 0.2054 | 0.1662 | [kg/s] |
| Butane mass flow | 0.2180 | 0.1126 | [kg/s] |
| CO2 Secondary Circuit mass flow | 0.2212 | 0.2247 | [kg/s] |
| Propane Compressor Suction Superheat | 15.0 | 15.0 | [K] |
| Butane Compressor Suction Superheat | 20.0 | 20.0 | [K] |
| Propane Compressor Discharge Temp. | 69.72 | 69.77 | [°C] |
| Butane Compressor Discharge Temp. | 92.18 | 94.55 | [°C] |
| Propane Compressor Shaft Power | 23.46 | 18.70 | [kW] |
| Butane Compressor Shaft Power | 16.82 | 9.15 | [kW] |
| Delivered Cooling | 60.36 | 60.36 | [kW] |
| Delivered Heat | 95.83 | 51.30+33.95 | [kW] |
| Heat Sink Water Volume flow | 0.3470 | 0.3087 | [l/s] |

Figure 5.23 and 5.24 on the following page show an comparison of COP heating, COP Combined and Refrigerant mass flow of the Dymola steady state and initial EES Calculation for the Model B1 and B2 configurations. The comparison show the developed Dymola models have close to identical refrigerant mass flows of the Propane and Butane cycle and in general lower COP compared to the initial EES Calculations. The small variation of refrigerant mass flow between the Dymola models and the EES calculations is so small that it is assumed to be caused only by numerical errors. The difference in COP is more noticeable and as should be expected because the Dymola models distinguish between isentropic- and effective isentropic efficiency in order to accommodate the effect of heat losses in the compressor. This results in increased compressor shaft power for the same discharge gas conditions and the COP should decrease accordingly.

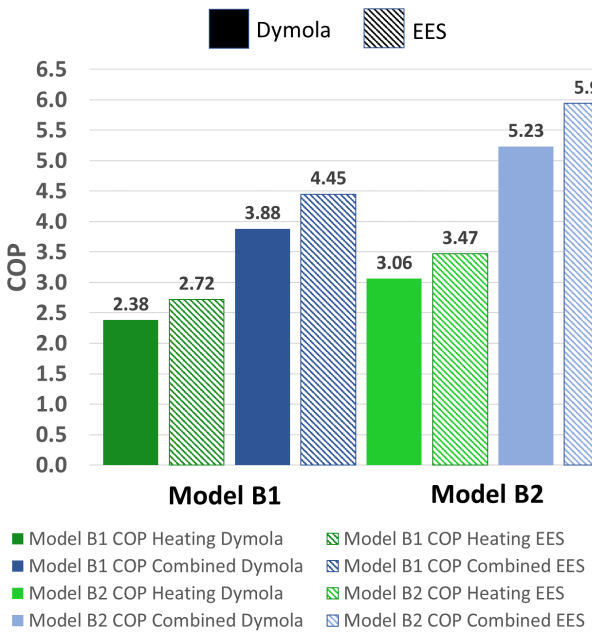


**Figure 5.23:** Comparison COP of model B1 and B2 from Dymola and EES.

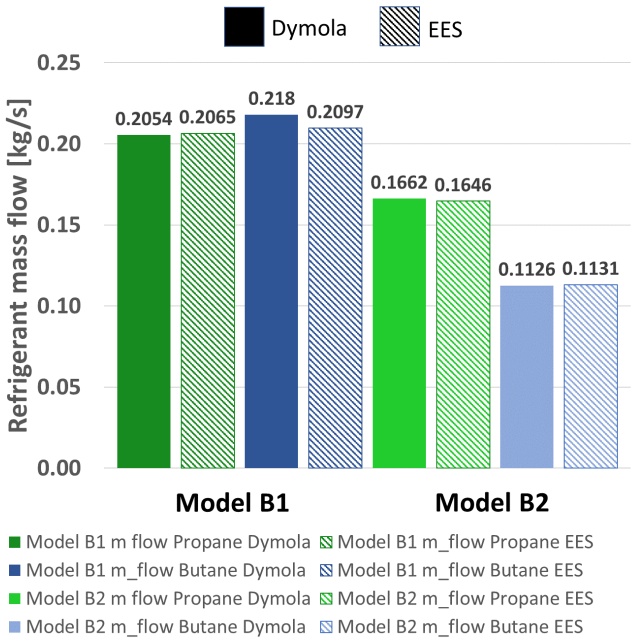


**Figure 5.24:** Comparison Refrigerant mass flow of model B1 and B2 from Dymola and EES.

The Model B1 and B2 heat pump configuration have been simulated for the same ”Weekly simulation” as the Model A1 and A2 heat pump configuration. The results of the simulations showed that the Model B1 and B2 heat pump configuration was able to follow the cooling demand at both the ”Testing-pulse” and ”Weekly simulation”. Since the results of the ”Testing-pulse” and ”Weekly simulation” of the Model B1 and B2 heat pump configurations showed a similar behaviour as the Model A1 and A2 heat pump configuration shown in Figure 5.14-5.20, the results of Model B1 and B2 are only attached in Appendix D.

## 5.4 Heat recovery by $CO_2$ Heat pump — Model C1

### 5.4.1 Model C1 — Steady state simulations

Figure 5.25 and Table 5.11 on the following page show the results of the steady state simulation for the Model C1 $CO_2$ hot water heat recovery heat pump configuration. As for the Model B1 and B2 configurations the Model C1 heat pump operates at steady state as intended by the initial EES calculations (indicated by the shaded area in Figure 5.25 ) and stabilized as quick as the model A1 and A2 configurations in Figure 5.9-5.11. The steady state results of the Model C1 configuration are therefore also only shown in a table.

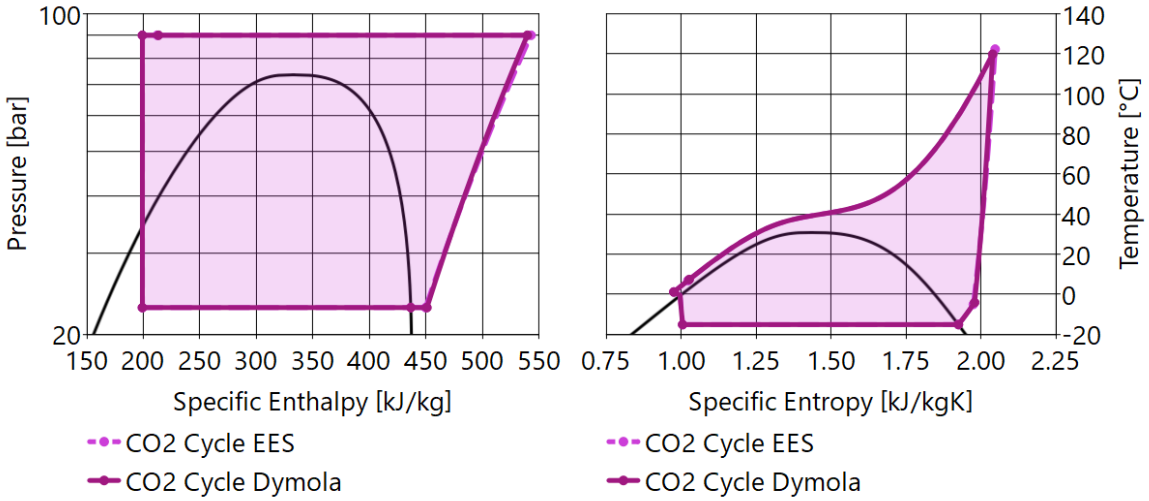


**Figure 5.25:** Model C1 — Steady state pH- and Ts-Chart From Dymola.

**Table 5.11:** Model C1 — Results of steady state simulation

| Parameter | Model C1 | Unit |
|---|---|---|
| COP Heating | 3.28 | [-] |
| COP Combined | 5.66 | [-] |
| $CO_2$ Refrigerant mass flow | 0.2542 | [kg/s] |
| $CO_2$ Secondary Circuit mass flow | 0.2209 | [kg/s] |
| $CO_2$ Compressor Suction Superheat | 11.0 | [K] |
| $CO_2$ Compressor Speed | 49.36 | [Hz] |
| $CO_2$ Compressor Discharge Temperature | 120.1 | [°C] |
| $CO_2$ Compressor Shaft Power | 25.31 | [kW] |
| Delivered Cooling | 60.36 | [kW] |
| Delivered Heat | 82.94 | [kW] |
| Heat Sink Water Volume flow | 0.3004 | [l/s] |

The Model C1 heat pump configuration have been simulated for the same ”Weekly simulation” as the Model A1 and A2 heat pump configuration. The results of the simulations showed that the Model C1 heat pump configuration also was able to follow the cooling demand at both the ”Testing-pulse” and ”Weekly simulation”. Since the results of the ”Testing-pulse” and ”Weekly simulation” of the Model C1 heat pump configurations showed a similar behaviour as the Model A1 and A2 heat pump configuration shown in Figure 5.14-5.20, the results of Model C1 are also only attached in Appendix D.

### Impact of heat sink inlet temperature

As mentioned in the theory (Section 2.4.3) it is important with low heat sink inlet water temperatures in order to achieve high COP for trans-critical $CO_2$ heat pumps. At increasing water inlet temperatures the specific cooling capacity of the $CO_2$ heat pump decreases, resulting in a decrease in COP as well. The decreased specific cooling capacity at increased heat sink inlet water temperatures is illustrated in Figure 5.26 below for 4, 10 and 15°C water temperatures. This effect is present for the other developed heat recovery heat pump configurations as well, but due to the low critical point of $CO_2$ the detrimental effect of increased heat sink inlet water temperature is larger for the Model C1 $CO_2$ heat pump. The steady state COP of the Model C1 and Model B2 Dymola models at 4, 10 and 15°C heat sink water inlet temperatures can be seen in Figure 5.27. The Model B2 heat pump configuration achieves 7%, 6% and 4% lower COP compared to the Model C1 heat pump configuration for the three mentioned water inlet temperatures, indicating that increased inlet water temperature has a more detrimental effect on COP for Model C1 compared to Model B2.

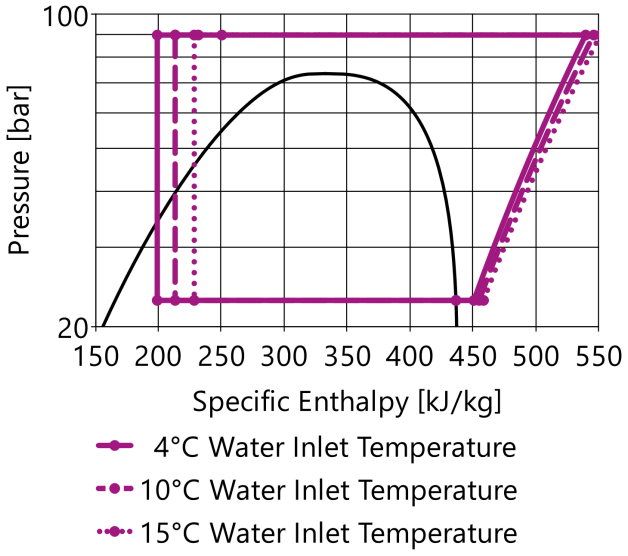


**Figure 5.26:** Model C1 — pH-Chart at different heat sink inlet water temperatures.

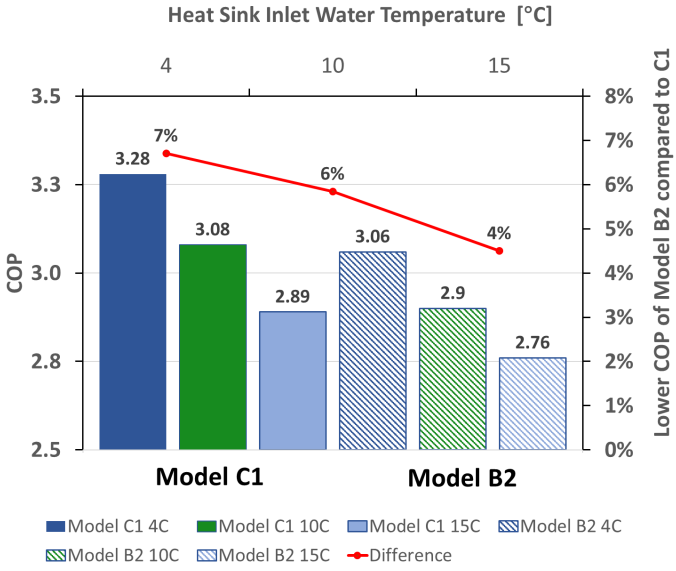


**Figure 5.27:** Comparison Model C1 and Model B2 COP at different heat sink Water inlet temperatures.

## 5.5 Comparison of Models

### 5.5.1 Steady State

Figure 5.28 below shown an comparison between steady state COPs and average COPs of the weekly simulations for all the developed Dymola simulation models. The COPs for the weekly simulations are an average value of the COP achieved from hour 1 to 168 of the simulation, the first hour of simulation was not included in order to eliminate incorrect initialisation values as a source of error. The results show that the average COPs of the weekly simulations are for all developed models slightly larger than the steady state COP. In real life conditions the weekly simulated COP which is performed at part load should achieve lower COP than the steady state simulation at design operation point due to reduced compressor efficiency at part load. The reduction of compressor efficiency at part load is not included in the simulation models, this is therefore a model limitation and possible source of error of the simulated results. The increase in COPs for the weekly simulation is believed to be caused by an minor decrease of heat exchanger LMTD at part load, resulting in reduced simulated compression ratio, compressor shaft power and increased COP. In real life conditions the decrease in compressor efficiencies at part load is likely to have a larger detrimental impact on COP than the slightly reduced compression ratio. The results of the weekly simulations are therefore likely not to be a better representation of real life performance of the heat pumps than the steady state results. Due to this it has in this thesis been decided to use the results of the steady state simulations as a basis for the following energy flow and economical analysis of the developed heat pump models.

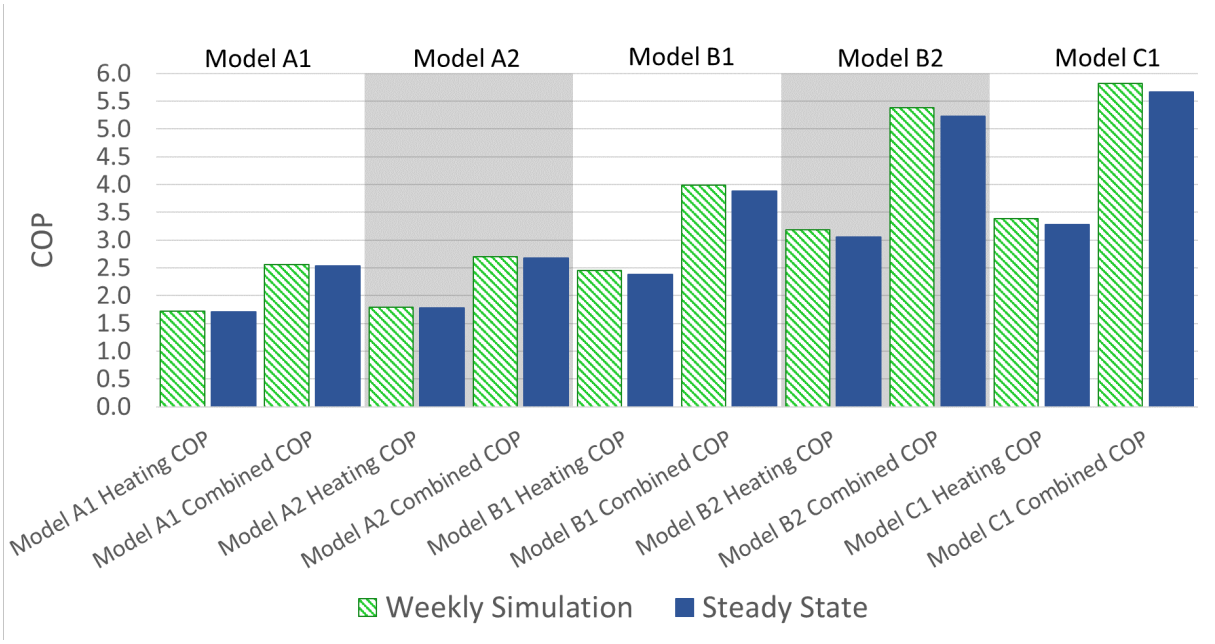


**Figure 5.28:** Model comparison — Steady state COP and Average COP of weekly simulation.

Figure 5.29 below show a comparison between the simulated design point heating COP at steady state for all developed simulation models and the maximum theoretical COP, the Carnot COP calculated with Equation 2.6. The achieved heating COP of the simulation models is in the range of 48.2% to 71.9% of the Carnot COP, where the minimum and maximum value was achieved for the Model A1 and Model C1 heat pump configuration respectively.

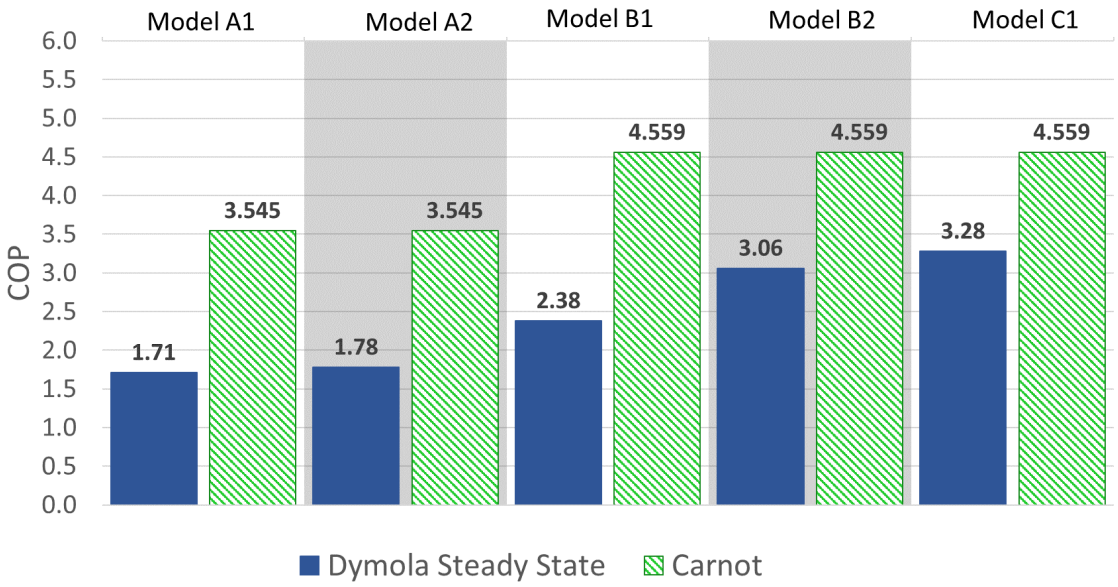


**Figure 5.29:** Model comparison — Steady state COP Heating and Carnot COP.

### 5.5.2 Accumulated Water Volume

Figure 5.30 on the following page show the accumulated hot water volume produced during the weekly simulation for all five developed Dymola models. Since all models have the same evaporator capacity the accumulated volume of hot water is directly correlated with the COP of the heat recovery heat pump configuration, the heat pump configurations to district heating Model A1 and A2 a low COP, indicating large compressor shaft power demand compared to the other models. As a result of this the A1 and A2 configuration produce accordingly more hot water. Also the heat sink water temperature lift is smaller for the Model A1 and A2 configuration (100-65°C) compared to the other models (70-4°C). Resulting in an even larger volume of hot water produced per kW of condenser power.

The results of the weekly simulation show that the Model B1, B2 and C1 heat recovery heat pump configuration produce; 191.5, 172.5 and 168.2 $m^3$ of hot water during the weekly simulation. The estimated annual hot water demand of Austmann is 483750 liters and for 3T the estimated hot water demand is either 2 155 200 or 426 700 liters depending on the standard SN/TS 3031:2016 or SN-NSPEK3031:2020 is used for calculation or the hot water demand. Even if the largest estimate for hot water demand is used the Model C1 heat pump configuration, which has the smallest hot water volume production rate would be able to deliver the same amount of hot water in approximately 15.7 weeks or 2640 hours of operation.

If the hot water demand for 3T is calculated with values from SN/TS 3031:2016 the annual estimated hot water demand 2 155 200 liters, equivalent to 5900 liters per day. Which intuitively seems like too much hot water demand. This might be the reason why the energy demand for hot water is significantly lower in SN-NSPEK3031:2020. If the 2020 version of the standard is used this results in a daily hot water demand of 1200 liters, which seems like a more reasonable hot water consumption. Using the values from the updated standard results in the Model C1 heat pump configuration being able to cover the annual estimated hot water demand of Austmann and 3T in only 910 hour of operation. The other developed heat recovery heat pump models would be able to cover the demand in an even shorter amount of time. The combined hot water demand of Austmann and 3T is therefore likely to not be large enough to be the sole recipient of hot water from a heat recovery heat pump with 60 kW of evaporator capacity.

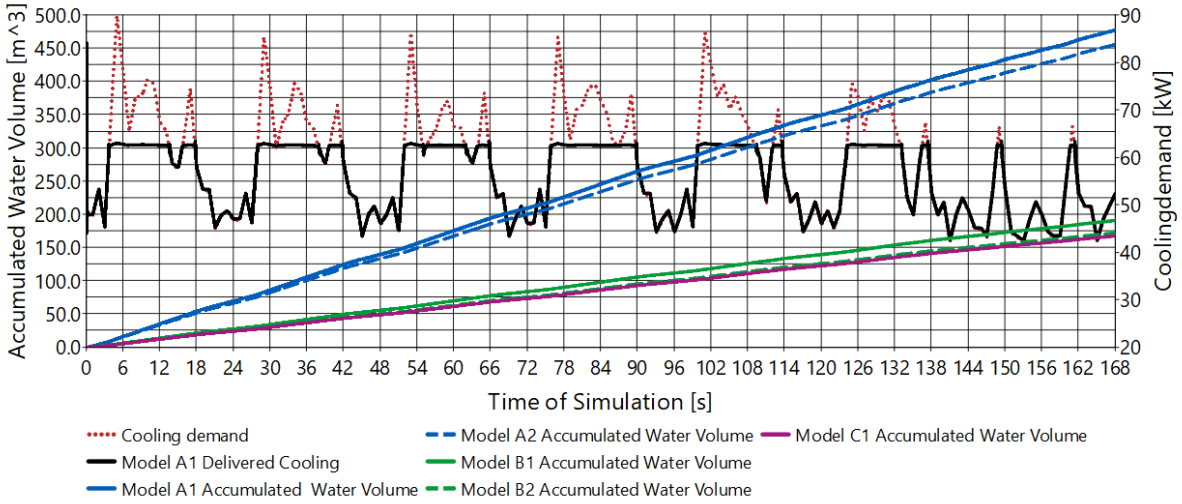


**Figure 5.30:** Model comparison — Accumulated Water Volume Weekly Simulation.

## 5.6 Energy analysis

Figure 5.31 and 5.32 below show the energy flows of the developed heat pump models at design condition assuming 8500 full load hours annually. In Figure 5.31 the delivered cooling and compressor shaft power of the individual compressors is shown. From the figure it is evident that the extra heat delivery of the other models compared to the Model C1 configuration is due to extra electrical consumption of the compressors. It can also be seen from the figure that the delivered heating of each models is slightly lower than the sum of delivered cooling and compressor shaft power, this is because the Dymola models include compressor heat losses to the ambient.

In Figure 5.32 the total heat recovery heat pump compressor electricity consumption and estimated reduced electricity consumption of the existing chillers can be seen. From the figure it can be seen that for the hot water producing heat pumps the net additional electricity consumption of the electric chillers is very small. The Model B2 and C1 heat recovery heat pumps are therefore the best options from an energy point of view and for achieving a positive energy district.

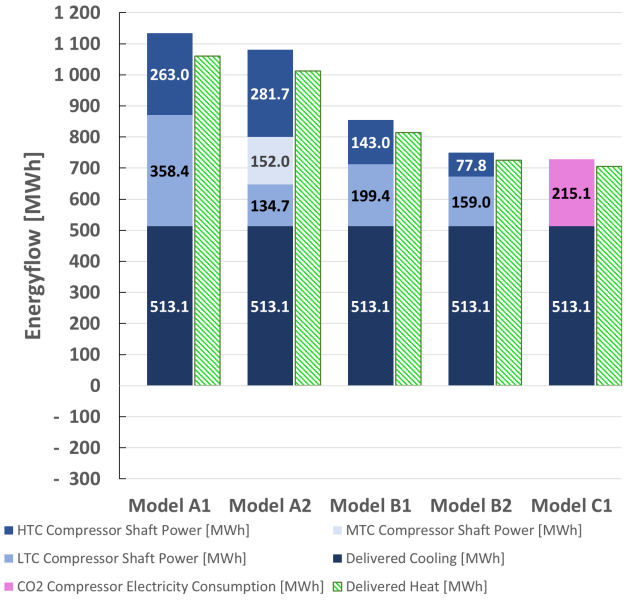


**Figure 5.31:** Energy analysis — Delivered cooling, compressor shaft power and delivered heat at 8500 Full-load-Hours.

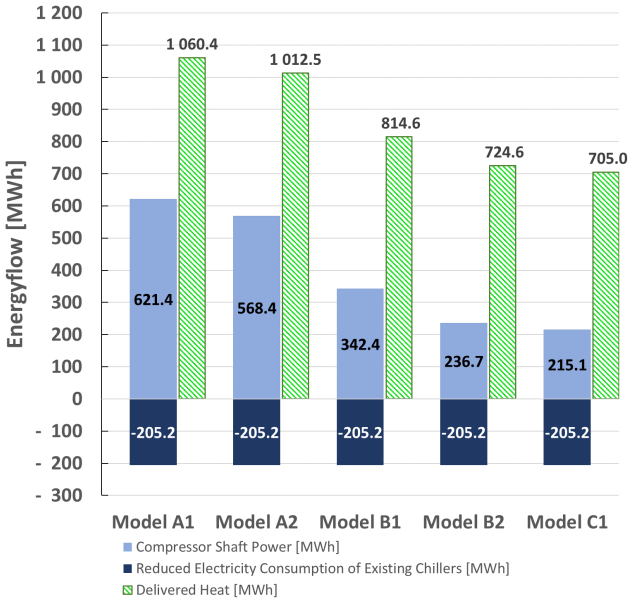


**Figure 5.32:** Energy analysis — Delivered heat, compressor electricity consumption and reduced electricity consumption of existing chillers at 8500 Full-load-Hours.

## 5.7 Costs & Profitability Analysis

### 5.7.1 Investment costs

Table 5.12 below show the estimated investment costs and fixed annual operating costs of the developed heat recovery heat pump configurations. The values are only a rough estimation estimated from general cost of heat pumps according to NVE [78]. The actual investment cost of the unit may differ from the values in Table 5.12 but since the price of heat pump installations often is considered as confidential information it has not been possible to estimate the costs more precisely.

In order to illustrate that the costs are not known exactly the rounded costs in the bottom of the table used in the following economical analysis. The investment cost of the Model A1 and A2 configuration were set equal to each other because they are identical besides the Model A2 configuration has two propane compressors. The compressors of the model A2 configuration is however smaller than the model A1 Propane compressor. It is therefore assumed that the two configurations would have a similar investment cost.

**Table 5.12:** Investment Costs — Calculated Investment and Operating Cost of Developed heat recovery heat pump configurations using data from Table 2.5 and 2.6.

| | Model A1 | Model A2 | Model B1 | Model B2 | Model C1 | Unit |
|---|---|---|---|---|---|---|
| LTC Condenser Power | 98.24 | 90.74 | 81.41 | 77.4 | - | kW |
| HTC Condenser Power | 124.75 | 119.12 | 95.83 | 51.3 | 82.94 | kW |
| Total Delivered Heat | 124.75 | 119.12 | 95.83 | 85.25 | 82.94 | kW |
| Specific Investment Costs LTC | 2184 | 2211 | 2244 | 2258 | - | NOK/kW |
| Fixed Operation Costs LTC | 40 | 40 | 40 | 40 | - | NOK/kW/year |
| Specific Investment Costs HTC | 4577 | 4855 | 6002 | 8197 | 6638 | NOK/kW |
| Fixed Operation Costs HTC | 70 | 70 | 70 | 70 | 70 | NOK/kW/year |
| Spesific Construction Interests | 351 | 364 | 415 | 438 | 443 | NOK/kW |
| Spesific Installation Costs | 5630 | 5651 | 5738 | 5777 | 5785 | NOK/kW |
| LTC Unit Costs | 214582 | 200623 | 182699 | 174804 | - | NOK |
| HTC Unit Costs | 713769 | 722867 | 719013 | 525618 | 688153 | NOK |
| Sum Unit Costs | 928351 | 923490 | 901712 | 700422 | 688153 | NOK |
| Installation Costs | 702334 | 673132 | 549826 | 492478 | 479846 | NOK |
| Total Operation Costs | 12662 | 11968 | 9965 | 6687 | 5806 | NOK/year |
| Construction Interest costs | 43828 | 43320 | 39741 | 37330 | 36738 | NOK |
| Total Investment Costs | 1674513 | 1639942 | 1491278 | 1230230 | 1204738 | NOK |
| Rounded Investment Cost | 1650 000 | 1 650 000 | 1 500 000 | 1230 000 | 1205 000 | NOK |
| Rounded Operation Costs | 12 000 | 12 000 | 10 000 | 7000 | 6000 | NOK |

The model B1, B2 and C1 configuration have smaller investment costs compared to the A1 and A2 configuration due to the lower heat sink capacity. Especially for the Model C1 configuration the costs are lower because it is a more commercially available solution and there is not a need for the cost intensive Butane Cycle, which has to be custom ordered.

### 5.7.2 Annual Costs and LCOG

#### Cost of Electricity

Table 5.13 on the following page show the estimated annual additional electricity cost of the developed heat recovery heat pump configurations. The net additional electricity costs were calculated by subtracting the value of the reduced electricity consumption of the existing chillers. The results show that the Model A1, A2 and B1 configuration lead to an annual increased electricity cost of approximately 25 000 -150 000 NOK depending on the type of model and number of hours of operation. In general the developed models with the highest COP results in the lowest additional increased electricity cost, as should be expected. Especially for the Model C1 $CO_2$ heat pump model results in almost no additional net electricity consumption due to the electricity consumption of the compressor being cancelled out by reduced electricity consumption of the existing chillers.

**Table 5.13:** Model Comparison — Annual cost of electricity and value of delivered cooling. Assumed average cost of electricity of 0.36 NOK/kWh incl. 25% VAT.

| | | Reduced Cost of Electricity Chiller | Cost of Compressor Electricity Consumption | Net Cost of Electricity |
|---|---|---|---|---|
| | FLH [h/year] | NOK/Year | NOK/Year | NOK/Year |
| Model A1 | 4250 | -36893 | 111701 | 74807 |
| | 6375 | -55340 | 167551 | 112211 |
| | 8500 | -73787 | 223401 | 149615 |
| Model A2 | 4250 | -36893 | 102181 | 65288 |
| | 6375 | -55340 | 153271 | 97931 |
| | 8500 | -73787 | 204362 | 130575 |
| Model B1 | 4250 | -36893 | 61550 | 24657 |
| | 6375 | -55340 | 92325 | 36985 |
| | 8500 | -73787 | 123100 | 49313 |
| Model B2 | 4250 | -36893 | 42556 | 5663 |
| | 6375 | -55340 | 63834 | 8494 |
| | 8500 | -73787 | 85113 | 11326 |
| Model C1 | 4250 | -36893 | 38675 | 1782 |
| | 6375 | -55340 | 58012 | 2673 |
| | 8500 | -73787 | 77350 | 3563 |

Table 5.14 on the following page show the results of the cost analysis. The table shows the annual costs and LCOG for 4250, 6375 and 8500 full load hours correlating to 50%, 75% and 100% of the estimated cooling demand based on the electricity measurements presented in Section 3.2. Since the economical lifetime of the heat recovery heat pumps also is uncertain the annual cost and LCOG have been calculated for 10, 15 and 20 years of lifetime, as seen in the table. Similar calculations have also been performed for an interest rate of 12% and 18%. The results of the cost analysis for an interest rate of 12% and 18% is attached in Table D.1 and D.2 in Appendix D. The break even LCOG for an economical life time of 15 years is estimated to be approximately 0.31 NOK/kWh for the district heating heat recovery heat pumps Model A1 and Model A2. For the hot water producing heat recovery heat pumps Model B1, Model B2 and Model C1, the LCOG is estimated to approximately 0.81, 0.74 and 0.73 NOK/kWh. The LCOG for the hot water producing heat pumps is larger than the LCOG for the district heating heat recovery heat pumps despite the lower investment costs and higher COP of the hot water heat pumps. This is because the estimated hot water demand of Austmann and 3T is to small to accommodate so large heat recovery heat pumps, the excess hot water produced therefore have to be exported out of the area by M-TES. The price of M-TES is assumed to be 0.6 NOK/kWh based on the presented theory.

**Table 5.14:** Annual costs and break even LCOG for 6% interest rate and various full load hours and economical life times.

| Interest rate 6% | | Annual Costs Economical Life time years | | | LCOE Economical Life time | | |
|---|---|---|---|---|---|---|---|
| | FLH [h/year] | 10 | 15 | 20 | 10 | 15 | 20 |
| Model A1 | 4250 | 310989 | 256696 | 230662 | 0.5866 | 0.4842 | 0.4351 |
| | 6375 | 348393 | 294100 | 268065 | 0.4381 | 0.3698 | 0.3371 |
| | 8500 | 385797 | 331503 | 305469 | 0.3638 | 0.3126 | 0.2881 |
| Model A2 | 4250 | 301470 | 247176 | 221142 | 0.5955 | 0.4882 | 0.4368 |
| | 6375 | 334113 | 279820 | 253786 | 0.4400 | 0.3685 | 0.3342 |
| | 8500 | 366757 | 312464 | 286430 | 0.3622 | 0.3086 | 0.2829 |
| Model B1 | 4250 | 440769 | 391411 | 367744 | 1.0822 | 0.9610 | 0.9029 |
| | 6375 | 575281 | 525923 | 502255 | 0.9417 | 0.8609 | 0.8221 |
| | 8500 | 709792 | 660434 | 636767 | 0.8714 | 0.8108 | 0.7817 |
| Model B2 | 4250 | 355112 | 314639 | 295231 | 0.9801 | 0.8684 | 0.8149 |
| | 6375 | 466637 | 426164 | 406757 | 0.8586 | 0.7842 | 0.7484 |
| | 8500 | 578162 | 537689 | 518282 | 0.7979 | 0.7420 | 0.7152 |
| Model C1 | 4250 | 340944 | 301293 | 282280 | 0.9672 | 0.8547 | 0.8008 |
| | 6375 | 447583 | 407932 | 388919 | 0.8465 | 0.7715 | 0.7356 |
| | 8500 | 554222 | 514571 | 495559 | 0.7861 | 0.7299 | 0.7029 |

Figure 5.33 and 5.34 on the following page show the calculated annual cost and LCOG of the developed heat recovery heat pump configurations for full load hours from 1 to 8760. The results show that for very low cooling demands and little operation of the heat recovery heat pumps, the hot water producing heat pumps result in the lowest annual costs. This is because of the lower investment cost of these heat pumps compared to the district heating heat pumps. However if the hot water production is larger than the hot water demand of Austmann and 3T, meaning that hot water has to be exported out of the area, the annual costs of the hot water heat pumps increase significantly with the number of full load hours. Due to this the heat recovery to district heating heat pumps achieve the lowest annual costs for large full load hours. The results in Figure 5.33 and 5.34 are calculated using the tax-reduced electricity price. If the electricity is bought with full tax the annual costs of especially the Model A1 and A2 heat pump configurations increase, but are still lower than the hot water heat pumps for large full load hours. The annual cost of the hot water heat pumps are less affected by the electricity tax due to the low electricity consumption of these heat pumps and high cost of M-TES.

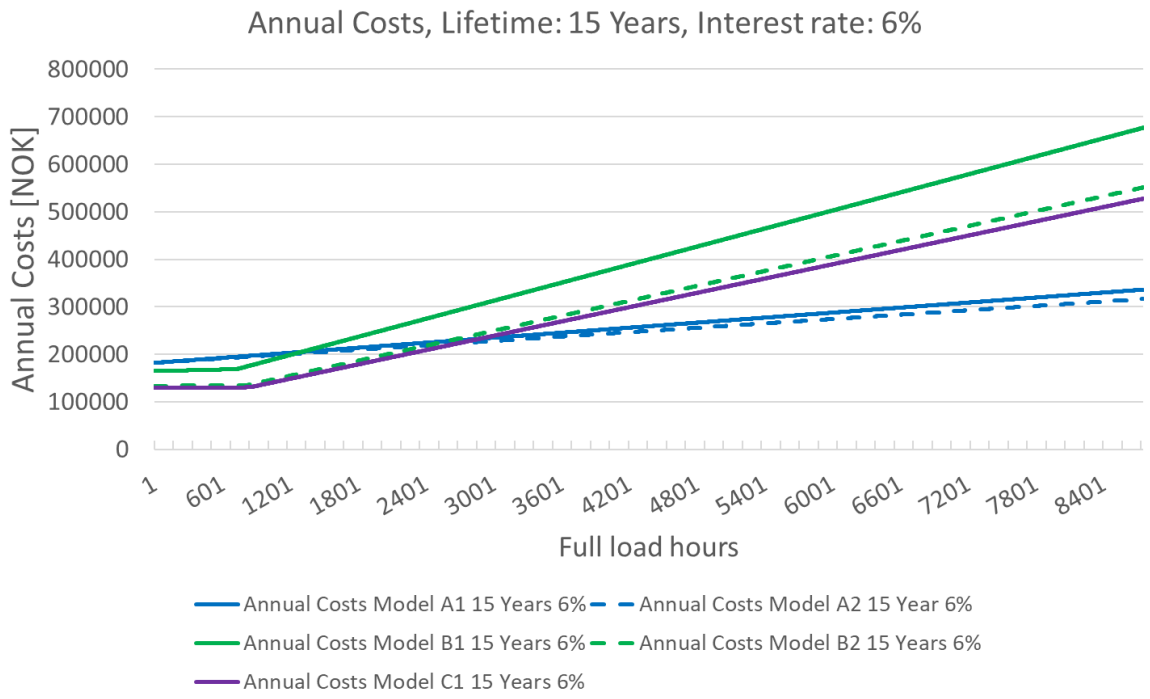


**Figure 5.33:** Annual Costs of heat recovery heat pumps with 15 year economical lifetime and 6% interest rate.

The break even LCOG of the developed heat recovery heat pumps at 15 years lifetime and 6% interest is shown in figure 5.34 below. The results show that the LCOG for the district heating heat recovery heat pumps achieve lower LCOG compared to the hot water heat pumps because of the high amount of delivered heat and lower annual cost. According to SSB the average district heating price in Norway lies between 0.55 and 0.65 NOK/kWh [93] this is illustrated with red dotted lines in the figure. It is evident from the calculated LCOG that the hot water producing heat pumps are not competitive with district heating as a source of hot water production due to the LCOG being higher than the average district heating price. This even before demand for pay-back period and profitability is considered.

In the case of the Model A1 and A2 heat recovery heat pumps delivering heat to the district heating grid the break even LCOG is lower than the average district heating price for full load hours above 3600. If the heat pumps are profitable or not depends on the demanded pay-back time, profitability requirement and what the district heating company is willing to pay for the delivered heat. Since the heat is being recovered from a cold storage facility it is reasonable to assume that most heat is going to be recovered during the summer period. A period of time when the district heating grid in Trondheim typically have an excess amount of heat it could therefore be challenging to persuade the district heating grid company to be willing to accept the heat and definitely pay for it. Whether or not the district heating company is willing to accept the heat is not further discussed in this thesis.

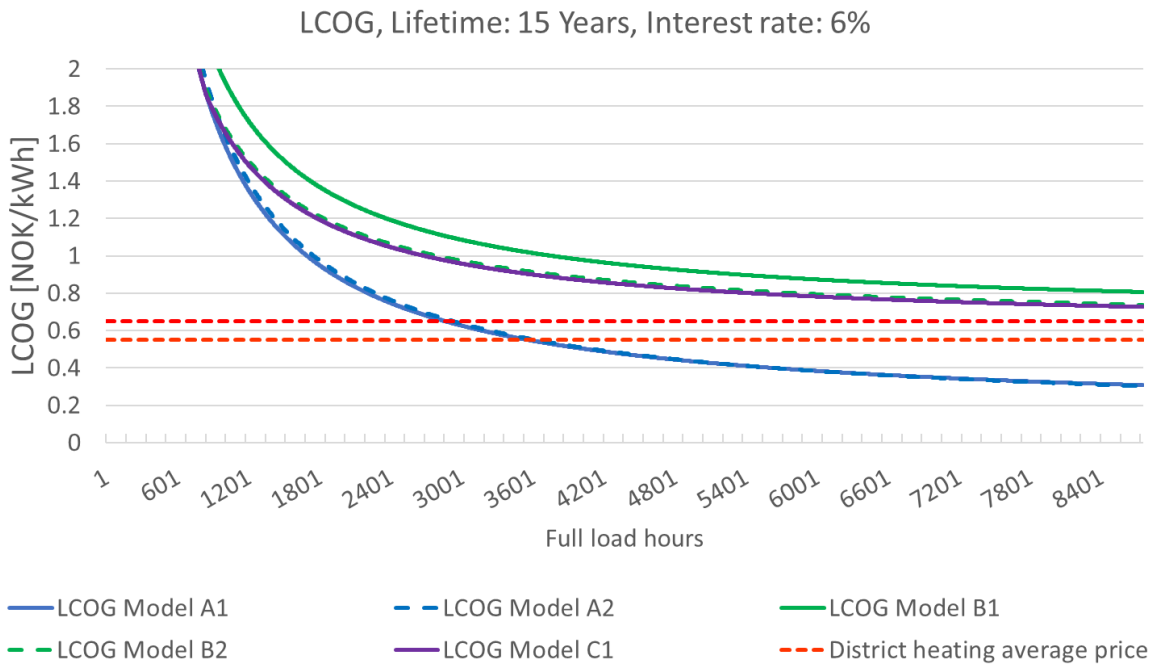


**Figure 5.34:** LCOG of heat recovery heat pumps with 15 year economical lifetime and 6% interest rate.

### 5.7.3 Maximum Investment costs

Figure 5.35 below show the maximum investment cost for the model A1 and A2 configurations calculated with a pay back time of 5 years. Two different maximum investment costs have been calculated, one for 20% interest rate and one for 6% interest rate. The maximum investment cost for 20% interest rate illustrate the maximum investment cost of a real project with a demand for profitability in order to account for risk of the investment. The investment cost for 6% interest rate have been calculated to show the absolute maximum investment cost of the heat pumps only accounting for inflation and no profit. Table 5.15 below show the calculated maximum investment cost of the Model A1 and Model A2 heat pump configuration for 4250, 6375 and 8500 full load hours, correlating to 50%, 75% and 100% of the estimated cooling demand. The maximum investment costs have been estimated to the closest 500 kr.

**Table 5.15:** Maximum investment cost of model A1 and A2 assuming 5 years pay back time.

| | Model A1 | | Model A2 | |
|---|---|---|---|---|
| FlH | 20% Interest rate | 6% Interest rate | 20% Interest rate | 6% Interest rate |
| 4250 | 216 000 | 304 500 | 223 000 | 314 000 |
| 6375 | 342 000 | 482 000 | 496 500 | 494 000 |
| 8500 | 468 000 | 659 000 | 482 000 | 679 000 |

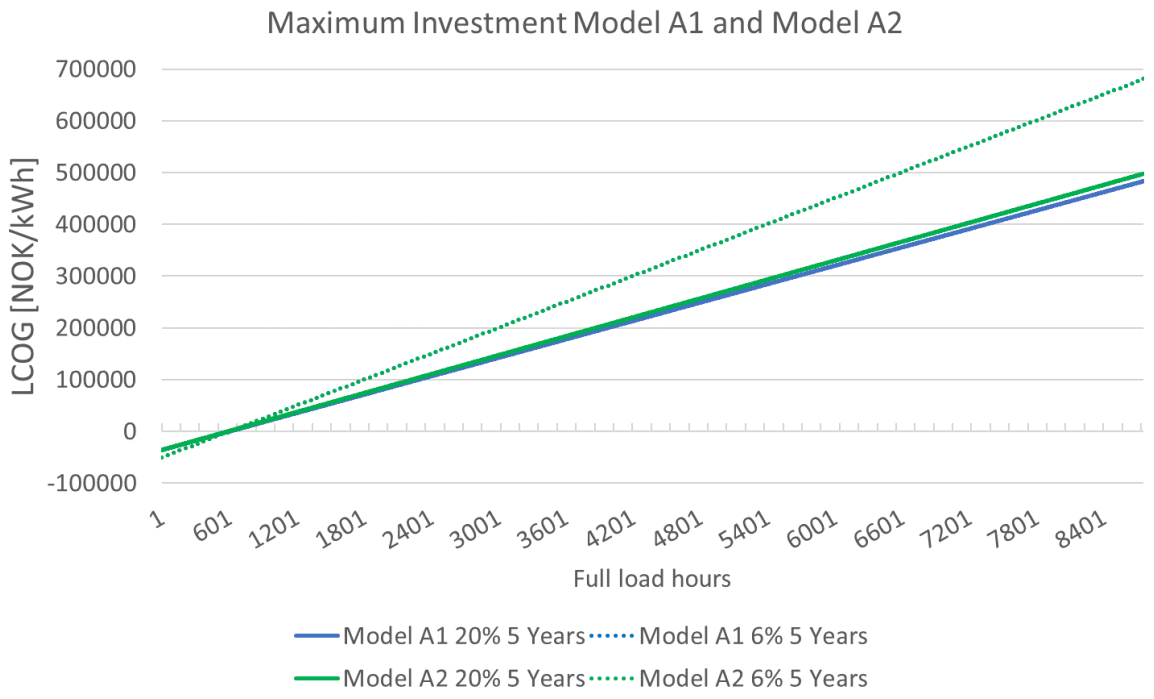


**Figure 5.35:** Maximum investment cost of Model A1 and A2 heat pump configuration at 5 years pay back time.

Chapter 6

# Conclusion

From the literature study it can be concluded that high temperature heat pumps capable of heat sink temperatures above 100°$C$ are available from a series of manufacturers. Cascade CVCC heat pumps are capable of heat sink temperatures above 100°$C$ and low temperature heat recovery, with the right choice of working fluid and configuration. Propane (R290) and Butane (R600) are a good choice of working fluids from a performance and environmental point of view. The main disadvantage with Propane and Butane is the high flammability, but safe and reliable operation is possible with safety precautions. High temperature CVCC heat pumps are limited by the available compressor technology. For hydrocarbons the suction- and discharge gas temperature is in practice limited to about 75 and 130°$C$, due to problems with oil an lubrication. Existing installations are therefore limited to small scale test and pilot heat pump not commercially available. In order to make the technology commercially available there is a need for larger scale pilot projects as +CityxChange, to test the reliability and performance under real life conditions.

Different methods of heat recovery from the cold storage facility at Sluppenveien 10 have been investigated, both recovery to the district heating grid and hot water production. As a result of this thesis five dynamic simulation models of heat potential heat recovery heat pump configurations for +CityXChange have been developed in Dymola [1]. The heat recovery heat pumps were tested for realistic operating conditions showing that the models were able to follow a average weekly cooling demand curve of the cold store down from 62.5 kW down to 45 kW. For cooling demands over 62.5 kW additional cooling has to be delivered by the existing chillers. The developed models achieved a heating/cooling COP in the range of 1.71-3.28/2.53-5.66 respectively. Where the heat pumps producing hot water achieved the highest COP and the maximum COP was achieved by the $CO_2$ heat pump. The developed R290/R600 cascade heat pump is able to recover heat to both district heating and produce hot water, however for hot water production it is overly complicated and a less advanced heat pump can deliver the same setpoint water temperature.

The hot water demand of Austmann and 3T is not known, but estimated using relevant literature and standards. The results show that the annual hot water demand of Austmann/3T is small compared to the possible hot water production by the heat recovery heat pumps. If heat should be recovered by means of hot water production large amounts of water has to be exported out of the area with M-TES.

The electricity measurements performed by the building owner show a strong degree of correlation with the activity of the cold storage facility, therefore a good indication of the weekly operation of the chillers. However the results show little correlation with ambient temperature, which it should. The measured electricity consumption increases at both high and low ambient temperatures. It is therefore likely that the electric heaters in the cold storage facility are installed on the same electrical circuit as the chillers. The measurements can therefore not be used to calculate the annual cooling demand of the cold storage.

The developed models have also been compared through an energy and economical analysis. The results show that at 8500 full load hours (FLH) 513.1 MWh of heat can be recovered from the cold storage facility. At the same FLH 1060.4-705.0 MWh of heat can be delivered to either the district heating grid or as hot water depending on which method of heat recovery and heat pump configuration is chosen. Because of the higher COP the hot water producing heat pumps are the best alternative from an energy point of view and for achieving positive energy district at Sluppen.

The economical analysis show that the Model A1 and A2 heat pump configurations recovering heat to the district heating grid, have the highest investment costs estimated to 1 650 000 NOK. Similar for the hot water producing heat pumps B1, B2 and C1 the investment cost is estimated to be in the range of 1 500 000- 1 205 000 NOK. In general heat recovery to the district heating grid requires a larger investment cost, fixed operation and maintenance costs and annual costs of electricity than heat recovery by hot water production. At very low FLH the hot water producing heat pumps achieve the lowest annual costs due to the lower investment cost, however with FLH the annual costs of heat recovery by hot water increases significantly due to the high cost of M-TES. The calculated LCOG of heat recovery to district heating and hot water production is approximately 0.31 NOK/kWh and 0.81-0.73 NOK/kWh respectively, assuming an economical lifetime of 15 years, 6% interest rate and 8500 FLH per year. Heat recovery by hot water production is not profitable compared to district heating due to higher LCOG than the average district heating price. For FLH over 3600 hours heat recovery to the district heating grid achieves a LCOG lower than the average district heating price. However the most amount of heat is likely to be recovered in the summer when there is an excess of heat in the district heating grid in Trondheim. The value of the recovered heat is therefore low from the district heating company's point of view. Assuming the heat is sold for half the district heating price, the maximum investment cost of the Model A1 and A2 configuration is estimated to be in the range of 468 000-482 000 and 659 000-679 000 for a pay back time of 5 years and 20% and 6% rate of return respectively. Substantial investment support from +CityXChange is therefore needed.

The results of this thesis are however largely dependent on the assumptions and simplifications made both in the simulation models and the energy- and economical investigation. Both the annual cooling demand and hot water demand are uncertain and have a grate impact on the results. More research and measurements is therefore needed to draw final conclusion on how and if waste heat should be recovered from Sluppenveien 10.

Chapter 7

# Further work

**Measurements**

The findings of this thesis are limited by the simplifications and assumptions made. Especially the results of the energy and economical analysis are greatly dependent on the assumed investment and operation costs as well as the cooling and hot water demand in the area. It is therefore important to perform measurements of the cooling demand of the cold storage facility and hot water demand of Austmann and 3T. When more information regarding cooling and hot water demand is known a more detailed energy and economical analysis could be performed. I a more detailed economical analysis it is also important to know more detailed information of investment costs, maintenance costs as well as selling price of delivered cooling and heat needs to be agreed on with the cold storage facility and possible recipient of recovered heat.

**Detailed energy- and economical analysis**

After a more detailed energy- and economical analysis have been performed final conclusions whether and how heat should be recovered from Sluppenveien 10. As an alternative to heat recovery installing more PV-panels could be investigated as a possible alternative to heat recovery in order to achieve the PED goal of +CityXChange.

**Detailed simulations in Dymola**

The focus of this thesis have been to investigate several possible methods heat recovery at Sluppenveien 10, it has therefore not been possible to investigate each method in great detail. When a particular method of heat recovery is chosen and measurements conducted, it would be interesting to perform more detailed simulations in Dymola. Some interesting parts of the simulation models in need of more detailed simulations are:

- **Heat Exchangers** — The heat exchanger models in this thesis are simplified using constant heat transfer rates from literature. In order to precisely determine the actual heat transfer rate and necessary heat transfer area a more detailed investigation is needed.

- **Heat and pressure losses** — In this thesis heat losses to the ambient is only regarded in the compressor models and pressure losses in the system is not considered. In order to investigate the performance of the system in detail this should be investigated.
- **Part load operation** — Several attempts of implementing variable compressor efficiencies at different operating conditions were unsuccessfully due to limitations in the ”EffCompressor” model used. To determine the part load performance of the systems a more advanced custom compressor model need to be crated enabling different compressor efficiencies at various speeds.

# Bibliography


[1] Dassault Systemes. Dymola 2020. https://www.3ds.com/products-services/catia/products/dymola/?woc=%7B%22category%22%3A%5B%22category%2Fdymola%22%5D%7D&wockw=card_content_cta_1_url%3A%22https%3A%2F%2Fblogs.3ds.com%2Fcatia%2F%22 [Accessed: 27.08.2019].

[2] Newell. R.G, Raimi. D, and Aldana G. Global energy outlook 2019: The next generation of energy. *Resources of the future*, 2019.

[3] United Nations UN. About the sustainable development goals, 2019. https://www.un.org/sustainabledevelopment/sustainable-development-goals/ [Accessed: 2019-09-26].

[4] Erostat. Europe 2020 - overview, 2019. https://ec.europa.eu/eurostat/web/europe-2020-indicators [Accessed: 2019-09-26].

[5] Skree J and Vatndal J.D. Energibruk i bygg – rammer, krav og muligheter. *Norsk Teknologi*, 2008.

[6] Norsk Energi. and Enova. Utnyttelse av spillvarme fra norsk industri, 2007. https://www.enova.no/download/?objectPath=upload_images/44EB7A65846B4824A6EB704198C3F6BC.pdf [Accessed: 2019-09-26].

[7] +CityxChange. About +cityxchange, 2019. https://cityxchange.eu/about-cityxchange/ [Accessed: 2019-09-26].

[8] European Commission. What is horizon 2020?, 2019. https://ec.europa.eu/programmes/horizon2020/what-horizon-2020 [Accessed: 2019-09-26].

[9] +CityxChange. Our cities, 2019. https://cityxchange.eu/our-cities/
Accessed: 2019-09-26
.

[10] +CityxChange. Demo Projects, 2019. https://cityxchange.eu/wp-content/uploads/2019/03/trondheim-city-map.jpg [Accessed: 2019-09-19].

[11] Medicon Village. Looking ahead, 2020. https://www.mediconvillage.se/en/looking-ahead [Accessed: 2020-02-19].

[12] Ectogrid. E.on is building the world's first ectogrid™at medicon village, 2020. http://ectogrid.com/use-cases/medicon-village/ [Accessed: 2020-02-19].

[13] Ectogrid. The ectogrid™ technology, 2020. http://ectogrid.com/business-customer/ [Accessed: 2020-02-19].

[14] Ectogrid. An illustrative view of the ectogrid™ at medicon village, 2020. http://ectogrid.com/wp-content/uploads/2018/04/MediconMap-1920-v2-no-kam.mp4 [Accessed: 2020-02-18].

[15] ZUG Estates AG. Architektonische relevanz und vorbildlichkeit auf dem areal., 2020. https://www.suurstoffi.ch/bau-projekte [Accessed: 2020-02-20].

[16] Vetterli N and Sulzer M. Dynamic analysis of the low-temperature district network. In *Conference paper, Lucerne School of Engineering and Architecture.*

[17] Prasanna A, Vetterli N, Dorer V, and M,Sulzer. Modelling the suurstoffi district based on monitored data to analyse future scenarios for energy self-sufficiency. In *Conference: 19. Status-Seminar Forschen für den Bau im Kontext von Energie und Umwelt At: ETH Zürich*, pages 1–16, 2016. https://www.researchgate.net/publication/307965462_Modelling_the_Suurstoffi_district_based_on_monitored_data_to_analyse_future_scenarios_for_energy_self-sufficiency [Accessed: 20.02.2020].

[18] ZugEstates. Suurstoffi zero-zero area, 2020. https://www.zugestates.ch/fileadmin/user_upload/redakteure/bilder/nachhaltigkeit/img_zero_zero_energiesystem.jpg [Accessed: 2020-02-18].

[19] Hesselgreaves J.E. *Compact Heat Exchangers, Selection, Design and Operation.* PERGAMON, Elsevier Science Ltd, 2001.

[20] Stene J. *Varmepumper - Grunnelggende varmepumpeteknikk*. SINTEF Energiforskning AS, Klima- og kuldeteknikk, 2001.

[21] Koelet P.C. *Industrial Refrigeration*. Macmillan, 1992.

[22] United Nations UN. About montreal protocol, 2019. https://www.unenvironment.org/ozonaction/who-we-are/about-montreal-protocol [Accessed: 2019-10-12].

[23] United Nations UN. What is the kyoto protocol?, 2019. https://unfccc.int/kyoto_protocol
Accessed: 2019-10-12

.

[24] European Commission. Eu legislation to control f-gases, 2019. https://ec.europa.eu/clima/policies/f-gas/legislation_en
Accessed: 2019-10-12

.

[25] Hafner A. The advantages of natural working fluids. In *25th IIR International Congress of Refrigeration*, pages 2456–2464, 2019.

[26] The Norwegian Environment Agency. Study on environmental and health effects of hfo refrigerants, 2017. https://www.miljodirektoratet.no/globalassets/publikasjoner/M917/M917.pdf [Accessed: 2019-10-14].

[27] Standard Norge. NS-EN 378-1:2016 — Kuldeanlegg og varmepumper - Sikkerhets- og miljøkrav - Del 1: Grunnleggende krav, definisjoner, klassifisering og vurderingskriterier, 2016.

[28] Bamigbetan. O, Eikevik. T.M, and Bantle P, Nekså.and M. Review of vapour compression heat pumps for high temperature heating using natural working fluids. *International Journal of Refrigeration*, 80:197 – 211, 2017. https://doi.org/10.1016/j.ijrefrig.2017.04.021.

[29] Brodowicz K and Dyakowski T. *Heat Pumps*. Butterworth-Heinemann Ltd 1990, 1993.

[30] Nekså P, Bantle M, Schlemminger C, and Bamigbetan O. High temperature industrial heat pumps utilising natural working fluids. In *25th IIR International Congress of Refrigeration*, pages 4729–4735, 2019.

[31] Rath S. *Brannfarlige kuldemedier*. Stig Rath Consulting, 2018.

[32] Standard Norge. NS-EN 378-2:2016 — Kuldeanlegg og varmepumper - Sikkerhets- og miljøkrav - Del 2: Utforming, bygging, prøving, merking og dokumentasjon, 2016.

[33] Standard Norge. NS-EN 378-3:2016 — Kuldeanlegg og varmepumper - Sikkerhets- og miljøkrav - Del 3: Oppstillingssted og personvern, 2016.

[34] Standard Norge. NS-EN 378-4:2016 — Kuldeanlegg og varmepumper - Sikkerhets- og miljøkrav - Del 4: Drift, vedlikehold, reparasjon og gjenbruk, 2016.

[35] Allymehr E, Eikevik T.M, and Hafner A. Experimental investigation of evaporation of propane (R290) in small pipes. In *25th IIR International Congress of Refrigeration*, pages 18559–1862, 2019.

[36] Bamigbetan. O, Eikevik. T.M, Nekså. P, Bantle M, and Schlemminger C. Theoretical analysis of suitable fluids for high temperature heat pumps up to 125°C heat delivery. *International Journal of Refrigeration*, 92:185 – 195, 2018. https://doi.org/10.1016/j.ijrefrig.2018.05.017.

[37] Schlemminger C, Svendsen E.S, Foslie S.S, Bantle M, Bamigbetan O, and Nekså P. Performance of high temperature heat pump for simultaneous and efficient production of ice water and process heat. In *25th IIR International Congress of Refrigeration*, pages 4632–4639, 2019.

[38] Koelet P.C. *Industrial Refrigeration*. Macmillan, 1992.

[39] Haukås H.T. *Norsk kulde- og varmepumpenorm 2018*. Norsk kjøleteknisk forening, 2018.

[40] Chen Y.G. Optimal heat rejection pressure of co2 heat pump water heaters based on pinch point analysis. *International Journal of Refrigeration*, 106:592 – 603, 2019. https://doi.org/10.1016/j.ijrefrig.2019.04.003.

[41] Zijdemans D. *Vannbaserte oppvarmings- og kjølesystemer*. Skarland Press AS, 2014.

[42] Direktoratet for byggkvalitet. Byggteknisk forskrift (tek17) med veiledning. https://dibk.no/byggereglene/byggteknisk-forskrift-tek17/15/ii/15-5/ [Accessed: 06.05.2020].

[43] Canadian Industry Program for Energy Conservation. Guide to energy efficiency opportunities in the canadian brewing industry. https://www.nrcan.gc.ca/sites/www.nrcan.gc.ca/files/oee/files/pdf/publications/industry/Brewers_Guide_access_e.pdf [Accessed: 13.02.2020].

[44] Kubule A, Zogla L, Ikaunieks J, and Rosa M. Highlights on energy efficiency improvements: a case of a small brewery. *Journal of Cleaner Production*, 138:275 – 286, 2016. https://doi.org/10.1016/j.jclepro.2016.02.131.

[45] Muster Slawitsch B, Weiss W, Schnitzer H, and Brunner C. The green brewery concept – energy efficiency and the use of renewable energy sources in breweries. *Applied Thermal Engineering*, 31(13):2123 – 2134, 2011. Selected Papers from the 13th Conference on Process Integration, Modelling and Optimisation for Energy Saving and Pollution Reduction.

[46] Giner Santonja G, Karlis P, Stubdrup K, Brinkmann T, and Roudier S. Best available techniques (bat) reference document for the food, drink and milk industries. industrial emissions directive 2010/75/eu (integrated pollution prevention and control), eur 29978 en, publications office of the european union, luxembourg. 2019. https://doi.org/10.2760/243911.

[47] B. Sturm, S. Hugenschmidt, S. Joyce, W. Hofacker, and A.P Roskilly. Opportunities and barriers for efficient energy use in a medium-sized brewery. *Applied Thermal Engineering*, 53(2):397 – 404, 2013. Includes Special Issue: PRO-TEM Special Issue.

[48] Brewers Association. Energy usage, ghg reduction, efficiency and load management manual. https://www.brewersassociation.org/attachments/0001/1530/Sustainability_Energy_Manual.pdf [Accessed: 13.02.2020].

[49] Campden BRI. About us – sites. https://www.campdenbri.co.uk/about.php [Accessed: 01.05.2020].

[50] Campden BRI. Worldwide brewery industry water and energy benchmarking survey. https://www.campdenbri.co.uk/images/WaterEnergy.pdf [Accessed: 01.05.2020].

[51] Arpagaus C, Bless. F, Uhlmann. M, Schiffmann J, and Bertsch S.S. High temperature heat pumps: Market overview, state of the art, research status, refrigerants, and application potentials. *Energy*, 152:985 – 1010, 2018. https://doi.org/10.1016/j.energy.2018.03.166.

[52] Jensen J.K, Markussen W.B, Reinholdt L, and Elmegaard B. On the development of high temperature ammonia–water hybrid absorption–compression heat pumps. *International Journal of Refrigeration*, 58:79 – 89, 2015. https://doi.org/10.1016/j.ijrefrig.2015.06.006.

[53] Bamigbetan. O, Eikevik. T.M, Nekså P, Bantle M, and Schlemminger C. The development of a hydrocarbon high temperature heat pump for waste heat recovery. *Energy*, 173:1141–1153, 2019. https://doi.org/10.1016/j.energy.2019.02.159.

[54] G.F. Frate, L. Ferrari, and U. Desideri. Analysis of suitability ranges of high temperature heat pump working fluids. *Applied Thermal Engineering*, 150:628 – 640, 2019. https://doi.org/10.1016/j.applthermaleng.2019.01.034.

[55] Verdnik M, Rieberer R, and H. Mosi. Trans-critical vapor compression cycle using butane (R600) as refrigerant for industrial waste heat recovery. In *25th IIR International Congress of Refrigeration*, pages 4697–4704, 2019.

[56] Wemmers A.K, Van Haasteren A.W.M.B, Kremers P, and Van der Kamp J. Test results R600 pilot heat pump. In *12th IEA Heat Pump Conference*, 2017.

[57] Bamigbetan. O, Eikevik. T.M, Nekså. P, Bantle M, and Schlemminger C. Experimental investigation of a prototype R-600 compressor for high temperature heat pump. *Energy*, 169:730 – 738, 2019. https://doi.org/10.1016/j.energy.2018.12.020.

[58] Kosmadakis. G. Estimating the potential of industrial (high-temperature) heat pumps for exploiting waste heat in eu industries. *Applied Thermal Engineering*, 156:287 – 298, 2019. https://doi.org/10.1016/j.applthermaleng.2019.04.082.

[59] Koomey J. Growth in data center electricity use 2005 to 2010. *A report by Analytical Press, completed at the request of The New York Times*, 9:161, 2011.

[60] Lu T, Lü X, Remes M, and Viljanen M. Investigation of air management and energy performance in a data center in finland: Case study. *Energy and Buildings*, 43(12):3360 – 3372, 2011. https://doi.org/10.1016/j.enbuild.2011.08.0340.

[61] Wahlroos. M, Pärssinen. M, Rinne. S, Syri. S, and Manner J. Future views on waste heat utilization – case of data centers in northern europe. *Renewable and Sustainable Energy Reviews*, 82:1749 – 1764, 2018. https://doi.org/10.1016/j.rser.2017.10.058.

[62] Stenberg SÅ. Tietokonesalien hukkalämmön hyödyntämismahdollisuuksien teknis-taloudellinen optimointi (technical and economical optimization of data center waste heat utilization). Master's thesis, Master's thesis. Espoo, Finland: Aalto University, 2015.

[63] ASHRAE. *ASHRAE Handbook Refrigeration*, chapter 9,13. 2010. ISBN :978-1-933742-82-3.

[64] Lund H, Werner S, Wiltshire R, Svendsen S, Thorsen J.E, Hvelplund F, and Vad Mathiesen B. 4th generation district heating (4gdh): Integrating smart thermal grids into future sustainable energy systems. *Energy*, 68:1 – 11, 2014. https://doi.org/10.1016/j.energy.2014.02.089.

[65] Hongwei Li and Svendsen S. Energy and exergy analysis of low temperature district heating network. *Energy*, 45(1):237 – 246, 2012. The 24th International Conference on Efficiency, Cost, Optimization, Simulation and Environmental Impact of Energy, ECOS 2011.

[66] Kallert A and Schmidt D. Future low temperature district heating design guidebook, 2017. https://www.euroheat.org/publications/reports-and-studies/future-low-temperature-district-heating-design-guidebook/ (Accessed: 15.01.2020).

[67] Incoperta F.P, Dewitt D.P, Bergman T.L, and Lavine A.S. *Incopera's Principles of Heat and Mass Transfer.* John Wiley & Sons Singapore Pte. Ltd., 2018.

[68] Zenhai G. *Principles of Reinforced Concrete*. Elsevier Inc, 2014. https://doi.org/10.1016/C2013-0-13698-7.

[69] D.R.Legates. *Encyclopedia of World Climatology, Latent Heat*, pages 450–451. Springer Netherlands, Dordrecht, 2005. https://doi.org/10.1007/1-4020-3266-8_124.

[70] Kalaiselvam S and Parameshwaran R. *Thermal Energy Storage Technologies for Sustainability*. Academic Press Elsevier Inc. 32 Jamestown Road, London NW1 7BY, UK, 2014.

[71] Eggen G and Vangsnes G. Heat pump for district cooling and heating at oslo airport gardermoen. In *Proceedings 8th IEA Heat Pump Conference, Las Vegas, Nevada*, volume 30, 2005.

[72] Chiu J.NW, Castro Flores J, Martin V, and Lacarrière B. Industrial surplus heat transportation for use in district heating. *Energy*, 110:139 – 147, 2016. https://doi.org/10.1016/j.energy.2016.05.003.

[73] Li H, Wang W, Yan J, and Dahlquist E. Economic assessment of the mobilized thermal energy storage (m-tes) system for distributed heat supply. *Applied Energy*, 104:178 – 186, 2013. https://doi.org/10.1016/j.apenergy.2012.11.010.

[74] Wang W, Guo S, Li H, Yan J, Zhao J, Li X, and Ding J. Experimental study on the direct/indirect contact energy storage container in mobilized thermal energy system (m-tes). *Applied Energy*, 119:181 – 189, 2014. https://doi.org/10.1016/j.apenergy.2013.12.058.

[75] Guo S, Li H, Zhao J, Li X, and Yan J. Numerical simulation study on optimizing charging process of the direct contact mobilized thermal energy storage. *Applied Energy*, 112:1416 – 1423, 2013. https://doi.org/10.1016/j.apenergy.2013.01.020.

[76] Deckert M, Scholz R, Binder S, and Hornung A. Economic efficiency of mobile latent heat storages. *Energy Procedia*, 46:171 – 177, 2014.

[77] Stene J. Investeringsanalyse for varmepumpesystemer. In ., page 9, 2019.

[78] NVE. Dokumentasjon for kostnadar i energisektoren, 24.04.2020. https://www.nve.no/energiforsyning/energiforsyningsdata/dokumentasjon-for-kostnadar-i-energisektoren/.

[79] NORSK KLIMA SERVICE SENTER. Observasjoner og værstatistikk, homogenisert middeltemperatur trondheim voll, 2020. https://klimaservicesenter.no/observations/, [Acccsessed: 2020-03-17].

[80] DAIKIN. *DAIKIN Chiller selection software SERIES: EWAD D-*. Daikin.

[81] Leonhardsen S. Elektrisitetsforbruk sluppenveien 10, 12.03.2020. Email correspandance: sondre.leonhardsen@kjeldsberg.no to erlendnb@stud.ntnu.no.

[82] NORSK KLIMA SERVICE SENTER. Observasjoner og værstatistikk, lufttemperatur (timer) trondheim risvollan. https://klimaservicesenter.no/observations/, [Accessed: 2020-03-16].

[83] Mosling Vonstad C. +cityxchange — energiforbruk kjølemaskiner sluppenveien 10, 19.03.2020. Email correspandance: Cato.Vonstad@bama.no to erlendnb@stud.ntnu.no.

[84] Wikipedia. Austmann bryggeri. https://no.wikipedia.org/wiki/Austmann_Bryggeri[Accessed: 28.05.2020].

[85] Standard Norge. SN/TS 3031:2016 — Bygningers energiytelse, Beregning av energibehov og energiforsyning., 2016.

[86] Standard Norge. SN-NSPEK 3031:2020 — Bygningers energiytelse, Beregning av energibehov og energiforsyning., 2020.

[87] Dr Wolf Srl. Dorin software 19.10. https://www.dorin.com/en/Software [Accessed: 17.10.2019].

[88] BITZER Kühlmaschinenbau GmbH. Bitzer software v6.13.0 rev2417. https://www.bitzer.de/websoftware/ [Accessed: 05.05.2020].

[89] F Chart Software. Engineering equations solver, 2019.

[90] Institut für Thermodynamik Technische Universität Braunschweig: TLK-Thermo GmbH & IfT. Til media & til component library 3.5.0. [Accessed: 27.08.2019].

[91] Stistisk Sentralbyrå. Elektrisitetspriser. https://www.ssb.no/statbank/table/09363/tableViewLayout1/[Accessed: 02.06.2020].

[92] Skattedirektoratet. Avgift pÅ elektrisk kraft 2019. https://www.skatteetaten.no/globalassets/bedrift-og-organisasjon/avgifter/saravgifter/elektrisk-kraft/2019-el-kraft.pdf[Accessed: 02.06.2020].

[93] Stistisk Sentralbyrå. Fjernvarme og fjernkjøling i norge. https://www.ssb.no/energi-og-industri/artikler-og-publikasjoner/fjernvarme-og-fjernkjoling-i-norge[Accessed: 02.06.2020].

[94] ACM Kälte Klima. Scaey air cooled water chillers air cooled reversible heat pumps from 45 kw to 320 kw, 2011. http://interfrigo.co.rs/PDF/ACM/CatalogoSCAEYDE88rev0411.pdf [Accessed: 2020-03-15].

[95] Zeta Echos. Chillers and heat pumps air/water 41-125 kw, 2014. http://www.easyairconditioning.com/images/bluebox/bluebox-pdfs/zeta-echos-aircooled-water-chillers-and-heat-pumps-41-to-125-kw.pdf [Accsessed: 2020-03-15].

[96] DAIKIN EUROPE N.V. Air cooled multiple scroll chi, 2014. https://www.daikin.fr/content/dam/document-library/catalogues/as/air-cooled-chiller/ewaq-dayn/EWAQ-DAYN_EWYQ-DAYN_ECPEN09-422_Catalogues_English.pdf [Accessed: 2020-03-15].

Appendix A

# Draft of Scientific Paper

# Evaluation of possible heat pump configurations for waste heat recovery at +CityXChange Sluppen

**Erlend Nytrø Balstad**[1]

[1]Institutt for energi- og prosessteknikk, NTNU, Trondheim, 7439, Norway
[1]Email: erlendnb@stud.ntnu.no

10.06.2020

## ABSTRACT

Waste heat utilization is important for improving energy efficiency and reducing $CO_2$ emissions in Norway. The purpose of this thesis is to evaluate different heat pump configurations for waste heat recovery at +CityXChange Sluppen, both for district heating and production of hot water. Through developing five dynamic simulation models in Dymola. Simulated at both design point and at a realistic weekly cooling demand curve derived from electricity measurements. The measurements show a strong degree of correlation with the activity in the cold storage, but little correlation with ambient temperature. The models achieved a heating/cooling COP of 1.71-3.28/2.53-5.66 with the minimum and maximum COP was achieved by district heating and hot water producing heat pumps respectively. Estimated hot water demand is small compared to the possible production, large amounts of hot water therefore has to be exported with M-TES. Due to the uncertainty in cooling demand, an energy- and economical analysis have been performed as a function of full load hours (FLH). The results show that at 8500 FLH 513.1 MWh of heat can be recovered and 705.0-1060.4 MWh heat delivered, depending on chosen heat pump configuration. The annual costs of hot water production increases with FLH due to the high cost of M-TES. Heat recovery by hot water production is therefore most energy efficient, but not profitable compared to district heating. For FLH over 3600 hours heat recovery to district heating achieves lower LCOG than the average district heating price, but the maximum profitable investment cost is less than the estimated investment costs. Substantial investment support from +CityXChange is therefore needed.

# 1 INTRODUCTION

Climate change is a growing threat to our common future, the sea level is rising and weather patterns are changing. At the same time the worlds demand for energy is increasing, and is expected to grow by 20-30% within 2040 [1]. Facing climate change while maintaining economic growth is a tremendous challenge in need of new solutions. For instance $\approx 36\%$ of the total energy consumption in Norway is related to building use and operation [2]. At the same time a study by Norsk Energi in collaboration with Enova [3] found that Norway has $19.2\ TWh$ of available waste heat from industry. Thereof $3.3\ TWh$ is in the low temperature range 25 to $40°C$. Developing new methods to utilize this excess heat is therefore vital to reducing the energy consumption and $CO_2$ emissions in Norway. This can be achieved through use of state of the art heat pump technology.

## 1.1 About the Master Thesis

The objective of this thesis is to evaluate possible heat recovery heat pump configurations for waste heat recovery at Sluppenveien 10, a part of developing Positive energy block (PEB) at Sluppen-Tempe in Trondheim. Both heat recovery to the district heating grid and for hot water production are considered, with a focus on heat pumps utilizing natural refrigerants. This work is the results of the Master Thesis conducted during the spring of 2020 and a continuation of the Project thesis and a summer internship for Statkraft Varme AS, one of the participants of the +CityXChange project.

## 1.2 +CityXChange

+CityxChange is a smart city project funded by the European Union [4]. The project is a part of the European Unions research and innovation program *Horizon 2020* , under the scope *Smart cities and communities* [5]. The goal of the project is to develop sustainable cities for the future. The two *Light house cities* Trondheim and Limerick are to develop sustainable and climate-friendly demo projects in urban environments. Positive Energy Blocks (PEB) are to be created through innovative solutions in energy markets, implementing new technology and business models.

+CityxChange in Trondheim consists of three demonetisation areas: DA1 Sluppen-Tempe, DA2 Brattøra and DA3 Campus Gløshaugen. This thesis will focus on thermal energy solutions of DA1 Sluppen-Tempe. Positive Energy Block Sluppen-Tempe consist of in total eight buildings. The location of all +CityxChange buildings at Sluppen-Tempe except Ola Frost vei as well as a simplified overview of the road and district heating infrastructure in the area is shown in Figure 1 below. Figure 2 shows which of the buildings in the area are currently connected to the district heating grid as well as sources of, and potential recipients of waste heat in the area.

SLV10 and SLV17A both have excess waste heat which can be utilized. The heat sources in the two buildings are cold storage and cooling of a computer centre for SLV10 and SLV17A respectively. Unlike SLV17A is SLV10 not connected to the existing district heating grid. The lack of district heating connection and period of waste heat availability is of importance when considering potential methods of waste heat recovery. Some of the most promising possible recipients of the excess waste heat are; Austmann a local brewery located in the same building and 3T Sluppen a fitness center as well as heat recovery the building to the existing district heating grid.

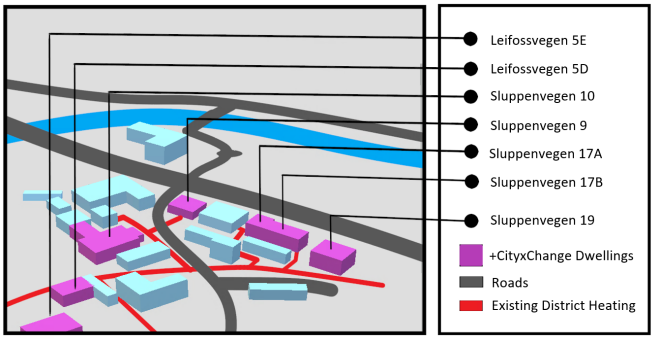


Figure 1: Simplified 3D overview of the +Cityx-Change buildings at Sluppen-Tempe.

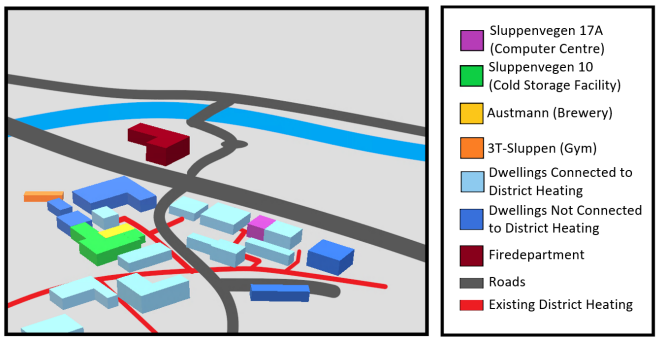


Figure 2: Simplified 3D overview of the Sluppen-Tempe Area.

# 2 Theory & Literature

## 2.1 High temperature heat pumps

The temperature level of high temperature heat pumps (HTHP) is not consistently defined in literature. In this thesis it is therefore decided to use Arpagaus' definition of HTHP, which is heat sink outlet temperatures (HSiOT) above 100°$C$ [6]. Arpagaus performed a thorough market overview, reviewing current research and technology status of HTHPs capable of HSiOT of 90-160°$C$. Among the most important findings of the study are; There is a large potential for waste heat recovery from industry in Europe. Over 20 HTHPs from 13 manufacturers are capable of HSiOT above 90°$C$, but few are able to deliver HSiOTs over 120 °$C$. Arpagaus also concludes that some important barriers to development in HTHP technology are; Long pay back periods, usually above 3 years. Limited availability of low GWP working fluids and few pilot and demonstration heat pumps. Different HTHP technologies exist, for instance Bamigbetan [7] has developed a prototype vapor-compression HTHP using a two-cascade system with Propane (R290) and Butane (R600) as working fluids. Consistent with the goals of +CityXChange and to aid further developments in HTHPs with natural working fluids, this study will focus on high temperature vapor-compression heat pumps with natural working fluids.

Of the low GWP hydrocarbons, Butane, Pentane and their respective isomers is well suited for high temperature delivery due to their high critical temperature. Bamigbetan, Eikevik, Nekså, Bantle and Schlemminger performed a theoretical analysis of suitable working fluids for high temperature heat delivery [8]. They found that R601 and R601a is capable of delivering a

maximum heat sink outlet temperature (HSiOT) of 134 °C and for R600 and R600a the maximum HSiOT was 128 °C. According to Bamigbetan, Eikevik, Nekså, Bantle and Schlemminger R601 achieved the highest simulated COP, however the suction temperature is more restricted for R601 and R601a compared to R600 and R600a. The low volumetric heating capacity of R601 results in a 2-3 times larger compressor size compared to R600. Increasing investment costs. R600 also has the advantage of a broader operating range and is thermodynamically closer to R290 [8]. There exists commercially available compressor technology for R290 which can be used with R600 with small modifications.

Bamigbetan has in collaboration with SINTEF Energy Research, developed a 20 kW prototype cascade heat pump using Propane (R290) and Butane (R600) as working fluids [7]. The heat pump is capable of waste heat recovery at 30°$C$ and HSiOT of 115°$C$. For temperature lifts of 58-72 and 98-101 $K$ the average heating COPs was found to be 3.1 and 2.1 respectively [7]. The heat pump is also tested with a evaporation temperature of -1°$C$ to +1°$C$ and 113°$C$ to 118°$C$ condensation temperature, delivering chilled ice-water at 4°$C$ and hot water at 85°$C$ to 116°$C$ [9]. The combined heating and cooling COP achieved was 2.6-2.8 [9].

Often the maximum HSiOT is not restricted by $T_{Crit}$, but by the maximum compressor discharge temperature (CDT) or maximum compressor suction temperature (CST), given by the available compressor technology. For hydrocarbons the maximum CDT is 140°$C$ and the highest CST is 80°$C$ [8]. No commercially available hydrocarbon compressors are able to handle these temperature conditions, Bamigbetan therefore developed a prototype R600 semi-hermetic piston compressor [10]. The compressor is a modified R290 compressor with 4 cylinders manufactured by Mario Dorin S.p.A., with a displacement of 48.82 $m^3/h$ and a rated maximum operating pressure of 31 $bar$ [7], [10]. The maximum operating pressure was under 22 bar significantly lower than the maximum rated pressure [7]. The HTC prototype R600 compressor achieved an average isentropic efficiency of 84%, average total compressor efficiency of 74% and an average volumetric efficiency of 82% [7]. The average isentropic, total and volumetric efficiency of the LTC was 65%, 60% and 74% [7].

## 2.2 Breweries

The brewery process and beer production in particular is very intensive in both energy and water consumption [11]. A literature study have been performed in order to investigate the energy consumption of the brewery process.Table 1 below shows an overview of several studies investigating the energy consumption of breweries.

Table 1: Literature overview: Energy consumption of beer production.

| Source | Brewery Size | Production | Thermal Energy Consumption | Electricity Consumption |
|---|---|---|---|---|
| Kubule 2016 [12] | Small Size | 15 000 - 17000 hl/y | 219.2-231.3 $^{(a)}$ MJ/hl | 81-92 MJ/hl |
| Muster-Slawitsch 2011 [13] | Small Size | 20 000 - 50 000 hl/y | 104.5 $^{(b)}$ MJ/hl | - |
| Muster-Slawitsch 2011 [13] | Medium Size | 800 000 hl/y | 43.6 $^{(b)}$ MJ/hl | - |
| EU Commission 2019 [14] | All Sizes | 20 000 -500 000 hl/y | 87-121 $^{(c)}$ MJ/hl | - |
| Canadian Brewing Industry [11] | All Sizes | <100 000 to >500 000 | 150 $^{(c)}$ MJ/hl | |
| Campden BRI [15] | Large breweries | > 500000 hl/y | 141-207 $^{(d)}$ MJ/hl | |

$^{(a)}$ Inclusive space heating, $^{(b)}$ Exclusive space heating, $^{(c)}$ Not specified, $^{(d)}$ Total energy consumption.

**Water Consumption in Breweries**
As previously mentioned the brewing of beer has a high water consumption. Campden BRI a part of Bristol University [15], have in collaboration with the brewing industry performed a global study of energy and water consumption in 225 breweries [16]. The study concluded that the average water consumption had dropped by 17% from 5.2 hl/hl in 2008 to 4.3 hl/hl in 2012. Few studies found have investigated the distribution of water within the brewery, but according to the Canadian Industry Program for Energy Conservation report "Guide to energy efficiency opportunities in the Canadian brewing industry" [11] is; 20% of water used as raw material in product, 10% For heat transfer, 45% fro cleaning and 25% Other applications including losses.

## 2.3 Mobile thermal energy storage — M-TES

When the heat source and heat customer are not located in near proximity to each other mobile thermal energy storage (M-TES) can be viable option for transporting thermal energy. Some studies suggest Latent M-TES using Erythritol as phase change material (PCM) is a good option for waste heat recovery from the industry [17]. In Västerås Sweden, a pilot project investigated using M-TES with Erythritol as PCM for waste heat recovery from the industry [17], [18], [19], [20]. The M-TES system was for a transportation distance of 30 km more attractive than an oil boiler , and the cost estimated to be in the range of 0.03-0.06 USD/kWh. The price of PCM had the most impact on cost of heat transportation [18]. They also evaluated using sensible M-TES

with water, concluding that Water M-TES is competitive to Erythritol M-TES, especially for small transportation distances and small building areas [18]. An economical assessment of M-TES by Chiu, Castro Flores, Martin and Lacarriere [17] considered transportation by both rail and maritime. They found a levelized cost of thermal energy of; 49, 62 and 86 Eur/MWh for maritime, rail and road transportation. Deckert, Scholz, Binder and Hornung [21] investigated the economical efficiency of Latatent M-TES using Sodium Acetate Hydrate. Their economic assessment resulted in costs of 5 ct/kWh. Table 2 below summarises the found costs of M-TES in literature.

Table 2: Literature overview: Specific costs of mobile thermal storage (M-TES)

| Source | Technology | Specific energy storage cost | Storage cost in NOK/MWh |
|---|---|---|---|
| Li 2013 [18] | PCM Erythritol | 0.03-0.06 USD/kWh | 300-600* NOK/MWh |
| Deckert 2014 [21] | PCM Sodium Acetate Hydrate | 5 ct/kWh | 550* NOK/MWh |
| Chiu 2016 [17] | PCM Erythritol | $49^{(a)}$, $62^{(b)}$, $86^{(c)}$ EUR/MWh | 539-946* NOK/MWh |

Transportation method:$^{(a)}$ Maritime, $^{(b)}$ Rail, $^{(c)}$ Road.
*Assuming an exchange rate of EUR/NOK of 11. and USD/NOK of 10.

## 2.4 Principles of Cost & Investment analysis

Heat pumps are complex technical installations and typically large capital investments. Norges Vassdrags- og Energidirektorat (NVE) have developed an Excel-sheet of standard values for documentation of costs in the Norwegian energy sector [22]. Heat pump costs according to NVE [22] for geothermal heat pumps with capacities from 35 to 150 kW delivering hot water at 55 °C and 70 °C respectively, excluding energy wells and heat extraction system is shown in Table 3 below. Geothermal heat pumps was chosen because they were considered to be most comparable to the intended SLV10 heat pump installation.

Table 3: Heat Pump Costs According to NVE: Heat Pump Brine to Water [22].

| | Brine to Water 55 C | | | Brine to Water 70 C | | Unit |
|---|---|---|---|---|---|---|
| Capacity | 35 | 75 | 150 | 35 | 150 | kW |
| Heat Pump Unit | 100 000 | 170 000 | 300 000 | 315 000 | 500 000 | NOK/Unit |
| Installation Cost | 115 500 | 247 500 | 495 000 | 115 500 | 495 000 | NOK/Installation |
| Specific Unit Cost | 2 875 | 2 267 | 2 000 | 9 000 | 3 333 | NOK/kW |
| Spcsific Installation Cost | 3 300 | 3 300 | 3 300 | 3 300 | 3 300 | NOK/kW |
| Specific Construction Interests | 274 | 248 | 236 | 548 | 296 | NOK/kW |
| Sum Specific Investment Costs | 6449 | 5815 | 5536 | 12848 | 6929 | NOK/kW |
| Fixed Operational Costs | 40 | 40 | 40 | 70 | 70 | NOK/kW/year |
| Total Specific Costs | 6489 | 5855 | 5576 | 12918 | 6999 | NOK/kW |

Some frequently used parameters for comparison of the costs and profitability of energy systems are; Annual Costs (AC), Levelized cost of generation (LCOG) and the maximum investment costs. The definition of these economical parameters are shown in Equation 1-3 below.Both AC and LCOG can be used to compare different methods of energy production.

$$AC = \sum I_0 * a + \sum W_E * e + \sum O\&M \quad [23] \tag{1}$$

$$LCOG = \frac{AC}{\sum Q_{Produced}} \quad [23] \tag{2}$$

$$Maximum\ investment\ cost = \sum_{i}^{n} \left(\frac{B_i}{(1+r)^i}\right) \approx B \cdot \frac{1-(1+r)^{-n}}{r} \quad [24] \tag{3}$$

# 3 Existing Technical Installations

## 3.1 Cold Storage Facility

Sluppenveien 10 is an old light-industry building constructed in the 1970s. Today the building is mainly a cold storage facility. The building has over 6600 $m^2$ of cold storage areas, mainly used for storing pre-refrigerated fruit and vegetables until redistribution to local supermarkets. Besides from being a cold storage facility the building also have office areas and a local brewery, Austmann. The building has available waste heat from the existing chillers of the cold storage facilities, the exact amount is however unknown due to a lack of measurements.

The existing refrigeration system consists of in total 4 cooling machines. Each cooling machine has an air cooled condenser placed on the outside of the building. The temperature of the storage rooms wary from 2-20°C (Mostly 2-4°C), depending on the type of products stored in the room. The room partitioning of the chillers can be seen in Figure 3.

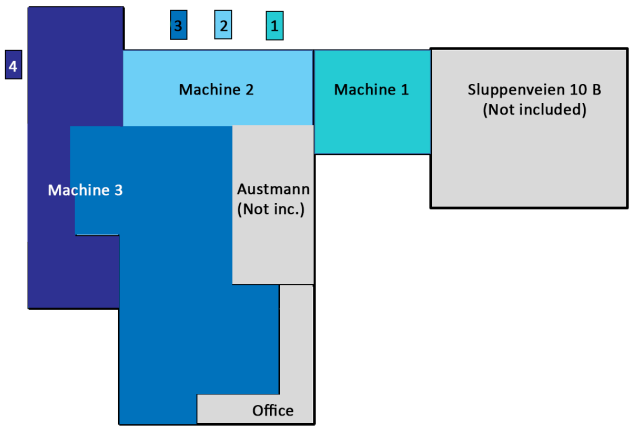


Figure 3: SLV10: Cooling machine zone overview

Chiller 1,2 and 3, have an installed cooling capacity of 117, 121 and 338 kW respectively. Chiller 3 is however newer and likely to have better energy efficiency. From a system performance point of view it is therefore desirable to operate chiller 3 as much as possible. Little is known about chiller 4. An overview of the existing chiller information can be seen in Table 4. Most information is known about the newest and largest unit, chiller 3. It was installed in 2013 and is a DAIKIN EWAD-480D-SL air cooled chiller. Table 5 below shows the energy performance of the Daikin EWAD 480D-SL under variable part load operation.

Table 4: SLV10 — Existing Chiller Information. Numbers according to Figure 3.

| Chiller | $\dot{Q}_{Evap}$ | Refrigerant | Ref. Charge | Installation date | Model |
|---|---|---|---|---|---|
| 1 | 121 kW | R410a | 20 kg | Unknown | ACM SCAEYJ-F 151 PAC1 |
| 2 | 117 kW | R410A | 23.7 kg | Unknown | BlueBox ZETA ECHOS/ST 12.2 |
| 3 | 338 kW | R134a | 68 kg | 08.2014 | DAIKIN EWAD 480D-SL |
| 4 | 145 kW | R410A | 2x26 kg | 11.2010 | DAIKIN EWYQ 150 DAYNB-Q |

Table 5: DAIKIN EWAD-480D-SL Energy performance according to the user manual [25]

| Part Load [%] | $T_E$ In [$°C$] | $T_E$ Out [$°C$] | T Ambient [$°C$] | $\dot{Q}_{Evap}$ [kW] | $\dot{W}_{Comp+Pump}$ [kW] | $\dot{W}_{Fan}$ [kW] | COP [-] |
|---|---|---|---|---|---|---|---|
| 100 | -2.0 | -6.0 | 28.0 | 338 | 129 | 6.27 | 2.49 |
| 75 | -3.0 | -6.0 | 28.0 | 253 | 100 | 6.27 | 2.37 |
| 50 | -4.0 | -6.0 | 28.0 | 168 | 68.9 | 3.14 | 2.33 |
| 25 | -5.0 | -6.0 | 28.0 | 107 | 44.2 | 3.14 | 2.27 |

## 3.2 Electricity Measurements

No measurements of available thermal energy have been performed at SLV10, the exact potential for waste heat recovery is therefore uncertain. However the electric energy consumption of chiller 3 have been measured daily since the beginning of 2015 by the building owner, Kjeldsberg Eiendomsforvaltning AS [26]. Detailed measurements of the electricity consumption of the same chiller also exists in hourly increments since 08.02.2019. The electricity measurements have therefore been used a basis for estimating the cooling demand and potential for waste heat recovery of SLV10. According to the cold store manager Cato Mosling Vonstad most of the rooms have installed electrical heating leading which also have high electricity consumption during the winter period [27]. It is however unknown if these heaters are included in the electricity measurements.

The electricity consumption of the chiller unit is stable around 1200 kWh/day throughout the year. Not as would be expected of a cold storage facility, which is an increase in cooling demand during summer due to increased infiltration and transmission losses. The measured electricity consumption show little correlation with ambient temperature and has a tendency of increased electricity consumption both at high and low ambient temperatures. The lack of correspondence between cooling demand and outdoor temperature might be caused by low chiller efficiencies at part load or the electricity consumption of the electric heaters are included in the measurements. Figure 4 show the hourly measured electricity consumption of chiller 3 for most of 2019. The data show a visible peaks in electricity consumption correlating to when the storage facility receives trucks with new products. It is therefore assumed that the electricity measurements are a good indication of the short therm cooling demand of the cold storage facility in the summer period, but not for the annual cooling demand.

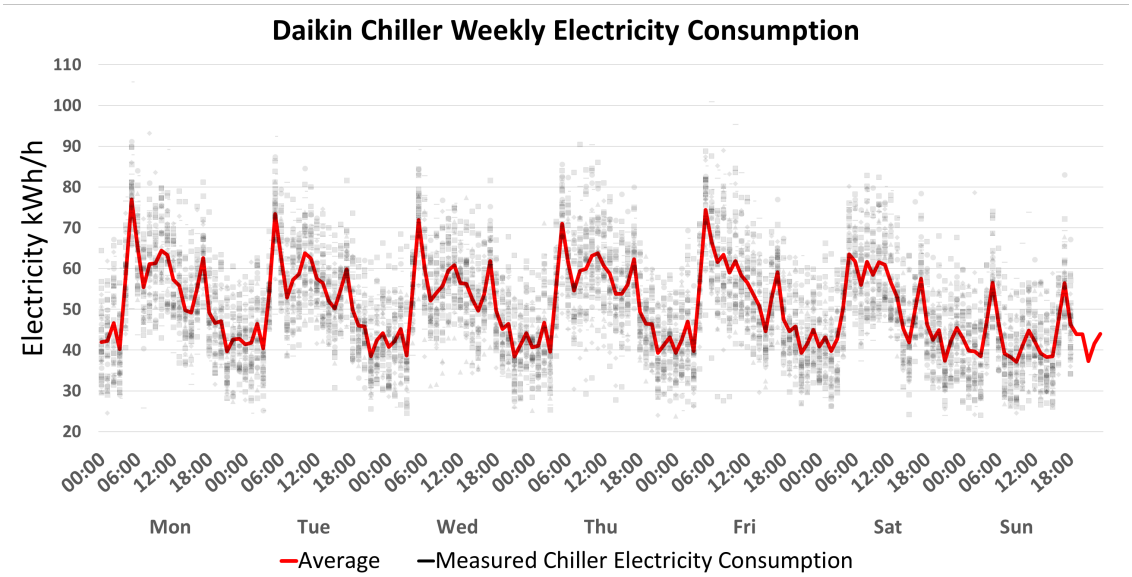


Figure 4: Chiller, weekly electricity consumption for 2019, measured in hourly increments [26].

# 4 Method

## 4.1 General Modeling Approach

Five dynamic simulation models of possible HTHP configurations have been developed using the program Dymola [28], and the TLK-Thermo GmbH refrigerant and component libraries [29]. Dymola and the TLK-Thermo GmbH libraries provide tools to model advanced thermal systems and run transient simulations of complex heat pump configurations. Two configurations (Model A1 and A2) for recovery to district heating and 3 for tap water production (B1, B2 and C1), have been studied. Configuration A1 and A2 are both R290/R600 cascade heat pumps similar to the prototype HTHP developed by Bamigbetan [7]. The R290/R600 cascade solution have been chosen for heat recovery at Sluppenveien 17A. It is therefore beneficial for +CityXChange if the same solution can be used for Sluppenveien 10. The A1 and A2 configuration were set to have an evaporation/condensation temperature of -15/56 °C and 53/103 °C of the LTC and HTC respectively. The configurations are identical except the A2 configuration has two compression and expansion steps. The intermediate pressure of the A2 configuration was set according to Equation 4 below.

$$P_m = \sqrt{P_E \cdot P_C} \quad [30] \tag{4}$$

The R290/R600 cascade solution is also considered for heat recovery by producing hot water at 70 °C with the B1 and B2 configurations. The models were set to have an evaporation/condensation temperature of -15/33 °C and 30/70 °C of the LTC and HTC respectively. The B2 configuration was created to investigate the impact of increased Propane sub-cooling on the system performance. For production of hot water the heat sink inlet water temperature is significantly lower compared to re-heating of district heating return line water to the supply line. This opens up the possibility to use $CO_2$ heat pumps which are inefficient for high heat sink inlet temperatures. It has therefore been decided to compare the performance the R290/R600 cascade solution to a more conventional $CO_2$ heat pump for production of hot water. Figure 5 below show all the developed heat pump configurations.

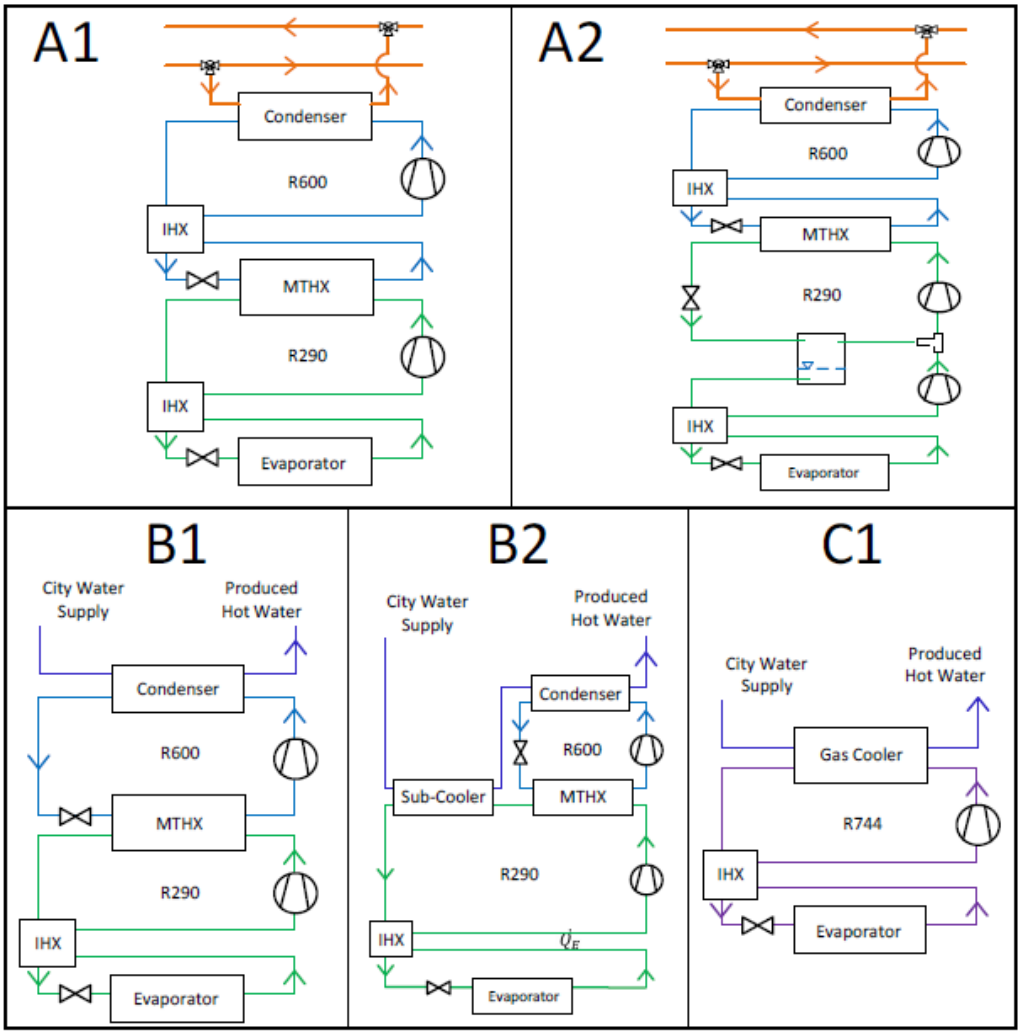


Figure 5: Developed heat pump configurations:
Heat recovery to district heating; Model A1 & A2. — Heat recovery by hot water production; Model B1, B2, & C1.

The TIL 3.5.0 component library contains several pre-modeled components such as; heat exchangers, valves, pumps and compressors. The refrigerant library TIL-Media contains a variety of commonly used refrigerants and secondary fluids. Which were used to create the simulation models. Each heat pump cycle was modeled with heat exchangers, expansion valve and compressors. All evaporators, condensers and internal heat exchangers were modeled as counter flow plate heat exchangers. For each CVCC the amount of superheat is regulated by the expansion valve through a PI-controller. The Compressor speed is regulated by PI-controllers as well to maintain a set evaporation pressure. Initial iteration values for all models except A2 were calculated in Engineering Equations Solver (EES) by assuming an volumetric and isentropic compressor efficiency of 0.8 and 0.7. Suitable compressors were then selected using the software provided by the compressor manufacturers Dorin [31] and Bitzer [32]. The compressor displacement, volumetric-, isentropic and effective isentropic efficiency of each compressor were then calculated with Equation 5, 6a, 6b and 6c combined with compressor shaft power and refrigerant calculated using Equation 7 and coefficients C1-C10 given by the compressor manufacturers. The polynomial for the $CO_2$ compressor was similar, but with Gas cooler pressure $P_{GC}$ instead of condensation temperature. The resulting input parameters for the A1 configuration is shown in Table 6.

$$V_{Disp} = \frac{V_{Nom}}{3600 \cdot 50} \tag{5}$$

$$\lambda_{Vol} = \frac{\dot{m}_R}{V_{Disp} \cdot n \cdot \rho_{Suction}} \quad (6a) \qquad \eta_{Is} = \frac{h_{is.Disch} - hsuction}{h_{Disch} - h_{Suction}} \quad (6b) \qquad \eta_{Is} = \frac{\dot{m}_R \cdot (h_{is.Disch} - hsuction)}{P_{Shaft}} \quad (6c)$$

$$y = C1 + C2 \cdot T_E + C3 \cdot T_C + C4 \cdot T_E^2 + C5 \cdot T_E \cdot T_C + C6 \cdot T_C^2 + C7 \cdot T_E^3 + C8 \cdot T_C \cdot T_E^2 + C9 \cdot T_E \cdot T_C^2 + C10 \cdot T_C^3 \quad (7)$$

$$A_{Valve} = \frac{\dot{m}_{Ref}}{\sqrt{(P_C - P_E) \cdot 2\rho_{inlet}}} \quad (8)$$

$$\dot{Q} = \dot{V} \cdot \rho \cdot C_P \cdot \Delta T = U \cdot A \cdot LMTD_{HX} = \dot{m}_R \cdot \Delta h \quad (9)$$

Table 6: Model A1 — Compressor input parameters in Dymola Model

| | LTC (R290) | HTC (R600) | Unit |
|---|---|---|---|
| Chosen Compressor | HEX7501CS | HEX5000CC | $[kg/s]$ |
| Nominal Displacement (50 Hz) | 221.75 | 153.52 | $[m^3/h]$ |
| Displacement in Dymola | $1.2319 \cdot 10^-3$ | $8.5288 \cdot 10^-4$ | $[m^3]$ |
| Pressure ratio $\pi$ | 6.68 | 3.01 | $[--]$ |
| Volumetric Efficiency | 0.70 | $\approx 0.8$ | $[--]$ |
| Isentropic Efficiency | 0.69 | $\approx 0.7$ | $[--]$ |
| Eff. Isentropic Efficiency | 0.62 | $\approx 0.6$ | $[--]$ |

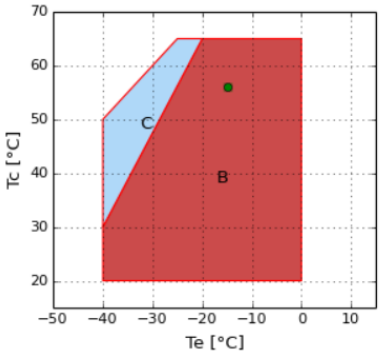


Figure 6: Model A1 — Operation point of HEX7501CS Compressor, Snipped from Dorin Software [31]

The expansion valve effective flow area and heat exchanger heat transfer area were set using Equation 8 and 9 above. Due to the buildings lack of district heating connection a secondary $CO_2$ circuit is created to transport the waste heat from the source to the heat recovery heat pump as seen in Figure 7 and 6 shows a simplified version of the Model A1 Dymola model and the design operation point of the A1 Propane compressor respectively. Figure 7 also shows the PI-Controllers regulating; suction superheat, suction pressure, heat sink outlet temperature and heat source outlet temperature by controlling the; Expansion valve effective flow area, compressor speed, water volume flow and $CO_2$ mass flow respectively. The same modeling approach was also used for the four other developed simulation models. The models were simulated for an realistic weekly cooling load-curve estimated from the average electricity measurements seen in Figure 4 and chiller COP in Table 5.

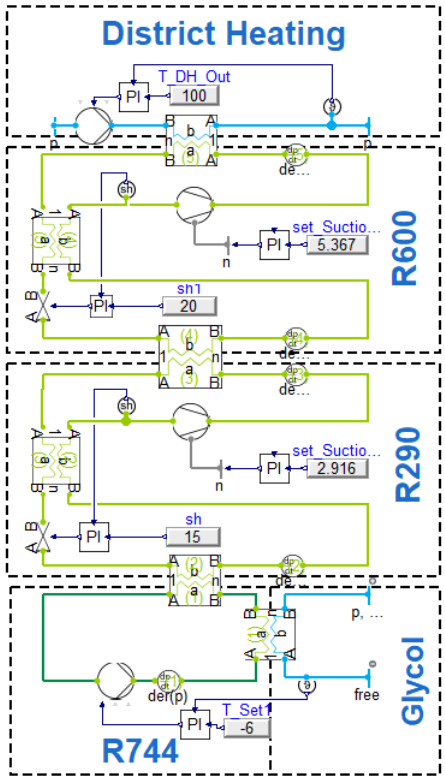


Figure 7: Model A1 — Simplified Cascade HTHP model snipped from Dymola.

## 4.2 Energy, Costs & Profitability Analysis

The annual cooling demand of the cold storage facility is not known, it was therefore decided to perform and energy- and economical analysis as a function of the amount of full load hours (FLH) of the heat recovery heat pump. The investment and operation cost were estimated from Table 3 assuming the costs are linear between the tabulated capacities. For the LTC/HTC the heat transfer in the cascade heat exchanger/condenser and values for Brine to water 55°C/70°C were used respectively. It was also assumed an 25% increase of costs for the Butane cycle because it has to be custom ordered. The annual costs of electricity and value of delivered cooling were both calculated with an electricity price of 0.36 NOK/kWh including 25% VAT and 0.5 Øre/kWh electricity tax [33]. The electricity price was set to the average quarterly price according to SSB [34]. Value of delivered cooling was assumed to be the value of reduced chiller electricity consumption estimated with a COP of 2.49 from Table 5. The maximum Chiller COP was chosen to not over estimate the reduced electricity consumption of the existing chillers. The LCOG of the systems were subsequently compared to the average price of district heating of 0.55-0.65 NOK/kWh [35].

### 4.3 Recipients of hot water

In the case of +CityxChange Austmann and 3T, a local brewery and fitness center is believed to have large hot water demands. Their actual power demand for hot water production is dependent on user behaviour which is not known, because the attempts on contacting the respective companies have been unsuccessful. In this thesis the hot water demand is therefore investigated in an annual energy point of view through estimating the average annual power demand for hot water. It is therefore assumed that the two recipients have large accumulation tanks to account for hourly or daily variations in hot water demand. For the case of Austmann the hot water demand is estimated based on the presented theory to be $0.45 \cdot 4.3$ hl/hl of beer. The annual production capacity of Austmann is also unknown it is therefore assumed to be 250 000 liters. This results in an annual hot water demand of approximately 483750 liters. For the fitness center 3T, the hot water demand have been calculated using standard values from SN-NSPEK 3031:2020 "Energy performance of buildings, Calculation of energy needs and energy supply" [36]. The most suitable building category for 3T Sluppen is "Idrettsbygg". The energy demand for hot water is therefore set to 4.5 $Wh/m^2$ from 07:00 to 18:00 and 0 $Wh/m^2$ the remaining hours of the day. The Standard SN-NSPEK 3031:2020 also has standardized values for annual operating days of five days a week and 44 weeks of operation annually. The same number of operating days as for school buildings. This is not the case for 3T Sluppen which are open all days of the week the entire year. It has therefore been decided to use operating days to 7/52 days/weeks because it is assumed to be more suitable for 3T Sluppen. 3T Sluppen is estimated total area of approximately 2000 $m^2$. The hot water demand of 3T Sluppen were then calculated using Equation 10 and 11 below, where P is the average hourly power demand for hot water according to the mentioned standards and $h_d$ is the amount of hours with hot water demand per day. The main focus of this paper is heat pump configurations for waste heat recovery, it is therefore assumed that excess hot water production over the demands of Austmann and 3T Sluppen is exported out of the area by for instance mobile thermal energy storage (M-TES).

$$E_{HotWater} = \frac{P \cdot h_d \cdot days \cdot Area}{10^3}[kWh] \tag{10}$$

$$V_{Hot_Water} = \frac{E_{HotWater}}{3600 \cdot C_p \cdot \Delta T_{Water} \cdot \rho} \cdot 1000[liter] \tag{11}$$

## 5 Results & Discussion

### 5.1 Steady State

Figure 8 below shown the Ts-chart of the Model A1 and A2 configuration under design conditions with 60 KW of cooling demand. The results show that the A2 configuration achieves 11.3 K lower propane compressor discharge gas temperature and 103.9 $kJ/kg$ lover enthalpy of propane at the evaporator inlet compared to the A1 configuration. This can also be seen in the Ts-Chart below, where the results of the initial EES calculations of Model A1 is indicated by the shaded area in the cycles. The steady state performance of the B1, B2 and C1 configuration also were close to identical to the initial cycle points from the EES calculations, indicating that the steady state performance of the Dymola models are as intended.

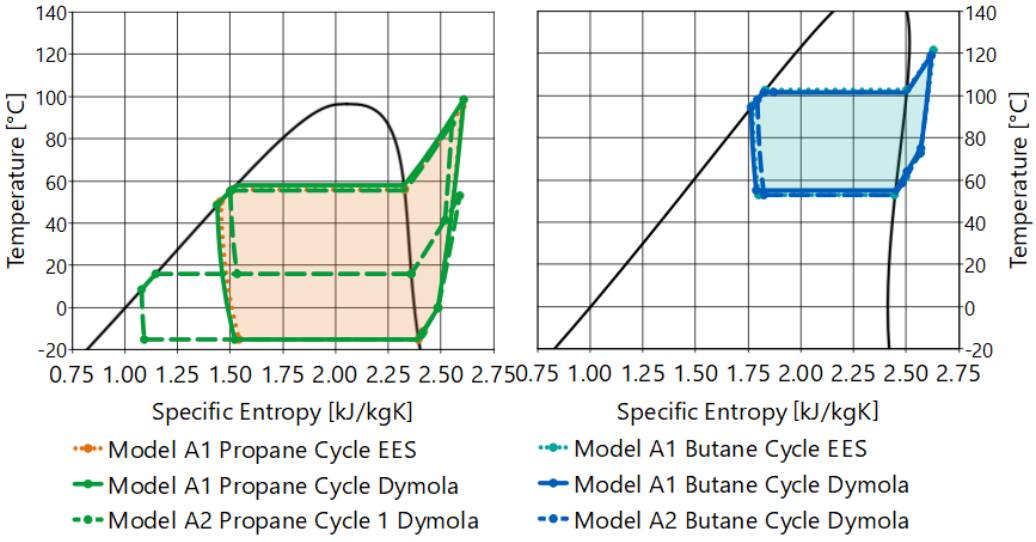


Figure 8: Model A1 and A2 — Steady state Ts-Chart From Dymola.

Table 7 show the most important results of the steady state simulations of the five developed simulation models. The models achieved a heating/cooling COP in the range of 1.71-3.28/2.53-5.66 where minimum and maximum COP was achieved by the A1 and C1 configuration respectively. For the Model B2 configuration it can be seen that increasing the sub-cooling of the propane cycle significantly increases the COP. Making it closer, but still lower than the COP of the C1 configuration. It can also be seen that the compressor discharge temperature of the hot water producing heat pumps B1 and B2 are significantly lower than the A1 and A2 configuration due to the lower condensation temperature. All models are able to deliver 60.36 kW of cooling and compressor shaft power and delivered heat varies from 25.31-73.10 kW and 82.94-124.75 kW depending on heat recovery configuration.

Table 7: Results of steady state simulations

| Model | A1 | A2 | B1 | B2 | C1 | Unit |
|---|---|---|---|---|---|---|
| COP Heating | 1.71 | 1.78 | 2.38 | 3.06 | 3.28 | |
| COP Combined | 2.53 | 2.68 | 3.88 | 5.23 | 5.66 | |
| Propane CDT | 98.8 | 87.5 | 69.7 | 69.8 | 120.1* | C |
| Butane CDT | 119.2 | 119.4 | 92.2 | 94.6 | | C |
| Delivered Cooling | 60.36 | 60.36 | 60.36 | 60.36 | 60.36 | kW |
| Compressor Shaft Power | 73.10 | 66.87 | 40.28 | 27.85 | 25.31 | kW |
| Delivered Heat | 124.75 | 119.12 | 95.83 | 85.25* | 82.94 | kW |

## 5.2 Weekly load-curve Simulation

Figure 9 and 10 below show the results of the weekly simulations for the A1 configuration. The weekly simulation results of the remaining models show the same behavior as the A1 configuration and is therefore not presented in this paper. Figure 9 show the cooling demand input, delivered cooling as well as the heat sink and heat source outlet temperature. The results show that for all models the set heat sink outlet water temperature is maintained at all simulated conditions and the heat recovery heat pumps are able cover the cooling demand between 45 and 62.5 kW. During weekdays from 05:00-18:00 the heat recovery heat pumps operate mostly at full load, not able to cover the entire input cooling demand. This can be seen in the heat source outlet glycol temperature which increases above the -6°C set point in this period, indicating that the additional cooling demand has to be covered by the existing chillers. The simulated cooling demand input is 50% of the peak estimated cooling demand curve from the electricity measurements, correlating to a realistic operating condition in spring or autumn with low cooling demand. In summer conditions the estimated cooling demand is higher than the maximum capacity of the heat recovery heat pumps, resulting in the heat pumps operating at steady state design conditions.

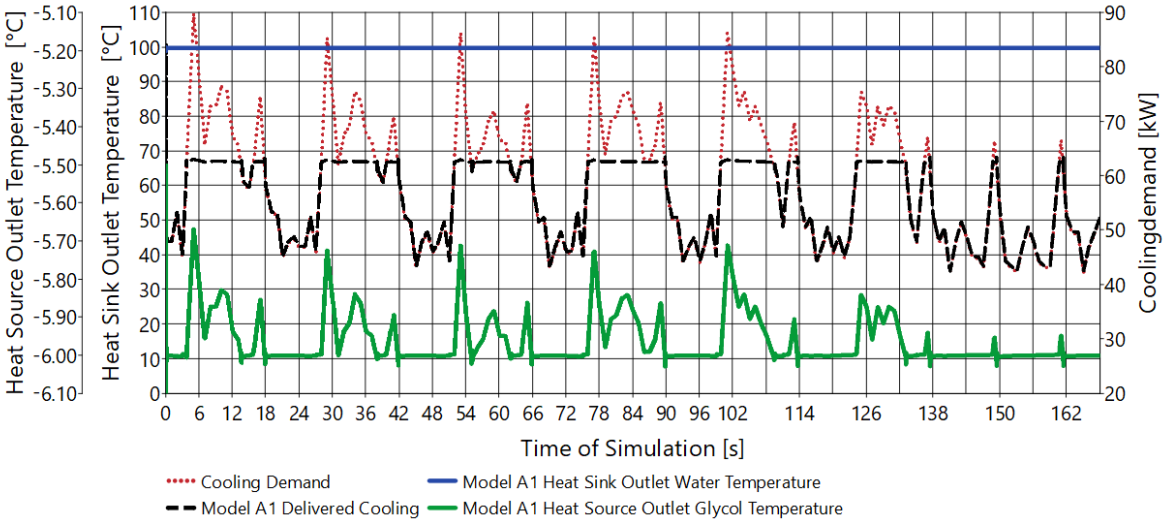


Figure 9: Model A1 — Weekly Simulation, Heat sink outlet water temperature and heat source outlet glycol temperature at 50% of estimated cooling demand.

Figure 10 below show the compressor speed of the R290 and R600 compressors for the A1 configuration. The results show that the compressor are operating close to the design speed of 50 Hz at design conditions with $\approx$ 60 kW delivered cooling, indicating that the selected compressors are suitable for this heat pump configuration. At low load conditions during the night and weekends the compressor speeds drops down to approximately 35 Hz, assumed to be within the valid area of operation for the compressor with variable speed control.

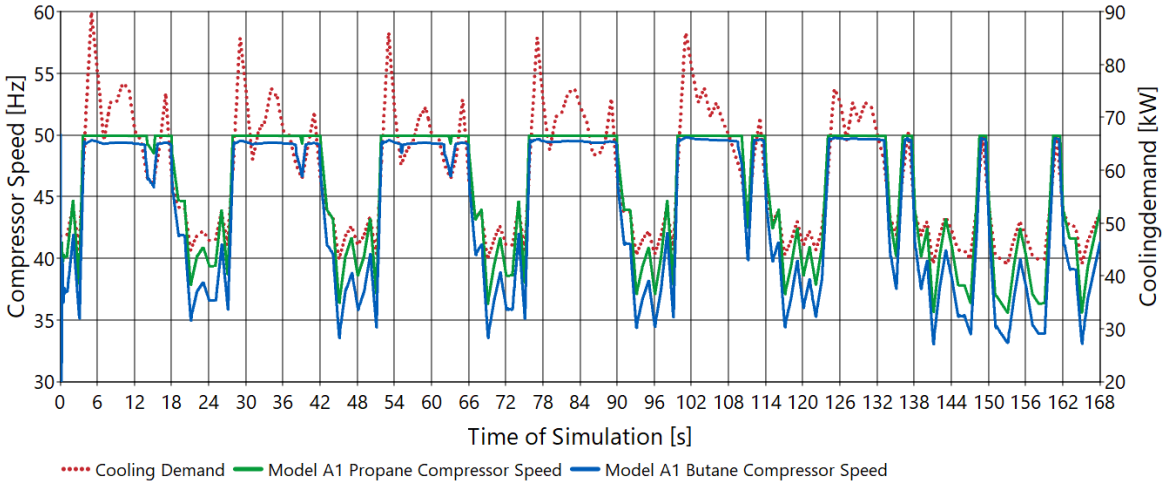


Figure 10: Model A1 — Weekly Simulation, Compressor speed at 50% of estimated cooling demand.

The results of the weekly simulations for all models showed a slightly higher COP than for the steady state simulations. This effect is likely to be caused by the LMTD of the heat exchangers decreasing with reduced heat transfer, resulting in a lower compression ratio, compressor shaft power and thus an increase in COP. In real heat pump installations the COP at part load operation is lower than the design point COP due to reduced compressor efficiencies at part load. This effect of reduced compressor efficiencies is not included and a limitation of the simulation models. The results of the steady state simulations were therefore used in the following energy- and economical analysis.

## 5.3 Energy- and Costs & Profitability Analysis

Because of the uncertainty of the annual cooling demand of the cold storage facility the energy- and the following costs and profitability analysis have been performed as function of the annual full load hours (FLH) of the heat recovery heat pumps. Figure 11 and 12 on the following page show the; delivered heating, cooling and compressor shaft power of the developed heat pump configurations at 8500 FLH. The results of the energy analysis show that at 8500 full load hours (FLH) 513.1 MWh of heat can be recovered and 705.0-1060.4 MWh heat delivered to either the district heating grid or as produced hot water, depending of chosen method of heat recovery and heat pump configuration. From Figure 11 it can be seen that all models deliver the same amount of cooling and the increased heat delivery of the A1, A2, B1 and B2 configuration is due a higher compressor electricity consumption. The hot water heat pumps are therefore the best alternative from an energy point of view and for achieving PED at Sluppen due to the highest simulated COP. From the figure it is also evident that the delivered heat is less than the sum of delivered cooling and compressor shaft power, this is because the simulation models include 10% heat losses in the compressor implemented by lower effective isentropic efficiencies than the isentropic efficiency. From Figure 12 it can be seen that the reduced cooling demand of the existing chillers due to the delivered cooling from the heat recovery heat pumps is estimated to be 205.2 MWh per year.

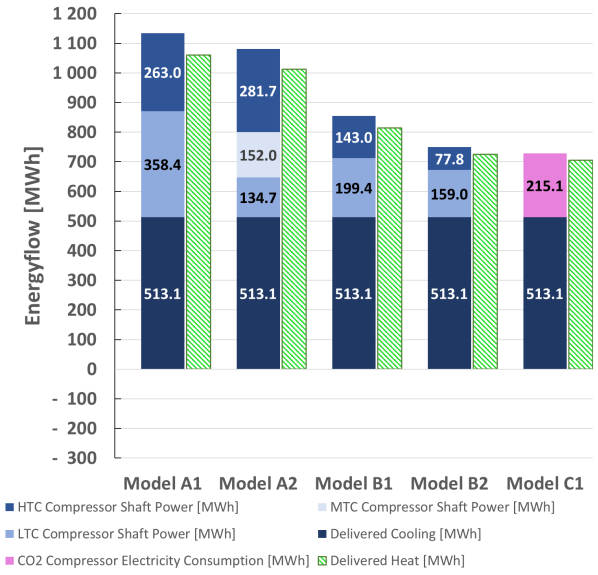


Figure 11: Energy analysis — Delivered cooling, compressor shaft power and delivered heat at 8500 Full-load-Hours.

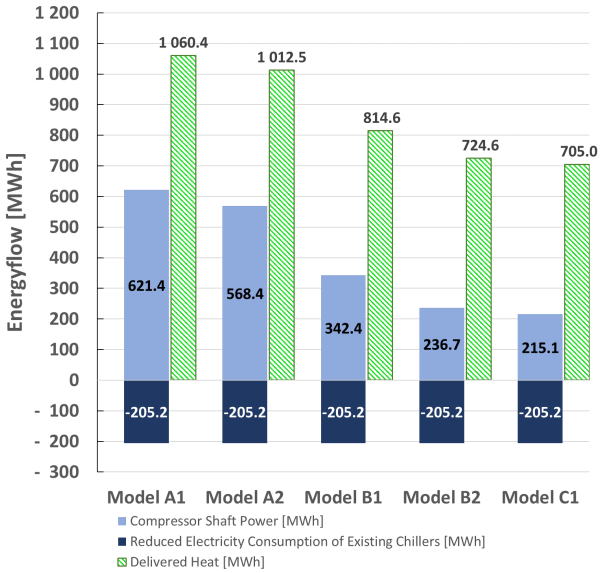


Figure 12: Energy analysis — Delivered heat, compressor electricity consumption and reduced electricity consumption of existing chillers at 8500 Full-load-Hours.

The cost analysis show that the Model A1 and A2 heat pump configurations recovering heat to the district heating grid, have the highest investment costs estimated to 1 650 000 NOK. Similar for the hot water producing heat pumps B1, B2 and C1 the investment cost is estimated to be in the range of 1 500 000- 1 205 000 NOK. The calculated LCOG of heat recovery to district heating and hot water production is approximately 0.31 NOK/kWh and 0.81-0.73 NOK/kWh respectively, assuming an economical lifetime of 15 years, 6% interest rate and 8500 FLH per year. Figure 13 and 14 below show the calculated annual costs and LCOG for the developed modes as a function of FLH. The calculations are based on an assumed economical lifetime of 15 years and 6% interest rate. The results show that the annual costs of the hot water producing heat pumps are lowest for small FLH, but increasing significantly around 1000 FLH due to the high costs of M-TES. The calculated LCOG is high for low FLH due to the high annual costs compared to delivered heat. It is therefore important with high FLH from both an energy- and economical point of view.

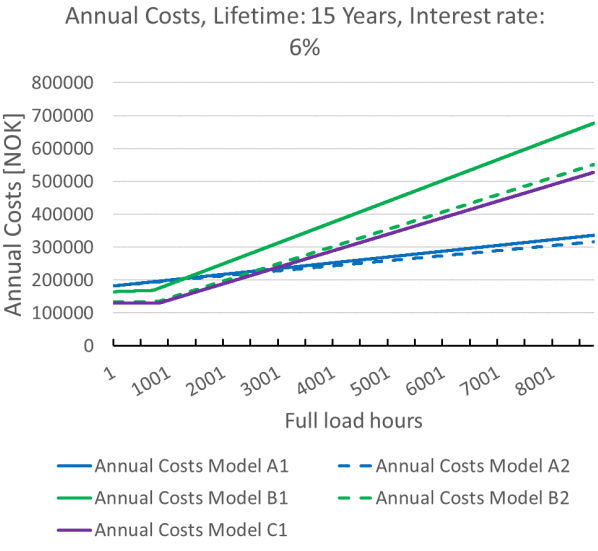


Figure 13: Annual Costs of heat recovery heat pumps with 15 year economical lifetime and 6% interest rate.

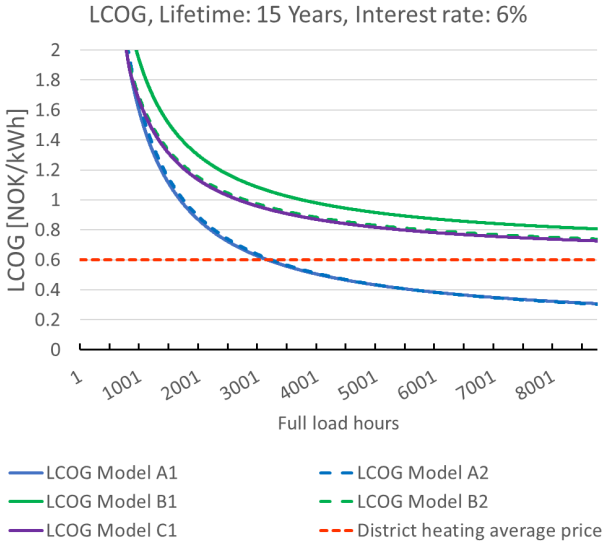


Figure 14: LCOG of heat recovery heat pumps with 15 year economical lifetime and 6% interest rate.

With increased FLH the LCOG decreases caused by the larger increase in delivered heat compared to the annual costs. The results in Figure 14 are compared to the average district heating price of 0.6 NOK/kWh. It is then clear that heat recovery by hot water production would not be profitable compared to district heating due to the higher LCOG than average district heating price. For FLH over 3600 hours heat recovery to the district heating grid achieves a LCOG lower than the average district heating price. However the most amount of heat is likely to be recovered in the summer when there is an excess of heat in the district heating grid in Trondheim. The value of the recovered heat is therefore low from the district heating company's point of view. Assuming the heat is sold for half the district heating price, the maximum investment cost of the Model A1 and A2 configuration is estimated to be in the range of 468 000-482 000 and 659 000-679 000 for a pay back time of 5 years and 20% and 6% rate of return respectively. Substantial investment support from +CityXChange is therefore needed.

# 6 CONCLUSION

High temperature heat pumps capable of heat sink temperatures above $100°C$ are exists, but limited to small scale test and pilot heat pumps not commercially available. Cascade CVCC heat pumps are capable of heat sink temperatures above $100°C$ and low temperature heat recovery. R290 and R600 are a performance-vise and environmentally good choice of working fluids. The main disadvantage with hydrocarbons as refrigerants is the high flammability and limited suction- and discharge gas temperature. Which in practice is limited to about 75 and $130°C$. To make the technology commercially available there is a need for large scale pilot projects as +CityxChange, to test the reliability and performance under real life conditions.

Five dynamic simulation models of heat potential heat recovery heat pump configurations for +CityXChange have been developed in Dymola [28], to investigate potential methods of heat recovery at Sluppenveien 10. The models were tested for realistic operating conditions and able to follow a average weekly cooling demand curve of the cold store down from 62.5 kW down to 45 kW. The developed models achieved a heating/cooling COP in the range of 1.71-3.28/2.53-5.66 respectively. The minimum and maximum COP was achieved by the A1 and C1 configuration respectively. The developed R290/R600 cascade heat pump is able to recover heat to both district heating and produce hot water, but is considered overly complicated for hot water production.

The hot water demand of Austmann and 3T is not known, but estimated to be small compared to the possible hot water production of the heat pumps. Heat recovery by hot water production therefore requires large amounts of water to be exported out of the area with M-TES. The electricity measurements performed by the building owner show a strong degree of correlation with the activity of the cold storage facility, but little correlation with ambient temperature. The electricity consumption of the heaters are therefore likely to be included in the measurements. The measurements are therefore not suitable for calculation of the annual cooling demand. The results of the energy analysis show that at 8500 full load hours (FLH) 513.1 MWh of heat can be recovered and 705.0-1060.4 MWh heat delivered depending on method of heat recovery. The hot water heat pumps are the best alternative from an energy point of view and for achieving PED at Sluppen due to the highest simulated COP.

The Model A1 and A2 heat pump configurations recovering heat to the district heating grid requires a larger investment cost, fixed operation and maintenance costs and annual costs of electricity than heat recovery by hot water production. At low FLH the hot water producing heat pumps achieve the lowest annual costs, but with FLH the annual costs increases significantly due to the high cost of M-TES. Heat recovery by hot water production is therefore likely not profitable compared to district heating. For FLH over 3600 hours heat recovery to the district heating grid achieves a LCOG lower than the average district heating price. The most amount of heat is likely to be recovered in the summer, the value of the recovered heat is therefore low from the district heating company's point of view. The maximum profitable investment cost of all models is less than the estimated investment costs, substantial investment support from +CityXChange is therefore needed. The least unprofitable configuration is A2, but other methods of achieving PED at Sluppen than heat recovery should be considered.

The results of this thesis are dependent on the assumptions and simplifications made, both in the simulation models and the energy- and economical investigation. Both the demand for cooling and hot water are uncertain. More research and measurements is therefore needed to draw final conclusion on how and if waste heat should be recovered from Sluppenveien 10.

## ACKNOWLEDGEMENTS

I would like to thank Professor Armin Hafner (NTNU) for valuable guidance and advises, helping me realize this thesis. Also a special thanks should be granted to Morten Einar Fossum and Åmund Utne (Statkraft Varme AS), who as advisors during the summer internship provided me with valuable experiences and insights into Statkraft Varme and the +CityxChange project. I would also like to thank Bjørn Ove Berthelsen, Trondheim Kommune and the other +CityxChange partners for allowing students to participate in the project. Further thanks to; Ignat Tolstorebrov for providing the EES software, Marcel Ahrens for advice and insight into the Dymola/Modelica software. Vegard Klungtveit (ABK-Qviller) providing practical advises and technical knowledge about HTHPs. Sondre Leonhardsen (Kjeldsberg Eiendomsforvaltning AS) for providing accesses to the electricity measurements at Sluppenveien 10.

## NOMENACLATURE

### Abbreviations

| | | |
|---|---|---|
| AC | = | Annual Costs |
| CDT | = | Compressor discharge temperature |
| +CityxChange | = | Positive city exchange |
| COP | = | Coefficient of performance |
| CST | = | Compressor suction temperature |
| CVCC | = | Closed vapour compression cycle |
| DA | = | Demonstration area |
| EES | = | Engineering equations solver |
| EUR | = | Euro |
| FLH | = | Full load hours |
| GWP | = | Global warming potential |
| HSiOT | = | Heat sink outlet temperature |
| HTC | = | High temperature cycle (compressor) |
| HTHP | = | High temperature heat pump |
| IHX | = | Internal heat exchanger |
| LCOG | = | Levelized costs of generation |
| LMTD | = | Logarithmic mean temperature difference |
| LTC | = | Low temperature cycle (compressor) |
| M-TES | = | Mobile thermal energy storage |
| MTHX | = | Cascade heat exchanger |
| NOK | = | Norwegian kroner |
| NTNU | = | Norwegian university of science and technology |
| NVE | = | Norges vassdrags- og energidirektorat |
| O&M | = | Operation and maintenance costs |
| PEB | = | Positive energy block |
| PED | = | Positive energy district |
| PCM | = | Phase changing material |
| SLV10 | = | Sluppenvegen 10 |
| SLV17A | = | Sluppenvegen 17A |
| USD | = | US Dollar |
| VAT | = | Value added tax |
| VCHP | = | Vapor compression heat pump |

### Symbols

| | | | |
|---|---|---|---|
| a | = | annuity factor | [-] |
| A | = | Area | [$m^2$] |
| $A_{Valve}$ | = | Valve effective flow area | [$m^2$] |
| $B_i$ | = | Annual net benefit | [NOK/year] |
| $C_P$ | = | Heat capacity | [$kJ/kgK$] |
| e | = | electricity price | [NOK/kWh] |
| $h$ | = | Enthalpy | [$kJ/kg$] |
| $I_0$ | = | Investment cost | [NOK] |
| $\dot{m}_R$ | = | Refrigerant mass flow | [kg/s] |
| n | = | Economical lifetime | [years] |
| $P_C$ | = | Condensation pressure | [Pa] |
| $P_E$ | = | Evaporation pressure | [Pa] |
| $P_{GC}$ | = | Gas cooler pressure | [bar] |
| $P_m$ | = | Intermediate pressure | [Pa] |
| $P_{Shaft}$ | = | Compressor shaft power | [kW] |
| $\dot{Q}$ | = | Heat flow | [kW] |
| r | = | rate of interest | [-] |
| $T_C$ | = | Condensation temperature | [°C] |
| $T_{Crit}$ | = | Critical temperature | [°C] |
| $T_E$ | = | Evaporation temperature | [°C] |
| $U$ | = | Overall heat transfer coefficient | [$W/m^2K$] |
| $V_{Disp}$ | = | Compressor displacement | [$m^3$] |
| $V_{Nom}$ | = | Nominal compressor displacement | [$m^3/h$] |
| $W_E$ | = | Electricity consumption | [kWh] |
| $\lambda_{vol}$ | = | Volumetric efficiency | [-] |
| $\eta_{Is}$ | = | Isentropic efficiency | [-] |
| $\eta_{Eff.Is}$ | = | Effective isentropic efficiency | [-] |
| $\rho_{Suction}$ | = | Suction gas density | [kg/$m^3$] |
| $\rho_{Inlet}$ | = | Expansion valve inlet density | [kg/$m^3$] |
| $\pi$ | = | pressure ratio | [-] |

# REFERENCES


[1] Newell. R.G, Raimi. D, and Aldana G. Global energy outlook 2019: The next generation of energy. *Resources of the future*, 2019.

[2] Skree J and Vatndal J.D. Energibruk i bygg – rammer, krav og muligheter. *Norsk Teknologi*, 2008.

[3] Norsk Energi. and Enova. Utnyttelse av spillvarme fra norsk industri, 2007. https://www.enova.no/download/?objectPath=upload_images/44EB7A65846B4824A6EB704198C3F6BC.pdf [Accessed: 2019-09-26].

[4] +CityxChange. About +cityxchange, 2019. https://cityxchange.eu/about-cityxchange/ [Accessed: 2019-09-26].

[5] European Commission. What is horizon 2020?, 2019. https://ec.europa.eu/programmes/horizon2020/what-horizon-2020 [Accessed: 2019-09-26].

[6] Arpagaus C, Bless. F, Uhlmann. M, Schiffmann J, and Bertsch S.S. High temperature heat pumps: Market overview, state of the art, research status, refrigerants, and application potentials. *Energy*, 152:985 – 1010, 2018. https://doi.org/10.1016/j.energy.2018.03.166.

[7] Bamigbetan. O, Eikevik. T.M, Nekså P, Bantle M, and Schlemminger C. The development of a hydrocarbon high temperature heat pump for waste heat recovery. *Energy*, 173:1141–1153, 2019. https://doi.org/10.1016/j.energy.2019.02.159.

[8] Bamigbetan. O, Eikevik. T.M, Nekså. P, Bantle M, and Schlemminger C. Theoretical analysis of suitable fluids for high temperature heat pumps up to 125°C heat delivery. *International Journal of Refrigeration*, 92:185 – 195, 2018. https://doi.org/10.1016/j.ijrefrig.2018.05.017.

[9] Schlemminger C, Svendsen E.S, Foslie S.S, Bantle M, Bamigbetan O, and Nekså P. Performance of high temperature heat pump for simultaneous and efficient production of ice water and process heat. In *25th IIR International Congress of Refrigeration*, pages 4632–4639, 2019.

[10] Bamigbetan. O, Eikevik. T.M, Nekså. P, Bantle M, and Schlemminger C. Experimental investigation of a prototype R-600 compressor for high temperature heat pump. *Energy*, 169:730 – 738, 2019. https://doi.org/10.1016/j.energy.2018.12.020.

[11] Canadian Industry Program for Energy Conservation. Guide to energy efficiency opportunities in the canadian brewing industry. https://www.nrcan.gc.ca/sites/www.nrcan.gc.ca/files/oee/files/pdf/publications/industry/Brewers_Guide_access_e.pdf [Accessed: 13.02.2020].

[12] Kubule A, Zogla L, Ikaunieks J, and Rosa M. Highlights on energy efficiency improvements: a case of a small brewery. *Journal of Cleaner Production*, 138:275 – 286, 2016. https://doi.org/10.1016/j.jclepro.2016.02.131.

[13] Muster Slawitsch B, Weiss W, Schnitzer H, and Brunner C. The green brewery concept – energy efficiency and the use of renewable energy sources in breweries. *Applied Thermal Engineering*, 31(13):2123 – 2134, 2011. Selected Papers from the 13th Conference on Process Integration, Modelling and Optimisation for Energy Saving and Pollution Reduction.

[14] Giner Santonja G, Karlis P, Stubdrup K, Brinkmann T, and Roudier S. Best available techniques (bat) reference document for the food, drink and milk industries. industrial emissions directive 2010/75/eu (integrated pollution prevention and control), eur 29978 en, publications office of the european union, luxembourg. 2019. https://doi.org/10.2760/243911.

[15] Campden BRI. About us – sites. https://www.campdenbri.co.uk/about.php [Accessed: 01.05.2020].

[16] Campden BRI. Worldwide brewery industry water and energy benchmarking survey. https://www.campdenbri.co.uk/images/WaterEnergy.pdf [Accessed: 01.05.2020].

[17] Chiu J.NW, Castro Flores J, Martin V, and Lacarrière B. Industrial surplus heat transportation for use in district heating. *Energy*, 110:139 – 147, 2016. https://doi.org/10.1016/j.energy.2016.05.003.

[18] Li H, Wang W, Yan J, and Dahlquist E. Economic assessment of the mobilized thermal energy storage (m-tes) system for distributed heat supply. *Applied Energy*, 104:178 – 186, 2013. https://doi.org/10.1016/j.apenergy.2012.11.010.

[19] Wang W, Guo S, Li H, Yan J, Zhao J, Li X, and Ding J. Experimental study on the direct/indirect contact energy storage container in mobilized thermal energy system (m-tes). *Applied Energy*, 119:181 – 189, 2014. https://doi.org/10.1016/j.apenergy.2013.12.058.

[20] Guo S, Li H, Zhao J, Li X, and Yan J. Numerical simulation study on optimizing charging process of the direct contact mobilized thermal energy storage. *Applied Energy*, 112:1416 – 1423, 2013. https://doi.org/10.1016/j.apenergy.2013.01.020.

[21] Deckert M, Scholz R, Binder S, and Hornung A. Economic efficiency of mobile latent heat storages. *Energy Procedia*, 46:171 – 177, 2014.

[22] NVE. Dokumentasjon for kostnadar i energisektoren, 24.04.2020. https://www.nve.no/energiforsyning/energiforsyningsdata/dokumentasjon-for-kostnadar-i-energisektoren/.

[23] Stene J. Investeringsanalyse for varmepumpesystemer. In ., page 9, 2019.

[24] Stene J. *Varmepumper - Grunnelggende varmepumpeteknikk*. SINTEF Energiforskning AS, Klima- og kuldeteknikk, 2001.

[25] DAIKIN. *DAIKIN Chiller selection software SERIES: EWAD D-*. Daikin.

[26] Leonhardsen S. Elektrisitetsforbruk sluppenveien 10, 12.03.2020. Email correspandance: sondre.leonhardsen@kjeldsberg.no to erlendnb@stud.ntnu.no.

[27] Mosling Vonstad C. +cityxchange — energiforbruk kjølemaskiner sluppenveien 10, 19.03.2020. Email correspandance: Cato.Vonstad@bama.no to erlendnb@stud.ntnu.no.

[28] Dassault Systemes. Dymola 2020. https://www.3ds.com/products-services/catia/products/dymola/?woc=%7B%22category%22%3A%5B%22category%2Fdymola%22%5D%7D&wockw=card_content_cta_1_url%3A%22https%3A%2F%2Fblogs.3ds.com%2Fcatia%2F%22 [Accessed: 27.08.2019].

[29] Institut für Thermodynamik Technische Universität Braunschweig: TLK-Thermo GmbH & IfT. Til media & til component library 3.5.0. [Accessed: 27.08.2019].

[30] Koelet P.C. *Industrial Refrigeration*. Macmillan, 1992.

[31] Dr Wolf Srl. Dorin software 19.10. https://www.dorin.com/en/Software [Accessed: 17.10.2019].

[32] BITZER Kühlmaschinenbau GmbH. Bitzer software v6.13.0 rev2417. https://www.bitzer.de/websoftware/ [Accessed: 05.05.2020].

[33] Skattedirektoratet. Avgift pÅ elektrisk kraft 2019. https://www.skatteetaten.no/globalassets/bedrift-og-organisasjon/avgifter/saravgifter/elektrisk-kraft/2019-el-kraft.pdf[Accessed: 02.06.2020].

[34] Stistisk Sentralbyrå. Elektrisitetspriser. https://www.ssb.no/statbank/table/09363/tableViewLayout1/[Accessed: 02.06.2020].

[35] Stistisk Sentralbyrå. Fjernvarme og fjernkjøling i norge. https://www.ssb.no/energi-og-industri/artikler-og-publikasjoner/fjernvarme-og-fjernkjoling-i-norge[Accessed: 02.06.2020].

[36] Standard Norge. SN-NSPEK 3031:2020 — Bygningers energiytelse, Beregning av energibehov og energiforsyning., 2020.

# Appendix B

# Chiller Information

**Table B.1:** SLV10 Chiller 1 Information. Information marked* from manufacturer data-sheet [94]

| Chiller 1 — Information | | |
|---|---|---|
| Model | ACM SCAEYJ-F 151 PAC1 | |
| Coling Capacity | 121* | kW |
| Unit Power input | 48* | kW |
| EER | 2.52* | |
| ESEER | Not stated | |
| Refrigerant | R410A | |
| Refrigerant Charge | 20 | kg |
| Compressor | 2xHermetic Scroll* | |
| Part-Load Operation | | |

**Figure B.1:** AMC Chiller

**Table B.2:** SLV10 Chiller 2 Information. Information marked* from manufacturer data-sheet [95]

| Chiller 2 — Information | | |
|---|---|---|
| Model | BlueBox ZETA ECHOS /ST 2PS 12.2 | |
| Coling Capacity | 116.4* | kW |
| Unit Power input | 40.8* | kW |
| EER | 2.81* | |
| ESEER | 4.09* | |
| Refrigerant | R410A | |
| Refrigerant Charge | 23.7* | kg |
| Compressor | 2xSemi Hermetic Scroll | |
| Part-Load Operation | Step 0-50-100% | |

**Figure B.2:** BlueBox Chiller

**Table B.3:** SLV10 Chiller 3 Information

| Chiller 3 — Information | | |
|---|---|---|
| Model | DAIKIN EWAD-480D-SL | |
| Coling Capacity | 338 | kW |
| Unit Power input | 136 | kW |
| EER | 2.49 | |
| ESEER | 3.46 | |
| Fluid | Ethylene Glycol 40% | |
| Water temp. (In/Out) | -2.0 / -6.0* | $°C$ |
| Nominal Water flow | 21.5* | l/s |
| Refrigerant | R134a | |
| Refrigerant Charge | 68* | kg |
| Compressor | 2xSymetric Single Screw* | |
| Part-Load Operation | Stepless 100-25%* | |


**Figure B.3:** DAIKIN EWAD 480D-SL Chiller

**Table B.4:** SLV10 Chiller 4 Information. Information marked* from manufacturer data-sheet [96]

| Chiller 4 — Information | | |
|---|---|---|
| Model | DAIKIN EWYQ 150 DAYNB | |
| Coling Capacity | 145* | kW |
| Unit Power input | 55.7* | kW |
| EER | 2.81* | |
| ESEER | 4.07* | |
| Refrigerant | R410A | |
| Refrigerant Charge | 2x26 | kg |
| Compressor | 4xScroll SJ180* | |
| Part-Load Operation | Step 0-25-50-75-100%* | |


**Figure B.4:** DAIKIN EWYQ 150 DAYN Chiller

Appendix C

# Detailed Dymola Model Parameters

## C.1 Model A1

**LTC - Propane (R290) Cycle**

**Table C.1:** Model A1 — Evaporator key parameters

| Evaporator | | |
|---|---|---|
| Heat sink | Propane (R290) | [–] |
| Heat source | $CO_2$ | [–] |
| $T_{In}$ $CO_2$ | -5.3 | [°C] |
| $T_{Out}$ $CO_2$ | -12.7 | [°C] |
| $T_{In}$ R290 | -15 | [°C] |
| $T_{Out}$ R290 | -11 | [°C] |
| $Q_{Evap}$ | 60.36 | [kW] |
| Thermal conductivity | 600 | $[W/m^2K]$ |
| Length | 0.6 | $[m]$ |
| Width | 0.3 | $[m]$ |
| Number of Plates | 205 | $[-]$ |

**HTC - Butane (R600) Cycle**

**Table C.2:** Model A1 — Condenser key parameters

| Condenser | | |
|---|---|---|
| Heat sink | Water | [–] |
| Heat source | Butane (R600) | [–] |
| $T_{In}$ Water | 65 | [°C] |
| $T_{Out}$ Water | 100 | [°C] |
| $T_{In}$ R600 | 119.2 | [°C] |
| $T_{Out}$ R600 | 101.6 | [°C] |
| $Q_{Cond}$ | 124.76 | [kW] |
| Thermal conductivity | 800 | $[W/m^2K]$ |
| Length | 0.6 | $[m]$ |
| Width | 0.3 | $[m]$ |
| Number of Plates | 81 | $[-]$ |

**Table C.3:** Model A1 — Propane IHX, key parameters

| Internal Heat Exchanger (R290) | | |
|---|---|---|
| Heat sink | Propane (R290) | [–] |
| Heat source | Propane (R290) | [–] |
| $T_{In}$ Source | 53.3 | [°C] |
| $T_{Out}$ Source | 46.5 | [°C] |
| $T_{In}$ Sink | -11 | [°C] |
| $T_{Out}$ Sink | 0 | [°C] |
| Thermal conductivity | 100 | $[W/m^2K]$ |
| Length | 0.3 | $[m]$ |
| Width | 0.1 | $[m]$ |
| Number of Plates | 55 | $[-]$ |

**Table C.4:** Model A1 — Butane IHX key parameters

| Internal Heat Exchanger (R600) | | |
|---|---|---|
| Heat sink | Propane (R600) | [–] |
| Heat source | Propane (R600) | [–] |
| $T_{In}$ Source | 99.9 | [C] |
| $T_{Out}$ Source | 92.1 | [C] |
| $T_{In}$ Sink | 61.5 | [C] |
| $T_{Out}$ Sink | 73 | [C] |
| Thermal conductivity | 100 | $[W/m^2K]$ |
| Length | 0.3 | $[m]$ |
| Width | 0.1 | $[m]$ |
| Number of Plates | 190 | $[-]$ |

**Table C.5:** Model A1 — Cascade Heat Exchanger key parameters

| Cascade Heat Exchanger | | |
|---|---|---|
| Heat sink | Butane (R600) | [–] |
| Heat source | Propane (R290) | [–] |
| $T_{In}$ R290 | 98.8 | [°C] |
| $T_{Out}$ R290 | 55.6 | [°C] |
| $T_{In}$ R600 | 53 | [°C] |
| $T_{Out}$ R600 | 64.2 | [°C] |
| Q | 83.3 | [kW] |
| Thermal conductivity | 800/500 | $[W/m^2K]$ |
| Length | 0.6 | $[m]$ |
| Width | 0.3 | $[m]$ |
| Number of Plates | 540 | $[-]$ |

**Table C.6:** Model A1 — Propane Compressor key parameters

| Propane (R290) Compressor | | |
|---|---|---|
| Compressor Model | HEX7501CS | [–] |
| Displacement | $1.232 \cdot 10^{-}4m^3$ | $[m^3]$ |
| Frequency | 50 | [Hz] |
| Eff.Isentropic Efficiency | 0.62 | [–] |
| Isentropic Efficiency | 0.69 | [–] |
| Volumetric Efficiency | 0.70 | [–] |
| $\dot{m}_R$ | 0.264 | $[kg/s]$ |
| $\dot{V}_S$ | 224.35 | $[m^3/h]$ |
| $\dot{W}_C$ | 42.16 | $[kW]$ |
| Suction Temperature | 0 | $[°C]$ |
| Discharge Temperature | 98.8 | $[°C]$ |

**Table C.7:** Model A1 — Butane Compressor key parameters

| Butane (R600) Compressor | | |
|---|---|---|
| Compressor Model | HEX5000CC | [–] |
| Displacement | $8.529 \cdot 10^{-}4m^3$ | $[m^3]$ |
| Frequency | 50 | [Hz] |
| Eff.Isentropic Efficiency | 0.6 | [–] |
| Isentropic Efficiency | 0.7 | [–] |
| Volumetric Efficiency | 0.8 | [–] |
| $\dot{m}_R$ | 0.417 | $[kg/s]$ |
| $\dot{V}_S$ | 147.23 | $[m^3/h]$ |
| $\dot{W}_C$ | 30.94 | $[kW]$ |
| Suction Temperature | 73 | $[°C]$ |
| Discharge Temperature | 119.2 | $[°C]$ |

## C.2 Model A2

**LTC - Propane (R290) Cycle**

**Table C.8:** Model A2 — Evaporator key parameters

| Evaporator | | |
|---|---|---|
| Heat sink | Propane (R290) | [–] |
| Heat source | $CO_2$ | [–] |
| $T_{In}$ $CO_2$ | -5.3 | [C] |
| $T_{Out}$ $CO_2$ | -12.7 | [C] |
| $T_{In}$ R290 | -15 | [C] |
| $T_{Out}$ R290 | -11 | [C] |
| $Q_{Evap}$ | 60.36 | [kW] |
| Thermal conductivity | 600 | $[W/m^2K]$ |
| Length | 0.6 | $[m]$ |
| Width | 0.3 | $[m]$ |
| Number of Plates | 205 | $[-]$ |

**HTC - Butane (R600) Cycle**

**Table C.9:** Model A2 — Condenser key parameters

| Condenser | | |
|---|---|---|
| Heat sink | Water | [–] |
| Heat source | Butane (R600) | [–] |
| $T_{In}$ Water | 65 | [C] |
| $T_{Out}$ Water | 100 | [C] |
| $T_{In}$ R600 | 119.4 | [C] |
| $T_{Out}$ R600 | 101.9 | [C] |
| $Q_{Cond}$ | 119.09 | [kW] |
| Thermal conductivity | 800 | $[W/m^2K]$ |
| Length | 0.6 | $[m]$ |
| Width | 0.3 | $[m]$ |
| Number of Plates | 75 | $[-]$ |

**Table C.10:** Model A2 — Propane IHX, key parameters

| Internal Heat Exchanger (R290) | | |
|---|---|---|
| Heat sink | Propane (R290) | [–] |
| Heat source | Propane (R290) | [–] |
| $T_{In}$ Source | 16.1 | [C] |
| $T_{Out}$ Source | 8.7 | [C] |
| $T_{In}$ Sink | -11 | [C] |
| $T_{Out}$ Sink | 0 | [C] |
| Thermal conductivity | 100 | $[W/m^2K]$ |
| Length | 0.3 | $[m]$ |
| Width | 0.1 | $[m]$ |
| Number of Plates | 110 | $[-]$ |

**Table C.11:** Model A2 — Butane IHX key parameters

| Internal Heat Exchanger (R600) | | |
|---|---|---|
| Heat sink | Propane (R600) | [–] |
| Heat source | Propane (R600) | [–] |
| $T_{In}$ Source | 101.9 | [C] |
| $T_{Out}$ Source | 97.6 | [C] |
| $T_{In}$ Sink | 58.7 | [C] |
| $T_{Out}$ Sink | 73.1 | [C] |
| Thermal conductivity | 100 | $[W/m^2K]$ |
| Length | 0.3 | $[m]$ |
| Width | 0.1 | $[m]$ |
| Number of Plates | 200 | $[-]$ |

**Table C.12:** Model A2 — Cascade Heat Exchanger key parameters

| Cascade Heat Exchanger | | |
|---|---|---|
| Heat sink | Butane (R600) | [–] |
| Heat source | Propane (R290) | [–] |
| $T_{In}$ R290 | 87.7 | [C] |
| $T_{Out}$ R290 | 55.6 | [C] |
| $T_{In}$ R600 | 53.1 | [C] |
| $T_{Out}$ R600 | 58.7 | [C] |
| $\dot{Q}$ | 90.88 | [kW] |
| Thermal conductivity | 800/500 | $[W/m^2K]$ |
| Length | 0.6 | $[m]$ |
| Width | 0.3 | $[m]$ |
| Number of Plates | 440 | $[-]$ |

**Table C.13:** Model A2 — LTC Propane Compressor key parameters

| LTC (R290) Compressor | |
|---|---|
| Compressor Model | HEX4000CC |
| Displacement | $7.08 \cdot 10^{-}4$ |
| Frequency | 50 |
| Eff.Isen. Efficiency | 0.53 |
| Isentropic Efficiency | 0.59 |
| Volumetric Efficiency | 0.82 |
| $\dot{m}_R$ | 0.177 |
| $\dot{V}_S$ | 128.37 |
| $\dot{W}_C$ | 15.85 |
| Suction Temperature | 0 |
| Discharge Temperature | 53.2 |

**Table C.14:** Model A2 — MTC Propane Compressor key parameters

| MTC (R290) Compressor | |
|---|---|
| Compressor Model | HEX2500CC |
| Displacement | $4.21 \cdot 10^{-}4$ |
| Frequency | 50 |
| Eff. Isen. Efficiency | 0.73 |
| Isentropic Efficiency | 0.81 |
| Volumetric Efficiency | 0.92 |
| $\dot{m}_R$ | 0.261 |
| $\dot{V}_S$ | 71.39 |
| $\dot{W}_C$ | 17.88 |
| Suction Temperature | 41.4 |
| Discharge Temperature | 87.7 |

**Table C.15:** Model A2 — Butane Compressor key parameters

| Butane (R600) Compressor | | |
|---|---|---|
| Compressor Model | HEX5000CC | [–] |
| Displacement | $8.53 \cdot 10^{-}4$ | $[m^3]$ |
| Frequency | 50 | [Hz] |
| Eff. Isen. Efficiency | 0.6 | [–] |
| Isentropic Efficiency | 0.7 | [–] |
| Volumetric Efficiency | 0.8 | [–] |
| $\dot{m}_R$ | 0.420 | $[kg/s]$ |
| $\dot{V}_S$ | 156.28 | $[m^3/h]$ |
| $\dot{W}_C$ | 33.14 | $[kW]$ |
| Suction Temperature | 73.1 | $[°C]$ |
| Discharge Temperature | 119.4 | $[°C]$ |

## C.3 Model B1

**LTC - Propane (R290) Cycle**

**Table C.16:** Model B1 — Evaporator key parameters

| Evaporator | | |
|---|---|---|
| Heat sink | Propane (R290) | [–] |
| Heat source | $CO_2$ | [–] |
| $T_{In}$ $CO_2$ | -5.3 | [C] |
| $T_{Out}$ $CO_2$ | -12.7 | [°C] |
| $T_{In}$ R290 | -15 | [°C] |
| $T_{Out}$ R290 | -11 | [°C] |
| $Q_{Evap}$ | 60.36 | [kW] |
| Thermal conductivity | 600 | $[W/m^2K]$ |
| Length | 0.6 | $[m]$ |
| Width | 0.3 | $[m]$ |
| Number of Plates | 210 | $[-]$ |

**HTC - Butane (R600) Cycle**

**Table C.17:** Model B1 — Condenser key parameters

| Condenser | | |
|---|---|---|
| Heat sink | Water | [–] |
| Heat source | Butane (R600) | [–] |
| $T_{In}$ Water | 4 | [°C] |
| $T_{Out}$ Water | 70 | [°C] |
| $T_{In}$ R600 | 92.2 | [°C] |
| $T_{Out}$ R600 | 38.1 | [°C] |
| $Q_{Cond}$ | 95.82 | [kW] |
| Thermal conductivity | 800 | $[W/m^2K]$ |
| Length | 0.6 | $[m]$ |
| Width | 0.3 | $[m]$ |
| Number of Plates | 48 | $[-]$ |

**Table C.18:** Model B1 — Propane IHX, key parameters

| Internal Heat Exchanger (R290) | | |
|---|---|---|
| Heat sink | Propane (R290) | [–] |
| Heat source | Propane (R290) | [–] |
| $T_{In}$ Source | 32.8 | [°C] |
| $T_{Out}$ Source | 25.2 | [°C] |
| $T_{In}$ Sink | -13.9 | [°C] |
| $T_{Out}$ Sink | 0 | [°C] |
| Thermal conductivity | 100 | $[W/m^2K]$ |
| Length | 0.3 | $[m]$ |
| Width | 0.1 | $[m]$ |
| Number of Plates | 75 | $[-]$ |

**Table C.19:** Model B1 — Cascade Heat Exchanger key parameters

| Cascade Heat Exchanger | | |
|---|---|---|
| Heat sink | Butane (R600) | [–] |
| Heat source | Propane (R290) | [–] |
| $T_{In}$ R290 | 69.7 | [°C] |
| $T_{Out}$ R290 | 32.9 | [°C] |
| $T_{In}$ R600 | 30.1 | [°C] |
| $T_{Out}$ R600 | 50.1 | [°C] |
| Q | 83.3 | [kW] |
| Thermal conductivity | 800/500 | $[W/m^2K]$ |
| Length | 0.6 | $[m]$ |
| Width | 0.3 | $[m]$ |
| Number of Plates | 440 | $[-]$ |

**Table C.20:** Model B1 — Propane Compressor key parameters

| Propane (R290) Compressor | | |
|---|---|---|
| Compressor Model | HEX4500CS | [–] |
| Displacement | $8.53 \cdot 10^-4m^3$ | $[m^3]$ |
| Frequency | 50 | [Hz] |
| Eff. Isen. Efficiency | 0.61 | [–] |
| Isentropic Efficiency | 0.68 | [–] |
| Volumetric Efficiency | 0.78 | [–] |
| $\dot{m}_R$ | 0.205 | $[kg/s]$ |
| $\dot{V}_S$ | 156.59 | $[m^3/h]$ |
| $\dot{W}_C$ | 23.46 | $[kW]$ |
| Suction Temperature | 0 | $[°C]$ |
| Discharge Temperature | 69.7 | $[°C]$ |

**Table C.21:** Model B1 — Butane Compressor key parameters

| Butane (R600) Compressor | | |
|---|---|---|
| Compressor Model | HEX5000CC | [–] |
| Displacement | $X \cdot 10^-4m^3$ | $[m^3]$ |
| Frequency | 50 | [Hz] |
| Eff. Isen. Efficiency | 0.6 | [–] |
| Isentropic Efficiency | 0.7 | [–] |
| Volumetric Efficiency | 0.8 | [–] |
| $\dot{m}_R$ | 0.218 | $[kg/s]$ |
| $\dot{V}_S$ | 149.19 | $[m^3/h]$ |
| $\dot{W}_C$ | 16.82 | $[kW]$ |
| Suction Temperature | 50.1 | $[°C]$ |
| Discharge Temperature | 92.2 | $[°C]$ |

## C.4 Model B2

**LTC - Propane (R290) Cycle**

**Table C.22:** Model B2 — Evaporator key parameters

| Evaporator | |
|---|---|
| Heat sink | Propane |
| Heat source | $CO_2$ |
| $T_{In}$ $CO_2$ | -5.3 |
| $T_{Out}$ $CO_2$ | -10.9 |
| $T_{In}$ R290 | -15 |
| $T_{Out}$ R290 | -11.5 |
| $Q_{Evap}$ | 60.36 |
| Thermal conductivity | 600 |
| Length | 0.6 |
| Width | 0.3 |
| Number of Plates | 205 |

**LTC — Sub-cooler**

**Table C.23:** Model B2 — Sub-cooler key parameters

| Sub-cooler | |
|---|---|
| Heat sink | Water |
| Heat source | Propane |
| $T_{In}$ Water | 4 |
| $T_{Out}$ Water | 30.3 |
| $T_{In}$ R290 | 32.9 |
| $T_{Out}$ R290 | 11.6 |
| $Q_{Cond1}$ | 33.95 |
| Thermal conductivity | 600 |
| Length | 0.6 |
| Width | 0.3 |
| Number of Plates | 47 |

**HTC - Butane (R600) Cycle**

**Table C.24:** Model B2 — Condenser key parameters

| Condenser | | |
|---|---|---|
| Heat sink | Water | [–] |
| Heat source | Butane (R600) | [–] |
| $T_{In}$ Water | 30.3 | [°C] |
| $T_{Out}$ Water | 70 | [°C] |
| $T_{In}$ R600 | 94.6 | [°C] |
| $T_{Out}$ R600 | 33.0 | [°C] |
| $Q_{Cond2}$ | 51.30 | [kW] |
| Thermal conductivity | 800 | $[W/m^2K]$ |
| Length | 0.6 | $[m]$ |
| Width | 0.3 | $[m]$ |
| Number of Plates | 45 | $[-]$ |

**Table C.25:** Model B2 — Propane IHX, key parameters

| Internal Heat Exchanger (R290) | | |
|---|---|---|
| Heat sink | Propane (R290) | [–] |
| Heat source | Propane (R290) | [–] |
| $T_{In}$ Source | 7.5 | [C] |
| $T_{Out}$ Source | 0 | [C] |
| $T_{In}$ Sink | -11.5 | [C] |
| $T_{Out}$ Sink | 0 | [C] |
| Thermal conductivity | 100 | $[W/m^2K]$ |
| Length | 0.3 | $[m]$ |
| Width | 0.1 | $[m]$ |
| Number of Plates | 205 | $[-]$ |

**Table C.26:** Model B2 — Cascade Heat Exchanger key parameters

| Cascade Heat Exchanger | | |
|---|---|---|
| Heat sink | Butane (R600) | [–] |
| Heat source | Propane (R290) | [–] |
| $T_{In}$ R290 | 69.8 | [C] |
| $T_{Out}$ R290 | 32.9 | [C] |
| $T_{In}$ R600 | 30 | [C] |
| $T_{Out}$ R600 | 50 | [C] |
| Q | 43.45 | [kW] |
| Thermal conductivity | 800/500 | $[W/m^2K]$ |
| Length | 0.6 | $[m]$ |
| Width | 0.3 | $[m]$ |
| Number of Plates | 205 | $[-]$ |

**Table C.27:** Model B2 — Propane Compressor key parameters

| Propane (R290) Compressor | | |
|---|---|---|
| Compressor Model | HEX3500CS | [–] |
| Displacement | $7.08 \cdot 10^{-}4m^3$ | $[m^3]$ |
| Frequency | 50 | [Hz] |
| Eff. Isen. Efficiency | 0.62 | [–] |
| Isentropic Efficiency | 0.68 | [–] |
| Volumetric Efficiency | 0.78 | [–] |
| $\dot{m}_R$ | 0.166 | $[kg/s]$ |
| $\dot{V}_S$ | 126.77 | $[m^3/h]$ |
| $\dot{W}_C$ | 18.70 | $[kW]$ |
| Suction Temperature | 0.0 | $[°C]$ |
| Discharge Temperature | 69.8 | $[°C]$ |

**Table C.28:** Model B2 — Butane Compressor key parameters

| Butane (R600) Compressor | | |
|---|---|---|
| Compressor Model | HEX2500CC | [–] |
| Displacement | $4.21 \cdot 10^{-}4m^3$ | $[m^3]$ |
| Frequency | 50 | [Hz] |
| Eff. Isen. Efficiency | 0.6 | [–] |
| Isentropic Efficiency | 0.7 | [–] |
| Volumetric Efficiency | 0.8 | [–] |
| $\dot{m}_R$ | 0.113 | $[kg/s]$ |
| $\dot{V}_S$ | 77.02 | $[m^3/h]$ |
| $\dot{W}_C$ | 9.15 | $[kW]$ |
| Suction Temperature | 50.1 | $[°C]$ |
| Discharge Temperature | 94.6 | $[°C]$ |

## C.5 Model C1

**Table C.29:** Model C1 — Evaporator key parameters

| Evaporator | | |
|---|---|---|
| Heat sink | $CO_2$ (R744) | [–] |
| Heat source | $CO_2$ | [–] |
| $T_{In}$ $CO_2$ | -5.3 | [C] |
| $T_{Out}$ $CO_2$ | -12.2 | [°C] |
| $T_{In}$ R290 | -15 | [°C] |
| $T_{Out}$ R290 | -15 | [°C] |
| $Q_{Evap}$ | 60.36 | [kW] |
| Thermal conductivity | 600 | $[W/m^2K]$ |
| Length | 0.6 | $[m]$ |
| Width | 0.3 | $[m]$ |
| Number of Plates | 260 | $[-]$ |

**Table C.30:** Model C1 — Gas Cooler key parameters

| Gas Cooler | | |
|---|---|---|
| Heat sink | Water | [–] |
| Heat source | $CO_2$ (R744) | [–] |
| $T_{In}$ Water | 4 | [°C] |
| $T_{Out}$ Water | 70 | [°C] |
| $T_{In}$ R744 | 120.1 | [°C] |
| $T_{Out}$ R744 | 7.5 | [°C] |
| $Q_{G.Cooler}$ | 82.94 | [kW] |
| Thermal conductivity | 800 | $[W/m^2K]$ |
| Length | 0.6 | $[m]$ |
| Width | 0.3 | $[m]$ |
| Number of Plates | 125 | $[-]$ |

**Table C.31:** Model C1 — $CO_2$ IHX, key parameters

| Internal Heat Exchanger (R744) | | |
|---|---|---|
| Heat sink | $CO_2$ (R744) | [–] |
| Heat source | $CO_2$ (R744) | [–] |
| $T_{In}$ Source | 7.5 | [°C] |
| $T_{Out}$ Source | 1.3 | [°C] |
| $T_{In}$ Sink | -15 | [°C] |
| $T_{Out}$ Sink | -3.9 | [°C] |
| Thermal conductivity | 100 | $[W/m^2K]$ |
| Length | 0.3 | $[m]$ |
| Width | 0.1 | $[m]$ |
| Number of Plates | 150 | $[-]$ |

**Table C.32:** Model C1 — $CO_2$ Compressor key parameters

| $CO_2$ (R744) Compressor | | |
|---|---|---|
| Compressor Model | | [–] |
| Displacement | $\cdot 10^-4 m^3$ | $[m^3]$ |
| Frequency | 50 | [Hz] |
| Eff. Isen. Efficiency | 0.66 | [–] |
| Isentropic Efficiency | 0.74 | [–] |
| Volumetric Efficiency | 0.76 | [–] |
| $\dot{m}_R$ | 0.254 | $[kg/s]$ |
| $\dot{V}_S$ | 21.71 | $[m^3/h]$ |
| $\dot{W}_C$ | 25.31 | $[kW]$ |
| Suction Temperature | -3.9 | $[°C]$ |
| Discharge Temperature | 120.1 | $[°C]$ |

## C.6 Compressor Polynomials

**Table C.33:** Polonmial coefficents for chosen Dorin Compressor models.

| Compressor model | Parameter | C1 | C2 | C3 | C4 | C5 | C6 | C7 | C8 | C9 | C10 |
|---|---|---|---|---|---|---|---|---|---|---|---|
| Propane Compressors | | y = C1 + C2*to + C3*tc + C4*to^2 + C5*to*tc + C6*tc^2 + C7*to^3 + C8*tc*to^2 + C9*to*tc^2 + C10*tc^3 | | | | | | | | | |
| HEX2500CC | P [kW] | 6363.56885 | -87.6602102 | 185.57118 | -3.23238283 | 3.65306878 | -0.09213245 | -0.01526615 | 0.00770597 | 0.01809947 | 0.00348669 |
| | m [kg/s] | 0.189619 | 0.00657854 | -0.00026548 | 8.97E-05 | -4.04E-06 | -2.94E-06 | 5.21E-07 | -4.67E-08 | -1.50E-08 | -1.69E-09 |
| HEX3500CS | P [kW] | 11544.757 | -132.889619 | 372.410853 | -6.22828777 | 7.11582823 | -3.20459239 | -0.03746204 | 0.04545711 | 0.03679449 | 0.04513509 |
| | m [kg/s] | 0.33035753 | 0.01127631 | -0.00120157 | 0.00014704 | -2.23E-05 | 7.51E-06 | 8.03E-07 | -9.31E-08 | 1.76E-07 | -2.83E-08 |
| HEX4000CC | P [kW] | 13664.2239 | -72.935816 | 207.714722 | -4.58862609 | 4.3011884 | 0.78513678 | -0.01881844 | 0.00534511 | 0.04795095 | 0.00901818 |
| | m [kg/s] | 0.32523774 | 0.01117375 | -0.00089112 | 0.00015024 | -1.48E-05 | 1.31E-06 | 8.74E-07 | -6.59E-08 | 8.28E-08 | -1.30E-09 |
| HEX4500CS | P [kW] | 17458.1834 | 60.8873847 | 214.261731 | -2.50580963 | 1.21287462 | 1.86804801 | -0.00710211 | -0.04440028 | 0.07633736 | 0.00086204 |
| | m [kg/s] | 0.38719446 | 0.01330643 | -0.00087079 | 0.00017444 | -1.47E-05 | 4.86E-07 | 9.42E-07 | -9.05E-08 | 6.11E-08 | -1.53E-08 |
| HEX5000CC | P [kW] | 15446.4356 | -111.047664 | 307.188431 | -5.85219334 | 6.56457387 | 0.57974672 | -0.02522575 | 0.01252942 | 0.03975558 | 0.00318081 |
| | m [kg/s] | 0.38359404 | 0.01333507 | -0.00055334 | 0.00018139 | -7.91E-06 | -6.23E-06 | 1.05E-06 | -8.10E-08 | -4.13E-08 | 1.28E-08 |
| HEX7501CS | P [kW] | 22175.9004 | -122.005351 | 465.470555 | -8.16534231 | 9.62961857 | -0.04949522 | -0.04248839 | 0.02755988 | 0.04607727 | 0.01295913 |
| | m [kg/s] | 0.57363991 | 0.01941071 | -0.00175787 | 0.0002494 | -2.91E-05 | 1.81E-06 | 1.33E-06 | -1.14E-07 | 9.03E-08 | 3.99E-09 |
| $CO_2$ Compressors | | y = C1 + C2*to + C3*pc + C4*to^2 + C5*to*pc + C6*pc^2 + C7*to^3 + C8*pc*to^2 + C9*to*pc^2 + C10*pc^3 | | | | | | | | | |
| CD3501H | P [kW] | 0.62237435 | 0.01653057 | -0.00259578 | 0.00014839 | -1.41E-05 | 8.32E-06 | 0 | 0 | 0 | 0 |
| | m [kg/s] | -27961.7519 | -987.871628 | 1136.88462 | -9.51298473 | 14.5115321 | -7.76555559 | -0.00892134 | 0.0267851 | -0.04061483 | 0.02347348 |
| 4DTE-25K | P [kW] | -9255,877783 | -614,3494637 | 512,7094997 | -5,20330968 | 8,655358232 | -0,80352 | 0,040227912 | 0,011010826 | -0,008399747 | -0,003012281 |
| | m* [kg/h] | 2182,614111 | 64,9405461 | -7,719038619 | 0,797023684 | -0,117852936 | 0,017707736 | 0,005406015 | -0,00048252 | -2,00179E-05 | -4,25862E-05 |

Bitzer compressor mass flow given in [kg/h]

Appendix D

# Additional Results

## D.1 Model B1 & B2

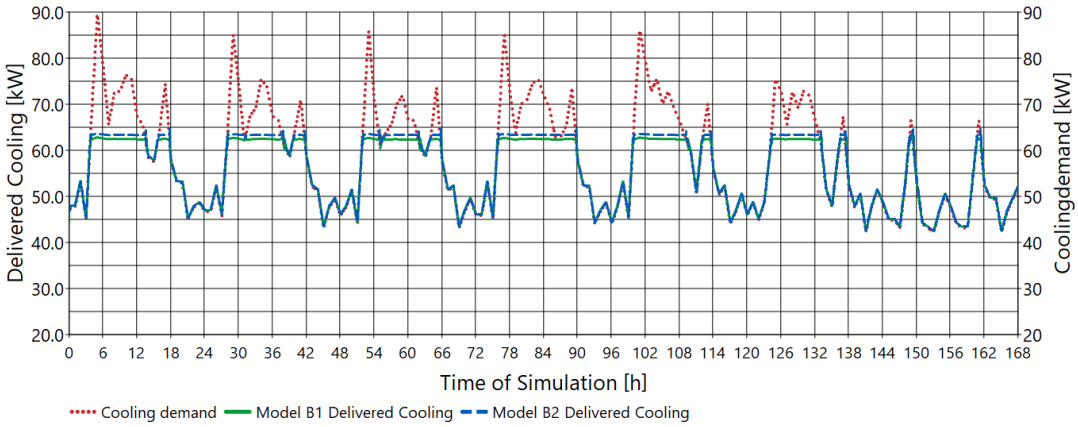


**Figure D.1:** Model B1 and B2 — Weekly Simulation, delivered cooling. Input 50% of estimated cooling demand.

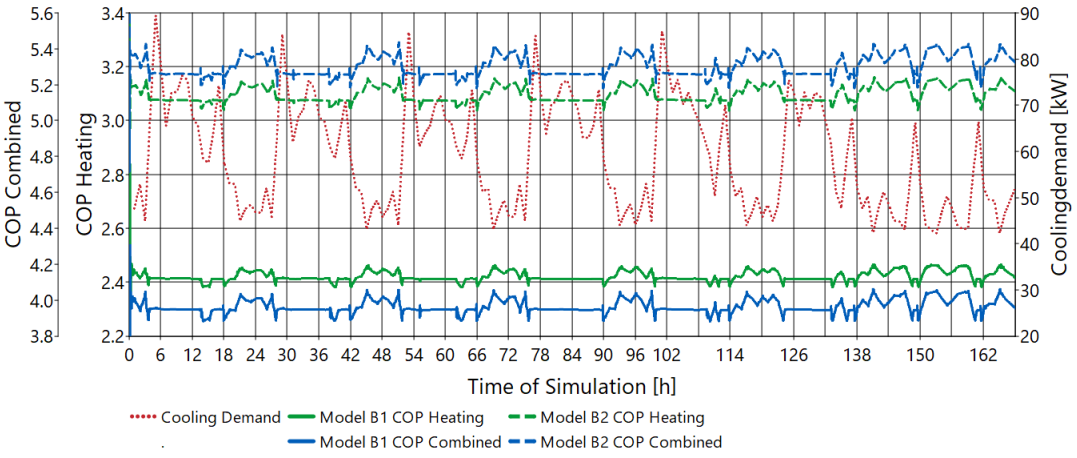


**Figure D.2:** Model B1 and B2 — Weekly Simulation, COP Heating and Combined COP Heating & Cooling.

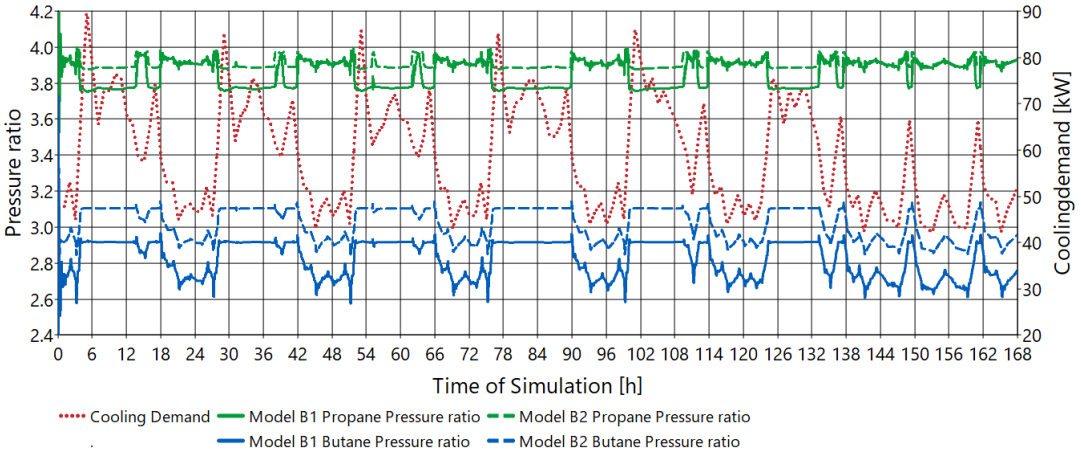


**Figure D.3:** Model B1 and B2 — Weekly Simulation, Cycle pressure ratio. Input 50% of estimated cooling demand

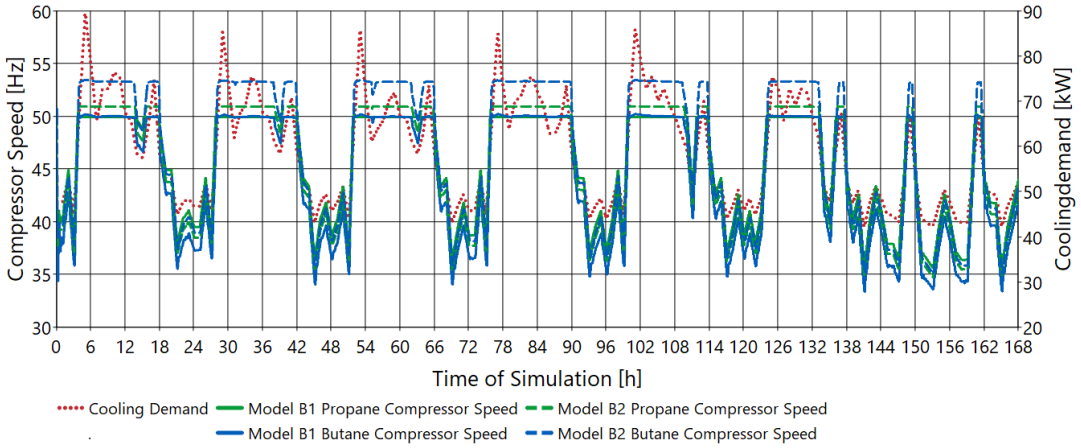


**Figure D.4:** Model B1 and B2 — Weekly Simulation, Compressor speed at 50% of estimated cooling demand.

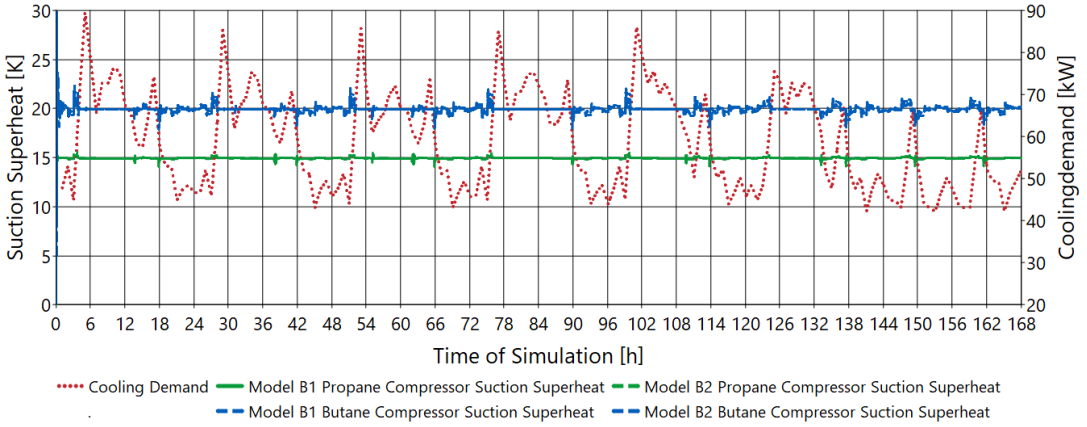


**Figure D.5:** Model B1 and B2 — Weekly Simulation, Compressor suction superheat. Input 50% of estimated cooling demand.

## D.2 Model C1

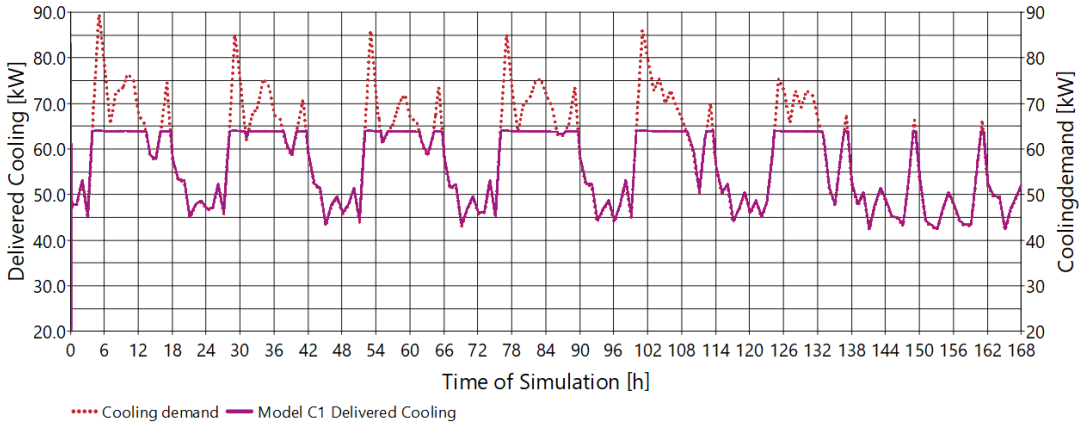


**Figure D.6:** Model C1 — Weekly Simulation, delivered cooling. Input 50% of estimated cooling demand.

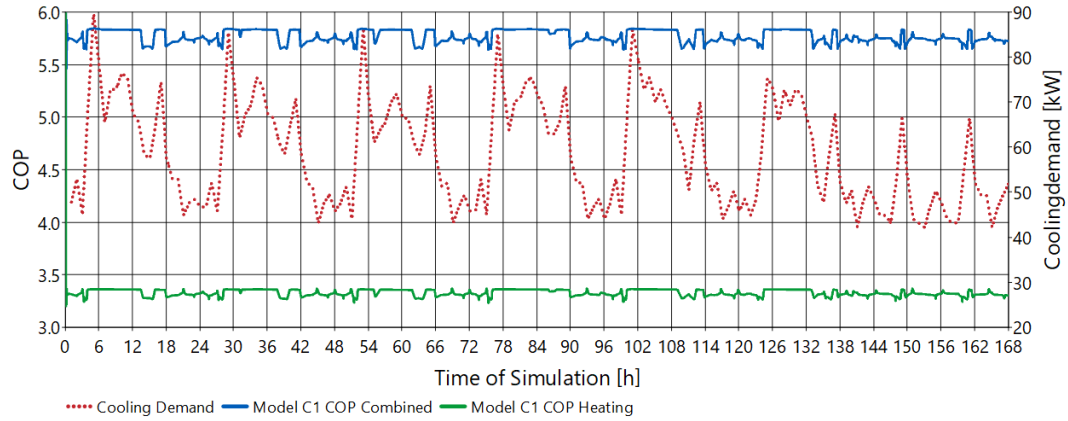


**Figure D.7:** Model C1 — Weekly Simulation, COP Heating and Combined COP Heating & Cooling.

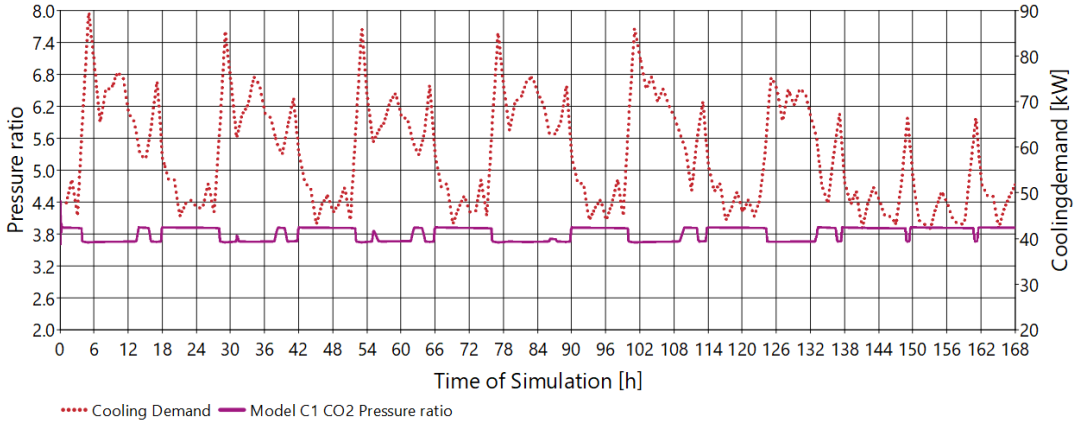


**Figure D.8:** Model C1 — Weekly Simulation, Cycle pressure ratio. Input 50% of estimated cooling demand

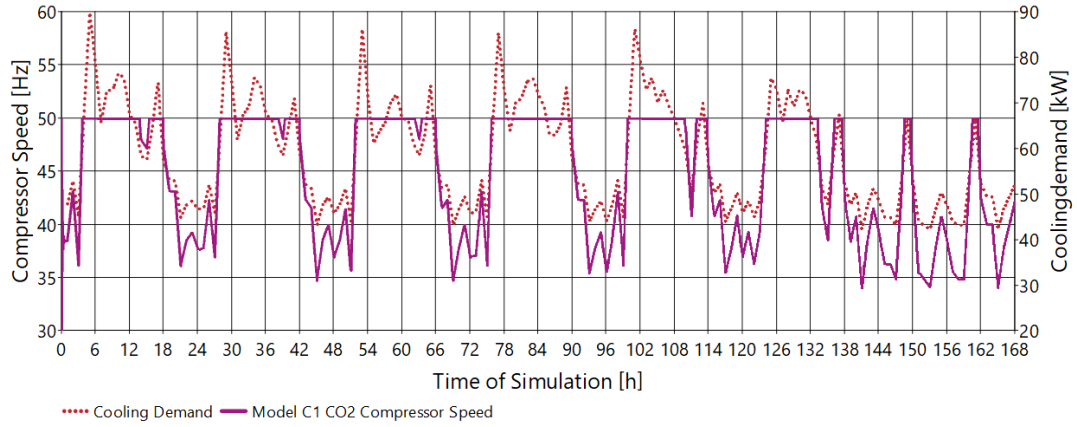


**Figure D.9:** Model C1 — Weekly Simulation, Compressor speed at 50% of estimated cooling demand.

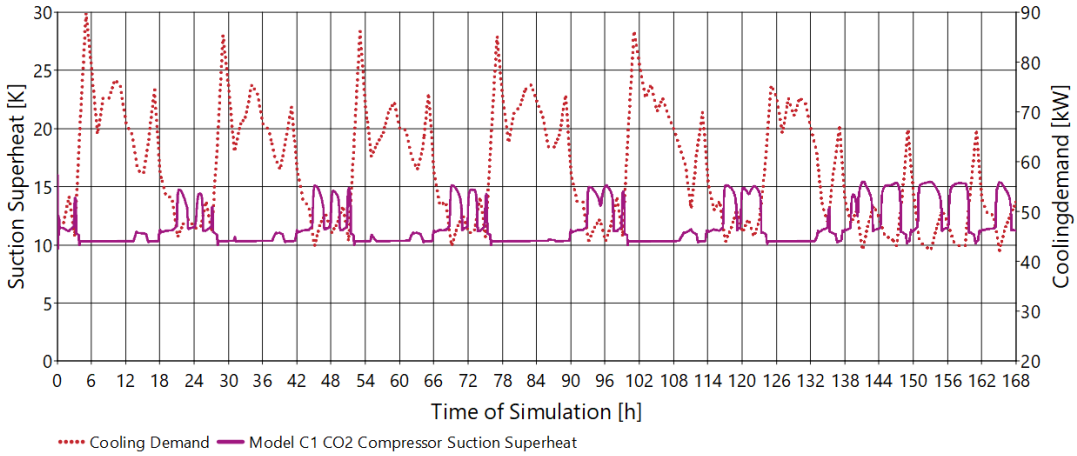


**Figure D.10:** Model C1 — Weekly Simulation, Compressor suction superheat. Input 50% of estimated cooling demand.

### D.2.1 Annual Costs

**Table D.1:** Calculated annual costs for 3 different, full load hours, economical life times and interest rates.

| Annual Costs | | Interest rate 6% Economical Life time years | | | Interest rate 12% Economical Life time | | | Interest rate 18% Economical Life time | | |
|---|---|---|---|---|---|---|---|---|---|---|
| | FLH [h/year] | 10 | 15 | 20 | 10 | 15 | 20 | 10 | 15 | 20 |
| Model A1 | 4250 | 310989 | 256696 | 230662 | 378831 | 329067 | 307707 | 453956 | 410872 | 395060 |
| | 6375 | 348393 | 294100 | 268065 | 416235 | 366471 | 345111 | 491360 | 448276 | 432464 |
| | 8500 | 385797 | 331503 | 305469 | 453639 | 403875 | 382515 | 528764 | 485679 | 469868 |
| Model A2 | 4250 | 301470 | 247176 | 221142 | 369311 | 319548 | 298188 | 444437 | 401352 | 385541 |
| | 6375 | 334113 | 279820 | 253786 | 401955 | 352191 | 330831 | 477080 | 433996 | 418184 |
| | 8500 | 366757 | 312464 | 286430 | 434599 | 384835 | 363475 | 509724 | 466640 | 450828 |
| Model B1 | 4250 | 440769 | 391411 | 367744 | 502443 | 457203 | 437785 | 570739 | 531571 | 517197 |
| | 6375 | 575281 | 525923 | 502255 | 636955 | 591715 | 572297 | 705251 | 666083 | 651709 |
| | 8500 | 709792 | 660434 | 636767 | 771466 | 726227 | 706808 | 839762 | 800594 | 786220 |
| Model B2 | 4250 | 355112 | 314639 | 295231 | 405685 | 368588 | 352665 | 461687 | 429570 | 417783 |
| | 6375 | 466637 | 426164 | 406757 | 517210 | 480113 | 464190 | 573213 | 541095 | 529308 |
| | 8500 | 578162 | 537689 | 518282 | 628735 | 591639 | 575716 | 684738 | 652620 | 640833 |
| Model C1 | 4250 | 340944 | 301293 | 282280 | 390489 | 354146 | 338547 | 445353 | 413888 | 402341 |
| | 6375 | 447583 | 407932 | 388919 | 497128 | 460785 | 445186 | 551992 | 520527 | 508980 |
| | 8500 | 554222 | 514571 | 495559 | 603767 | 567425 | 551825 | 658631 | 627167 | 615619 |

### D.2.2 Levelized Cost of generation, LCOG

**Table D.2:** Calculated LCOG for 3 different, full load hours, economical life times and interest rates.

| LCOE | | Interest rate 6% Economical Life time years | | | Interest rate 12% Economical Life time | | | Interest rate 18% Economical Life time | | |
|---|---|---|---|---|---|---|---|---|---|---|
| | FLH [h/year] | 10 | 15 | 20 | 10 | 15 | 20 | 10 | 15 | 20 |
| | 4250 | 0.5866 | 0.4842 | 0.4351 | 0.7145 | 0.6207 | 0.5804 | 0.8562 | 0.7750 | 0.7451 |
| Model A1 | 6375 | 0.4381 | 0.3698 | 0.3371 | 0.5234 | 0.4608 | 0.4339 | 0.6178 | 0.5637 | 0.5438 |
| | 8500 | 0.3638 | 0.3126 | 0.2881 | 0.4278 | 0.3809 | 0.3607 | 0.4987 | 0.4580 | 0.4431 |
| | 4250 | 0.5955 | 0.4882 | 0.4368 | 0.7295 | 0.6312 | 0.5890 | 0.8779 | 0.7928 | 0.7615 |
| Model A2 | 6375 | 0.4400 | 0.3685 | 0.3342 | 0.5293 | 0.4638 | 0.4357 | 0.6282 | 0.5715 | 0.5507 |
| | 8500 | 0.3622 | 0.3086 | 0.2829 | 0.4292 | 0.3801 | 0.3590 | 0.5034 | 0.4609 | 0.4453 |
| | 4250 | 1.0822 | 0.9610 | 0.9029 | 1.2337 | 1.1226 | 1.0749 | 1.4014 | 1.3052 | 1.2699 |
| Model B1 | 6375 | 0.9417 | 0.8609 | 0.8221 | 1.0426 | 0.9686 | 0.9368 | 1.1544 | 1.0903 | 1.0668 |
| | 8500 | 0.8714 | 0.8108 | 0.7817 | 0.9471 | 0.8916 | 0.8677 | 1.0309 | 0.9829 | 0.9652 |
| | 4250 | 0.9801 | 0.8684 | 0.8149 | 1.1197 | 1.0173 | 0.9734 | 1.2743 | 1.1856 | 1.1531 |
| Model B2 | 6375 | 0.8586 | 0.7842 | 0.7484 | 0.9517 | 0.8834 | 0.8541 | 1.0547 | 0.9956 | 0.9739 |
| | 8500 | 0.7979 | 0.7420 | 0.7152 | 0.8677 | 0.8165 | 0.7945 | 0.9450 | 0.9006 | 0.8844 |
| | 4250 | 0.9672 | 0.8547 | 0.8008 | 1.1078 | 1.0047 | 0.9604 | 1.2634 | 1.1742 | 1.1414 |
| Model C1 | 6375 | 0.8465 | 0.7715 | 0.7356 | 0.9402 | 0.8715 | 0.8420 | 1.0440 | 0.9845 | 0.9626 |
| | 8500 | 0.7861 | 0.7299 | 0.7029 | 0.8564 | 0.8049 | 0.7827 | 0.9342 | 0.8896 | 0.8732 |

Appendix E

# EES Scripts

The developed EES scripst for the initial heat recovery heat pump calculations are attached below. The srcipt for the B1 configuration is not attached because it is identical as the A1 scrip besides the changed evaporation and condensation temperatures.

```
T_E[1]  = -15    [C]                    {Evaporation    Temp Propane Cycle}
T_C[1]  = 56     [C]                    {Condensation Temp Propane Cycle}

T_E[2]  = 53     [C]                    {Evaporation    Temp Butane Cycle}
T_C[2]  = 103    [C]                    {Condensation Temp Butane Cycle}

DT_Sh[1]  = 4  [C]                      {Amount of Superheat out of Propane Cycle Evaporator}
DT_Sh[2]  = 9  [C]                      {Amount of Superheat out of Butane   Cycle Evaporator}

DT_IHX[1]  = 11  [C]                    {Added superheat in Propane IHX}
DT_IHX[2]  = 11  [C]                    {Added superheat in Propane IHX}


T_Water_In[1]=65

P_E[1]=p_sat(R290,T=T_E[1])             {Evaporation Pressure of Propane Cycle}
P_E[2]=p_sat(R600,T=T_E[2])             {Evaporation Pressure of Butane Cycle}

P_C[1]=p_sat(R290,T=T_C[1])             {Condensation Pressure of Propane Cycle}
P_C[2]=p_sat(R600,T=T_C[2])             {Condensation Pressure of Butane Cycle}

Pi[1]=P_C[1]/P_E[1]                     {Pressure ratio Propane Cycle}
Pi[2]=P_C[2]/P_E[2]                     {Pressure ratio Butane Cycle}


{!First Cycle (Propane R290)}

my[1]=0.8                               {Volumetric Efficiency Propane Compressor}
eta_is[1]=0.7                           {Isntropic Efficiency Propane Compressor}

{!Saturated gas}
Q_E[1]  = 60 [kW]                       {Evaporator Capacity Propane Cycle}

T_1[1] = T_E[1]                         {Set Evaporation Temperature Propane Cycle}
P_1[1] = p_sat(R290,T=T_E[1])           {Evaporation Pressure Propane Cycle}
h_1[1] = enthalpy(R290, P=P_1[1],x=1)   {Enthalpy of Saturated Propane gas at set Evaporation Temperature
and Pressure}
s_1[1] = entropy(R290, P=P_1[1],x=1)    {Entropy of Saturated Propane gas at set Evaporation Temperture
and Pressure}

{!Out of Evaporator}
T_2[1] = T_1[1]+DT_Sh[1]                {Temperature of Gas out of Propane Cycle Evaporator}
P_2[1] = P_1[1]                         {Evaporation pressure Propane Cycle}
h_2[1] = enthalpy(R290, P=P_2[1],T=T_2[1])  {Enthalpy of Propane Gas out of Evaporator}
s_2[1] = entropy(R290, P=P_2[1],T=T_2[1])   {Entropy  of Propane Gas out of Evaporator}

{!Suction Gas}
T_2b[1] = T_2[1]+DT_IHX[1]              {Suction Gas Temperature at Propane Compressor inlet}
P_2b[1] = P_2[1]                        {Suction pressure of Propane Compressor}
h_2b[1] = enthalpy(R290, P=P_2b[1],T=T_2b[1])  {Enthalpy of Proapane Suction gas}
s_2b[1] = entropy(R290, P=P_2b[1],T=T_2b[1])   {Entropy  of  Proapane Suction gas}

D_Enthalpy_IXH[1] = h_2b[1]-h_2[1]      {Enthalpy increase in Propane IHX}

{!Discharge Gas}
P_3[1] = p_sat(R290,T=T_C[1])           {Condensation Pressure of Propane Condenser at set T_C}
h_3is[1] = enthalpy(R290, P=P_3[1],s=s_2b[1])  {Enthalpy of Propane Discharge Gas assuming isentropic
compression}
h_3[1] = h_2b[1]+(h_3is[1]-h_2b[1])/eta_is[1]  {Enthalpy of Propane Discharge Gas, assuming a fixed isentropic
efficiency}
s_3[1] = entropy(R290, P=P_3[1],h=h_3[1])      {Entropy  of Propane Discharge Gas}
T_3[1] = temperature(R290, P=P_3[1], h=h_3[1])  {Temperature of Propane Discharge Gas}
```

```
{!Saturated Gas}
P_4[1] = P_3[1]                                  {Condensation Pressure of Propane Condenser at T_C}
T_4[1] = temperature(R290, P=P_4[1],x=1)         {Condensation Temperature of Propane Cycle}
h_4[1] = enthalpy(R290,P=P_4[1], x=1)            {Enthalpy of saturated Propane Gas at set Condensation
Temperature}
s_4[1] = entropy(R290, P=P_4[1],h=h_4[1])        {Enthalpy of saturated Propane Gas at set Condensation
Temperature}

{!Saturated Liquid}
P_5[1] = P_3[1]                                  {Condensation Pressure of Propane Condenser at T_C}
T_5[1] = temperature(R290, P=P_5[1],x=0)         {Condensation Temperature of Propane Cycle}
h_5[1] = enthalpy(R290,P=P_5[1], x=0)            {Enthalpy of saturated Propane Liquid at set Condensation
Temperature}
s_5[1] = entropy(R290, P=P_5[1],h=h_5[1])        {Entropy  of saturated Propane Liquid at set Condensation
Temperature}

{!Subcooled Liquid}
P_6[1] = P_3[1]                                  {Condensation pressure of Propane Condenser at T_C}
h_6[1] =h_5[1] - D_Enthalpy_IXH[1]               {Removed heat from hot gas in Propane IHX}
T_6[1] = temperature(R290, P=P_6[1],h=h_6[1])    {Temperature of subcooled Propane Liquid after IHX}
s_6[1] = entropy(R290, P=P_6[1],h=h_6[1])        {Entropy of subcooled Propane Liquid after IHX}
 DT_SC[1]=T_6[1]-T_5[1]                         {Temperature decrease in subcooling IHX}

{!Out of expansion valve}
P_7[1] = P_1[1]                                  {Evaporation pressure of Propane Evaporatior at set T_E}
h_7[1] = h_6[1]                                  {Enthalpy after expansion valve assuming insenthalpic expansion}
s_7[1] = entropy(R290, P=P_7[1],h=h_7[1])        {Entropy  after expansion valve assuming insenthalpic expansion}
T_7[1] = temperature(R290,P=P_7[1], h=h_7[1])    {Temperature of Propane after Expansion Valve}

h_Vec_1[1]=h_1[1];  h_Vec_1[2]=h_2[1];  h_Vec_1[3]=h_2b[1];  h_Vec_1[4]=h_3[1];  h_Vec_1[5]=h_4[1];  h_Vec_1[6]=
h_5[1];  h_Vec_1[7]=h_6[1];  h_Vec_1[8]=h_7[1];  h_Vec_1[9]=h_1[1];
p_Vec_1[1]=P_1[1];  p_Vec_1[2]=P_2[1];  p_Vec_1[3]=P_2b[1];  p_Vec_1[4]=P_3[1];  p_Vec_1[5]=P_4[1];  p_Vec_1[6]=
P_5[1];  p_Vec_1[7]=P_6[1];  p_Vec_1[8]=P_7[1];  p_Vec_1[9]=P_1[1];
T_Vec_1[1]=T_1[1];  T_Vec_1[2]=T_2[1];  T_Vec_1[3]=T_2b[1];  T_Vec_1[4]=T_3[1];  T_Vec_1[5]=T_4[1];
T_Vec_1[6]=T_5[1];  T_Vec_1[7]=T_6[1];  T_Vec_1[8]=T_7[1];  T_Vec_1[9]=T_1[1];
s_Vec_1[1]=s_1[1];  s_Vec_1[2]=s_2[1];  s_Vec_1[3]=s_2b[1];  s_Vec_1[4]=s_3[1];  s_Vec_1[5]=s_4[1];  s_Vec_1[6]=
s_5[1];  s_Vec_1[7]=s_6[1];  s_Vec_1[8]=s_7[1];  s_Vec_1[9]=s_1[1];

{!Calculations for first cycle}
m_flow[1]  = Q_E[1]/(h_2[1]-h_7[1])                                                {Needed Mass
flow of Propane to achieve desired Evaporation Capacity}
W_C[1]     = m_flow[1]*(h_3[1]-h_2b[1])                                            {Compressor
Work Propane Cycle}
V_s[1]     = ((m_flow[1]*volume(R290,T=T_2b[1],P=P_2[1]))/my[1])*3600 [m3/h]       {Volume flow of
propane Compressor [m^3/h]}
Q_C[1]     = Q_E[1]+W_C[1]                                                         {Condensator
heat transfer of Propane Cycle}
Q_E[2]     = Q_C[1]                                                                {Butane
Evaporator Capacity assuming zero heat loss in Cascade Heat Exchanger}
P_Ratio[1]=P_3[1]/P_1[1]                                                           {Propane Cycle
Pressure Ratio}

{%%%%  %%%%  %%%%  %%%%  Start of Butane Cycle calculations  %%%%  %%%%  %%%%  %%%%}

{!Second Cycle Calculations (Butane R600)}

eta_is[2]  = 0.66                                {Isentropic  Efficiency of Butane Compressor}
```

```
my[2]  = 0.84                                   {Volumetric Efficiency of Butane Compressor}

{!Saturated Gas}

T_1[2] = T_E[2]                                 {Evaporation Temperature of Butane Cycle}
P_1[2] = p_sat(R600,T=T_E[2])                   {Evaporation Pressure of Butane Cycle}
h_1[2] = enthalpy(R600, P=P_1[2],x=1)           {Enthalpy of saturated Butane Gas at set T_E}
s_1[2] = entropy(R600, P=P_1[2],x=1)            {Entropy  of saturated Butane Gas at set T_E}


{!Out of Evaporator}
T_2[2] = T_1[2]+DT_Sh[2]                        {Temperature of Butane Gas out of Evaporator}
P_2[2] = P_1[2]                                 {Evaporation Pressure of Butane Cycle}
h_2[2] = enthalpy(R600, P=P_2[2],T=T_2[2])      {Enthalpy of Butane Gas out of Evaporator}
s_2[2] = entropy(R600, P=P_2[2],T=T_2[2])       {Entropy  of Butane Gas out of Evaporator}

{!Suction Gas}
T_2b[2] = T_2[2]+DT_IHX[2]                      {Temperature of suction gas into Butane Compressor}
P_2b[2] = P_2[2]                                {Evaporation Pressure of Butane Cycle}
h_2b[2] = enthalpy(R600, P=P_2b[2],T=T_2b[2])   {Enthalpy of Butane Suction Gas into Compressor}
s_2b[2] = entropy(R600, P=P_2b[2],T=T_2b[2])    {Entropy of Butane Suction Gas into Compressor}


D_Enthalpy_IXH[2] = h_2b[2]-h_2[2]              {Enthalpy increase of suction gas in Butane IHX}


{!Discharge Gas}
P_3[2] = p_sat(R600,T=T_C[2])                   {Condensation Butane of Butane Cycle}
h_3is[2] = enthalpy(R600, P=P_3[2],s=s_2b[2])   {Enthalpy of Butane Discharge Gas assuming isentropic
compression}
h_3[2] = h_2b[2]+(h_3is[2]-h_2b[2])/eta_is[2]   {Enthalpy of Butane Discharge Gas}
s_3[2] = entropy(R600, P=P_3[2],h=h_3[2])       {Entropy  of Butane Discharge Gas}
T_3[2] = temperature(R600, P=P_3[2], h=h_3[2])  {Temperature of Butane Discharge Gas}


{!Saturated Gas}
P_4[2] = P_3[2]                                 {Condensation pressure of Butane Condenser at set T_C}
T_4[2] = temperature(R600, P=P_4[2],x=1)        {Condensation Temperature of Butane Cycle}
h_4[2] = enthalpy(R600,P=P_4[2], x=1)           {Enthalpy of saturated Butane Gas at set Condensation
Temperature}
s_4[2] = entropy(R600, P=P_4[2],h=h_4[2])       {Entropy  of saturated Butane Gas at set Condensation Temperature}

{!Saturated Liquid}
P_5[2] = P_3[2]                                 {Condensation Pressure of Butane Condenser at set T_C}
T_5[2] = temperature(R600, P=P_5[2],x=0)        {Condensation Temperature of Butane Cycle}
h_5[2] = enthalpy(R600,P=P_5[2], x=0)           {Enthalpy of saturated Butane Liquid at set Condensation
Temperature}
s_5[2] = entropy(R600, P=P_5[2],h=h_5[2])       {Entropy of saturated Butane Liquid at set Condensation
Temperature}


{!Subcooled Liquid}
P_6[2] = P_3[2]                                 {Condensation Pressure of Butane Condenser at set T_C}
h_6[2] = h_5[2] - D_Enthalpy_IXH[2]             {Removed heat from hot gas in propane IHX when assuming 100%
IHX efficiency}
T_6[2] = temperature(R600, P=P_6[2],h=h_6[2])   {Temperature of subcooled Butane Liquid}
{T_6[2]=T_Water_In[1]+3}
{h_6[2]=enthalpy(R600,P=P_6[2], T=T_6[2])}
s_6[2] = entropy(R600, P=P_6[2],h=h_6[2])       {Entropy  of subcooled Butane Liquid}
 DT_SC[2]=T_6[2]-T_5[2]                         {Temperature decrease in subcooling IHX}

{!Out of expansion valve}
```

```
P_7[2] = P_1[2]                                  {Evaporation Pressure of Butane Condenser at set T_C}
h_7[2] = h_6[2]                                  {Enthalpy of Buatane out of Expansion valve}
s_7[2] = entropy(R600, P=P_7[2],h=h_7[2])        {Entropy  of Butane out of Expansion valve}
T_7[2] = temperature(R600,P=P_7[2], h=h_7[2])    {Evaporation Temperature of Butane Cycle}


h_Vec_2[1]=h_1[2];  h_Vec_2[2]=h_2[2];  h_Vec_2[3]=h_2b[2];  h_Vec_2[4]=h_3[2];  h_Vec_2[5]=h_4[2];  h_Vec_2[6]=
h_5[2];  h_Vec_2[7]=h_6[2];  h_Vec_2[8]=h_7[2];  h_Vec_2[9]=h_1[2];
p_Vec_2[1]=P_1[2];  p_Vec_2[2]=P_2[2];  p_Vec_2[3]=P_2b[2];  p_Vec_2[4]=P_3[2];  p_Vec_2[5]=P_4[2];  p_Vec_2[6]=
P_5[2];  p_Vec_2[7]=P_6[2];  p_Vec_2[8]=P_7[2];  p_Vec_2[9]=P_1[2];
T_Vec_2[1]=T_1[2];  T_Vec_2[2]=T_2[2];  T_Vec_2[3]=T_2b[2];  T_Vec_2[4]=T_3[2];  T_Vec_2[5]=T_4[2];
T_Vec_2[6]=T_5[2];  T_Vec_2[7]=T_6[2];  T_Vec_2[8]=T_7[2];  T_Vec_2[9]=T_1[2];
s_Vec_2[1]=s_1[2];  s_Vec_2[2]=s_2[2];  s_Vec_2[3]=s_2b[2];  s_Vec_2[4]=s_3[2];  s_Vec_2[5]=s_4[2];  s_Vec_2[6]=
s_5[2];  s_Vec_2[7]=s_6[2];  s_Vec_2[8]=s_7[2];  s_Vec_2[9]=s_1[2];


{!Calculations for 2nd cycle}
m_flow[2] = Q_E[2]/(h_2[2]-h_7[2])                                                {Needed Mass
flow of Butane to achieve desired Evaporation Capacity}
W_C[2]   = m_flow[2]*(h_3[2]-h_2b[2])                                             {Compressor
Work Butane Cycle}
V_s[2]   = ((m_flow[2]*volume(R600,T=T_2b[2],P=P_2[2]))/my[2])*3600 [m3/h]        {Volume flow of
Butane Compressor [m^3/h]}
Q_C[2]   = Q_E[2]+W_C[2]                                                          {Condensator
heat transfer of Butane Cycle}

P_Ratio[2]=P_3[2]/P_1[2]                         {Butane Cycle Pressure Ratio}

COP[1]=Q_C[1]/W_C[1]                             {Heating COP LTC}
COP[2]=Q_C[2]/W_C[2]                             {Heating COP MTC}

COP_Total[1]=Q_C[2]/(W_C[1]+W_C[2])              {Total Heating COP}
```

```
T_E[1]  = -15    [C]          {Evaporation    Temp Propane Cycle}
T_C[1]  = 33     [C]          {Condensation Temp Propane Cycle}

T_E[2]  = 30     [C]          {Evaporation    Temp Butane Cycle}
T_C[2]  = 73    [C]           {Condensation Temp Butane Cycle}


T_City_Water=4 [C]           {Inlet Water Temperature}
T_Set_DHW=70 [C]             {Outlet Water Temperature}

T_Water_In[1]=T_City_Water   {Heat Sink Inlet Water temperature}
T_Water_Out[1]=T_E[2]        {Heat Sink Water temperature out of water pre-heater}

T_Water_In[2]=T_Water_Out[1] {Heat Sink Water temperature in to Burane Condenser}
T_Water_Out[2]=T_Set_DHW     {Heat Sink Outlet Water Temperature}

DT_HX[1] =  3 [C]            {Assumed Temperature Difference in heat exchanger}
DT_Sh[1]  = 4  [C]           {Amount of Superheat out of Propane Cycle Evaporator}
DT_Sh[2]  = 20  [C]          {Amount of Superheat out of Butane   Cycle Evaporator}

DT_IHX[1]  = 11  [C]         {Added superheat in Propane IHX}
DT_IHX[2]  = 0  [C]          {Added superheat in Propane IHX}

DT_SC[2]=39                  {Subcooling of Butane Cycle}

P_E[1]=p_sat(R290,T=T_E[1])  {Evaporation pressure Propane Cycle}
P_E[2]=p_sat(R600,T=T_E[2])  {Evaporation pressure Butane Cycle}

P_C[1]=p_sat(R290,T=T_C[1])  {Condensation pressure Propane Cycle}
P_C[2]=p_sat(R600,T=T_C[2])  {Condensation pressure Propane Cycle}

Pi[1]=P_C[1]/P_E[1]          {Pressure ratio Propane Cycle}
Pi[2]=P_C[2]/P_E[2]          {Pressure ratio Butane Cycle}


{!First Cycle (Propane R290)}

my[1]  = 0.8                 {Volumetric Efficiency Propane Compressor}
eta_is[1]=0.7                {Isentropic Efficiency Propane Compressor}

{!Saturated gas}
Q_E[1]  = 60 [kW]            {Evaporator Capacity Propane Cycle from Measurements}

T_1[1] = T_E[1]              {Set Evaporation Temperature Propane Cycle}
P_1[1] = p_sat(R290,T=T_E[1])  {Evaporation Pressure Propane Cycle}
h_1[1] = enthalpy(R290, P=P_1[1],x=1)  {Enthalpy of Saturated Propane gas at set Evaporation Temperature
and Pressure}
s_1[1] = entropy(R290, P=P_1[1],x=1)  {Entropy of Saturated Propane gas at set Evaporation Temperture
and Pressure}

{!Out of Evaporator}
T_2[1] = T_1[1]+DT_Sh[1]     {Temperature of Gas out of Propane Cycle Evaporator}
P_2[1] = P_1[1]              {Evaporation pressure Propane Cycle}
h_2[1] = enthalpy(R290, P=P_2[1],T=T_2[1])  {Enthalpy of Propane Gas out of Evaporator}
s_2[1] = entropy(R290, P=P_2[1],T=T_2[1])  {Entropy  of Propane Gas out of Evaporator}

{!Suction Gas}
T_2b[1] = T_2[1]+DT_IHX[1]   {Suction Gas Temperature at Propane Compressor inlet}
P_2b[1] = P_2[1]             {Suction pressure of Propane Compressor}
h_2b[1] = enthalpy(R290, P=P_2b[1],T=T_2b[1])  {Enthalpy of Proapane Suction gas}
s_2b[1] = entropy(R290, P=P_2b[1],T=T_2b[1])  {Entropy  of  Proapane Suction gas}

D_Enthalpy_IXH[1] = h_2b[1]-h_2[1]  {Enthalpy increase in Propane IHX}
```

```
{!Discharge Gas}
P_3[1] = p_sat(R290,T=T_C[1])                    {Condensation Pressure of Propane Condenser at set T_C}
h_3is[1] = enthalpy(R290, P=P_3[1],s=s_2b[1])    {Enthalpy of Propane Discharge Gas assuming isentropic
compression}
h_3[1] = h_2b[1]+(h_3is[1]-h_2b[1])/eta_is[1]    {Enthalpy of Propane Discharge Gas, assuming an fixed isentropic
efficiency}
s_3[1] = entropy(R290, P=P_3[1],h=h_3[1])        {Entropy  of Propane Discharge Gas}
T_3[1] = temperature(R290, P=P_3[1], h=h_3[1])   {Temperature of Propane Discharge Gas}

{!Saturated Gas}
P_4[1] = P_3[1]                                  {Condensation Pressure of Propane Condenser at T_C}
T_4[1] = temperature(R290, P=P_4[1],x=1)         {Condensation Temperature of Propane Cycle}
h_4[1] = enthalpy(R290,P=P_4[1], x=1)            {Enthalpy of saturated Propane Gas at set Condensation
Temperature}
s_4[1] = entropy(R290, P=P_4[1],h=h_4[1])        {Enthalpy of saturated Propane Gas at set Condensation
Temperature}

{!Saturated Liquid}
P_6[1] = P_3[1]                                  {Condensation Pressure of Propane Condenser at T_C}
T_6[1] = temperature(R290, P=P_6[1],x=0)         {Condensation Temperature of Propane Cycle}
h_6[1] = enthalpy(R290,P=P_6[1], x=0)            {Enthalpy of saturated Propane Liquid at set Condensation
Temperature}
s_6[1] = entropy(R290, P=P_6[1],h=h_6[1])        {Entropy  of saturated Propane Liquid at set Condensation
Temperature}

{! Out of DHW Pre-Heater}
P_7[1]=P_3[1]                                    {Condensation pressure of Propane}
T_7[1]=T_Water_In[1]+DT_HX[1]                    {Assumed Propane Temperature out of Water pre-heater}
h_7[1]=enthalpy(R290,P=P_7[1], T=T_7[1])         {Enthalpy of propane out of water pre heater}
s_7[1] = entropy(R290, P=P_7[1],h=h_7[1])        {Entropy of propane out of water pre heater}

{!Subcooled Liquid}
P_8[1] = P_3[1]                                  {Condensation pressure of Propane Condenser at T_C}
h_8[1] =h_7[1] - D_Enthalpy_IXH[1]               {Removed heat from hot gas in Propane IHX}
T_8[1] = temperature(R290, P=P_8[1],h=h_8[1])    {Temperature of subcooled Propane Liquid after IHX}
s_8[1] = entropy(R290, P=P_8[1],h=h_8[1])        {Entropy of subcooled Propane Liquid after IHX}
DT_SC[1]=T_8[1]-T_6[1]                           {Temperature decrease in subcooling IHX}

{!Out of expansion valve}
P_9[1] = P_1[1]                                  {Evaporation pressure of Propane Evaporatior at set T_E}
h_9[1] = h_8[1]                                  {Enthalpy after expansion valve assuming insenthalpic expansion}
s_9[1] = entropy(R290, P=P_9[1],h=h_9[1])        {Entropy  after expansion valve assuming insenthalpic expansion}
T_9[1] = temperature(R290,P=P_9[1], h=h_9[1])    {Temperature of Propane after Expansion Valve}


m_flow[1]  = Q_E[1]/(h_2[1]-h_9[1])                                                {Needed Mass
flow of Propane to achieve desired Evaporation Capacity}
W_C[1]     = m_flow[1]*(h_3[1]-h_2b[1])                                            {Compressor
Work Propane Cycle}
V_s[1]     = ((m_flow[1]*volume(R290,T=T_2b[1],P=P_2[1]))/my[1])*3600 [m3/h]       {Volume flow of
propane Compressor [m^3/h]}
Q_C[1]     = Q_E[1]+W_C[1]                                                         {Condensator
heat transfer of Propane Cycle}

Q_C_Guess[1]=1.1*Q_C[1]                                                            {Guessed
condensation power of Water pre heater plus Butane Cycle condenser, assumed 1.1 times-}                {-
heat emitted from Propane Cycle}
P_Atm[1]=1.013 [Bar]                                                               {Water
pressure assumed atmospheric pressure}

cp[1]=cp(Water,T=(T_Water_In[1]+T_Water_Out[2])/2,P=P_Atm[1])                      {Average
Spesific heating capazity of water heated from 4 to 70 deg C.}
m_Flow_Water[1]=Q_C_Guess[1]/(cp[1]*(T_Water_Out[2]-T_Water_In[1]))                {Estimated
Mass flow of water heated}
```

```
Q_DHW_HX[1]=m_Flow_Water[1]*cp[1]*(T_Water_Out[1]-T_Water_In[1])        {Needed heat transfer in water pre heater}
Q_DHW_HX[2]=m_Flow_Water[1]*cp[1]*(T_Water_Out[2]-T_Water_In[2])        {Needed heat transfer in Butane Condenser}

{! Out of Cascade HX}
P_5[1]=P_3[1]                                                          {Condensation Pressure of Propane}
h_5[1]=(m_flow[1]*h_7[1]+Q_DHW_HX[1])/m_flow[1]                        {Propane enthalpy out of cascade HX}
T_5[1]=temperature(R290,P=P_5[1],h=h_5[1])                             {Propane temperature out of cascade HX}
s_5[1]=entropy(R290,P=P_5[1],h=h_5[1])                                 {Propane entropy out of cascade HX}


h_Vec_1[1]=h_1[1];  h_Vec_1[2]=h_2[1];  h_Vec_1[3]=h_2b[1];  h_Vec_1[4]=h_3[1];  h_Vec_1[5]=h_4[1];  h_Vec_1[6]=
h_5[1];  h_Vec_1[7]=h_6[1];  h_Vec_1[8]=h_7[1];  h_Vec_1[9]=h_8[1];  h_Vec_1[10]=h_9[1]; h_Vec_1[11]=h_1[1];
p_Vec_1[1]=P_1[1];  p_Vec_1[2]=P_2[1];  p_Vec_1[3]=P_2b[1];  p_Vec_1[4]=P_3[1];  p_Vec_1[5]=P_4[1];  p_Vec_1[6]=
P_5[1];  p_Vec_1[7]=P_6[1];  p_Vec_1[8]=P_7[1];  p_Vec_1[9]=P_8[1];  p_Vec_1[10]=P_9[1]; p_Vec_1[11]=P_1[1];
T_Vec_1[1]=T_1[1];  T_Vec_1[2]=T_2[1];  T_Vec_1[3]=T_2b[1];  T_Vec_1[4]=T_3[1];  T_Vec_1[5]=T_4[1];  T_Vec_1[6]=
T_5[1];  T_Vec_1[7]=T_6[1];  T_Vec_1[8]=T_7[1];  T_Vec_1[9]=T_8[1];  T_Vec_1[10]=T_9[1]; T_Vec_1[11]=T_1[1];
s_Vec_1[1]=s_1[1];  s_Vec_1[2]=s_2[1];  s_Vec_1[3]=s_2b[1];  s_Vec_1[4]=s_3[1];  s_Vec_1[5]=s_4[1];  s_Vec_1[6]=
s_5[1];  s_Vec_1[7]=s_6[1];  s_Vec_1[8]=s_7[1];  s_Vec_1[9]=s_8[1];  s_Vec_1[10]=s_9[1]; s_Vec_1[11]=s_1[1];


{!Calculations for first cycle}
Q_E[2]  = m_flow[1]*(h_3[1]-h_5[1])                                    {Butane Evaporator Capacity assuming zero heat loss in Cascade Heat Exchanger}
P_Ratio[1]=P_3[1]/P_1[1]                                               {Propane Cycle Pressure Ratio}


{%%%%  %%%%  %%%%  %%%%  Start of Butane Cycle calculations  %%%%  %%%%  %%%%  %%%%%}


{!Second Cycle Calculations (Butane R600)}

eta_is[2]  = 0.7                                                       {Isentropic  Efficiency of Butane Compressor from Literature}
my[2]  = 0.8                                                           {Volumetric Efficiency of Butane Compressor from Literature}

{!Saturated Gas}

T_1[2] = T_E[2]                                                        {Evaporation Temperature of Butane Cycle}
P_1[2] = p_sat(R600,T=T_E[2])                                          {Evaporation Pressure of Butane Cycle}
h_1[2] = enthalpy(R600, P=P_1[2],x=1)                                  {Enthalpy of saturated Butane Gas at set T_E}
s_1[2] = entropy(R600, P=P_1[2],x=1)                                   {Entropy  of saturated Butane Gas at set T_E}


{!Out of Evaporator}
T_2[2] = T_1[2]+DT_Sh[2]                                               {Temperature of Butane Gas out of Evaporator}
P_2[2] = P_1[2]                                                        {Evaporation Pressure of Butane Cycle}
h_2[2] = enthalpy(R600, P=P_2[2],T=T_2[2])                             {Enthalpy of Butane Gas out of Evaporator}
s_2[2] = entropy(R600, P=P_2[2],T=T_2[2])                              {Entropy  of Butane Gas out of Evaporator}

{!Suction Gas}
T_2b[2] = T_2[2]+DT_IHX[2]                                             {Temperature of suction gas into Butane Compressor}
P_2b[2] = P_2[2]                                                       {Evaporation Pressure of Butane Cycle}
h_2b[2] = enthalpy(R600, P=P_2b[2],T=T_2b[2])                          {Enthalpy of Butane Suction Gas into Compressor}
```

```
s_2b[2] = entropy(R600, P=P_2b[2],T=T_2b[2])        {Entropy of Butane Suction Gas into Compressor}

D_Enthalpy_IXH[2] = h_2b[2]-h_2[2]                  {Enthalpy increase of suction gas in Butane IHX}

{!Discharge Gas}
P_3[2] = p_sat(R600,T=T_C[2])                       {Condensation Butane of Butane Cycle}
h_3is[2] = enthalpy(R600, P=P_3[2],s=s_2b[2])       {Enthalpy of Butane Discharge Gas assuming isentropic
compression}
h_3[2] = h_2b[2]+(h_3is[2]-h_2b[2])/eta_is[2]       {Enthalpy of Butane Discharge Gas}
s_3[2] = entropy(R600, P=P_3[2],h=h_3[2])           {Entropy  of Butane Discharge Gas}
T_3[2] = temperature(R600, P=P_3[2], h=h_3[2])      {Temperature of Butane Discharge Gas}

{!Saturated Gas}
P_4[2] = P_3[2]                                     {Condensation pressure of Butane Condenser at set T_C}
T_4[2] = temperature(R600, P=P_4[2],x=1)            {Condensation Temperature of Butane Cycle}
h_4[2] = enthalpy(R600,P=P_4[2], x=1)               {Enthalpy of saturated Butane Gas at set Condensation
Temperature}
s_4[2] = entropy(R600, P=P_4[2],h=h_4[2])           {Entropy  of saturated Butane Gas at set Condensation Temperature}

{!Saturated Liquid}
P_5[2] = P_3[2]                                     {Condensation Pressure of Butane Condenser at set T_C}
T_5[2] = temperature(R600, P=P_5[2],x=0)            {Condensation Temperature of Butane Cycle}
h_5[2] = enthalpy(R600,P=P_5[2], x=0)               {Enthalpy of saturated Butane Liquid at set Condensation
Temperature}
s_5[2] = entropy(R600, P=P_5[2],h=h_5[2])           {Entropy of saturated Butane Liquid at set Condensation
Temperature}


{!Subcooled Liquid}
P_6[2] = P_3[2]                                     {Condensation Pressure of Butane Condenser at set T_C}

T_6[2] = T_5[2]-DT_SC[2]                            {Temperature of subcooled Butane Liquid}
h_6[2]=enthalpy(R600,P=P_6[2], T=T_6[2])
s_6[2] = entropy(R600, P=P_6[2],h=h_6[2])           {Entropy  of subcooled Butane Liquid}

{!Out of expansion valve}
P_7[2] = P_1[2]                                     {Evaporation Pressure of Butane Condenser at set T_C}
h_7[2] = h_6[2]                                     {Enthalpy of Buatane out of Expansion valve}
s_7[2] = entropy(R600, P=P_7[2],h=h_7[2])           {Entropy  of Butane out of Expansion valve}
T_7[2] = temperature(R600,P=P_7[2], h=h_7[2])       {Evaporation Temperature of Butane Cycle}

h_Vec_2[1]=h_1[2];  h_Vec_2[2]=h_2[2];  h_Vec_2[3]=h_2b[2];  h_Vec_2[4]=h_3[2];  h_Vec_2[5]=h_4[2];  h_Vec_2[6]=
h_5[2];  h_Vec_2[7]=h_6[2];  h_Vec_2[8]=h_7[2];  h_Vec_2[9]=h_1[2];
p_Vec_2[1]=P_1[2];  p_Vec_2[2]=P_2[2];  p_Vec_2[3]=P_2b[2];  p_Vec_2[4]=P_3[2];  p_Vec_2[5]=P_4[2];  p_Vec_2[6]=
P_5[2];  p_Vec_2[7]=P_6[2];  p_Vec_2[8]=P_7[2];  p_Vec_2[9]=P_1[2];
T_Vec_2[1]=T_1[2];  T_Vec_2[2]=T_2[2];  T_Vec_2[3]=T_2b[2];  T_Vec_2[4]=T_3[2];  T_Vec_2[5]=T_4[2];
T_Vec_2[6]=T_5[2];  T_Vec_2[7]=T_6[2];  T_Vec_2[8]=T_7[2];  T_Vec_2[9]=T_1[2];
s_Vec_2[1]=s_1[2];  s_Vec_2[2]=s_2[2];  s_Vec_2[3]=s_2b[2];  s_Vec_2[4]=s_3[2];  s_Vec_2[5]=s_4[2];  s_Vec_2[6]=
s_5[2];  s_Vec_2[7]=s_6[2];  s_Vec_2[8]=s_7[2];  s_Vec_2[9]=s_1[2];

{!Calculations for 2nd cycle}
m_flow[2] = Q_E[2]/(h_2[2]-h_7[2])                                  {Needed Mass
flow of Butane to achieve desired Evaporation Capacity}
W_C[2]  = m_flow[2]*(h_3[2]-h_2b[2])                                {Compressor
Work Butane Cycle}
V_s[2]  = ((m_flow[2]*volume(R600,T=T_2b[2],P=P_2[2]))/my[2])*3600 [m3/h]   {Volume flow of
Butane Compressor [m^3/h]}
Q_C[2]  = Q_E[2]+W_C[2]                                             {Condensator
```

heat transfer of Butane Cycle}

P_Ratio[2]=P_3[2]/P_1[2] {Butane Cycle Pressure Ratio}

COP[1]=Q_C[1]/W_C[1] {Heating COP LTC}
COP[2]=Q_C[2]/W_C[2] {Heating COP MTC}

COP_Total[1]=(Q_C[2]+(Q_C[1]-Q_E[2]))/(W_C[1]+W_C[2]) {Total Heating COP}

$Reference R744 IIR

```
T_E[1]  = -15    [C]                    {Evaporation    Temp CO2 Cycle}
P_C[1] = 95 [bar]                       {Condensing Pressure CO2}

T_Water_In[1] = 4 [C]                   {Inlet DHW Temperture}
T_Water_Out[1] = 70 [C]                 {Outlet DHW Temperature}

DT_HX[1] = 3 [C]
DT_Sh[1]  = 0.1  [C]                    {Amount of Superheat out of CO2 Evaporator was not possible to se
0.}
DT_IHX[1]  = 10  [C]                    {Added superheat in CO2 IHX}

{!First Cycle (CO2 R744)}

eta_is[1]  = 0.64                       {Istentropic Efficiency CO2 Compressor from Compressor
Manufacturer}
my[1]  = 0.74                           {Volumetric Efficiency Co2 Compressor from Compressor
Manufacturer}

{!Saturated gas}
Q_E[1]  = 60 [kW]                       {Evaporator Capacity CO2 Cycle from Measurements}

T_1[1] = T_E[1]                         {Set Evaporation Temperature CO2 Cycle}
P_1[1] = p_sat(R744,T=T_E[1])           {Evaporation Pressure CO2 Cycle}
h_1[1] = enthalpy(R744, P=P_1[1],x=1)   {Enthalpy of Saturated CO2 gas at set Evaporation Temperature and
Pressure}
s_1[1] = entropy(R744, P=P_1[1],x=1)    {Entropy of Saturated CO2 gas at set Evaporation Temperture and
Pressure}

{!Out of Evaporator}
T_2[1] = T_1[1]+DT_Sh[1]                {Temperature of Gas out of CO2 Cycle Evaporator}
P_2[1] = P_1[1]                         {Evaporation pressure CO2 Cycle}
h_2[1] = enthalpy(R744, P=P_2[1],T=T_2[1])  {Enthalpy of CO2 Gas out of Evaporator}
s_2[1] = entropy(R744, P=P_2[1],T=T_2[1])   {Entropy  of CO2 Gas out of Evaporator}

{!Suction Gas}
T_2b[1] = T_2[1]+DT_IHX[1]              {Suction Gas Temperature at CO2 Compressor inlet}
P_2b[1] = P_2[1]                        {Suction pressure of CO2 Compressor}
h_2b[1] = enthalpy(R744, P=P_2b[1],T=T_2b[1])  {Enthalpy of CO2 Suction gas}
s_2b[1] = entropy(R744, P=P_2b[1],T=T_2b[1])   {Entropy  of  CO2 Suction gas}

D_Enthalpy_IXH[1] = h_2b[1]-h_2[1]      {Enthalpy increase in CO2 IHX}

{!Discharge Gas}
P_3[1] = P_C[1]                         {Condensation Pressure of CO2 Condenser at set T_C}
h_3is[1] = enthalpy(R744, P=P_3[1],s=s_2b[1])  {Enthalpy of CO2 Discharge Gas assuming isentropic compression}
h_3[1] = h_2b[1]+(h_3is[1]-h_2b[1])/eta_is[1]  {Enthalpy of CO2 Discharge Gas, assuming an fixed isentropic
efficiency}
s_3[1] = entropy(R744, P=P_3[1],h=h_3[1])   {Entropy  of CO2 Discharge Gas}
T_3[1] = temperature(R744, P=P_3[1], h=h_3[1])  {Temperature of CO2 Discharge Gas}

{!Out of Condenser}
P_4[1] = P_3[1]                         {Condensation Pressure of CO2 Condenser at T_C}
T_4[1] = T_Water_In[1]+DT_HX[1]         {Condensation Temperature of CO2 Cycle}
{T_4[1] = 40}
h_4[1] = enthalpy(R744,P=P_4[1], T=T_4[1])  {Enthalpy of  CO2 Out of Condenser}
s_4[1] = entropy(R744, P=P_4[1],h=h_4[1])   {Entropy  of  CO2 out of Condenser}

{!Subcooled Liquid}
P_5[1] = P_3[1]                         {Condensation pressure of CO2 Condenser at T_C}
h_5[1] =h_4[1] - D_Enthalpy_IXH[1]      {Removed heat from hot gas in CO2 IHX}
T_5[1] = temperature(R744, P=P_5[1],h=h_5[1])  {Temperature of subcooled CO2 Liquid after IHX}
```

```
s_5[1] = entropy(R744, P=P_5[1],h=h_5[1])          {Entropy of subcooled CO2 Liquid after IHX}
 DT_SC[1]=T_5[1]-T_4[1]                            {Temperature decrease in subcooling IHX}

{!Out of expansion valve}
P_6[1] = P_1[1]                                    {Evaporation pressure of CO2 Evaporatior at set T_E}
h_6[1] = h_5[1]                                    {Enthalpy after expansion valve assuming insenthalpic expansion}
s_6[1] = entropy(R744, P=P_6[1],h=h_6[1])          {Entropy  after expansion valve assuming insenthalpic expansion}
T_6[1] = temperature(R744,P=P_6[1], h=h_6[1])      {Temperature of CO2 after Expansion Valve}

h_Vec_1[1]=h_1[1];  h_Vec_1[2]=h_2[1];  h_Vec_1[3]=h_2b[1];  h_Vec_1[4]=h_3[1];  h_Vec_1[5]=h_4[1];  h_Vec_1[6]=
h_5[1];  h_Vec_1[7]=h_6[1];  h_Vec_1[8]=h_1[1];
p_Vec_1[1]=P_1[1];  p_Vec_1[2]=P_2[1];  p_Vec_1[3]=P_2b[1];  p_Vec_1[4]=P_3[1];  p_Vec_1[5]=P_4[1];  p_Vec_1[6]=
P_5[1];  p_Vec_1[7]=P_6[1];  p_Vec_1[8]=P_1[1];
T_Vec_1[1]=T_1[1];  T_Vec_1[2]=T_2[1];  T_Vec_1[3]=T_2b[1];  T_Vec_1[4]=T_3[1];  T_Vec_1[5]=T_4[1];
T_Vec_1[6]=T_5[1];  T_Vec_1[7]=T_6[1];  T_Vec_1[8]=T_1[1];
s_Vec_1[1]=s_1[1];  s_Vec_1[2]=s_2[1];  s_Vec_1[3]=s_2b[1];  s_Vec_1[4]=s_3[1];  s_Vec_1[5]=s_4[1];  s_Vec_1[6]=
s_5[1];  s_Vec_1[7]=s_6[1];  s_Vec_1[8]=s_1[1];

{!Calculations for first cycle}
m_flow[1]  = Q_E[1]/(h_2[1]-h_6[1])                                                    {Needed Mass
flow of CO2 to achieve desired Evaporation Capacity}
W_C[1]     = m_flow[1]*(h_3[1]-h_2b[1])                                                {Compressor
Work CO2 Cycle}
V_s[1]     = ((m_flow[1]*volume(R744,T=T_2b[1],P=P_2[1]))/my[1])*3600 [m3/h]           {Volume flow of
CO2 Compressor [m^3/h]}
Q_C[1]     = Q_E[1]+W_C[1]                                                             {Condensator
heat transfer of CO2 Cycle}
P_Ratio[1]=P_3[1]/P_1[1]                                                               {Propane Cycle
Pressure Ratio}

{%%%%  %%%%  %%%%  %%%%  Start of Butane Cycle calculations  %%%%  %%%%  %%%%  %%%%%}
```

***Function*** **get_m_flow**(Compressor$,T_Evap,T_Cond) {Compressor polynomials calculating refrigerant mass flow}
***If*** Compressor$='HEX2500CC' ***Then*** C[1..10]=[0.189619, 0.006578541, -0.000265476, 8.97089E-05, -4.03522E-06, -2.94078E-06, 5.20551E-07, -4.6707E-08, -1.50127E-08, -1.69197E-09]
***If*** Compressor$='HEX3000CC' ***Then*** C[1..10]=[0.21983283, 0.007540326, -0.000623416, 0.000101274, -1.03422E-05, 8.36868E-07, 5.88038E-07, -4.7766E-08, 5.51753E-08, -6.87298E-09]
***If*** Compressor$='HEX3400CC' ***Then*** C[1..10]=[0.26330305, 0.009033515, -0.000744946, 0.000121327, -1.24768E-05, 9.11218E-07, 7.03961E-07, -5.93922E-08, 6.44097E-08, -7.37076E-09]
***If*** Compressor$='HEX3501CC' ***Then*** C[1..10]=[0.290623796, 0.009970847, -0.000822243, 0.000133917, -1.37714E-05, 1.00577E-06, 7.77006E-07, -6.55548E-08, 7.10929E-08, -8.13557E-09]
***If*** Compressor$='HEX3500CS' ***Then*** C[1..10]=[0.33035753, 0.011276312, -0.001201573, 0.000147041, -2.22568E-05, 7.50553E-06, 8.02957E-07, -9.30817E-08, 1.76099E-07, -2.83143E-08]
***If*** Compressor$='HEX4000CC' ***Then*** C[1..10]=[0.32523774,0.011173754,-0.000891115,0.000150241,-1.47825E-05, 1.3086E-06,8.74311E-07,-6.59074E-08,8.28134E-08,-1.30429E-09]
***If*** Compressor$='HEX4500CS' ***Then*** C[1..10]=[0.38719446, 0.013306434, -0.000870794, 0.000174444, -1.47322E-05, 4.8552E-07, 9.4235E-07, -9.04842E-08, 6.1055E-08, -1.53222E-08]
***If*** Compressor$='HEX5000CC' ***Then*** C[1..10]=[0.38359404, 0.013335073, -0.00055334, 0.000181387, -7.91486E-06, -6.22679E-06, 1.04838E-06, -8.09738E-08, -4.12656E-08, 1.27597E-08]
***If*** Compressor$='HEX5500CS' ***Then*** C[1..10]=[0.4634392,0.015834546,-0.00086284563,0.00020608003,-0.000014377313,-0.0000055474432,0.0000010969819,-0.00000012456188,-0.000000034728714,0.000000007494964]
***If*** Compressor$='HEX7501CS' ***Then*** C[1..10]=[0.57363991,0.019410714,-0.001757866, 0.000249396,-2.90778E-05, 1.81252E-06,1.32647E-06,-1.14467E-07,9.02694E-08,3.99124E-09]

m_flow= C[1] + C[2]*T_Evap + C[3]*T_Cond + C[4]*T_Evap^2 + C[5]*T_Evap*T_Cond + C[6]*T_Cond^2 + C[7]*T_Evap^3 + C[8]*T_Cond*T_Evap^2 + C[9]*T_Evap*T_Cond^2 + C[10]*T_Cond^3
**get_m_flow**=m_flow
***End***

***Function*** **get_p_shaft**(Compressor$,T_Evap,T_Cond) {Compressor polynomials calculating Compressor Shaft Power}
***If*** Compressor$='HEX2500CC' ***Then*** C[1..10]=[6363.56885, -87.66021016, 185.5711797, -3.232382834, 3.653068775, -0.092132446, -0.015266152, 0.007705966, 0.018099468, 0.003486694]
***If*** Compressor$='HEX3000CC' ***Then*** C[1..10]=[6881.055451, -175.9116905, 226.0293672, -6.107617545, 6.806090476, -0.256897156, -0.037708398, 0.053236185, 0.00512911, 0.002965109]
***If*** Compressor$='HEX3400CC' ***Then*** C[1..10]=[8935.011326,-134.2507474,233.3370201,-4.874422253,5.408268396, 0.028500636,-0.022920414,0.019340177,0.022229892,0.005573586]
***If*** Compressor$='HEX3501CC' ***Then*** C[1..10]=[9862.122418,-148.1808201,257.5484432,-5.380200116,5.969438991, 0.031457908,-0.025298673,0.021346944,0.024536501,0.00615191]
***If*** Compressor$='HEX3500CS' ***Then*** C[1..10]=[11544.75699,-132.8896188,372.4108528,-6.228287774,7.115828232,-3.204592388,-0.037462043,0.045457111,0.036794493,0.045135094]
***If*** Compressor$='HEX4000CC' ***Then*** C[1..10]=[13664.22386,-72.93581601,207.714722,-4.588626092,4.301188397, 0.785136775,-0.018818444,0.005345105,0.047950946,0.009018177]
***If*** Compressor$='HEX4500CS' ***Then*** C[1..10]=[17458.18343,60.88738474,214.2617314,-2.505809632,1.212874617, 1.868048013,-0.007102111,-0.044400283,0.076337364,0.000862036]
***If*** Compressor$='HEX5000CC' ***Then*** C[1..10]=[15446.43561,-111.0476636, 307.1884308, -5.852193338, 6.564573871, 0.579746723, -0.025225752, 0.01252942, 0.039755584, 0.003180807]
***If*** Compressor$='HEX5500CS' ***Then*** C[1..10]=[16825.16069,-126.6693808,482.1442766,-7.074356755,9.769403431,-0.889037249,-0.038765552,0.026710516,0.01574376,0.004362204]
***If*** Compressor$='HEX7501CS' ***Then*** C[1..10]=[22175.90041,-122.0053505,465.4705554,-8.165342312,9.629618573,-0.049495222,-0.042488389,0.027559875,0.046077272,0.012959132]

P_Shaft= C[1] + C[2]*T_Evap + C[3]*T_Cond + C[4]*T_Evap^2 + C[5]*T_Evap*T_Cond + C[6]*T_Cond^2 + C[7]*T_Evap^3 + C[8]*T_Cond*T_Evap^2 + C[9]*T_Evap*T_Cond^2 + C[10]*T_Cond^3
**get_p_shaft**=P_Shaft
***End***

***Function*** **get_v_displacement**(Compressor$) {Nominal Displacement of compressors at 50Hz}
***If*** Compressor$='HEX2500CC' ***Then*** V_D = 75.83 [m3/h]
***If*** Compressor$='HEX3000CC' ***Then*** V_D = 85.01 [m3/h]
***If*** Compressor$='HEX3400CC' ***Then*** V_D = 102.35 [m3/h]
***If*** Compressor$='HEX3501CC' ***Then*** V_D = 112.97 [m3/h]

```
    If Compressor$='HEX3500CS' Then V_D = 127.52 [m3/h]
    If Compressor$='HEX4000CC' Then V_D =  127.52 [m3/h]
    If Compressor$='HEX4500CS' Then V_D =  153.52 [m3/h]
    If Compressor$='HEX5000CC' Then V_D  =  153.52 [m3/h]
    If Compressor$='HEX5500CS' Then V_D =  184.19 [m3/h]
    If Compressor$='HEX7501CS' Then V_D = 221.75 [m3/h]

    V_Disp=V_D/(50*3600) [m3]                    {Displacement in Dymola Model}
    get_v_displacement=V_Disp
End

Function plot_vol_eff(WF$,Compressor$,T_E, T_C)   {Calculating Compressor Volumetric Efficiency}
    n=50                                          {Nominal compressor speed [Hz]}

    T_Suction=T_E+15 [C]                          {Assuming 15K Suction Superheat}

    P_Shaft=get_p_shaft(Compressor$,T_E,T_C)
    m_flow=get_m_flow(Compressor$,T_E,T_C)
    V_Disp=get_v_displacement(Compressor$)

    P_E=p_sat(WF$,T=T_E)
    P_C=p_sat(WF$,T=T_C)

    rho=density(WF$,T=T_Suction, P=P_E)

    Vol_Eff=m_flow/(V_Disp*n*rho)
    plot_vol_eff=Vol_Eff

End

Function plot_is_eff_hl(WF$,Compressor$,T_E, T_C, Heat_Loss_Factor) {Calculating Compressor Isentropic Efficiency}

    n=50                                          {Nominal compressor speed [Hz]}
    T_Suction=T_E+15 [C]                          {Assuming 15K Suction Superheat}


    P_Shaft=get_p_shaft(Compressor$,T_E,T_C)
    m_flow=get_m_flow(Compressor$,T_E,T_C)

    P_C=p_sat(WF$,T=T_C)
    P_E=p_sat(WF$,T=T_E)

    h_in=enthalpy(WF$,T=T_Suction, P=P_E)
    s_suction=entropy(WF$,T=T_Suction, P=P_E)

    h_isDisch=enthalpy(WF$,s=s_suction, P=P_C)
    P_is=m_flow*(h_isDisch-h_in)                  {Isentropic compression work}


    is_Eff_HL=(P_is*1000)/(P_Shaft*(1-Heat_Loss_Factor))                    {Calculating
Isentropic efficiency by assumin constant heat loss factor of compressor}
    plot_is_eff_hl=is_Eff_HL

End



Function plot_is_eff(WF$,Compressor$,T_E, T_C)
    n=50                                          {Nominal compressor speed [Hz]}
    T_Suction=T_E+15 [C]                          {Assuming 15K Suction Superheat}

    P_Shaft=get_p_shaft(Compressor$,T_E,T_C)
    m_flow=get_m_flow(Compressor$,T_E,T_C)
```

```
P_E=p_sat(WF$,T=T_E)
P_C=p_sat(WF$,T=T_C)

h_in=enthalpy(WF$,T=T_Suction, P=P_E)
s_suction=entropy(WF$,T=T_Suction, P=P_E)

h_isDisch=enthalpy(WF$,s=s_suction, P=P_C)
P_is=m_flow*(h_isDisch-h_in)                    {Isentropic compression work}


is_Eff=(P_is*1000)/P_Shaft                      {Calculating Effective Isentropic efficiency by assumin constant heat
loss factor of compressor}
plot_is_eff=is_Eff

End

Compressor$='HEX2500CC'                         { Compressor Model}
WF$='R290'                                      {Refrigerant: Propane}

T_E=-15 [C]                                     {Evaporation temperature for plotting}
T_E_Drift=-15 [C]                               {Evaporation temperature operating point}
T_C_Drift= 56 [C]                               {Condensation temperature operating point}

T_Cmax=90 [C]                                   {Maximum condensation temperature for plotting}
Heat_Loss_Factor = 0.1                          {Assuming 10% of compressor shaft power is emitted to
surroundings as heat}
DT_SH=15 [C]                                    {Suction gas superheat}
T_Suction=T_E+DT_SH                             {Suction gas temperature}
P_E=p_sat(WF$,T=T_E)
DT_Step=(T_Cmax-T_Suction)/20


{Rest of script for plotting the compressor efficiencies over a range of pressure ratios}
T_C[1..20]= [T_Suction+DT_Step,T_Suction+2*DT_Step,T_Suction+3*DT_Step,T_Suction+4*DT_Step, T_Suction+5*
DT_Step, T_Suction+6*DT_Step, T_Suction+7*DT_Step, T_Suction+8*DT_Step, T_Suction+9*DT_Step, T_Suction+10*
DT_Step, T_Suction+11*DT_Step, T_Suction+12*DT_Step,T_Suction+13*DT_Step, T_Suction+14*DT_Step, T_Suction+15*
DT_Step, T_Suction+16*DT_Step, T_Suction+17*DT_Step, T_Suction+18*DT_Step, T_Suction+19*DT_Step, T_Suction+20*
DT_Step]

P_C[1]=p_sat(WF$,T=T_C[1])
P_C[2]=p_sat(WF$,T=T_C[2])
P_C[3]=p_sat(WF$,T=T_C[3])
P_C[4]=p_sat(WF$,T=T_C[4])
P_C[5]=p_sat(WF$,T=T_C[5])
P_C[6]=p_sat(WF$,T=T_C[6])
P_C[7]=p_sat(WF$,T=T_C[7])
P_C[8]=p_sat(WF$,T=T_C[8])
P_C[9]=p_sat(WF$,T=T_C[9])
P_C[10]=p_sat(WF$,T=T_C[10])
P_C[11]=p_sat(WF$,T=T_C[11])
P_C[12]=p_sat(WF$,T=T_C[12])
P_C[13]=p_sat(WF$,T=T_C[13])
P_C[14]=p_sat(WF$,T=T_C[14])
P_C[15]=p_sat(WF$,T=T_C[15])
P_C[16]=p_sat(WF$,T=T_C[16])
P_C[17]=p_sat(WF$,T=T_C[17])
P_C[18]=p_sat(WF$,T=T_C[18])
P_C[19]=p_sat(WF$,T=T_C[19])
P_C[20]=p_sat(WF$,T=T_C[20])
```

Vol_Eff[1]= **plot_vol_eff**(WF$,Compressor$,T_E, T_C[1])
Vol_Eff[2]= **plot_vol_eff**(WF$,Compressor$,T_E, T_C[2])
Vol_Eff[3]= **plot_vol_eff**(WF$,Compressor$,T_E, T_C[3])
Vol_Eff[4]= **plot_vol_eff**(WF$,Compressor$,T_E, T_C[4])
Vol_Eff[5]= **plot_vol_eff**(WF$,Compressor$,T_E, T_C[5])
Vol_Eff[6]= **plot_vol_eff**(WF$,Compressor$,T_E, T_C[6])
Vol_Eff[7]= **plot_vol_eff**(WF$,Compressor$,T_E, T_C[7])
Vol_Eff[8]= **plot_vol_eff**(WF$,Compressor$,T_E, T_C[8])
Vol_Eff[9]= **plot_vol_eff**(WF$,Compressor$,T_E, T_C[9])
Vol_Eff[10]= **plot_vol_eff**(WF$,Compressor$,T_E, T_C[10])
Vol_Eff[11]= **plot_vol_eff**(WF$,Compressor$,T_E, T_C[11])
Vol_Eff[12]= **plot_vol_eff**(WF$,Compressor$,T_E, T_C[12])
Vol_Eff[13]= **plot_vol_eff**(WF$,Compressor$,T_E, T_C[13])
Vol_Eff[14]= **plot_vol_eff**(WF$,Compressor$,T_E, T_C[14])
Vol_Eff[15]= **plot_vol_eff**(WF$,Compressor$,T_E, T_C[15])
Vol_Eff[16]= **plot_vol_eff**(WF$,Compressor$,T_E, T_C[16])
Vol_Eff[17]= **plot_vol_eff**(WF$,Compressor$,T_E, T_C[17])
Vol_Eff[18]= **plot_vol_eff**(WF$,Compressor$,T_E, T_C[18])
Vol_Eff[19]= **plot_vol_eff**(WF$,Compressor$,T_E, T_C[19])
Vol_Eff[20]= **plot_vol_eff**(WF$,Compressor$,T_E, T_C[20])

Is_Eff[1]=**plot_is_eff**(WF$,Compressor$,T_E, T_C[1])
Is_Eff[2]=**plot_is_eff**(WF$,Compressor$,T_E, T_C[2])
Is_Eff[3]=**plot_is_eff**(WF$,Compressor$,T_E, T_C[3])
Is_Eff[4]=**plot_is_eff**(WF$,Compressor$,T_E, T_C[4])
Is_Eff[5]=**plot_is_eff**(WF$,Compressor$,T_E, T_C[5])
Is_Eff[6]=**plot_is_eff**(WF$,Compressor$,T_E, T_C[6])
Is_Eff[7]=**plot_is_eff**(WF$,Compressor$,T_E, T_C[7])
Is_Eff[8]=**plot_is_eff**(WF$,Compressor$,T_E, T_C[8])
Is_Eff[9]=**plot_is_eff**(WF$,Compressor$,T_E, T_C[9])
Is_Eff[10]=**plot_is_eff**(WF$,Compressor$,T_E, T_C[10])
Is_Eff[11]=**plot_is_eff**(WF$,Compressor$,T_E, T_C[11])
Is_Eff[12]=**plot_is_eff**(WF$,Compressor$,T_E, T_C[12])
Is_Eff[13]=**plot_is_eff**(WF$,Compressor$,T_E, T_C[13])
Is_Eff[14]=**plot_is_eff**(WF$,Compressor$,T_E, T_C[14])
Is_Eff[15]=**plot_is_eff**(WF$,Compressor$,T_E, T_C[15])
Is_Eff[16]=**plot_is_eff**(WF$,Compressor$,T_E, T_C[16])
Is_Eff[17]=**plot_is_eff**(WF$,Compressor$,T_E, T_C[17])
Is_Eff[18]=**plot_is_eff**(WF$,Compressor$,T_E, T_C[18])
Is_Eff[19]=**plot_is_eff**(WF$,Compressor$,T_E, T_C[19])
Is_Eff[20]=**plot_is_eff**(WF$,Compressor$,T_E, T_C[20])

Is_Eff_Heat_Loss[1]=**plot_is_eff_hl**(WF$,Compressor$,T_E, T_C[1],Heat_Loss_Factor)
Is_Eff_Heat_Loss[2]=**plot_is_eff_hl**(WF$,Compressor$,T_E, T_C[2],Heat_Loss_Factor)
Is_Eff_Heat_Loss[3]=**plot_is_eff_hl**(WF$,Compressor$,T_E, T_C[3],Heat_Loss_Factor)
Is_Eff_Heat_Loss[4]=**plot_is_eff_hl**(WF$,Compressor$,T_E, T_C[4],Heat_Loss_Factor)
Is_Eff_Heat_Loss[5]=**plot_is_eff_hl**(WF$,Compressor$,T_E, T_C[5],Heat_Loss_Factor)
Is_Eff_Heat_Loss[6]=**plot_is_eff_hl**(WF$,Compressor$,T_E, T_C[6],Heat_Loss_Factor)
Is_Eff_Heat_Loss[7]=**plot_is_eff_hl**(WF$,Compressor$,T_E, T_C[7],Heat_Loss_Factor)
Is_Eff_Heat_Loss[8]=**plot_is_eff_hl**(WF$,Compressor$,T_E, T_C[8],Heat_Loss_Factor)
Is_Eff_Heat_Loss[9]=**plot_is_eff_hl**(WF$,Compressor$,T_E, T_C[9],Heat_Loss_Factor)
Is_Eff_Heat_Loss[10]=**plot_is_eff_hl**(WF$,Compressor$,T_E, T_C[10],Heat_Loss_Factor)
Is_Eff_Heat_Loss[11]=**plot_is_eff_hl**(WF$,Compressor$,T_E, T_C[11],Heat_Loss_Factor)
Is_Eff_Heat_Loss[12]=**plot_is_eff_hl**(WF$,Compressor$,T_E, T_C[12],Heat_Loss_Factor)
Is_Eff_Heat_Loss[13]=**plot_is_eff_hl**(WF$,Compressor$,T_E, T_C[13],Heat_Loss_Factor)
Is_Eff_Heat_Loss[14]=**plot_is_eff_hl**(WF$,Compressor$,T_E, T_C[14],Heat_Loss_Factor)
Is_Eff_Heat_Loss[15]=**plot_is_eff_hl**(WF$,Compressor$,T_E, T_C[15],Heat_Loss_Factor)
Is_Eff_Heat_Loss[16]=**plot_is_eff_hl**(WF$,Compressor$,T_E, T_C[16],Heat_Loss_Factor)
Is_Eff_Heat_Loss[17]=**plot_is_eff_hl**(WF$,Compressor$,T_E, T_C[17],Heat_Loss_Factor)
Is_Eff_Heat_Loss[18]=**plot_is_eff_hl**(WF$,Compressor$,T_E, T_C[18],Heat_Loss_Factor)
Is_Eff_Heat_Loss[19]=**plot_is_eff_hl**(WF$,Compressor$,T_E, T_C[19],Heat_Loss_Factor)

Is_Eff_Heat_Loss[20]=**plot_is_eff_hl**(WF$,Compressor$,T_E, T_C[20],Heat_Loss_Factor)

P_Ratio[1]=P_C[1]/P_E
P_Ratio[2]=P_C[2]/P_E
P_Ratio[3]=P_C[3]/P_E
P_Ratio[4]=P_C[4]/P_E
P_Ratio[5]=P_C[5]/P_E
P_Ratio[6]=P_C[6]/P_E
P_Ratio[7]=P_C[7]/P_E
P_Ratio[8]=P_C[8]/P_E
P_Ratio[9]=P_C[9]/P_E
P_Ratio[10]=P_C[10]/P_E
P_Ratio[11]=P_C[11]/P_E
P_Ratio[12]=P_C[12]/P_E
P_Ratio[13]=P_C[13]/P_E
P_Ratio[14]=P_C[14]/P_E
P_Ratio[15]=P_C[15]/P_E
P_Ratio[16]=P_C[16]/P_E
P_Ratio[17]=P_C[17]/P_E
P_Ratio[18]=P_C[18]/P_E
P_Ratio[19]=P_C[19]/P_E
P_Ratio[20]=P_C[20]/P_E

P_Ratio_Max=(**p_sat**(WF$,***T***=65))/P_E
P_Ratio_Min=(**p_sat**(WF$,***T***=20))/P_E

Vol_Eff_Drift=**plot_vol_eff**(WF$,Compressor$,T_E_Drift, T_C_Drift)
Is_Eff_Drift=**plot_is_eff**(WF$,Compressor$,T_E_Drift, T_C_Drift)
Is_Eff_Drift_Incl_Heat_Losses=**plot_is_eff_hl**(WF$,Compressor$,T_E_Drift, T_C_Drift,Heat_Loss_Factor)

SOLUTION

**Unit Settings: SI C bar kJ mass deg**

Compressor$ = 'HEX2500CC'
$DT_{Step}$ = 4.5
$Is_{Eff,Drift}$ = 0.6153
$P_E$ = 2.916
$P_{Ratio,Min}$ = 2.869
$T_{C,Drift}$ = 56 [C]
$T_{E,Drift}$ = -15 [C]
$Vol_{Eff,Drift}$ = 0.6941
$DT_{SH}$ = 15 [C]
$Heat_{Loss,Factor}$ = 0.1
$Is_{Eff,Drift,Incl,Heat,Losses}$ = 0.6836
$P_{Ratio,Max}$ = 8.035
$T_{Cmax}$ = 90 [C]
$T_E$ = -15 [C]
$T_{Suction}$ = 0
WF$ = 'R290'

105 potential unit problems were detected.

Erlend Nytrø Balstad

# Evaluation of possible heat pump configurations for waste heat recovery at +CityXChange Sluppen

NTNU
Norwegian University of
Science and Technology